FUNCTIONAL ASSESSMENT OF AMPUTEE PERFORMANCE

by

JOHN MICAL MANSFIELD

B. S. in Mechanical Engineering, Purdue University (1985)

S. M. in Mechanical Engineering, Massachusetts Institute of Technology (1988)

Submitted to the
Department of Mechanical Engineering
in Partial Fulfillment of the Requirements for the Degree of

DOCTOR OF PHILOSOPHY

at the

MASSACHUSETTS INSTITUTE OF TECHNOLOGY

December 1992

© Massachusetts Institute of Technology 1992
All rights reserved

Signature of Author _____
Department of Mechanical Engineering
December 18, 1992

Certified by _____
Professor Neville Hogan
Thesis Supervisor

Certified by _____
Professor Ain A. Sonin
Chairman, Departmental Committee on Graduate Studies

MASSACHUSETTS INSTITUTE OF TECHNOLOGY
MAR 24 1993
ARCHIVES
LIBRARIES

FUNCTIONAL ASSESSMENT OF AMPUTEE PERFORMANCE

by

JOHN MICAL MANSFIELD

Submitted to the Department of Mechanical Engineering
on December 18, 1992 in partial fulfillment of the requirements for the
Degree of Doctor of Philosophy in Mechanical Engineering

ABSTRACT

The interaction of amputees with the environment while performing tasks is a very important and complex problem. Increased understanding of the problem provides revelations about human motor behavior, improved formulations for tools used in task performance, and kindred insights into more productive and diverse robots. Unfortunately, very little is known or has been *quantified* about amputee environmental interaction and task performance.

This thesis describes a human-machine-environment interface used to experimentally investigate and quantify amputee interaction with the environment while performing tasks. The human-machine subsystem consists of a unilateral, above-elbow amputee wearing a high performance, computer controlled, elbow prosthesis. The computer can immediately implement and modify a broad range of preprogrammed, prosthesis controller algorithms but still permits the amputee to perform a series of tasks without interruption. The process of changing controller architectures for the same task and environmental conditions provides a unique approach for investigating the different interactions among the amputee, the prosthesis, and the environment during task performance.

Four controllers were implemented during the experiments. The Boston Elbow and the NY Electric Elbow controllers simulate two commercially available, high output impedance prostheses. An Impedance controller crudely mimics the characteristics of an intact elbow and a Passive controller mirrors the popular, body-powered prosthesis but lacks both the clutch and cable. The latter two controllers exhibit a low output impedance. The selected tasks included a highly quantifiable crank turning task (constrained motion task) and three Activity of Daily Living tasks: cutting meat (an eating task), donning socks (a dressing task), and using a rolling pin to roll a ball of dough into a pie crust (a bimanual task).

Based on the experiments with four subjects, the crank task results show that high output impedance devices can produce adverse effects during task performance; this possibly explains the poor acceptance of externally powered prostheses. The comparison of the more similar kinematic measurements (positions and velocities) with the more variable dynamic measurements (forces and power flows) for the same task but with different subjects, controllers, and constraints provides strong evidence that humans perform tasks using kinematic objectives and have a hierarchical organization of motor behavior. Dynamic measurements, especially the rate of change of power, proved to be extremely useful for segregating controller characteristics, unveiling relatively advanced human strategies, and for quantifying task performance. The results also stress the importance of a variable output impedance design for performing a spectrum of unrelated tasks. Models and simulations demonstrate that task performance may be governed by humans trying to minimize the task's power dissipation.

Thesis Supervisor: Neville Hogan, Ph.D.
Title: Professor of Mechanical Engineering and Brain & Cognitive Sciences

MEMBERS OF THE COMMITTEE

Dr. Neville Hogan
Professor
Department of Mechanical Engineering
Department of Brain & Cognitive Sciences

Dr. Thomas B. Sheridan
Professor of Engineering and Applied Psychology
Department of Mechanical Engineering

Dr. William K. Durfee
D'Arbeloff Associate Professor
Department of Mechanical Engineering

Dr. Ferdinando Mussa-Ivaldi
Principal Research Scientist
Department of Brain & Cognitive Sciences

ACKNOWLEDGMENTS

There is no question that attending MIT was an educational experience. The education, however, consisted more than just taking a handful of courses and writing a thesis to fulfill the requirements necessary to graduate. This was only a portion, perhaps even a minor portion, of the *total* experience. The remaining experience came from the people with whom I interacted and the intense environment in which we all shared our lives. I will miss the environment and the countless people who helped me along the way.

I would like to thank my advisor, Prof. Neville Hogan, for his guidance and support. I will never understand the circumstances that brought me to MIT and gave me the privilege to be one of Neville's students. I do understand that the series of events was probably the best thing that could have ever happened to me. From welding a cracked moldboard on a plow to soldering a new IC chip on a digital I/O board, my transition from a farm to a research environment has been quite dramatic. I trust it was not too traumatic for Neville. I would also like to thank the remaining members of my committee: Prof. Thomas Sheridan, Prof. William Durfee, and Dr. Ferdinando Mussa-Ivaldi (Sandro). Their participation, comments, and suggestions were very helpful towards the completion of my thesis.

Without the amputees, I would have no results. The amputees that participated as subjects in the experiments were invaluable. The willingness each amputee demonstrated to voluntarily take a day off from work (often without pay) and to travel to MIT to participate in the experiments was more than I ever expected. Individual interests in tackling a very difficult problem truly shined throughout the experiments.

The interaction and experience I received while working in the Newman lab has been precious. I would like to thank Prof. Robert Mann and all my friends for creating an atmosphere of camaraderie that was difficult to find in other labs. Taking the extra time and effort to help others and to perform the various lab chores were very small prices to pay for the education and enjoyment received. The moral of the story was well learned.

Finally, my foundation of support has always been my family. Technical support is useful for research, but it can not compare to the love that I received from my wife, Beth, my mom, my dad, and my two sisters, Lois and Carol. Research can be a rocky road with many highs and lows. Beth can attest to that. Love, though, seems to smooth out the peaks and valleys and makes living with a graduate student more tolerable. I am deeply in debt for the contributions and sacrifices made by my family. Special thanks must go to a great friend and engineer who helped edit this thesis – my dad.

This research was performed in the Eric P. and Evelyn E. Newman Laboratory for Biomechanics and Human Rehabilitation at MIT and was funded under the following grants: National Institute of Arthritis & Musculoskeletal & Skin Diseases and National Institutes of Health, Grant No. 40029.

To my wife, Beth

God be with you always

CONTENTS

CHAPTER
ONE

INTRODUCTION

1.1 ISSUES

The field of robotics has made several important contributions to society. Tedious, repetitive tasks that were once performed by humans are now performed by robots in a more productive and efficient manner. Manufacturing processes that were once considered difficult or impossible are now routine. Robotics has even entered into the field of rehabilitation by providing the injured with therapeutic aids and enhancing the lifestyles of the handicapped.

Despite these advances, there are still limitations in the field of robotics. Most robots tend to be very good at performing only one set of specific tasks, such as positioning or item transport. The ability to perform several unrelated tasks, as humans can do, is still not possible. Besides lacking task flexibility, robots have a very difficult time interacting dynamically with the environment. Even the simplest of contact tasks can quickly lead to system instabilities [31]. Telerobotics, which uses remote human supervision to operate a robot within a given environment, is a more advanced form of robotics and can address the flexibility issue. Unfortunately, time delays, poor sensory feedback and the added complexity of human feedback have limited the results obtained to date.

Perhaps even more complicated than the field of telerobotics is the field of externally powered prostheses; that is, prostheses with self-contained actuators. An example of such a device (and the focus of this thesis) is the above-elbow prosthesis. In the field of externally powered prostheses, there is a *direct* human-machine-environment interface that must not only address all the above robotic and telerobotic issues, but must also be safe, reliable, lightweight and compact. These additional design constraints usually smother any creative ideas for improving a prosthesis and may, in turn, explain the current lack of acceptance in using such devices. Studies have shown that only fifty percent of the above-elbow amputee population wear a prosthesis and only five percent wear an externally powered prosthesis [26].

1.2 OBJECTIVE

Many reasons are given for the poor acceptance of the externally powered prosthesis by the amputee population. Most of these reasons originate from three contributing factors: function, comfort, and appearance. This thesis concentrates on function and its relevance to task performance. Although deemed important, comfort and appearance are not addressed at this time.

A functional prosthesis interacts with either the amputee, the environment, or both during the performance of a task. While not always the case, the ability to perform a larger set of diversified tasks with the prosthesis *usually* indicates greater functionality. In many ways the prosthesis acts as a *tool* to aid the amputee during the performance of a task. In addition, auxiliary tools, such as a fork for eating or a comb for grooming, may be attached to the prosthesis to perform more specific tasks. Such a situation, where a *human* uses a *tool* (or a machine) to interact with the *environment*, is a very common occurrence for both amputees and intacts (i.e., persons without an amputation). Any investigation which would reveal insights on how the trilogy of subsystems interact during the performance of a task would not only be useful in the field of prosthetics but could also benefit the fields of robotics and telerobotics.

Humans are very good at performing a seemingly endless variety of tasks. Humans are also very adept at performing the same task several different ways. This is readily apparent in amputees who, with a missing limb, must confront the same daily tasks encountered by intacts. It is improbable that humans treat the method of performance for *each* task as an individual kinematic and dynamic problem. Besides being a computational burden, a motion control process of this nature would not lend itself to categorizing similar tasks or similar outcomes of different tasks. A more plausible working hypothesis is that task performance is based on

fundamental sets of motion control processes and tools. Depending on how the processes and tools are combined, a different set of tasks can be performed. When one of the tools is missing, such as an arm or a leg, the remaining processes and tools can recombine to compensate for the missing entity and to permit future performances of the task.

The specific objective of this work was to investigate the interaction of above-elbow amputees as they used their prosthesis (i.e., a tool) to perform a selected set of tasks. Understanding the interactions occurring within the amputee-prosthesis-environment system may provide insights to a much broader goal of investigating the fundamental requirements for effective tool use. In particular, this research sought to find what factors are important for humans to effectively interact with tools and the environment to accomplish a diverse set of tasks. To explore the objective, several above-elbow amputees were asked to perform a series of tasks using a unique, prosthesis emulator system that enables different prosthesis controller architectures to be implemented while using identical hardware [5]. In this situation, the emulator represents a tool that replaces the amputee's lost limb and the different controller architectures reflect different tool behaviors. It was proposed that studying the effects of different controller architectures while performing the same set of tasks would illuminate some of the fundamental requirements for effective tool use.

1.3 BACKGROUND

In terms of above-elbow prosthesis designs and controllers, one should refer to the comprehensive, historical reviews written by Abul-Haj and Kishinchandani [3, 4, 21]. The most common above-elbow prostheses used to date are the body-powered prosthesis and several externally powered, velocity-controlled prostheses. The body-powered prosthesis, still the most popular prosthesis, was developed just after World War II and has changed very little since. The body-powered prosthesis uses an amputee's shoulder motion and a cable to flex and lock the elbow unit. The introduction of externally powered prostheses in the late 50's provided great hopes of supplying the amputee with a dramatically improved, functional prosthesis. Yet, the improvements have only been modest. Current externally powered prostheses use a self-contained battery pack to power a small electric motor that drives the elbow through a high, speed reduction transmission.

In terms of research, numerous studies have been performed to determine how effective prostheses are at performing a battery of tasks [8, 18, 19, 23, 24, 28, 29, 32, 36]. The tasks usually represent activities that amputees normally encounter on a daily basis and are often la-

beled Activities of Daily Living (ADL). The studies rate effectiveness using qualitative, time, or motion measurements. The criteria of effectiveness in these measurements have been: 1) the prosthesis displays a more graceful appearance, 2) it performs the task faster, 3) it produces fewer position errors when compared to another prosthesis (or no prosthesis). While the studies often conclude with a statistical number as to which prosthesis is "better", the studies only speculate why one prosthesis excels over another. No studies could be found which specifically tried to determine what essential features are required for an *effective* prosthesis. No studies attempted to functionally assess task performance by incorporating force interactions, power flows, or other *dynamic* measurements.

The reasons for the limited advancements in above-elbow (AE) prostheses are not obvious and emphasize the difficulty of the problem. One would have expected, after decades of research, a prosthesis that is technically more advanced than the body-powered prosthesis would have had a greater acceptance among the amputees. The scant acceptance suggests that there is something lacking in the externally powered prostheses that is present in the body-powered prostheses. Weight and cost have always made the body-powered prosthesis attractive; there may be other hidden advantages that make this prosthesis more practical or functional. In this study of investigating the important factors for effective tool use, an explanation of the body-powered paradox may be exposed.

1.4 APPROACH

As alluded to in the objective, this investigation had several above-elbow amputees don a prosthesis emulator and perform a series of tasks using different controller architectures. The participation of amputees provided an intimate interface among the three subsystems (human, machine, and environment) and facilitated acquisition of measurements not *directly* obtainable from intact humans (e.g., elbow torque, elbow power). In addition, the inclusion of only above-elbow amputees permitted the study to concentrate on limbs that are highly task oriented.

Miller showed that the prosthesis controller plays a significant role in amputee performance [30]. In addition, Abul-Haj and Hogan demonstrated that the output impedance of a prosthesis can have important implications to the prosthesis's functionality [6, 7]. Both studies suggest that the prosthesis's controller architecture can make a significant contribution towards effective tool use. With the emulator system, the same task can be performed using dramatically different controller architectures while maintaining the same amputee posture, socket-

harness attachment, prosthesis hardware, and EMG muscle sites. This allows one to concentrate on studying the effects of the different controllers utilized during each task performance and to preserve tightly controlled experiments.

The controllers implemented included two common velocity controllers that are currently available for amputees: the NY Electric Elbow (NY) produced by Hosmer Dorance Corporation and the Boston Elbow (BE) supported by Liberty Mutual Insurance Company [1, 2]. Also included were two experimental controllers: the *impedance controller* which crudely mimics the control of the intact arm and a *passive controller* which is similar to the body-powered prosthesis in swing phase [1, 6, 38]. The details of each controller are discussed in Chapter 3. The four controllers selected represented a wide assortment of input gains, output impedances, and signal processing algorithms.

Four tasks were performed by each subject. One task was a simple but highly informative crank turning task. The remaining three were bimanual tasks encountered throughout an amputee's activities of daily living (ADL) [7]. All tasks contained movements that were constrained or partially constrained. The reasons for this were twofold. First, tasks involving constrained motions required the subject to interact mechanically with the environment. Such interaction is fundamental for tool use and is pivotal for improving the functionality of future human-machine-environment systems. Second, constrained motion tasks reduced the number of uncontrolled factors in the experiment by reducing the degrees of freedom of the task. This not only simplified the complexity of performing the task but also made instrumentation and analysis easier.

1.5 THESIS OVERVIEW

Chapters 2 through 5 of the thesis concentrate on the investigative experiments. Chapter 2 briefly discusses the two key apparatuses used to quantify the experiments. These are the emulator system and the crank. Reasons why the crank task is such an informative task are discussed in some detail. Chapter 3 explains the requirements necessary for an amputee to participate as a subject for the experiments. Details are also given on the type of controllers implemented during the experiments and the tasks performed by each subject. Data reduction of each experiment was complex and required some extensive software development. Chapter 4 provides an overview of the data processing used to ascertain the experimental results. Chapter 5 summarizes the results obtained from all subjects, controllers, and tasks. This chapter is the core of the thesis. Because of the subtle intricacies among the data and because of the tre-

mendous amount of data collected, the potential findings from the data are considerable. Even though the results and discussion in Chapter 5 are conclusive, they also imply that a much longer, on-going analysis of the data should be initiated.

The experiments unveiled numerous questions, some of which have no immediate answers. The second part of the thesis tries to answer some of the questions that arose in the first part. Chapter 6 presents two simplified models and thermodynamic arguments that explain some of the experimental results. The arguments are based on minimizing power dissipation and minimizing entropy generation. Chapters 7 and 8 present simulations of these models and discuss each argument's soundness.

The conclusions in Chapter 9 summarize the results obtained from both parts of the thesis. The significant findings of the investigation are reemphasized and several interpretations of the results are presented. The chapter also provides several potential directions for future research.

CHAPTER
TWO

HARDWARE

2.1 EMULATOR SYSTEM

The emulator system consists of a harness, a socket, two surface electrodes, a uniquely designed, above-elbow, prosthesis emulator, and an off-board computer and power supply. The system is equipped to fit an assortment of stump sizes to accommodate a range of amputees with different physiques and amputations. This section of the chapter briefly describes the hardware used to attach the emulator system to a subject.

A subject was given one of two leather shoulder harnesses depending on the side of the amputation. The harness is equipped with several adjusting straps to ensure proper fit and to support the weight of the socket and emulator. When compared to the standard figure-eight harness, the shoulder harness distributes the weight of the prosthesis over a greater bearing surface and reduces the chance that the weight of the emulator will play a factor during the performances of the tasks. A lightweight cotton shirt was worn underneath the harness to help absorb perspiration and to improve comfort.

Two flexible sockets, each of a different size, permit the emulator to be donned onto stumps of various sizes. Each flexible socket is made of soft plastic with expansion slots and slips over the subject's stump, normally covered with a cotton sock, and attaches to the shoulder

harness. The socket is secured in place by tightening two velcro straps placed around the socket and adjusting two velcro straps attached to the shoulder harness. Attaching the socket to the stump is very similar to slipping a tennis shoe on a foot and tying the laces.

Most of the controllers implemented for the experiments used myoelectric activity (MEA) as a command input to operate the prosthesis. To measure the MEA signals, the most recent, high gain, surface electrodes manufactured by Liberty Mutual were placed over the appropriate biceps and triceps muscle sights and secured with surgical tape.

The above-elbow prosthesis emulator is described in great detail by its designer, Cary Abul-Haj [3-5]. Only a brief description of the device is necessary for this work. The emulator was attached to the bottom of the socket with a single bolt. A friction pad prevented humeral rotation of the emulator relative to the socket. The prosthesis was tethered to a computer and power supply with over twenty feet of wire. Having the power supply off-board permitted the emulator to carry a more powerful motor than found on any self-contained prosthesis. Tethers to the computer permitted immediate changes to the emulator's controller architecture without interfering with the amputee or the task. The emulator was instrumented to measure elbow position, elbow velocity, and elbow torque.

The computer used to monitor and control the emulator was a DEC LSI 11/73. Menu-driven software permitted the implementation of four, preprogrammed, real-time controllers. Changing controllers for the emulator was as simple as changing the selection from the main menu. The computer monitored and stored seven measurements required to control the emulator. These measurements were: biceps and triceps MEA's, elbow position, velocity, and torque, and motor voltage and current. The computer's sampling rate was 100 HZ.

To minimize potential distractions due to mismatched limb lengths, care was taken to ensure that the link lengths from the shoulder to the elbow pivot and from the elbow pivot to the terminal device were the same lengths the amputee used with his personal prosthesis. Velcro straps on the shoulder harness permitted one to change the distance from the shoulder to elbow pivot while variable length, wrist extension tubes at the end of the emulator allowed the distance from the emulator's elbow pivot to the terminal device to be properly adjusted.

Because all ADL tasks required a terminal device, the harnesses, sockets and emulator were equipped with the appropriate hardware to operate a standard, voluntary open, hook from Hosmer Dorance Corp. Two different sizes were available for both right and left sided ampu-

tations. An assortment of rubber bands permitted the subject to adjust the desired gripping strength of the hook.

2.2 CRANK SYSTEM

The crank system consists of a crank, a handle, and optional attachments. The crank is attached securely to a laboratory work bench and rotates in a vertical plane. A potentiometer measured the crank angle. The crank pivot was roughly 32 inches from the floor and a handle was attached to the crank arm 8 inches from the pivot. The 8 inch arm length proved in past studies to be a good distance that reduced the amount of shoulder motion recruited during the performance of the task. For attachment to the emulator, the crank handle contained a special adapter that replaced the emulator's standard hook. The handle contains a potentiometer and strain gages to measure handle angle, radial force, and tangential force. A universal joint at the handle and radial ball bearings at all joints minimized moment and frictional effects of the system. To statically balance the weight of the handle, a counterbalance was attached to the opposite side of the crank pivot.

The design of the crank allowed for optional attachments that could change the conditions under which the task was being performed. A pulley at the crank pivot permitted an assortment of weights to be hung from the pulley's rim and produced crank torques which could either assist or resist the subject's rotation of the crank. A bicycle caliper brake, grounded to the lab bench and acting on the pulley's rim, allowed various levels of Coulomb friction to be added for the task [34]. As with the emulator, one should refer to Abul-Haj's writings for additional details on the crank design [6, 7].

Figure 2.1 shows the typical geometry of the crank and emulator system as a subject is performing the task. During the task, a subject sits in a chair facing the crank and rotates the crank in a semicircular fashion from the bottom of the crank path to the top and then from the top of the crank path back down to the bottom. In both cases, the crank is turned *towards* the subject. The subject's shoulder is roughly 7 inches above the crank pivot and 19 inches away. The link lengths and shoulder position shown in Figure 2.1 are proportional to average distances recorded from all subjects. The directions of the angle and force vectors shown define *positive* measurements from their respective zero reference lines. Unconstrained elbow flexion produces increased elbow angles, positive elbow velocities, and positive elbow torques.

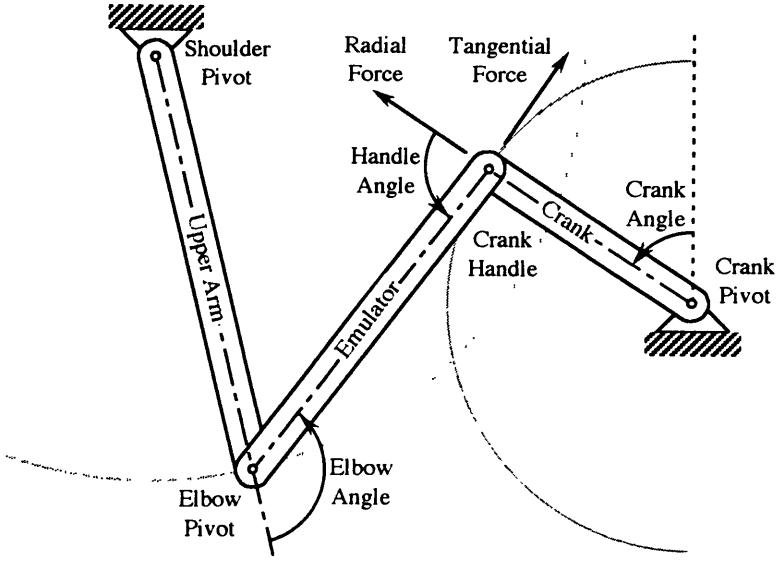

Figure 2.1 Emulator and Crank System

The elbow and shoulder reversals are two regions of the crank task that are often referenced. Figures 2.2 and 2.3 show the two reversals respectively. The elbow reversal is encountered when the centerline of the crank arm passes through the shoulder pivot. At this position, elbow torque can not contribute to the crank's tangential force vector. Elbow torque will only create radial forces in the crank arm. Passage through the reversal requires the subject to use some other means, such as shoulder torque, gravity, or momentum, if the task is to be completed. The shoulder reversal occurs when the crank arm centerline is collinear with the emulator centerline. At this position, shoulder torque will only produce radial forces and can not contribute to rotating the crank. The subject must rely on elbow torque or some other strategy if passage through the shoulder reversal is to be ensured.

The simplicity of the crank and the subtleties of the reversals are the primary reasons why the crank task has been the focus of several studies by researchers at MIT [7, 21, 30, 33, 34]. Most people are very familiar with the concept of turning a crank and do not require special training or practice. The reversals force the subject to interact and coordinate with all the system links. Any one link or any one actuator (muscle or motor) can not complete the task by itself unless the remaining links and actuators are properly coordinated. This is especially true when one of the joints possesses a high output impedance. Under the assumptions of planar motion, fixed link lengths, and fixed shoulder and crank pivot locations, the crank-emulator system becomes a four-bar linkage with one degree of freedom. In such a system, a joint with a high output impedance will dictate the kinematics of the entire system. The re-

maining joint positions, velocities and accelerations are all predetermined by the output of the high output impedance joint.

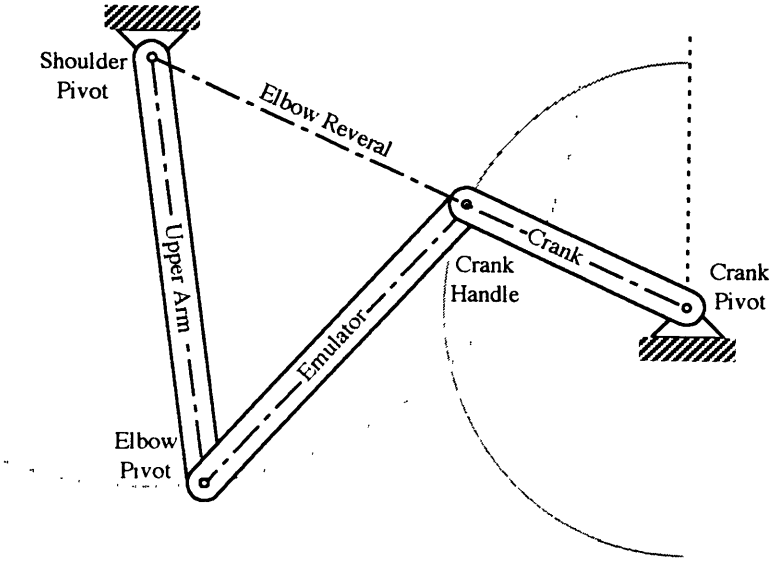

Figure 2.2 Elbow Reversal

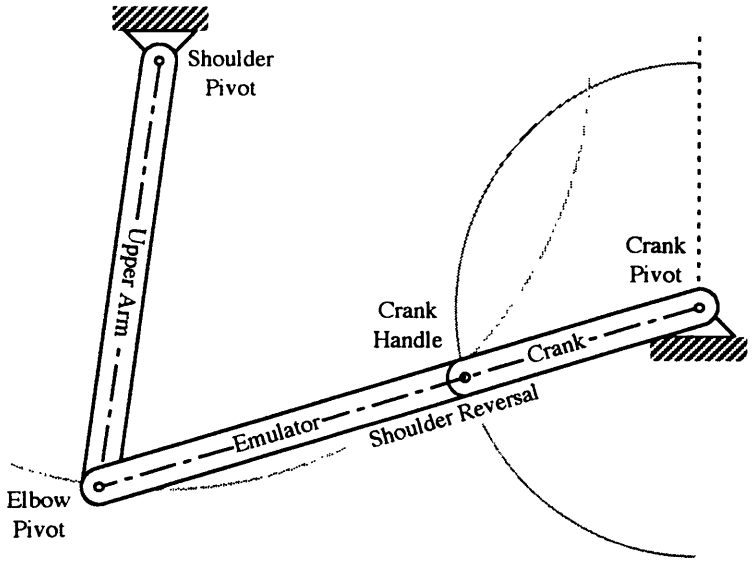

Figure 2.3 Shoulder Reversal

While the kinematics of the crank system can be dependent on the characteristics of one joint, this is not the case with the system's force interactions. Even with a high output impedance joint, the force interactions experienced by each link are dependent on the individual contri-

butions made by all the system's actuators. For example, assume that the 4-bar linkage is locked into place by a high output impedance joint. All the links have a fixed position with zero velocity and acceleration. However, the force interactions between the various linkages are not constrained and, in fact, can fluctuate dramatically depending on the contributions of the individual joint torques. This separation of joint kinematics from joint dynamics will become an important issue when discussing the experimental results.

2.3 ADL TASKS

Additional tasks performed by each subject were labeled Activities of Daily Living or ADL tasks. As the name suggests, the tasks represent activities that an amputee would normally encounter on a daily basis. While several previous studies have concentrated on the crank task for evaluating task performance, this investigation makes the first attempt to integrate the highly quantifiable crank results with the performances of ADL tasks. In the past, the crank task has shown some interesting experimental results but there has always been a question as to whether the results can be generalized to other tasks or whether they are specific to the one task: turning a crank. To see if any performance correlations exist between the crank and ADL tasks, a limited set of diversified ADL tasks were selected and studied in conjunction with the crank task.

Quantifying the ADL tasks unveils an interesting set of questions: What should be quantified and how? The emulator system provides a unique advantage for quantifying ADL tasks because of the seven on-board measurements it monitors. In addition, one can easily instrument other portions of the tasks to take full advantage of the data collection facilities on the off-board computer. While the advantage of the emulator system is its ability to collect measurements for quantification and comparison, its disadvantage is that the amount of data collected from the ADL tasks could become so overwhelming that one would not know where to begin the quantification process.

With very little prior evidence supporting the selection of any set of quantities as being useful measurements to quantify task performance, only the task completion times for each ADL task were selected. Three reasons justified this conservative choice. First, performing ADL tasks with the emulator system was an untested experiment in itself. In previous studies, the emulator had only been used for the crank task which is a constrained motion task. It was not obvious that the emulator would produce useful results for the unconstrained and partially constrained ADL tasks selected. Second, any one task could easily take several minutes to

complete. Storing several channels of data over such a long time span would quickly exceed the storage capabilities of the computer. Third, task completion times have been consistently used in past evaluation studies. Before collecting large amounts of data, it was deemed more prudent to observe the performances of the given battery of ADL tasks using time measurements and video tapes prior to deciding which quantities and which portions of a task would be more useful to measure in future experiments. This methodology would permit one to observe how informative the current set of ADL tasks is for evaluating performance, eliminate the problems associated with the data collection and storage, minimize the overhead involved with instrumenting the tasks, and investigate the correlation between a standardized method of measuring performance and the crank task performance results.

Three tasks were selected for the ADL tasks: donning-socks, cutting-meat, and rolling-dough. All tasks used the standard hook as a terminal device. The donning-socks task represents a common dressing task. A subject was given two, calf-high athletic socks, also known as "tube" socks, and asked to slip one sock onto each foot. All subjects wore a pair of calf-high hose during the task to help minimize individual skin, hair and perspiration effects as the subject donned the athletic socks. Subjects were given a chair to sit on while they performed the task.

The cutting-meat task is a common eating task and required the subject to sit at a table and pretend he was eating a meal. For the meal, the subject had to cut a piece of "meat" into bite-size pieces and bring each piece to his mouth. The task required a chair, a table, a wooden plate with a piece of "meat" on it, a fork, and a knife. The utensils possessed no special features for enhancing the amputee's ability to use them. The "meat" was a flattened piece of Play-Doh™.

The third task is also known as the rolling-pin task. The task was performed on a waist high table with the subject standing. On the table was a ball-shaped piece of Play-Doh, about the size of a baseball, centered on a cutting board. The task was to roll out the ball of Play-Doh with a rolling-pin. The rolling-pin was a typical rolling-pin found in most kitchens. The pin consisted of a wooden cylinder with handles attached at both ends. Friction bearings between the handles and the pin permitted the pin to rotate relative to the handles. While the rolling-pin task is not a common, everyday occurrence for most people, the task does represent a large number of *bimanual* tasks that are encountered daily. To roll out the Play-Doh requires the amputee to coordinate both their intact arm and their prosthesis "arm" to produce the proper rolling-pin motions and pressure distributions.

2.4 INSTRUMENTATION

Instruments for measuring elbow position, elbow velocity, and elbow torque were on-board the emulator system. Elbow position was measured using a single-turn potentiometer. Elbow velocity was obtained by electronically differentiating elbow position using an analog amplifier. Strain gages arranged in a Wheatstone bridge measured elbow torque at the elbow pivot. The crank arm angle and the crank handle angle were both measured using single-turn potentiometers. A single, square bending beam with strain gages on all sides enabled radial and tangential forces to be measured at the crank handle. The strain element produced a 4% positive correlation between force measurements under normal operation. For example, a 10 N radial force would create a 0.4 N tangential force. Motor current and voltage measurements were available from the motor's power supply. All signals were electronically amplified and scaled to accommodate the computer's analog-to-digital converter. Additional details of the instrumentation are discussed by Abul-Haj [4].

MEA signals were measured using the latest surface electrodes from Liberty Mutual. The MEA signals from each muscle were processed independently using an analog implementation of the conventional single-channel method described by Hogan and used by Abul-Haj [4, 16].

CHAPTER
THREE

EXPERIMENTS

3.1 SUBJECTS

Amputees who met the following specifications were eligible to participate as subjects for the experiments: 1) unilateral, above-elbow amputation, 2) stump length greater than 15 cm, 3) experienced user of myoelectrically controlled devices (MED's), 4) 18 years of age or older, and 5) physically able to don the emulator and perform the ADL and crank tasks.

Experienced users are amputees who had formal training on operating MED's. This does not necessarily mean the subjects had several years of experience using an MED. While not essential to operate the emulator, the requirement of formal training eliminated candidates who had physical inabilities to operate such a device. The requirement also permitted the experiments to concentrate on different controller architectures as opposed to subject limitations and learning curves.

Because of the weight of the emulator system, subjects were required to be physically strong enough to support the emulator for all tasks. This indirect requirement biased the subjects into a middle-age bracket from 20 to 50 years of age. To make sure weight was not an issue during the experiments, all candidates were asked to don the emulator and perform various reaching motions for different upper arm postures and to pick and place objects on a table

(Appendix E). Satisfactory completion of these preliminary tasks permitted the amputee to continue to the core set of experiments.

Before participating in *any* task, each subject was briefed on the emulator system and on the various tasks to be performed. An informed consent document, which outlines the experimental procedures, safety precautions, risks, and benefits (Appendix C), was presented, read and signed by each subject. A questionnaire (Appendix D) was also completed by each subject and provided general information about the subject's amputation and current prosthesis.

3.2 CONTROLLERS

Four controller architectures were implemented in the experiments. Of the four, three utilized myoelectric activity (MEA) as a command input. The MEA's were measured using surface electrodes placed over the subject's remnant biceps and triceps muscles. Controllers accepting the MEA's as inputs produced outputs based on the relative levels of the MEA's with respect to the subject's maximum voluntary contraction (MVC) levels.

Usually, MVC measurements are obtained through a series of contractions and resting periods and then averaged to obtain the best estimates [25]. With a limited amount of time to perform the entire battery of experiments for one subject, the common method of measuring MVC's was substituted by a quicker method. This method consisted of making two consecutive sets of MVC measurements (one second measurements with no specific resting period) for the biceps and triceps and then recording the average. Because of the inaccuracies involved with using the quicker method, occasionally electrode gain adjustments were necessary throughout the experiments; however, the adjustments were minor and did not influence the overall results obtained from the experiments.

3.2.1 NY ELECTRIC ELBOW

The NY controller simulates the commercially available NY Electric Elbow [1]. The controller operates on the *differences* of MEA's between the biceps and triceps to move the elbow at a *constant* speed. For differences below a specified threshold, normally 10% of MVC levels, the emulator locks at the current elbow position. The lock is simulated using a high position feedback gain to the motor. For MEA differences above the threshold, the prosthesis moves at a constant, preprogrammed speed. Since the controller is either moving at a con-

stant speed or locked at a particular position, the controller is one of the easiest to understand and operate.

The presence of a hysteresis window prevents "on-off chattering" when the MEA's fluctuate about the MVC threshold. After the MEA's exceed the initial threshold to disengage the simulated lock (10% MVC), a lower level of MEA's is required to lock the emulator at its new position (7% MVC). Similarly, when the proper level has been achieved to lock the clutch (7% MVC), a higher MEA level is necessary to disengage the clutch and move the emulator (10% MVC).

3.2.2 BOSTON ELBOW

The Boston Elbow controller is very similar to the NY [38]. Both are velocity controllers that exhibit a high output impedance and both incorporate a lock. The Boston Elbow controller also operates on the *differences* of MEA's. Below a specified threshold (10% MVC), the emulator locks at the current elbow position. However, unlike the NY controller, as the MEA difference increases above the threshold, the elbow begins to move at a speed that is *proportional* to the MEA difference minus the required threshold difference. At a specified MEA ceiling, usually 50% of MVC levels, the maximum speed of the emulator is achieved. Higher MEA differences past the ceiling have no affect on increasing the emulator's speed. Thus, the Boston Elbow controller permits the subject to adjust the speed of the prosthesis by changing the levels of MEA differences. MEA differences between 10% MVC and 50% MVC will proportionally change the speed of the prosthesis from zero velocity to maximum velocity. Chattering is not an issue with the Boston Elbow since small changes in MEA differences can not produce sudden changes in velocity.

3.2.3 IMPEDANCE

The impedance controller, also known as the "natural" controller, is significantly different from the two previous velocity controllers[4, 6, 14]. The impedance controller uses the differences and *sums* of the MEA's to control the emulator. The differences produce an elbow *torque* based on elbow position and velocity while the sums create elbow *stiffness* and *damping* characteristics. The controller adjusts the damping characteristics so that the emulator's damping ratio is always 0.5. The impedance controller has no simulated lock. Thus, when the subject relaxes muscle activation, the unconstrained emulator falls to a resting position with a low output impedance – much like an intact arm.

Greater MEA differences normally produce higher elbow torques and greater sums produce higher stiffness and damping characteristics. Because damping increases as the MEA differences increase, circumstances can develop in which the elbow torque must *decrease* despite the MEA increase. For example, increasing the MEA's for the biceps will normally increase motor flexion torque. However, if the emulator is *backdriven* sufficiently rapidly into flexion by an external force, the controller's damping characteristics will require elbow flexion torque to reduce or even produce extension torques to resist the elbow movement resulting from the external force. While this appears to be a fabricated situation, the experimental results will show that the circumstances can exist when performing a task rapidly.

Because the impedance controller does not have a lock or attempt to regulate the emulator's speed, the controller is more forgiving when interacting with the environment. If the environment prevents the controller from achieving its desired speed or position, the controller will comply to the larger environmental impedances and will not respond by applying higher and higher forces to achieve its desired objectives (e.g., a constant speed). This response crudely mimics the response of the natural arm. In addition, the controller's ability to vary the emulator's stiffness and damping characteristics for any one particular elbow posture permits the emulator to simulate antagonist muscle coactivation. Coactivation permits intact humans to vary joint output impedances during the performance of tasks and has been suggested to play an important role during human movement control [15].

3.2.4 PASSIVE

The passive controller is the simplest controller architecture of the four. The controller is in many ways no controller at all since implementing it simply requires unplugging the power leads to the motor. Without the motor active, the characteristics of the prosthesis become those of the mechanical design. Inertial properties are based on the emulator's mass distribution and transmission dynamics. Damping properties are created by bearing and transmission frictions. The power leads to the motor are left open to prevent dynamic braking. Elbow stiffness is zero. MEA's are measured but are not used.

The passive controller is similar to a body-powered prosthesis with no lock or cable attachment. The emulator is constantly in a free-swing mode and serves as a useful reference for comparing different controller architectures. The underlying assumption is that an active controller should be able to perform as well and hopefully better than a prosthesis with no con-

troller. If the active controller is worse, there is very little incentive for an amputee to purchase and use such a device.

3.3 ADL TASKS

All subjects performed the same three activities of daily living (ADL) tasks: rolling-pin, donning-socks, and cutting-meat. The protocol used for the experiments is listed in Appendix E. The order of the tasks and the controllers implemented were different for each subject. Each subject was given two controllers for performing their set of ADL tasks. Unbeknownst to the subjects, one controller was always the impedance controller and the second controller was one of the two velocity controllers. The subjects knew the controllers only as "A" and "B". For each of the three tasks, subjects performed the task twice with one controller and then twice with the second controller for a total of four trials before moving on to the next task. The only measurement taken from the trials was the time taken to complete the task.

3.3.1 ROLLING PIN

The rolling-pin task is very similar to that of rolling out a ball of dough for making a pie crust. The dough in this case was Play-Doh™. The standard procedure was for the subject to hold one handle of the rolling-pin with his intact hand and the other handle with his terminal device (TD). The subject was standing and facing a ball of Play-Doh that rested on a waist-high table. The subject rolled the dough out until it covered a marked, 4 inch by 4 inch square. The task began when the subject touched the ball of dough with the rolling-pin and ended when the square was completely covered.

The rolling-pin task attempts to represent various tasks that require some form of coordination between the intact arm and the prosthesis. To perform the task in the same manner that an intact human would, the subject needs to coordinate elbow flexions and extensions to move the rolling-pin back and forth while maintaining contact with the dough. In addition, if the dough is to fill the desired square, the subject must coordinate the necessary torques between the prosthesis and intact elbow to apply and distribute the proper forces across the dough. Thus, the task can represent situations found in both constrained and unconstrained movements.

3.3.2 DONNING SOCKS

The donning-socks task is a very common dressing task performed by most individuals every day. The subject's objective is to don a pair of athletic socks while sitting in a chair. The task begins when the subject receives the first sock and ends when the second sock is pulled above the calf muscle.

When given the choice, most amputees will don a sock using only their intact arm even though most humans will coordinate both arms to "shimmy" the sock up the leg. While the one handed strategy is very effective, it takes longer and requires excessive elbow and hand motions. The purpose of the donning-socks task is to see what controller limitations prevent the subject from using both hands to perform the task effectively.

3.3.3 CUTTING MEAT

Eating is another common task encountered every day. Most people use both hands to hold utensils and to manipulate food while eating. This is especially true when cutting-meat since one hand normally holds the meat stationary with the fork while the other hand cuts the meat with the knife. Like the donning-socks task, amputees usually prefer using only one hand or embarrassingly have someone else cut the meat.

The cutting-meat task tries to simulate what an amputee would encounter while eating at a table. The subject is given a knife and a fork and is asked to cut a flattened piece of Play-Doh into four bite-size pieces. The subject stabilizes the "meat" with a fork using the TD. After cutting a piece of meat, the subject must pick the meat up with the fork and flex the prosthesis as if they were going to place the meat in their mouth. In actuality, the subject passes the Play-Doh to a physical therapist who is standing behind his shoulder.

Again, the cutting-meat task tries to address the limitations of elbow prosthesis controllers. The task requires less coordination with the intact arm when compared to the other tasks but still involves constrained and unconstrained motions. One portion of the task that should not be under-appreciated is when the unconstrained prosthesis comes into contact with the meat during the "stabbing" phase of the task. Robotics experience has shown that contact tasks are not trivial and can often lead to instabilities [31].

3.4 CRANK TASK

After completing the entire set of ADL tasks, each subject performed a series of crank turning tasks. For the crank task, a subject was asked to sit in a chair facing the crank. The subject's TD and cable were removed so that the emulator could be attached to the crank handle. The subject was positioned so that the upper arm and prosthesis remained in the same sagital plane as the crank arm during the task. The length of the crank arm was 8 inches and provided a sufficient range of motion without overextending the subject. The subject's shoulder was approximately 7 inches above and 19 inches away from the crank pivot.

Each subject was asked to turn the crank, towards them, in a semicircular fashion from the bottom of the crank path to the top, pause, and then bring the crank, again towards them, back down to the bottom. The subjects were asked to repeat this process until they were told to stop and relax. As a subject turned the crank, 20 continuous seconds of data, which comprised one *trial*, was collected without the subject's knowledge. The data was later stored and assigned a specific *trial number*.

The crank task was divided into two phases. Phase I had the subject perform one set of trials (6 to 9 trials) with one controller and then a second set of trials (6 to 9 trials) with the second controller. One set used the impedance controller while the other set used a velocity controller. The controller used for a subject's first set was alternated between subjects. For example, Subject 1 used the NY controller in the first set and the impedance controller in the second set whereas Subject 2 used the impedance controller in the first set and the NY controller in the second set. The subjects were told they were using controller "A" for one set of trials and controller "B" for the other set. Friction or weights were not added during any of the trials and the crank arm was statically balanced with a counterweight.

For each set of trials in Phase I, the subject was asked to turn the crank at three different speeds: slow, medium, and fast. Two to three 20 second trials were recorded at each speed. Achieving the three different speeds for each controller was dependent on the controller implemented. For the NY, the emulator was programmed to flex and extend the elbow at a constant speed of 2 rad/sec, 4 rad/sec, or 6 rad/sec. The Boston Elbow's maximum speed was set at 2 rad/sec, 4 rad/sec, or 6 rad/sec. In the case of the impedance controller, the subjects were asked to turn the crank at a comfortable rate. This preferred rate approximated the 4 rad/sec rate programmed for the velocity controllers. To obtain faster or slower speeds, the subject was simply asked to increase or decrease the speed of the task.

Like Phase I, Phase II of the crank experiments had the subject perform two sets of trials. The first set (6 to 9 trials) *always* had the subject turn the crank with the passive controller. The subject was asked to turn the crank at three different speeds; similar to the speeds used for the impedance controller. No friction or weights were used in the first set. For the second set of trials, different combinations of friction and weights were added to the task and were performed at different speeds using either the passive or impedance controllers. The combinations given to a subject varied and were largely dependent on the performance of the subject's previous trial.

3.5 GENERAL PROCEDURE

A typical experiment involved two physical therapists, three engineers, and one amputee. At least one physical therapist and one engineer remained with the amputee at all times. The responsibilities of the therapist and engineer were to ensure proper fit and operation of the emulator system and to make sure appropriate care was given to the subject. *It can not be overstressed that the comfort of the subject was of the greatest importance during the entire set of experiments.* The remaining personnel were involved with video taping the experiments, operating the emulator's computer system, setting up amputee tasks, recording measurements of the ADL tasks, and monitoring the overall performance of the subject. With the given staff, a complete set of experiments could be performed within three hours.

Upon arrival, a subject was introduced to the laboratory, the emulator system, and the various tasks. After completing the informed consent document and questionnaire (Appendices C and D), the subject was asked to use his current myoelectric prosthesis to perform preliminary grasping and reaching tasks and the ADL tasks (Appendix E). Three objectives were accomplished by letting the amputee use his own prosthesis. First, the procedure permitted the subject to gain familiarity with the ADL tasks before donning the emulator. Second, the tasks gave a qualitative measure on how proficient the subject was at using his own prosthesis. Third, wearing the prosthesis made imprints of the electrode locations on the amputee's stump. This provided an excellent reference for where the emulator's electrodes should be placed so that the same set of EMG signals would be processed.

After practicing the ADL tasks with his own prosthesis, the subject was fitted with the emulator. Each subject was given two controllers named "A" and "B". While not given the specific names of the controllers implemented, the subject was informed of the basic features each controller possessed. Ample time (approximately 30 minutes) was given for the subject

to explore the two controllers and to make sure he could operate the emulator over its full range of motion (135 degrees) under different upper arm postures (anatomical, 90 degrees flexion, and 10 degrees extension). Two to three cycles of full flexion and extension were performed for each upper arm posture and controller. Next, the same grasping and reaching tasks performed with the subject's personal prosthesis (Appendix E) were performed with each controller. Once the subject, therapist, and engineer were confident that the emulator system was properly adjusted, the ADL and crank tasks were performed.

During the experiments, periodic checks were made to ensure that the subject was comfortable, the emulator was adjusted properly, and strong myoelectric signals were being measured from the subject's muscle sights. To help minimize the monotony of the experiments and to keep the subject's motivation high, occasional breaks (five to ten minutes) were taken between different sets of tasks. While making the total experimental time longer, the small breaks proved beneficial to both the subject and the investigators.

3.6 DATA COLLECTION

The DEC LSI 11/73, which ran the emulator's real-time controllers, also measured and stored eleven channels of data for each 20 second crank trial. The quantities measured were: 1) elbow position, 2) elbow velocity, 3) elbow torque, 4) crank arm angle, 5) crank handle angle, 6) crank handle radial force, 7) crank handle tangential force, 8) biceps MEA's, 9) triceps MEA's, 10) motor voltage, and 11) motor current. Data collection was initiated by a silent switch from the investigator and was automatically terminated by the computer after 20 seconds. Data collection began after the subject had successfully performed 2 to 3 cycles. During a trial, the data was stored in dynamic memory. At the end of a trial, data was transferred to a permanent file on a hard-drive with the appropriate header information for future processing.

Sampling was performed by a 12-bit analog-to-digital converter at 100 HZ. Precision was plus or minus 1 bit and accuracy was plus or minus 2 bits. One bit digital precisions produced *in the worst cases* analog precisions of 0.19 degrees for angles, 0.033 N for the forces, and 0.005 N-m for elbow torque. Appendix H describes the methods used for calibration and lists the results.

CHAPTER
FOUR

DATA PROCESSING

4.1 INTRODUCTION

The amount of data collected for one subject can quickly become overwhelming. Eleven channels of data were collected from each trial of the crank task. Having knowledge of the sampling rate permitted *time* to become a twelfth measurement. On average, each subject performed over 20 trials using different controllers under assorted crank conditions. If one were to plot each channel's time response for all trials, the number of plots for a particular subject would exceed 200 plots. If one made cross plots for the different variables, an additional 1000 plots would be necessary. Finally, keep in mind that the most informative plots may be *functions* of the measured variables. A simple example of this is the power plot (Chapter 5, Section 5.4.4), which is the product of a measured force and a measured velocity. With functions, the total number of plots for *one* subject can *easily* surpass the 3000 mark!

The purpose of this section is to explain how the raw data was processed. The objective of this section is not to give a line by line explanation of the code used for data processing but to give an overview of the process so that when looking at a set of plots, the reader will understand and feel comfortable with what is being displayed.

A flow chart of the main data processing algorithm used for making the plots is shown in Figure 4.1. Because of uncertainty about which variables would produce the most informative plots, the data processing routines were designed in an open architecture, pipeline fashion so that modules of code could easily be added or deleted from the primary processing algorithm. Overall, the algorithm takes a set of raw experimental data, processes the data depending on which modules have been turned on or off, and then plots the results using a graphics software package written by NCAR [20]. The data processing algorithm can be run in manual or automatic mode and can process one trial from one subject, several trials from different subjects, or all the trails from all the subjects.

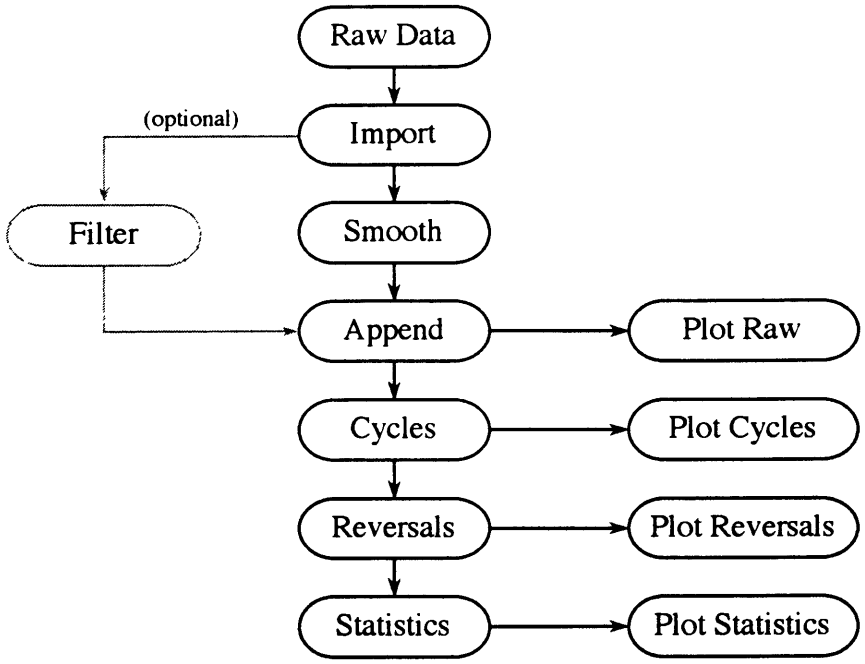

Figure 4.1 Data Processing Flow Chart

4.2 IMPORTING

During the experiments, data acquisition was performed using a DEC LSI 11/73 computer. Because of the intensity of the data processing, the data was transferred to a Sun 3 based microcomputer system. To act as a buffer between the two systems, an import module was created which converted the data to the proper system format. The import module also added time as an extra measurement, converted the digitized data to its analog equivalent, and made all measurements independent of the subject's side of amputation (right or left).

4.3 SMOOTHING

Despite taking the appropriate steps to minimize electrical noise, all trial measurements showed evidence of noise. Most of the measured electrical interference can be attributed to the emulator's power supply, the computer's electronics, and the laboratory environment. Measurements obtained from potentiometers had additional noise due to the manufacturing imperfections of potentiometer wipers riding on top of their conductive plastic films. Probably the measurement that contained the most noise was the emulator's elbow velocity. Since the elbow velocity was obtained by differentiating the elbow angle's potentiometer signal (Chapter 2, Section 2.4), any noise picked up by the potentiometer was accentuated by analog differentiation.

All potentiometers were single-turn styles (Chapter 2, Section 2.4). The single-turn potentiometers used for the experiments provided meaningful measurements for over 340 degrees of mechanical motion. Past 340 degrees, a potentiometer's wiper would separate from its conductive plastic film and would produce a discontinuous voltage drop (or rise) until the wiper re-seated. This mechanical limit of 340 degrees was not an issue for most angle measurements except for the crank arm angle. Occasionally, a subject would continue to rotate the crank passed the top of the crank path and exceed the potentiometer's electrical limitations. This produced discontinuities in the recorded measurements. Before the data could be analyzed, the discontinuities had to be eliminated.

The smoothing algorithm performed three functions. First, it eliminated the discontinuities existing in the crank angle measurements. Second, it removed the noise present in all recorded measurements using a smoothing algorithm written by Dohrmann, Busby, and Trujillo [11]. Third, after the data was smoothed, the crank angle measurement was linearly interpolated to make sure that a measurement existed for every degree of crank angle. The interpolating process was useful for statistical analysis.

One of the features of the smoothing algorithm was its ability to estimate higher time derivatives of a measurement. For example, given a noisy position measurement, the smoother would eliminate the noise on the position signal and would also return an estimate of the joint's relative velocity and acceleration. The velocity estimates proved to be in excellent agreement with the velocities measured by analog differentiation of the position signals. Higher derivative estimates obtained using the smoothing algorithm on position measurements included handle velocity, crank velocity, and crank acceleration.

The entire smoothing module can be bypassed using an optional filter module. This module permits one to customize the data by using different smoothers, implementing a various assortment of filters, or permitting portions of the data to pass to the next module untouched. With the filter module, one can be very specific about how each channel is processed.

4.4 APPENDING

In addition to the twelve recorded measurements and the smoothing algorithm's estimated higher derivative measurements, other measurements were calculated. The append module permitted one to add calculated measurements to each trial based on functions of the original measurements.

Elbow power, crank power, and shoulder position were all calculated with the append module. All calculations used smoothed measurements to minimize possible distortions often created when noisy measurements are multiplied and divided by each other. Elbow power was the product of elbow torque times elbow velocity. Crank power was the product of estimated crank velocity (obtained from the smoothing algorithm) times handle tangential force times the crank's eight inch moment arm. Shoulder position, relative to the crank pivot, was back-calculated using the crank angle, handle angle, and elbow angle measurements and the measured link lengths of the crank arm (crank pivot to handle pivot), emulator (handle pivot to elbow pivot), and upper arm (elbow pivot to shoulder). Link lengths for each subject are listed in Appendix G.

4.5 PLOTTING

After the append module and after all future modules, the data was displayed using various plotting modules. The plotting modules properly formatted the data so that a software graphics package called NCAR could plot the results on paper or on a monitor [20]. The plotting modules and scripts used to call NCAR were extremely versatile and produced a broad range and style of plots.

Although the first plotting module was not available until after the append module, the filter module could limit or eliminate the extent of data preprocessing. Figure 4.2 shows an example of how the various modules were used to plot the results from a single trial. The first plot shows the raw data with the smoothing, filtering, and appending modules "turned off". The trial contains one failed attempt at raising the crank and several smaller noise "spikes".

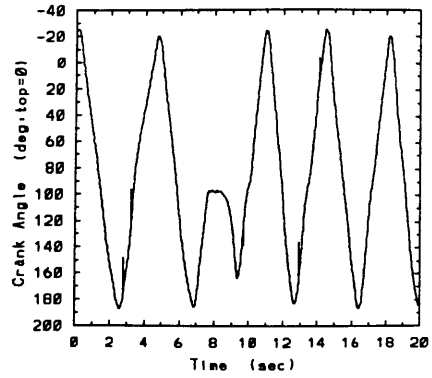

Crank Angle versus Time:
Unprocessed "raw" data

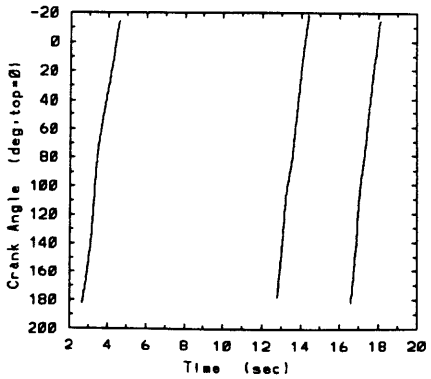

Crank Angle versus Time:
Smoothed, good, lifting cycles

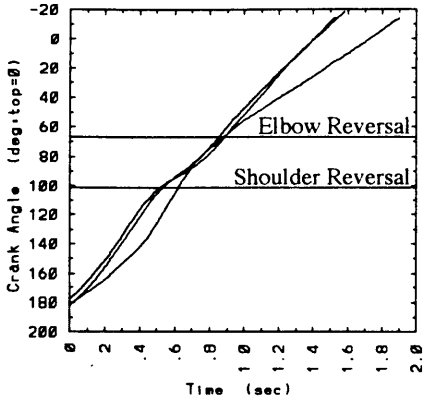

Crank Angle versus Time:
Cycles grouped with reversal lines

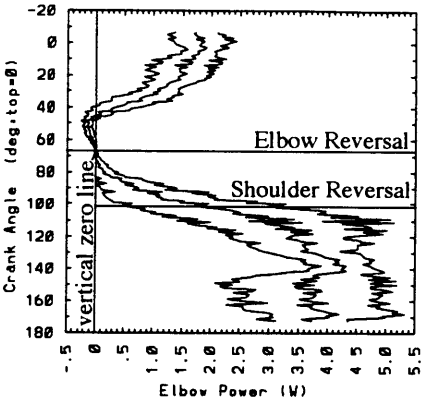

Crank Angle versus Elbow Power:
Average cycle with standard deviations

Figure 4.2 Plotting Results from Data Processing Algorithm

4.6 CYCLES

The crank turning task was separated into lifting, dropping, good, and bad cycles. Lifting cycles were periods when the subject was raising the crank arm from bottom (180 degrees) to the top (0 degrees). Dropping cycles were the opposite. Bad cycles were defined as any lifting or dropping cycle in which there was a change in the direction of crank motion. Thus, if the subject was lifting the crank and *decreasing* the crank angle, a bad cycle would occur only if the subject began to drop the crank and *increased* the crank angle during the lifting phase. Notice that if the subject started to lift the crank, slowed the crank down to zero velocity *without* dropping the crank, and then continued to lift the crank to the top, the cycle would be considered a good cycle. For a bad cycle, the direction of the crank *must* change during

the lifting or dropping phase. The cycle module also checked to ensure that a change in crank direction was not a result of noisy measurements. The second plot in Figure 4.2 shows the remains of the crank angle versus time raw data after being smoothed and selected as good, lifting cycles. Three of the trial's four lifting cycles were considered good.

4.7 REVERSALS

For a given set of lifting or dropping cycles, it was useful to know where the elbow and shoulder reversals were located with respect to the quantities being plotted. The reversal module scans the lifting and dropping cycles from each trial and determines the average crank angle location of the elbow and shoulder reversals (see Chapter 2, Figures 2.1, 2.2, and 2.3). The shoulder reversal is defined as the crank angle at which the handle angle is at zero degrees. This occurs when the emulator centerline is collinear with the crank arm centerline. The elbow reversal is defined as the crank angle at which the elbow angle is at maximum flexion. The third plot in Figure 4.2 shows the three good, lifting crank cycles grouped together. The time scale on the x-axis has changed to permit comparisons of cycle completion times. The horizontal lines represent the reversal locations. In all plots, the lower line will always represent the average shoulder reversal and the higher line will always represent the average elbow reversal for the set of cycles shown. While not shown in the crank angle versus time plots, the reversal module can also add a vertical line to a plot. This line represents the zero mark of the x-axis.

4.8 STATISTICS

Depending on the statistic, the statistics module will either print or plot the result. Information about an individual cycle such as its location in the trial, type, direction, and reversal locations are usually printed. Information about a group of cycles such as the overall average and standard deviations are usually plotted. The last plot in Figure 4.2 demonstrates the latter point by showing three crank angle versus elbow power curves. The middle curve represents the average of the trial's three good, lifting cycles. The additional curves are the average plus and minus one standard deviation. The statistics are based on the measurements found for *each degree of crank angle.* To ensure that a measurement existed for *each crank angle* (a measurement did not exist when the sampling rate was too slow), the crank angle and measurement were linearly interpolated in the smoothing module. The plot also demonstrates the usage of the vertical zero line (mentioned in Section 4.7).

CHAPTER
FIVE

RESULTS AND DISCUSSION

5.1 SUBJECTS

Four adult males were the subjects in the experiments. Table 5.1 provides some basic information about each. Subjects 1, 2, and 3 had several years of experience using the Boston Elbow and were very adept at using their prosthesis for an assortment of tasks. Subject 4 used the Utah Arm [2] and had the least experience of the four subjects using a myoelectrically controlled prosthesis. Subject 4 was, at best, an average user.

Table 5.1 Subject Information

	Subject 1	Subject 2	Subject 3	Subject 4
Age (yr.)	23	49	43	39
Sex	Male	Male	Male	Male
Amputation (yr.)	7	8	13	1
Cause	Trauma (Electrical)	Trauma (Electrical)	Trauma	Trauma
Side	Left	Left	Right	Right
Prosthesis (yr.)	7	7	9	0.8
Type	Boston	Boston	Boston	Utah

Subjects 2, 3, and 4 had no unusual complications with their amputation and each had remnant biceps and triceps for measuring myoelectric activity. Due to the nature of the electrical burn and required surgery, Subject 1's measured myoelectric activity at the biceps location originates from a separated portion of the remnant triceps muscle. This fact helps explain some of Subject 1's myoelectric activity results which are discussed in Section 5.4.8. Despite having both control signals coming from a similar muscle group, the subject showed excellent signal separation.

As a short note, a fifth subject who was only an experienced body-powered user participated in the experiments. The objective sought with the body-powered subject was to see if a totally inexperienced myoelectric user could don the emulator system and perform any of the investigation's ADL tasks. Because the impedance controller does not demand the typical muscle isolations required of a velocity controller, there was some question about an inexperienced user being able to operate the emulator. The results revealed that the subject had difficulty operating both the impedance controller and the velocity controller; he was unable to perform any of the given tasks. The subject was able to produce a reasonable triceps signal, but unable to create a meaningful biceps signal. The irregular biceps signal could be a result of inexperience, atrophy, or perhaps other unknown reasons.

5.2 CRANK TASK

To make the crank results more manageable and comprehensible, only lifting, good cycles were analyzed from all trials (Section 4.6). Lifting cycles possessed a natural tendency to recruit both biceps and triceps to complete the task. With the aid of gravity, dropping cycles for some of the controllers could be performed in a completely passive manner. Understanding how the different controllers and subsystems interacted in the dropping phase was more difficult to assess than in the lifting phase. Good cycles represented successful completions of the task, were more frequent than bad cycles, and offered a better chance of finding data trends within and between controllers and subjects.

During the crank experiments, a subject would perform several trials under the same conditions. Depending on the crank speed, a 20 second trial could include as few as two completed cycles for the slow speeds or have as many as 15 completed cycles for the faster speeds. A *completed* cycle consisted of one lifting cycle (bottom to top) followed by one dropping cycle (top to bottom).

Each trial's good, lifting cycles were grouped together with reversal lines and then plotted. The statistics module was not used to average the cycles (Section 4.8). Averaged data proved to be misleading when either a small number of cycles existed in a trial or when one of the cycles in a group deviated significantly from the norm. Removing irregular cycles from the data was considered but not implemented since pilot "cycle-filters" showed more information was lost than gained from the process.

For comparison purposes, trials were sorted into categories containing the same controller, speed and crank constraints (e.g., friction, hanging weights, etc.). A category usually contained two or three trials. From each category, a representative trial was selected. The selection process was based on qualitative notes written during the experiments, video tapes, and anomalies found in the measured data. Some reasons for trial rejections were: the subject changed sitting postures by moving the position of the chair relative to the crank, unexpected socket slippage, and the subject voluntarily stopped midway through a trial because he did not know data was being collected by the computer. Occasionally two trials from the same category were very similar. Under such a circumstance, one trial was chosen even though both were referenced when comparing categories.

Appendices A and B show the representative trials and their respective plots chosen for each subject. Appendix A contains the *kinematic plots* obtained from the four subjects. Each page in Appendix A contains a set of nine plots that show a trial's position, velocity, and acceleration measurements for a particular subject. Section 5.3 will discuss the kinematic plots in detail. Appendix B contains the *dynamic plots* for each subject. Each page contains a set of ten plots that display a trial's force, torque, power, and myoelectric activity measurements. Section 5.4 will discuss the dynamic plots. Since one trial has both a kinematic plot and a dynamic plot, the same trial shows up in both appendices but with different types of plotted information. Both the kinematic and dynamic plots show the trial's crank angle versus time plot of the good, lifting cycles in the upper left hand corner. This plot serves as a useful reference when comparing different trials.

Excluding the crank angle versus time plot, all plots shown are cross-plots. While showing interesting characteristics, time-response plots (measurement versus time) said little about the system's geometry and interactions. Since the crank turning system approximates a four-bar linkage, cross-plots of the crank angle versus other measured quantities proved to be more informative. With the addition of reversal lines, the crank angle cross-plots enabled one to en-

vision the system's geometry independently of crank speed and provided insights into the strategies and interactions occurring during the task.

Each set of plots has a title that explains the conditions of the trial. The following is a typical example of a title:

```
arm012 Sub:1/Ctrl:Imp/Spd:s/Fr:y/Wgt:n
```

`arm012` represents the trial number. Trial numbers ranged from `arm000` to as high as `arm028`. `Sub` identifies the subject. `Crtl` explains which controller was implemented for the trial: `NYU`, `BE`, `Imp`, and `Pas` stand for the NY Electric Elbow, Boston Elbow, Impedance, and Passive controllers respectively (NYU stands for New York University, the prosthesis's origin). `Spd` is the speed at which the crank was turned: `s`, `m`, and `f` stand for slow, medium, and fast. `Fr` informs one if friction was added to the crank: `y` and `n` stand for yes or no. `Wgt` tells if any weight was hung on the crank's pulley: `n` represents no weight while `1kg` represents 1 kilogram of mass. The same title is used for a trial's kinematic and dynamic plots. Thus, the above title will show up once in Appendix A and once in Appendix B.

The best method found for comparing representative trials and subjects was to organize the kinematic and dynamic plots into two separate but similar matrices. The rows represent the different speeds while the columns represent the different controllers and crank constraints. Tables 5.2 through 5.5 show the trial numbers (with the "`arm`" prefix removed) and matrices formed for each subject.

The first three columns of each table represent the three controllers given to each subject. Subjects 1 and 2 used the NY Electric Elbow while Subjects 3 and 4 used the Boston Elbow as their velocity controller. Subject 4's inexperience immediately shows up in the first three columns by the missing trials and reflects the subject's inability to perform the task. Table 5.5 suggests that the easiest controller for Subject 4 was the impedance controller since he could operate this controller over the broadest range of speeds. *This observation agrees with the subject's opinion.* Although Table 5.5 shows a trial for Subject 4's slow, Boston Elbow case, no good, lifting cycles occurred during the trail.

The remaining columns in each table show trials that had friction and weights added to the task. For all subjects, these additional cases were optional. Missing trials mean that the subject was not asked to perform the task. The passive, weight case is for a 1.0 kg mass. Subject 2 had other passive weight trials for medium speed. The additional trials were 024, 026, and 025 with the respective conditions: 1.9 kg, 4.5 kg, and 1.9 kg with friction. Subject 3 also

Table 5.2 Subject 1's Selected Trials

	NYU	Imp	Pas	Imp/Fr	Pas/Fr	Pas/Wgt
Slow	002	009	018	012	—	—
Medium	003	007	017	—	—	023
Fast	005	010	021	—	014	—

Table 5.3 Subject 2's Selected Trials

	NYU	Imp	Pas	Imp/Fr	Pas/Fr	Pas/Wgt
Slow	008	004	018	013	—	—
Medium	009	001	016	—	022	023
Fast	011	005	019	—	—	—

Table 5.4 Subject 3's Selected Trials

	BE	Imp	Pas	Imp/Fr	Pas/Fr	Pas/Wgt
Slow	000	009	020	014	—	—
Medium	003	010	016	—	024	025
Fast	006	012	021	—	—	—

Table 5.5 Subject 4's Selected Trials

	BE	Imp	Pas	Imp/Fr	Pas/Fr	Pas/Wgt
Slow	009	005	—	—	—	—
Medium	—	004	012	—	—	—
Fast	—	007	010	014	—	—

had additional passive medium speed trials. These trials were 026 with 1.9 kg and 027 with 1.9 kg and friction.

Comparison of the NY Electric Elbow and Boston Elbow controllers is not straightforward. The major difference between the two controllers was the proportional speed control capabil-

ity of the Boston Elbow (Section 3.2.2). The size of the subject's MEA Window that would enclose the Boston Elbow controller's proportional speed region was based on the subject's averaged maximum voluntary contraction (MVC) measurements taken before the experiments (10% MVC to 50% MVC). Since the MVC measurements were obtained with a quicker but less precise procedure than the normal procedure (Section 3.2), the possibility existed that improper MVC levels could be recorded in the computer and a subject's proportional window could be undersized or oversized.

Normally the quicker method proved to be sufficient. However, the Boston Elbow's proportional MEA Window may have been undersized for Subject 3. Undersizing the window produced a Boston Elbow emulation that closely resembled the NY Electric Elbow behavior. To further complicate matters, the manufacturers of the Boston Elbow believe that the proportional control feature of their product does not work as well as desired [39]. (Therefore, it is not clear if users of the Boston Elbow fully appreciate the feature.) For whatever reasons, the crank results were very similar for both velocity controllers. The major differences between the plots were the altered elbow speed transitions near the elbow reversals produced by the Boston Elbow's limited but still effective proportional control window (Section 5.3.6).

5.3 KINEMATIC PLOTS

Figure 5.1 shows an example of a trial's kinematic plots. The plots show the results obtained from `arm003` when Subject 1 used the NY Electric Elbow controller at medium speed with no friction or weight. The trial contains eight good, lifting cycles. By definition, the shoulder reversal line passes through the intersection of the zero vertical line and the *average* crank angle in the handle angle plot. The elbow reversal line passes through the *average* peak in the elbow angle plot. The elbow reversal also intersects the zero vertical line and the average crank angle in the elbow velocity plot. The difficulties subjects had when encountering the elbow reversal often show up in the data as unusual elbow position and velocity measurements during maximum flexion. While these irregularities can inhibit the data processing's reversal module from finding the precise location of an individual cycle's elbow reversal, the module's errors are minor in plot comparisons. The reversal lines calculated for the shoulder reversal proved to be very consistent and accurate. The average standard deviation of the reversal locations (in terms of crank angle) for all subjects and all trials (four subjects, 86 trials of good, lifting cycles) was 0.8 degrees for the shoulder reversal and 2.4 degrees for the elbow reversal.

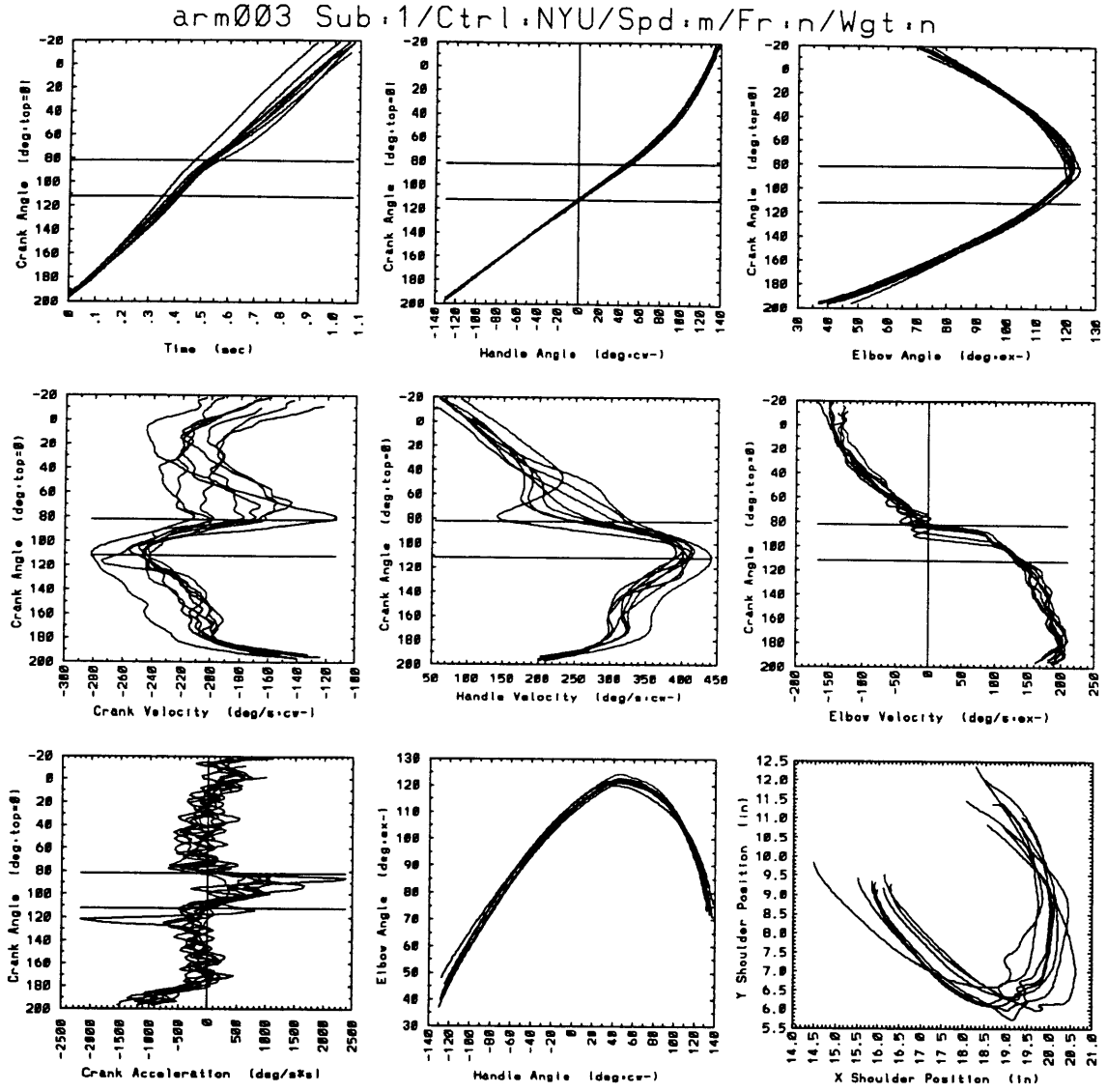

Figure 5.1 Kinematic Plots for Subject 1, Trial Number arm003

Crank angle, handle angle, elbow angle, and elbow velocity were smoothed using an algorithm written by Dohrmann, Busby, and Trujillo [11]. The algorithm took advantage of dynamic programming and generalized cross-validation to find the optimal smoothing parameter for a given set of equally spaced measurements. Crank velocity, crank acceleration, and handle velocity were estimated from the same smoothing algorithm. The "smoother" fitted the data using a cubic-spline algorithm that assumed constant jerk between sampling periods. With this algorithm, the velocity estimates proved to be quite accurate while the acceleration estimates were less accurate. During portions of the crank motion, especially at the shoulder

reversal, the sampling rate was too slow (100 Hz) for the assumption of constant jerk to always be valid. The under-sampling often produced aliasing and superfluous fluctuations in the smoothed, acceleration estimates.

All angles were plotted in units of degrees and are illustrated in Figure 2.1 of Section 2.2. A crank angle of 0° defined the top of the crank and 180° defined the bottom. All good, lifting cycles, independent of the subject's amputation, started at 180° and decreased to 0°. The handle angle was at zero degrees when the crank arm was collinear with the prosthesis. Counterclockwise rotation of the prosthesis relative to the crank arm increased the handle angle. Handle angles for the lifting cycles normally started at –120° and ended at 120°. The zero measurement for elbow angle occurred at full elbow extension. Elbow flexion increased elbow angle and produced positive velocities.

5.3.1 CRANK ANGLE VERSUS TIME

The times taken to complete a lifting cycle ranged from 0.4 seconds to almost 6.0 seconds. Subjects produced consistent times for each controller and speed. Times between subjects were usually consistent for the fast and medium speeds and showed the greatest variance at slow speeds. Time ranges for slow, medium, and fast speeds were 2.0-6.0, 1.0-1.5, and 0.5-0.8 seconds respectively.

Results showed that the crank task could be performed too fast or too slow. For times under 0.5 seconds, acceleration forces interacting between the various linkages became so high that the emulator socket would begin to slip off the subject's stump and the potential for damaging the hardware existed. In addition, the high speeds saturated the measurement devices and introduced aliasing into the data as a result of the relatively slow 100 Hz sampling rate. Times over 5.0 seconds proved to be too slow. Long time periods permitted the subject to become easily distracted and resulted in inconsistent strategies. A good time distribution for slow, medium, and fast speeds appeared to be 1.0, 2.0 and 4.0 seconds. As the data will show, such time spreads draw a clearer picture of the strategies and interactions occurring for the different subjects and controllers during the task.

The crank versus time plots are useful when comparing cycle completion times and to determine if a particular cycle is an exception to the trial's norm. The plots demonstrate that a subject can perform the task with different controllers, speeds, and constraints yet produce time-responses that have similar profiles. An example of this is shown in Figure 5.2. Figure 5.2 shows the crank angle versus time-response plots for Subject 1 turning the crank with three

different controllers at medium speed (arm003, arm007, and arm017). The subject produced similar profiles despite using dramatically different controllers. Only Subject 3's slow and medium passive cases (Appendix A: `arm020`, `arm016`) and Subject 2's slow, passive case (Appendix A: `arm018`) show significant differences. In these cases, the crank angle increases at a rapid rate up to the elbow reversal before slowing down to almost half the rate for the remainder of the cycle. Subject 1's passive case in Figure 5.2 shows evidence of a similar profile.

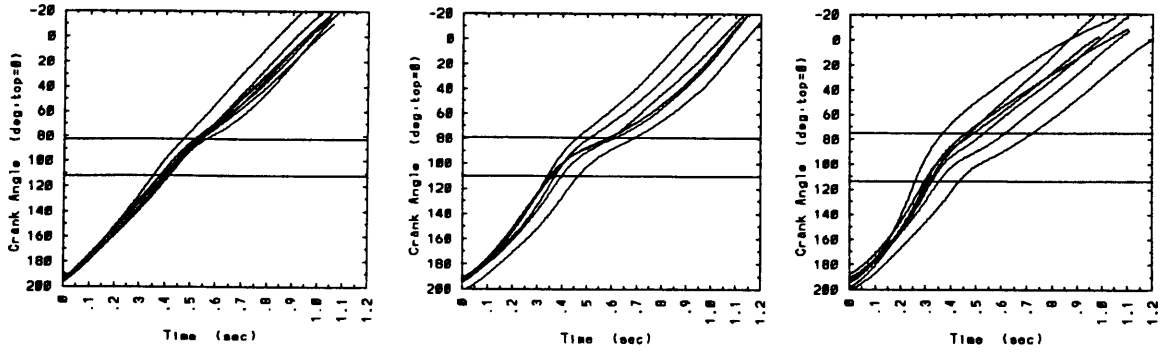

NY Electric Elbow Impedance Passive

Figure 5.2 Crank Angle versus Time Plots for Subject 1's Medium Speeds

In general, it is very difficult to obtain any useful information from the crank angle versus time plots in terms of performance and interactions. While the plots can show how long it took for a subject to complete the task and give some indications of the different speeds used during the task, the plots say little about the system's kinematic and dynamic interactions and how the subject is controlling the prosthesis to perform the task. In addition, a task performed with greater speed does not necessarily mean that the subject will have a greater acceptance of the prosthesis – a common assumption made in most timed, ADL studies. Subject 1's timed results from the ADL rolling pin task strengthens this statement (Section 5.5). Although the NY Electric Elbow permitted the subject to perform the rolling pin task in half the time, the subject preferred the impedance controller because of its "more natural feel". *For the crank task, time appears not to be a good measurement of task performance in terms of amputee acceptance.*

5.3.2 HANDLE ANGLE

The handle angle plots are *extremely* repeatable within and throughout all trials and subjects. No apparent differences exist between controllers and speeds. The repeatability is primarily a

result of the system's geometric constraints. With the majority of motion being performed in a vertical plane, only shoulder movement can provide additional degrees of freedom to the crank system. Since the handle angle is two link lengths away from the shoulder pivot, the measurement is insensitive to changes in shoulder position and largely dependent on crank angle. The handle angle versus crank angle plots are not a useful measurement of performance.

5.3.3 ELBOW ANGLE

Like the handle angle plots, the elbow angle plots are very repeatable and show no apparent differences between trials and subjects. Figure 5.3 shows the elbow angle plots for Subject 1's medium speeds. Since the elbow measurement is one link length closer to the shoulder pivot, elbow angle variances can be greater than their corresponding handle angle variances for the same shoulder movements. The default x-axis scale chosen for the elbow position plots emphasizes the variances when compared to the handle angle plots. The x-axis scale used for the handle angle plots is over twice the angle range used for the elbow angle plots (Figure 5.1).

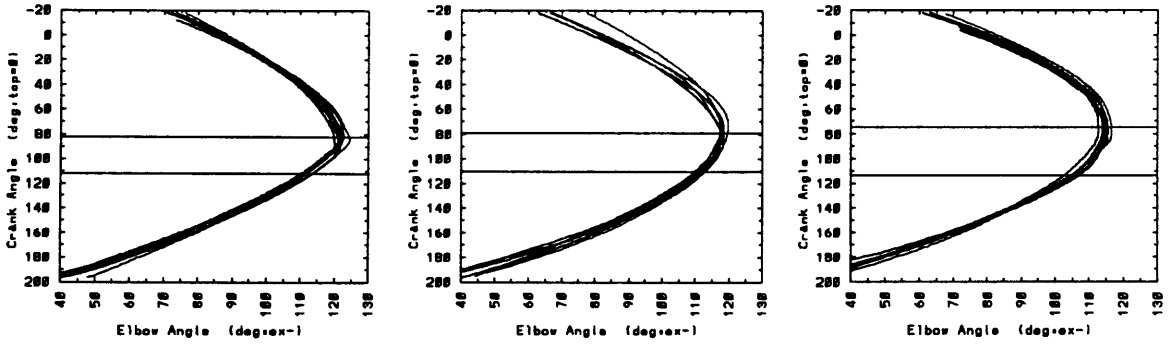

Figure 5.3 Elbow Angle Plots for Subject 1's Medium Speeds

The higher variances in Subject 4's measurements can be attributed to shoulder motion and socket slippage. While Subject 4's stump length was comparable to the other subjects, the subject's stump diameter was unusually small. This prevented a snug fit between the emulator's socket and the subject's stump and resulted in excessive slippage during the task. The unusually high variances found in Subject 4's fast, passive case (Appendix A, `arm010`) are largely due to shoulder motion. This is quite apparent in the video tapes. Higher flexion peaks correspond to cycles with less shoulder motion.

The elbow angle plots are useful for confirming the elbow reversal lines. While the plots show some subtle signs that different controllers produce different elbow motions near the elbow reversal, the differences do not appear to be significant enough to make any conclusive observations. The elbow angle plots would be difficult to use for quantifying task performance.

5.3.4 ELBOW ANGLE VERSUS HANDLE ANGLE

The elbow angle versus handle angle plots are the last in the series of angle versus angle cross-plots. As with the previous plots, these plots provide limited information for task performance and subsystem interactions. No significant differences exist between the various speeds and controllers.

The three plots: crank angle versus handle angle, crank angle versus elbow angle, and elbow angle versus handle angle all measure the *geometric coordination* of the system's linkages during the task and determine the system's geometric *state* at any given instance of time. All three measurements are required to define the system's geometric state because the shoulder pivot is *not* stationary during the task. *The experimental results depicted in the plots demonstrate that the system's geometric plots are extremely limited for comparing controller architectures, quantifying subsystem interactions, or evaluating subject performance.*

5.3.5 HANDLE AND CRANK VELOCITIES

Since the system geometry and the handle angle strongly depend on the crank angle, the handle angular velocity closely resembles the crank angular velocity. The striking mirror images shown between the two plots emphasize this point. High crank velocities correlated well with high handle velocities and low crank velocities correspond to low handle velocities. Because of the close association between the two profiles, discussion will concentrate only on the crank velocity.

Figure 5.4 illustrates the crank velocity plots for Subject 1's medium speeds. Any one of the subject's plots shows the base profile for the crank velocity. The profile can be described in three parts: 1) the velocity increases to a peak near the shoulder reversal, 2) drops while approaching the elbow reversal, 3) after "undershooting", stabilizes for the remaining portion of the task.

For the passive case, the higher speed fluctuations were necessary if the subject was to successfully pass through the shoulder reversal. The crank's initial speed increase results from the amputee transferring kinetic energy to the crank and the passive emulator. Past the shoulder reversal, the crank loses speed as the passive system's kinetic energy is transformed into potential energy. After the elbow reversal, the upper arm resumes control of the crank and increases or maintains the crank speed. As the crank approaches the end of the cycle, the velocity begins to reduce.

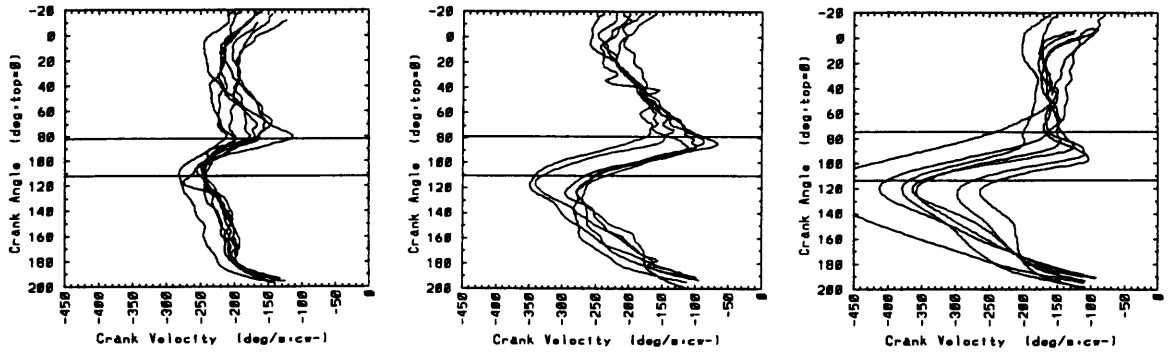

NY Electric Elbow Impedance Passive

Figure 5.4 Crank Velocity Plots for Subject 1's Medium Speeds

Because the task can be described in separate parts suggests that the subjects were segmenting the task. In other words, instead of performing the entire task using one continuous plan or strategy, the subjects might have been using two or three strategies combined in series. Russell shows some interesting simulations when *intact* subjects were turning the crank that support this segmentation hypothesis [34]. Since a consistent base profile is present with *all* controllers, the crank plots also suggest that the subject, *regardless of the controller architecture used*, attempted to use the same strategy (or set of strategies) to complete the task. Subjects showed a natural tendency to store kinetic energy into the system before encountering the shoulder reversal and then permitted the system's momentum to drive the *passive* system through the reversal.

All subjects were able to identify the crank location where they had the most difficulty lifting the crank and all mentioned that they needed to increase the speed of the crank to pass through the region. Unbeknownst to the subjects, the identified region was the shoulder reversal. Having the subjects admit to requiring different velocities at different crank positions along with showing signs of increasing or maintaining the velocity past the elbow reversal suggest that the subjects had a set of primary and secondary *kinematic objectives* in mind

when performing the task. The primary objective might have been to rotate the crank at a constant velocity or to optimize one (or all) of the task's movements. An example of optimizing a movement might have been to minimize the jerk (derivative of acceleration) of the emulator's endpoint (attached to the crank handle) in one of several possible coordinate systems. In the past, minimum jerk models have successfully simulated *unconstrained*, planar movements of intact humans quite well [12]. In addition, secondary objectives might have dealt with issues hindering the primary objective from being achieved. An example of a secondary objective might have been to increase the crank velocity to ensure passage through the shoulder reversal.

Of the three controllers, the velocity and impedance controllers permitted the subjects to minimize the crank speed fluctuations near the shoulder reversal, especially at slow speeds. This is not a very flattering statement considering that both controllers were being compared to a prosthesis that had no active actuator or controller. If not for the shoulder reversal, the passive controller may have regulated the crank velocity as well or better than the more elaborate controllers. Crank velocity plots do begin to show differences among the controllers and do start to give some insights into each subject's strategies and objectives. But, the plots do not reveal significant differences and often require additional *dynamic* measurements to achieve better comprehension.

5.3.6 ELBOW VELOCITY

The impedance and passive controllers display a common S-shaped pattern throughout all elbow velocity plots. Figure 5.5 illustrates this pattern for Subject 1. In preparation for the shoulder reversal, the elbow joint was quickly flexed to a peak velocity. As the emulator passed through the shoulder reversal and approached the elbow reversal, the elbow velocity decreased. At the elbow reversal, the elbow velocity made a *smooth* transition from flexion to extension. Past the reversal, the velocity increased as the emulator extended to complete the cycle. Differences between the two controllers are subtle. For medium and high speeds, the profiles can be indistinguishable. Only at the slow speeds do the limitations of the passive controller become obvious since the impedance controller permitted the subjects to significantly reduce the velocity peaks.

The velocity controllers show a less graceful S-pattern. Subject 1's NY Electric Elbow plot in Figure 5.5 serves as a good example. The NY Electric Elbow controller resembles a simple on-off controller. When on, the controller attempts to flex or extend the emulator at a con-

stant velocity. When off, the controller locks the emulator at the current elbow position. If the controller was perfect, the elbow velocity profile for the crank task would had been a square profile (Figure 5.5, dashed line). The emulator would had flexed at a constant speed up to the elbow reversal, locked, and then extended at a constant speed past the reversal until the cycle was complete.

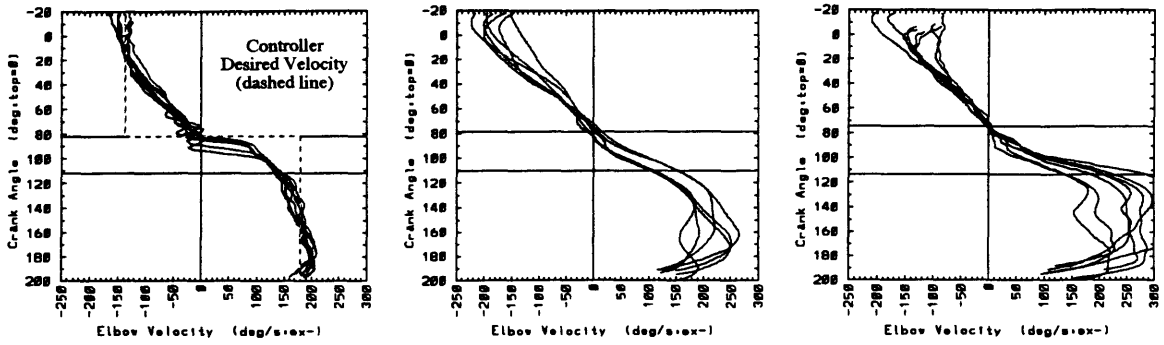

NY Electric Elbow Impedance Passive

Figure 5.5 Elbow Velocity Plots for Subject 1's Medium Speeds

The deviations from the ideal square pattern are not merely the effects of a poorly designed controller; instead, they are the results of the subjects' preferences. The dynamic plots show the subjects *forcibly* resisting the velocity controllers. When the elbow is not moving at the preferred speed, the subjects use their upper arm to assist or to impede the elbow motion. Impeded motion is most noticeable as the subjects approach and leave the elbow reversal and is often present at the start and finish of each cycle. Because of the proportional control provided by the Boston Elbow, Subject 3 was not constrained to one speed. While this permitted the subject to produce smoother speed transitions near the elbow reversal, the velocity profiles remain similar to the NY Electric Elbow controller.

Both velocity controllers produced a high output impedance and required the subjects to lock the prosthesis when passing through the elbow reversal. If a subject's *go-lock-go* timing was slightly off during the elbow reversal, the subject experienced high reactionary forces while trying to complete the cycle. Subject 2's medium speed profile (`arm009`) shown in Figure 5.6 demonstrates what can happen when the go-lock-go sequence is too slow. The elbow velocity's tiered effect and the elbow torque's dual peaks come from the subject's inability to enter and exit the locking phase quickly. It appears that velocity controllers can become a burden in tasks requiring elbow reversals.

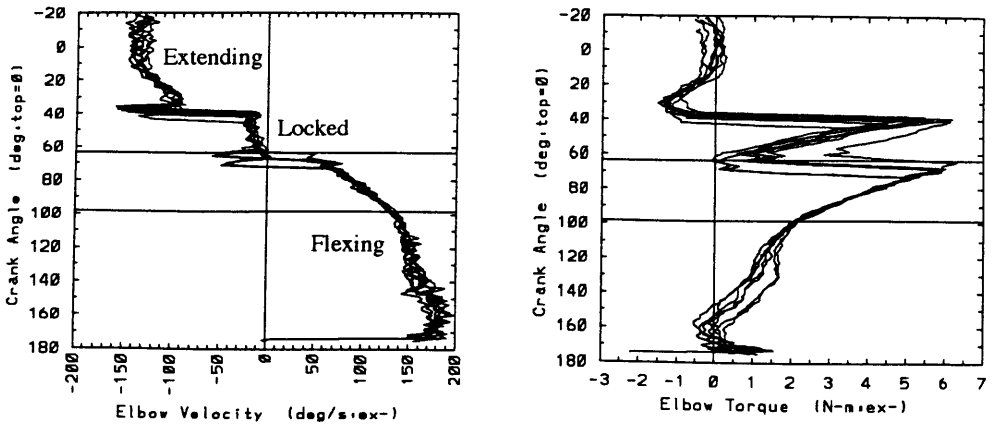

Elbow Velocity Elbow Torque

Figure 5.6 Velocity Controller's *go-lock-go* Effect

At the faster speeds, some of the subjects show small but consistent secondary velocity peaks near the elbow reversal. A good example is Subject 2's `arm019` trial (Appendix A). The peaks correlate well with sudden changes in shoulder movement shown in the shoulder position plots. Because of the method used to measure shoulder position (Section 4.4), the velocity peaks may be a result of shoulder movement or the relative motion between the emulator's socket and the subject's stump (Section 5.3.8). Some of the plots show the velocity controllers with small but rapid changes in elbow velocity near the reversals (Appendix A, Subject 1, `arm005`). These oscillations are the effects of the controllers' high output impedance and go-lock-go sequence instigating mechanical vibrations in the crank arm. The rapid changes in velocity shown in the plots are an alias of the actual vibrating frequency of the crank arm.

Of all the kinematic plots, the elbow velocity is the most informative. It is the only kinematic plot that begins to display some significant differences among the various controllers. The NY Electric Elbow and Boston Elbow show velocity discontinuities at the elbow reversal while the impedance and passive controllers permit smooth velocity transitions. The plots show evidence of amputee resistance to controllers with high output impedances. In Subject 2's case, substantial resistance occurs as the subject tries to implement the velocity controller's go-lock-go sequence yet *this is not reflected in the crank angle versus time plots nor is obvious in the angle cross-plots.*

The crank velocity plots suggest that the subjects have a set of kinematic objectives in mind when performing the task. One of the objectives may be to rotate the crank at a constant ve-

locity. The resistance displayed by the subjects in the elbow velocity plots strengthens the kinematic objective argument. The smooth elbow velocity transitions shown in the impedance and passive controller plots near the elbow reversals along with the reduction in speeds of the velocity controllers near the elbow reversals suggest that the subjects may desire smooth velocity transitions at the elbow reversal regardless of the controller architecture.

While revealing differences between the low and high output impedance controllers, *the elbow velocity plots are less informative for controllers within the same family.* Differences between the passive and impedance controllers, which are low output impedance controllers, are often indistinguishable for the medium and fast cases. Despite the Boston Elbow's proportional control feature, the Boston Elbow and the NY Electric Elbow, which are both high output impedance controllers, show remarkably similar profiles. Within the same family, individual controllers are easier to segregate using the more informative dynamic plots (Section 5.4).

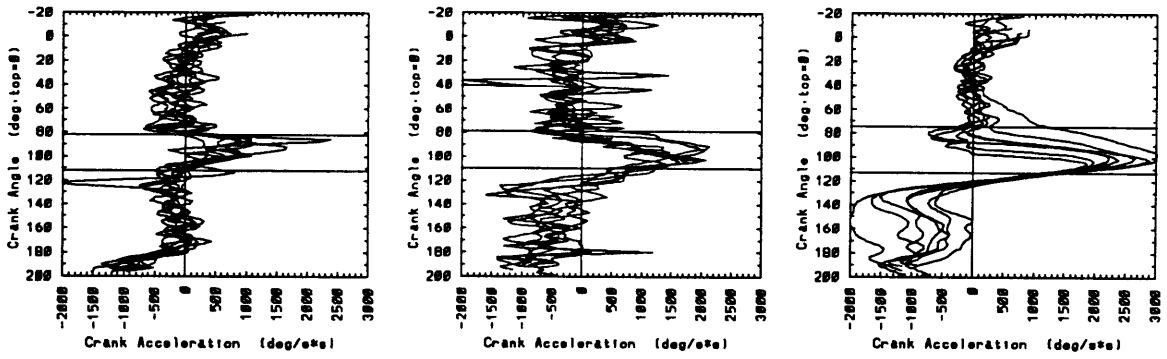

NY Electric Elbow Impedance Passive

Figure 5.7 Crank Acceleration Plots for Subject 1's Medium Speeds

5.3.7 CRANK ACCELERATION

A common pattern exists in most crank acceleration plots: At the beginning of each cycle, the subject produced high levels of acceleration (negative values) to start the crank motion. The acceleration then dropped to more moderate levels as the subject prepared for the shoulder reversal. Deceleration occurred during the reversals as the system exchanged kinetic energy for potential energy. Acceleration past the elbow reversal brought the system back up to speed. At the end of the cycle, high levels of deceleration often developed as the subject brought the crank to rest. Depending on how the cycles were cropped in the data processing,

cycle module (Section 4.6), the initial and final peak accelerations may be missing. Figure 5.7 shows Subject 1's medium speed profiles.

Figure 5.8 shows one of Subject 3's velocity controller profiles (arm003). The profile differs from the common acceleration pattern by showing peak accelerations (instead of decelerations) at the shoulder reversal. The peak accelerations resulted from the subject's "preload strategy" which will be discussed in greater detail when the radial force and tangential force plots are presented in Sections 5.4.2 and 5.4.3.

Crank acceleration was estimated from crank position using a cubic spline smoother that assumed constant jerk between sampling periods (Section 4.3). This assumption, coupled with potentiometer noise and a relative slow 100 Hz sampling rate, introduced errors in the smoothed results of the acceleration plots. The tangential force measurements in the dynamic plots proved to be more reliable, cleaner, and, in principle, are proportional. There was no additional information found in the crank acceleration plots that could not be found in other measurements.

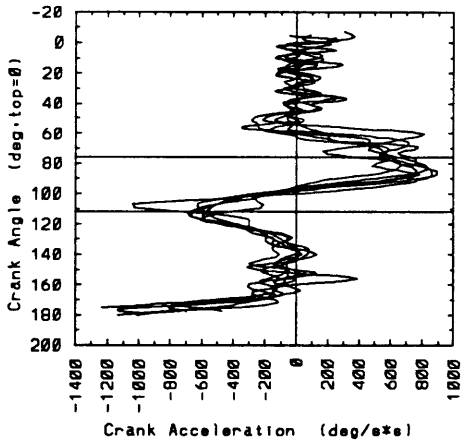

Figure 5.8 Crank Acceleration Profile using "Preload" Strategy

5.3.8 SHOULDER POSITION

The relative distance between a subject's shoulder pivot and the crank pivot during the task is shown in the shoulder position plots. Figure 5.9 demonstrates how the shoulder pivot moves relative to the crank pivot (Subject 1, arm003). The x and y axes represent the relative horizontal and vertical distances (in inches) of the shoulder pivot from the crank pivot. Higher x values mean the shoulder pivot is moving away from the crank pivot and higher y values

mean the shoulder is rising above the crank. A characteristic U-shaped pattern can be found in all plots. From the bottom of the crank to the shoulder reversal, the shoulder pivot moves away from the crank and drops. Past the shoulder reversal, the shoulder starts to rise. After the elbow reversal, the shoulder moves inward and upward until the top of the crank is reached.

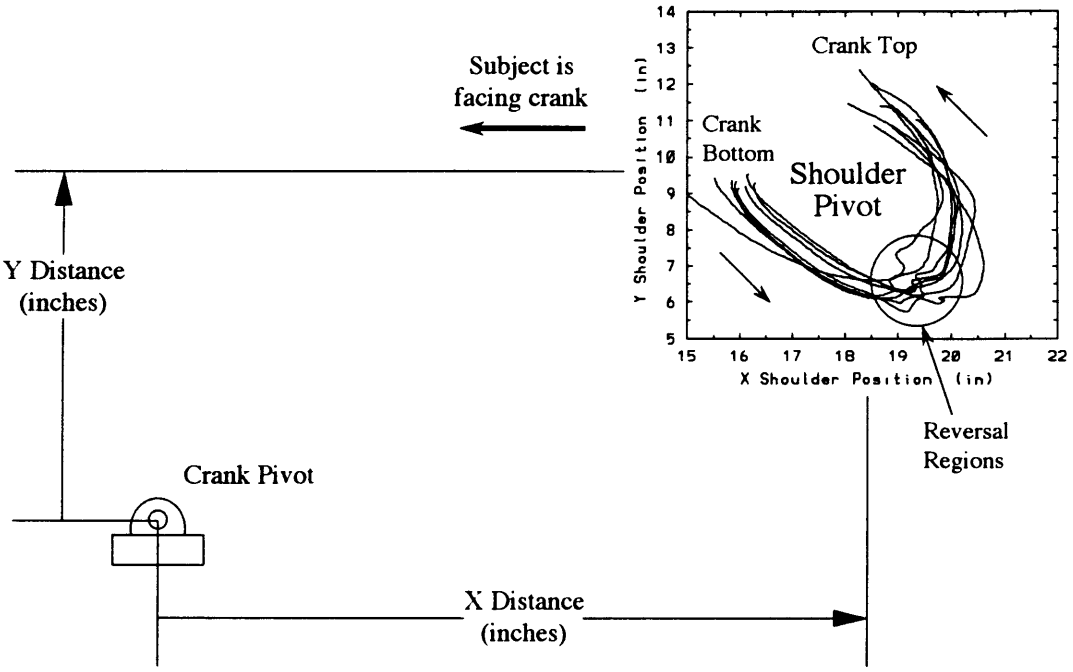

Figure 5.9 Shoulder Position Plot (relative to crank pivot)

The movements shown in the shoulder position plots do not agree with those observed in the video tapes. The plots show the shoulder pivot moving as much as 10 inches in either the x or y directions whereas the video tapes show only half this movement. The shoulder distances were back-calculated using measured link lengths and smoothed crank, handle, and elbow angles. Nonplanar movements, biased potentiometer readings, and potentiometer nonlinearities can not account for the large discrepancies between the plots and the video tapes. The discrepancies are most likely a result of the imprecisely measured link length between the elbow pivot and the shoulder pivot. For the plots, this measured length was assumed to be fixed. In actuality, the length was variable since there was relative motion between the subject's stump and the emulator's socket during the task. In addition, finding the precise location of the shoulder "pivot" was difficult since the shoulder is not a simple ball-and-socket connection. If under-measured, the upper arm link length will produce shoulder plot profiles

that swing back as the upper arm extends and move forward as the upper arm flexes – much like the recorded profiles.

During the slow speeds and especially for the passive, friction cases, a subject occasionally found himself in a situation where the crank was near the shoulder reversal and the crank velocity was quickly approaching zero. Not having enough kinetic energy stored in the crank system to pass through the reversal, the subject often dropped his shoulder to take advantage of the system's geometry and to effectively change the crank angle location of the shoulder reversal. This permitted the subject to pass through the shoulder reversal quicker so that the upper arm could regain control of the crank and complete the cycle. The shoulder movements for this tactic often show up in a shoulder position plots as subtle loops or deviations from the plot's U-shaped pattern. While appearing insignificant, these minor deviations help explain some of the force interactions recorded in the dynamic plots.

5.4 DYNAMIC PLOTS

Figure 5.10 shows ten plots that comprise Subject 1's dynamic plots for trial number `arm003`. The first two plots, crank angle versus time and crank angle versus elbow angle, serve as useful references when comparing speeds, reversals and subjects. The remaining plots display the trial's forces, power flows, and MEA measurements. Elbow torque, radial force, tangential force, and MEA's were measured and smoothed. Elbow power was calculated from smoothed elbow torque and elbow velocity. Crank power was calculated from smoothed tangential force and estimated crank velocity. The force magnitude plot is the square root of the sum of the squares of the smoothed radial and tangential force magnitudes.

At higher speeds, the crank arm began to vibrate and produce noisy measurements. The main source of vibration came from the crank handle which created excessive moments about the crank arm. Because of the high frequency vibration, aliasing occurred in some of the plots. Under such circumstances, localized trends in a plot should be disregarded. Only overall trends are credible. Higher speeds also produce saturation problems. Subject 1's fast, passive case (Appendix B, `arm021`) well illustrates this saturation and its consequences. The radial force plot shows forces that contain flat peaks near 65 N. These flat peaks are a result of the force sensor being pushed beyond its measuring capabilities (saturated). Normally, the radial and tangential sensors show excellent decoupling characteristics despite being mounted on the same strain element. When saturation occurs, the two sensors show strong correlations.

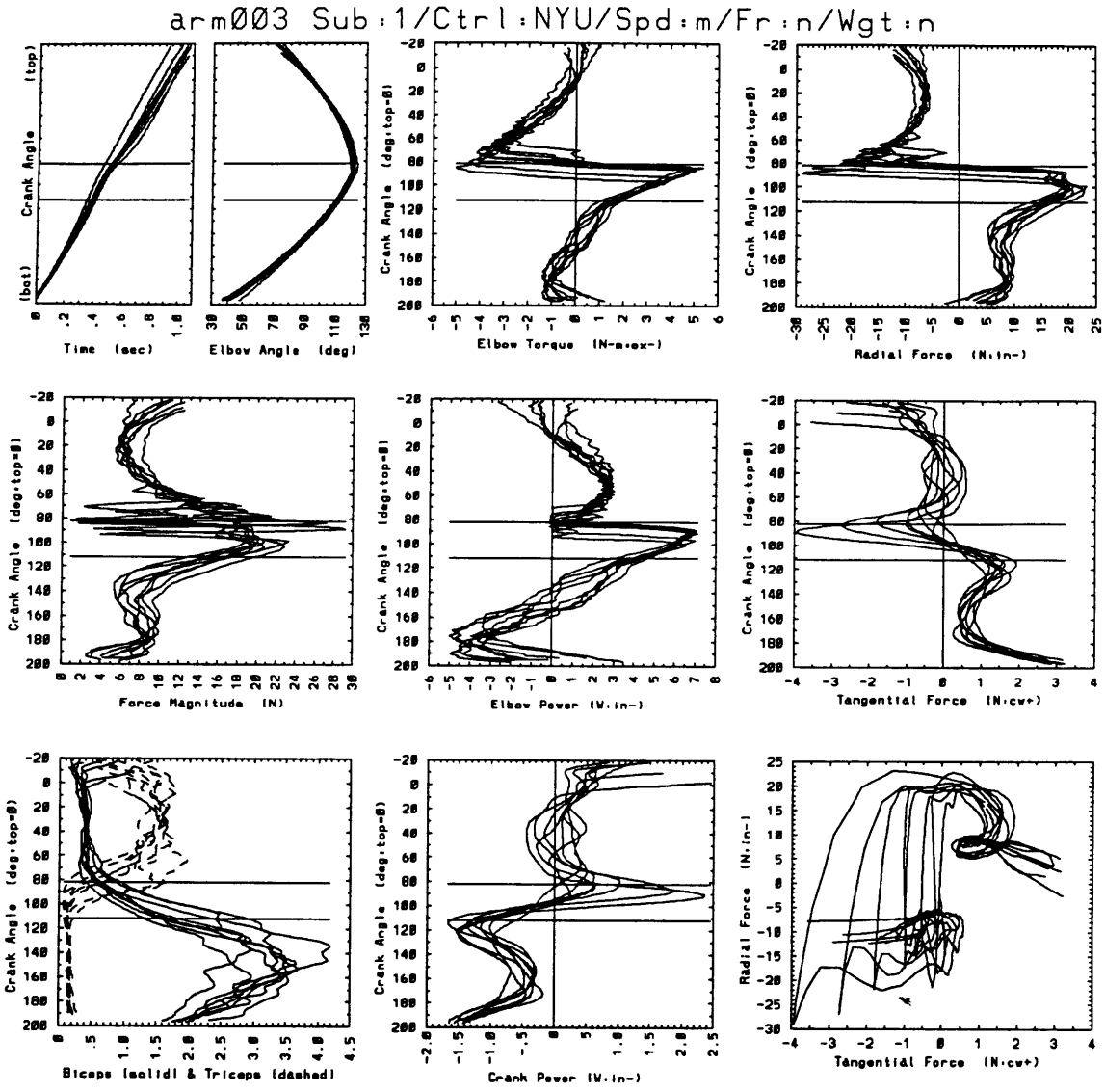

Figure 5.10 Dynamic Plots for Subject 1, Trial Number `arm003`

High radial forces produce sudden increases in the tangential forces. The correlation is most obvious in the tangential versus radial force cross-plots (Section 5.4.6).

5.4.1 ELBOW TORQUE

The measuring units for torque were Newton-meters. When the emulator's *motor* was flexing the elbow, any external resistance to the desired *flexion* motion produced *positive* elbow torques while resistance to desired *extension* motions produced *negative* torques. All measurements contained a 0.1 N-m positive bias which did not prove to be significant enough to

warrant correction. For the elbow torque plots, the different controllers produced significantly different results. Each controller is addressed separately.

Passive: When the emulator was *backdriven* in passive mode, the intrinsic friction in the hardware's transmission and sealed bearings produced *negative* elbow torques during *flexion* movements and *positive* torques during *extension* movements. Notice that the passive case produced flexion and extension torque measurements that were the negatives of the active controller measurements. Coulomb friction, which accounted for 0.4 N-m of the elbow torque, dominated the passive measurements. Torque and velocity feedback attenuated the coulomb friction for the active controllers.

For most of the lifting cycle, elbow flexion before the elbow reversal produced negative torques and elbow extension after the reversal produced positive torques. However, when high levels of elbow acceleration (or deceleration) occurred, an interesting phenomenon developed. Although the emulator was *electrically* turned off, the emulator's transmission and motor armature were still *mechanically* intact. Backdriving the emulator's elbow joint also backdrove the emulator's drive train. If the elbow joint was accelerated fast enough, the forces required to accelerate the emulator's drive train inertia would show up in the elbow torque measurements. Subject 1's `arm018` trial, shown in Figure 5.11, illustrates the drive train phenomenon quite well. Approximately 25° before the shoulder reversal, the subject rapidly accelerated the emulator to ensure passage through the reversal. Accelerating the emulator's elbow joint indirectly accelerated the emulator's transmission and produced negative, peak elbow torques in the subject's elbow torque plot.

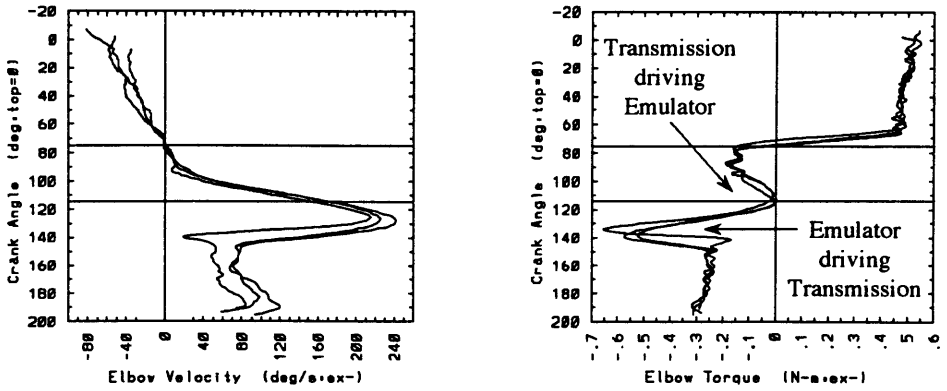

Figure 5.11 Elbow Velocity and Torque Plots for the Passive Controller

At the shoulder reversal, the emulator's transmission dynamics continued to affect the elbow torque measurements. By definition, only the elbow joint can drive the crank system at the reversal. Since the emulator motor was inactive for the passive case, only the system's stored kinetic energy could be used to lift the emulator through the reversal. A portion of this stored energy manifested itself as rotational momentum in the emulator's drive train. As the emulator approached the reversal, the emulator began to decelerate as its kinetic energy was transferred to potential energy to lift the crank. The elbow joint deceleration permitted the emulator's transmission to start driving the elbow with its stored kinetic energy. The transmission driving force was not only sufficient to eliminate the effects of Coulomb friction but was often high enough to produce positive elbow flexion torques at the shoulder reversal – flexion torques which are normally produced by an *active* motor. The phenomenon can be seen in the elbow torque plot's as sudden reductions in negative elbow torque values or as positive torque peaks at the shoulder reversal. All subjects show the phenomenon.

The drive train dynamic behavior suggests an interesting question: How important are a system's *passive dynamics* during task performance? While the phenomenon may have only played a minimal role in aiding the subjects through the shoulder reversal, other transmission designs, particularly those that are not easily backdrivable or exhibit a high output impedance, could have made the storage and exchange of energies between the various subsystems nearly impossible. Regardless of what objectives or strategies an amputee may have had, prosthesis designs or controllers that prevent the subject from taking advantage of this energy transfer phenomenon through the system's *passive dynamics* may limit the functionality of the device.

Currently, all powered prostheses that are commercially available to amputees contain high output impedance controllers that would limit the usage of the energy transport phenomenon during task performance. The body-powered prosthesis, on the other hand, has a low output impedance during swing phase and permits, or may even encourage, the usage of the system's passive dynamics. The benefits of the body-powered's passive dynamics may help explain why it is so popular and why the acceptance of the externally powered prosthesis is significantly lower [26].

Impedance: The slow cases illustrate the base profile for the impedance controller. Before the elbow reversal, the prosthesis provided flexion torque. Past the reversal, the prosthesis applied extension torque. This profile is similar to the elbow torques calculated by Russell when intact subjects turned the crank [34]. Figure 5.12 compares a measured elbow torque

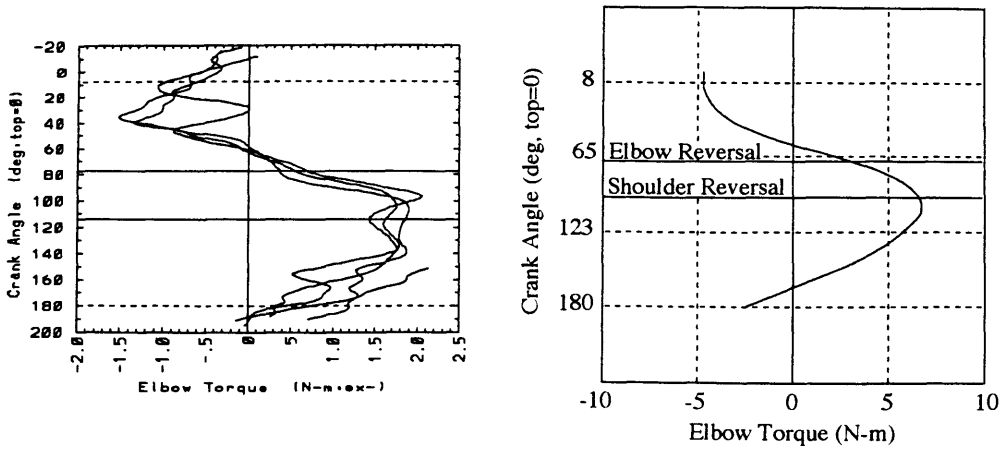

Amputee Measured Torque

Intact Calculated Torque

Figure 5.12 Amputee versus Intact Elbow Torques

trial obtained from an amputee (Subject 1, arm009) with a calculated elbow torque plot obtained from an intact subject (Russell [34], DLR Right).

The transition from flexion to extension torque consistently occurs *after* the elbow reversal. At faster speeds, some transitions do not occur until 40° past the reversal. The transition delay may be a consequence of the subject implementing the preload *strategy* which will be discussed in Section 5.4.2. The subject may also be using the shoulder reversal as a cue to initiate elbow extension. The radial force plots and the videos show that the shoulder reversal may provide a strong and very consistent force feedback signal to the subjects about the system's current geometric state. The subjects could use the radial force information as a guide for executing the elbow torque transition. The elapsed time from shoulder reversal to elbow torque transition is between 300 – 400 ms. This is more than enough time to react since human kinesthetic reaction times are usually less than 200 ms [17]. Torque plots at faster crank speeds support the "cueing" hypothesis by showing similar time delays and larger crank angle delays.

Because of the controller's low output impedance, the timing of the elbow torque transition about the elbow reversal is not crucial. If the subject inadvertently extends or flexes too soon or too late about the elbow reversal, he can easily compensate for the error by continuing to flex the upper arm. This permits the subject to be less concerned about controlling the execution of the task and may explain why all subjects thought the impedance controller was the easiest controller to use for the task.

The fast case results are substantially different from the slower cases because of the controller's *viscous* impedance. In the fast cases, the emulator was backdriven at such a high speed that the controller's damping characteristics began to dominate the elbow torque (Section 3.2.3). As in the passive case, this resulted in negative torques during elbow flexion and positive torques during elbow extension. The impedance controller's damping feature at the higher speeds may have been a mixed blessing. The plots suggest that the subjects were being hindered from performing the task. Normally, this would be looked upon as a fault in the controller architecture. However, the task completion times were very fast, usually less than 0.6 seconds, and the force plots show that the subjects were experiencing very abrupt force interactions. The controller's damping characteristic might have been a hidden asset to the subjects by preventing the task from being performed at speeds that would have otherwise been considered unsafe. Further investigation is required to determine the importance of the impedance controller's damping characteristics and whether the controller should incorporate variable damping ratios. For the experiments, a constant damping ratio of 0.5 was used for the impedance controller.

Subject 4 used only elbow flexion torque to perform the task. The MEA plots confirm that this was the subject's intent. The reason is not clear. The subject might have deduced that task completion did not require extension torques from the impedance controller. Most likely, the subject's triceps became fatigued. The extension torque found in Subject 4's slow case, `arm005`, was **not** a result of triceps activation. The torque arose from the controller's emulated stiffness and the deviation of the emulator's actual position from the controller's desired position.

NY Electric & Boston Elbow: Both controllers produce similar results. Since the Boston Elbow provides proportional velocity control, some of the plots show smoother torque transitions as the emulator's speed changes.

To understand the elbow torque plots, one must understand a consequence of the high output impedance, velocity controller. When an external force acts on the prosthesis, the velocity controller will counter the force to maintain its desired speed. Thus, even though the prosthesis may be flexing, external forces may require the controller to apply extension torques to maintain the desired flexion speed. The opposite is true for extension. Subject 1's slow trial, `arm002`, is a good example of this phenomenon and is shown in Figure 5.13

At the beginning of Subject 1's lifting cycle, the prosthesis is flexing even though the actuator is applying extension torques. In this phase, external forces produced by the subject and

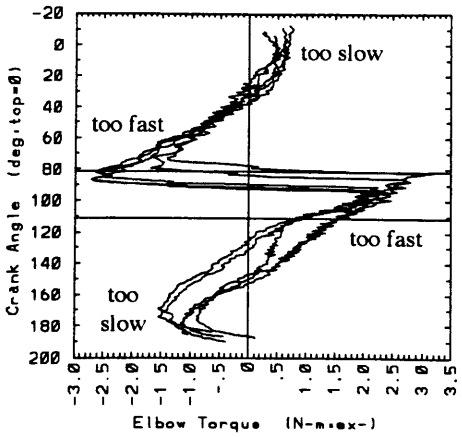

Figure 5.13 Elbow Torque Plot for the NY Electric Elbow Controller

the crank are driving the prosthesis faster than the controller desires. In other words, the prosthesis is moving too slowly for the subject. The controller attempts to maintain its desired speed by applying an extension torque that counters the external driving forces.

Not long after moving too slow, the prosthesis begins to move too fast. As the subject approaches the elbow reversal, the prosthesis is moving faster than the subject desires. The subject responds by applying extension torques to reduce the prosthesis's speed. Again, the controller counters these external forces by producing higher flexion torques that peak near the elbow reversal.

At the elbow reversal, the prosthesis must change directions. Sudden shifts in elbow torque occur as the controller attempts to achieve its newly desired extension speed. Initially, the extension torques are high because the amputee is not permitting the prosthesis to move as fast as the controller desires. By the end of the cycle, elbow flexion torques reveal that the prosthesis is extending too slowly for the subject.

All subjects and speeds show similar profiles. The torque discontinuities and the higher peak torques easily separate the velocity controllers from the impedance and passive controllers. For the faster, programmed elbow velocity speeds, the velocity controllers' profiles show higher torque peaks near the elbow reversals. This is because the subjects are less likely to be in a situation where the prosthesis is moving too slow and more prone to be in situations where the prosthesis is moving too fast. The fast cases do not show the high peaks one might expect because the motor's amplifier limited the emulator's output torque. An electrical current limit was set on the motor's amplifier to protect the motor from overheating. This pre-

vented the emulator elbow torque from exceeding 7 N-m. Subject 1's `arm005` trial and Subject 2's `arm011` trial (Appendix B) both show evidence of reaching the amplifier's current limit by producing elbow torques with flat peaks at about 7 N-m.

Subject 2's slow go-lock-go transitions discussed for the elbow velocity plots show up in the elbow torque plots as double peaks (Section 5.3.6, Figure 5.6). Interestingly enough, the double peaks consistently occur at the same magnitudes. Contingent on further investigation, the plots give one the impression that the subject was using the elbow resistance as a cue for elbow control. While not as pronounced or as consistent, Subject 3 shows similar double peaks. Subject 3 refrained from overdriving the system as much as the other subjects.

Summary: The crank velocity, elbow velocity, and elbow torque profiles make it more apparent that the subjects use similar strategies to perform the crank task. It is also more apparent that the subjects will attempt to implement their strategy regardless of the emulator's controller architecture. If the controller does not complement the strategy, the torque profiles show that the subjects will *forcibly oppose* the controller to achieve their objectives. When asked which controller a subject preferred, each subject described either the passive controller or the impedance controller. The elbow torque plots reveal that both of these controllers contained fewer cases of resistance when compared to the velocity controllers.

Both the passive and impedance controllers showed advantages of a low output impedance device. At the elbow reversal, the subject's timing of elbow flexion to extension did not have to be precise. Errors in execution could be compensated by the upper arm with little or no penalty. At the shoulder reversal, low impedances permitted the subject to take advantage of the system's passive dynamics. Utilization of basic momentum principles allowed the subjects to turn the crank for the passive controller with as much ease as any of the powered emulations. Using the video tapes to distinguish between the passive and impedance controllers by sight alone was often impossible.

The elbow torque plots provide significantly more information than found in any of the kinematic plots. By showing the force interactions between the human and the prosthesis, considerably more insights are gained on how the subjects cope with the different controllers. Because each controller has substantially different output torque control laws, distinguishing between the controllers is much easier. For these reasons, the elbow torque is a good measurement for quantifying amputee performance.

5.4.2 RADIAL FORCE

Radial force plots recorded the compression and tension forces experienced by the crank arm. Negative forces signify that the crank arm is in compression. Positive forces represent tension. At very high forces (60 – 70 N), the force transducer saturated and produced flat peaks.

Passive: The radial force profiles for the passive controller are very similar for all subjects. The profiles are best explained using a quasi-static force analysis. At the beginning of a lifting cycle, the emulator is at the bottom of the crank path. Both the upper arm and the crank arm must be in tension to support the emulator weight. Figure 5.14 shows a *simplified* free-body diagram of the force vectors required to support the emulator. The crank arm, force vector is always collinear with the crank arm centerline. To support its portion of the emulator, the crank arm must produce a force vector *component* that partly compensates for the emulator's weight vector. This crank arm component is labeled the emulator force component in Figure 5.14. As the emulator approaches the shoulder reversal, the crank arm centerline becomes collinear with the emulator centerline. The crank arm must continue to support its portion of the emulator weight. To do this, the crank arm's force vector must *increase* in magnitude to produce the required emulator force component. At the shoulder reversal, the magnitude of the force vector becomes infinite as it tries to support the emulator weight.

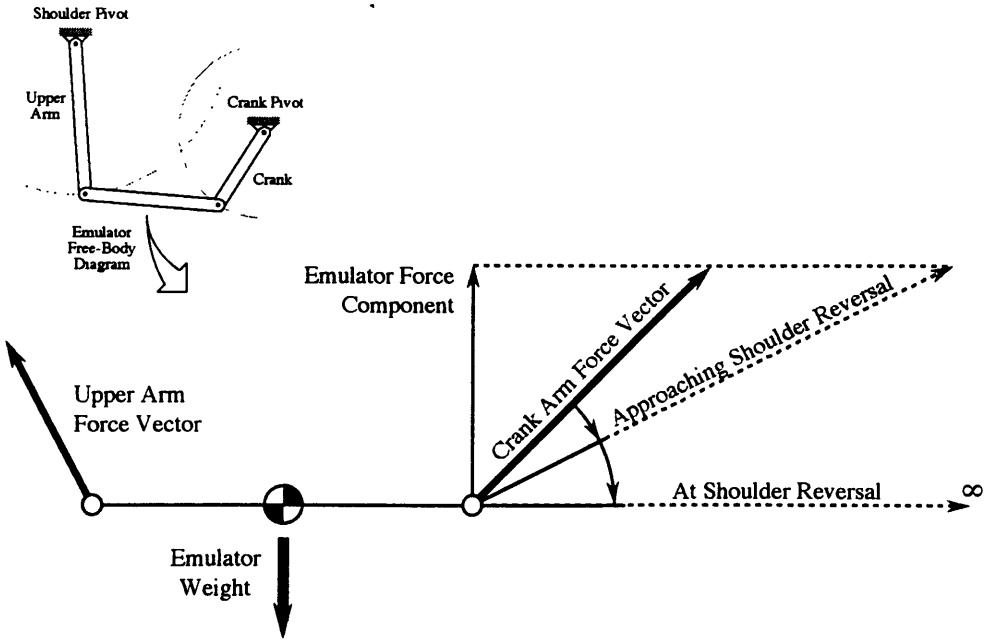

Figure 5.14 Crank Arm Force Analysis

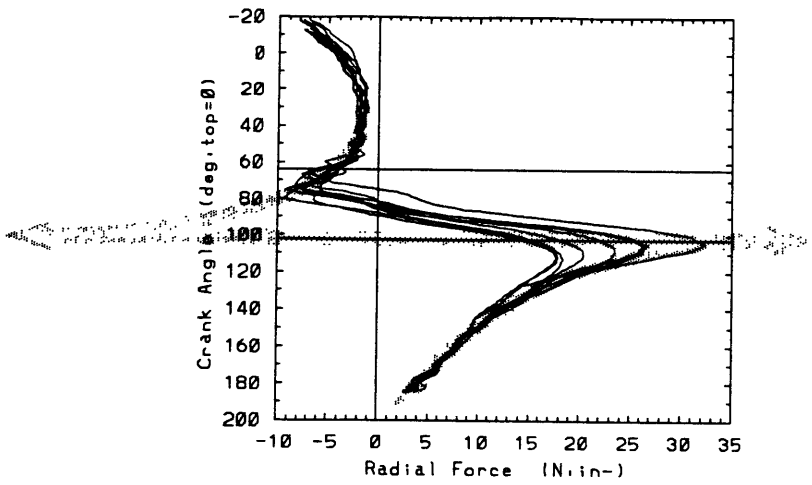

Figure 5.15 Radial Force Plot for the Passive Controller

As the emulator toggles through the reversal, the crank force vector must abruptly change from an infinite *tensile* force to an infinite *compressive* force to maintain the same emulator force component. From the reversal to the top of the crank path, the crank's compressive force vector decreases since a greater fraction of the vector contributes to the emulator force component. Figure 5.15 compares the hypothetical, quasi-static force analysis (shaded line) with an actual trial (Subject 2, `arm016`).

Figure 5.15 shows that the subjects do not produce infinite forces during the task. This is because the task was not performed in a quasi-static manner. As a subject approached the shoulder reversal, the subject stored kinetic energy into the system by increasing the crank and emulator's speed using rapid upper arm extension. At the shoulder reversal, the subject took advantage of the system's momentum to carry the emulator through the reversal without having to supply high forces. In cases when not enough kinetic energy was stored in the system, a subject would often move his shoulder pivot to help pass through the reversal quicker (Section 5.3.5).

Radial tension peaks increased with increasing crank speed as greater forces were required to decelerate the upper arm near the shoulder reversal. After the shoulder reversal, compression peaks decreased with increasing speed since the system's momentum reduced the need for high static, compressive forces. Secondary peaks found near the elbow reversals for the fast speeds are consequences of vibration and aliasing.

Subject 4's medium speed, `arm012` trial (Appendix B), contains a high compressive force cycle that resulted from the subject not storing enough kinetic energy into the system before the reversal. With the crank almost reaching zero velocity, the cycle came very close to reversing directions and becoming a "bad" cycle. Figure 5.16 shows Subject 4's fast speed, `arm010` trail. The trial contains two cycles with very low tension peaks. For these two cycles, the subject accelerated the crank sooner in the cycle (approximately 30° earlier) and then permitted the system's momentum to carry the emulator through the reversal. The strategy resulted in lower tension peaks and higher compression peaks. Notice that before the shoulder reversal, both cycles show the crank arm in compression and made the crank arm *unstable* at the reversal. Producing an unstable crank at the shoulder reversal also shows up in the impedance controller plots where it will be discussed in greater detail.

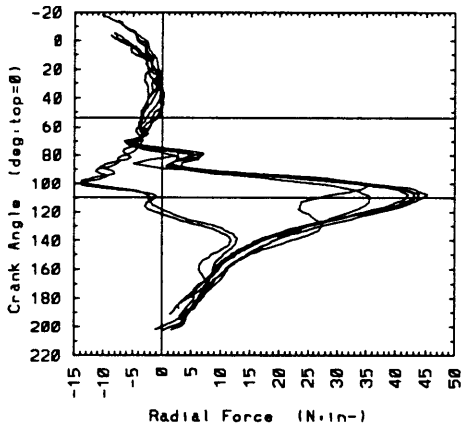

Figure 5.16 Radial Force Plot for the Passive Controller

Impedance: The common pattern found in the passive controller is also present in impedance controller. This is especially true for the faster speeds. At the slower speeds, the impedance controller's active motor reduced the crank's radial force peaks and produced smoother force transitions near the shoulder reversal. Faster cases often contained cycles starting in compression because the subject commanded flexion torque levels exceeded the weight of the emulator. Some of the faster cases also had tension forces occurring past the elbow reversal. These forces were the result of elbow torque transition delays (Section 5.4.1) and the domination of the controller's damping characteristics (Section 3.2.3).

Figure 5.17 illustrates an interesting phenomenon that was present in all subjects to some degree. The particular example is from Subject 3 (`arm009`, `arm010`, `arm012`). As can be seen, the impedance trial was very similar to the passive trial for the fast speed. The subject

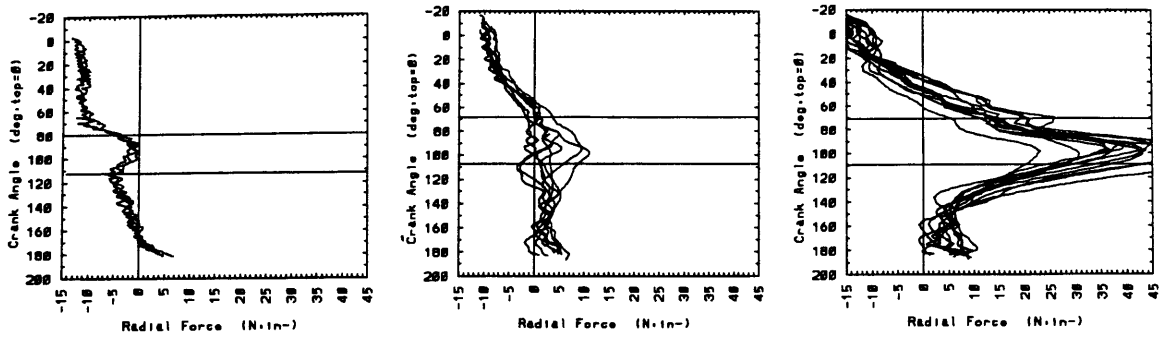

Figure 5.17 Radial Force Plots for Impedance Controller

demonstrated strong evidence of letting the passive dynamics of the system play a significant role in performing the task – even with an active controller. As the crank speed decreased, the subject began to rely more on the controller's active motor to reduce the radial force peaks. In the slow case, *the radial force peaks at the shoulder reversal are in compression instead of tension.*

The compression peaks have two interesting consequences. First, *crank arm compressive forces at the shoulder reversal make the system statically unstable.* Starting from rest, any perturbation to the compressed crank arm at the reversal will cause the crank to swing away from the reversal position to a new equilibrium position – much like a balanced, inverted pendulum. Second, all subjects show elbow flexion torques near the shoulder reversal. With the given crank geometry, elbow flexion torques can only produce radial tension forces. For the crank to be experiencing *compressive forces near the reversal requires the upper arm to be applying flexion torques.* The result is somewhat counterintuitive since the flexion torques from the upper arm are being applied while it is extending (before the shoulder reversal).

The slow cases reveal a strategy that coordinates both the upper arm and elbow flexion torques together to pass through the shoulder reversal. "Preloading" the upper arm with flexion torques creates an instability at the shoulder reversal and prepares the subject to push the crank to the top of the cycle once the reversal has been passed. "Preloading" the elbow with flexion torques aids in lifting the crank from the bottom of the cycle to the elbow reversal and ensures the crank arm will "toggle" upward when encountering the *unstable* shoulder reversal.

The advantage of such a strategy is that the subject does not need precise knowledge of the shoulder or elbow reversal locations to perform the task. Elbow flexion will help carry the crank from the bottom of the crank to the elbow reversal while shoulder flexion will push the crank from the shoulder reversal to the top. The subject has 20° to 30° of crank angle overlap between the two reversal locations to coordinate the transitions between elbow torque and shoulder torque. Because the controller exhibited a low output impedance, errors made while making the transitions produced minimal force interactions.

NY Electric & Boston Elbow: The high output impedance devices carry the same base profiles found with the other controllers. Figure 5.18 compares the three controllers for Subject 1's medium speed (`arm003`, `arm007`, `arm017`). Like the impedance controller, the velocity controller significantly reduced the positive radial force peaks when compared to the passive controller. However, the NY Electric Elbow and Boston Elbow produced negative peaks that were equivalent or worse than the passive controller. Both velocity controllers showed the sharpest force transitions of all the controllers at the elbow reversal.

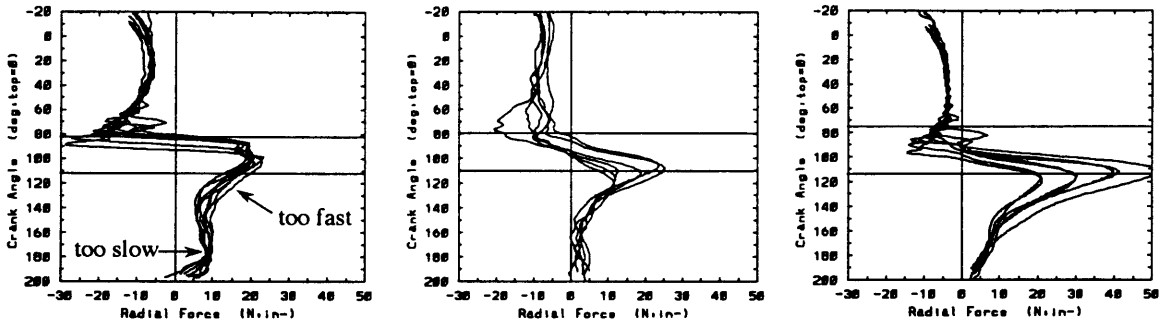

NY Electric Elbow Impedance Passive

Figure 5.18 Radial Force Plots for Subject 1's Medium Speeds

The NY Electric Elbow and Boston Elbow display a distinct, rise-and-fall force profile before the shoulder reversal. The profile is related to the conflicting speeds desired by the controllers and those desired by the subjects (Section 5.3.6). At the beginning of the lifting cycle, the prosthesis moved too slowly for the subject. To increase the emulator's speed, the subject forced the emulator to flex faster than the controller desired by applying shoulder extension torques. Such a strategy for the given geometry created a small tension peak in the radial force profiles during the first 20 degrees of the lifting cycle. Once the prosthesis was moving at a satisfactory speed, the radial forces plateaued or began to decrease. As the subject approached the elbow reversal, the prosthesis started to move too fast. Shoulder extension

torques were again used but in this case to *reduce* the emulator's speed. Trying to reduce the emulator's speed resulted in increasing the radial tension forces near the shoulder reversal.

Summary: The radial force plots unveiled two strategies that were present by all subjects to some degree. One strategy took advantage of the system's passive dynamics or more specifically, the system's momentum. At the start of the cycle, the subject used upper arm extension to increase the speed of the system so that enough kinetic energy was stored in the system to ensure passage through the shoulder reversal. The strategy produced high radial tension forces before the elbow reversal and high compression forces after the reversal. The second strategy "preloaded" the system with shoulder and elbow flexion torques before encountering the shoulder reversal. This strategy often created radial compression peaks and made the crank arm unstable at the shoulder reversal. Elbow flexion torques ensured that the crank successfully passed through the reversal.

Subjects showed evidence of using the *preload strategy* at the slower speeds. As the task became faster, the preload strategy yielded to the *passive dynamic strategy*. Figure 5.17 shows an excellent example of a subject making the transition between the two strategies as the task is performed at faster crank speeds. One advantage that both strategies possess is that they do not require precise knowledge of the reversal locations. Once the crank is up to speed for the passive dynamic strategy, the subject can let the system's momentum address the shoulder reversal location. Subject 4 demonstrated (Figure 5.16) that the strategy can be successful even if the execution of the strategy differs by as much as 30° in crank angle location. The preload strategy shows a similar "transition window" which occurs between the shoulder and elbow reversals.

All subjects showed evidence of implementing the passive dynamic strategy at the faster speeds regardless of the controller being used. This is supported by the similar radial force profiles. It is less obvious that the subjects were trying to implement the same preload strategy for all controllers at the slower speeds. Despite not having an active motor, the passive controller does show some significant myoelectric activity for Subjects 2 and 3 during their slow, passive cases (Section 5.4.8). The activity was the command flexion torque that would have been required to preload the emulator if an active motor was present. Subject 3 also shows the unstable, radial compression peaks for his velocity controller during the slow speed trial, `arm000` (Appendix B).

The radial force plots are useful for understanding the possible strategies implemented by the subjects to perform the task. However, when compared to elbow torque plots, the radial force

plots are not recommended for quantifying performance. Trying to separate the radial force results that are a consequence of different strategies as oppose to different performances appears to be difficult. Although the radial forces do not directly contribute to performing the task (only tangential forces do) and might be considered unnecessary, the forces can be a consequence of a very effective strategy. Both the slow and fast case trials show strategies that indirectly create radial forces while enabling the subjects to pass through the shoulder reversal without requiring precise knowledge of its location.

5.4.3 TANGENT FORCE

Pushing or pulling the crank in the *clockwise* direction created *positive* forces. All good, lifting cycles rotated the crank in a *clockwise* direction from the bottom of the crank path to the top. The general pattern found for the tangential force profile is shown in Figure 5.19 (Subject 1, `arm003`) and consists of the following: 1) an initial high force to accelerate the crank from rest, 2) a lower, relatively constant force to counter frictional effects and to accelerate the crank further, 3) an increase in force to provide the system with additional kinetic energy just before encountering the shoulder reversal, 4) a shift towards negative forces as the crank begins to drive the system, 5) a constant (usually near zero) force past the elbow reversal, and 6) a relatively high negative force to bring the crank to rest at the top of the cycle. Depending on how the cycles were cropped in the cycle module of the data processor, (Section 4.6), the initial and final peak forces may be missing. The unusually high forces present in the fast cases were an artifact caused by saturation of the force transducer in the radial direction. High frequency vibrations and aliasing also distorted the measurements.

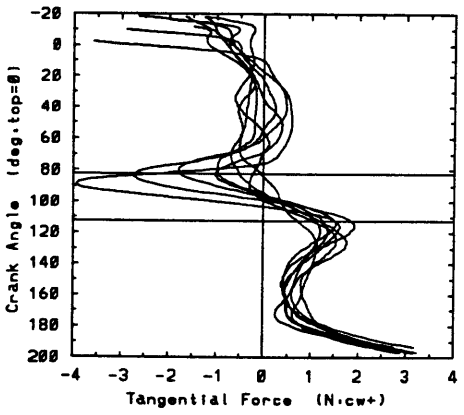

Figure 5.19 Tangential Force Profile

Passive: The passive controller follows the aforementioned general pattern. At the slower speeds, the force peaks before the shoulder reversal were higher since the subjects had to accelerate the crank faster to store more kinetic energy into the crank system. The negative force peaks after the reversal were also higher since the subjects relied more on the crank's stored momentum to push the emulator through the reversal. Normally, the zero crossovers of the tangential forces occurred *before* the shoulder reversal. This was a result of the crank arm's momentum starting to assist the subject in pushing the emulator through the reversal. The tangential force results for the passive controller strengthen the previous arguments that the subjects took advantage of the system's passive dynamics to successfully pass through the shoulder reversal.

Impedance: The impedance controller's medium and fast speeds show profiles that are similar to the passive controller's. With the active motor, the force peaks were lower since less kinetic energy needed to be transferred to the crank arm to complete the task. Zero tangential crossovers before or at the shoulder reversal demonstrate that the crank arm, to some extent, assisted the low output impedance, active controller through the reversal.

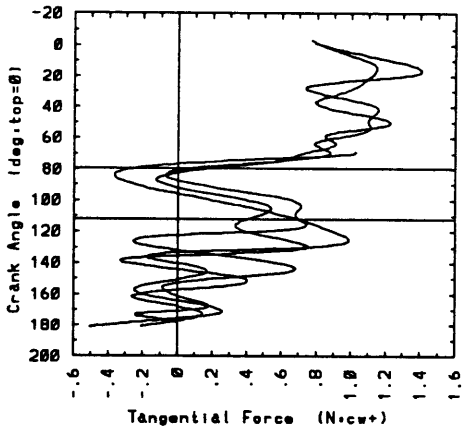

Figure 5.20 Tangential Force Profile for Slow, Impedance Case

The slow cases can show significant reductions in force levels and changes in the force profiles. Figure 5.20 shows Subject 3's results (`arm009`). The lower force levels can be attributed to turning the crank at a slower speed and requiring lower crank accelerations since the subject had an active prosthesis. The changes in force profiles are not as well understood. Some of the changes appear to be a result of the preload strategy. Before the shoulder reversal, the subject preloaded the emulator with elbow flexion. As the subject approached the reversal, a smaller and smaller portion of the crank arm's radial force could restrain the emula-

tor from flexing. At the reversal, the emulator was no longer restrained by the crank arm (by definition of the shoulder reversal) and permitted the emulator to freely flex and to direct its elbow torque entirely as tangential force at the crank handle. This "toggle joint effect" produced peak positive forces in the tangential force plots and speed increases in the crank velocity plots at the shoulder reversal. Once past the reversal, the crank arm's radial force resumed partially restraining the emulator's flexion torques. This unrestrained "toggle effect" that occurred at the shoulder reversal is also present in the velocity controller plots.

NY Electric & Boston Elbow: Like the impedance controller, the velocity controllers show peak forces that are less than those created by the passive controller. When compared to the impedance controller, the velocity controller force peaks appear to be equivalent. Only Subject 1's slow case shows force discontinuities that are normally the trademark of the high output impedance devices.

The force peaks for the velocity controllers normally occur *at* the shoulder reversal and the zero crossovers occur *after* the reversal. The peaks are most likely the result of the "toggle effect" discussed for the impedance controller's slow cases. Just before the shoulder reversal, the emulator is typically flexing at a speed slower than the velocity controller desires (Section 5.3.6). At the reversal, the emulator becomes unconstrained and permits the velocity controller to achieved its desired speed. This produces higher tangential forces on the crank arm and increases the crank's speed. The crank velocity plots reflect the speed increases.

Summary: In the kinematic plots, it is very difficult to see the shoulder reversal's "toggle effect" produced by the active controllers. If not for the tangential and radial force profiles, the preload strategy and the toggle effect would have been overlooked. The force plots stress the usefulness of dynamic measurements for quantifying interactions and performances.

The tangential force plots are helpful for investigating the force interactions between the crank handle and the emulator. They are also effective for confirming strategies speculated from the radial force and elbow torque plots. Unfortunately, the similarities between the plots make it difficult to establish differences between controllers and speeds. Quantifying performance based on the tangential force plots is not recommended.

5.4.4 ELBOW POWER

By definition, the elbow power plots (units of Watts) show the rate and direction of energy flowing into or out of the emulator. Positive power is defined as power being supplied from

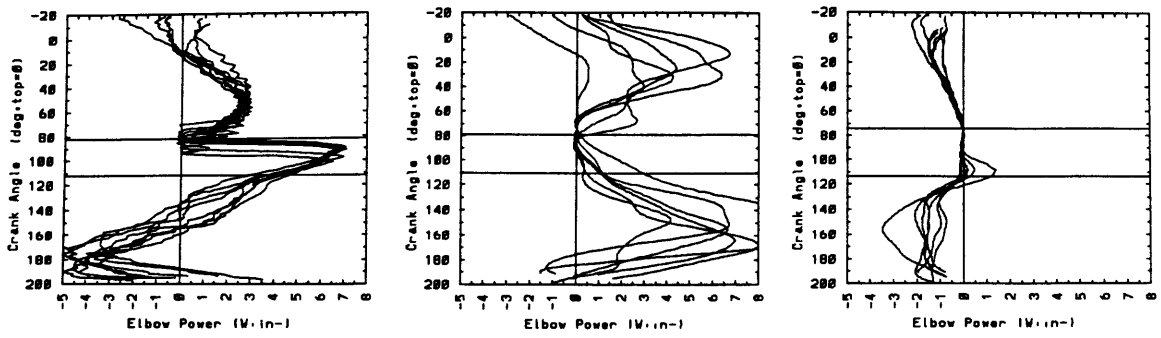

Figure 5.21 Elbow Power Plots for Subject 1's Medium Speeds

the emulator to the surroundings (e.g., amputee, crank, etc.). Negative power means the emulator is absorbing power (e.g., acting as a high-tech damper). Figure 5.21 shows the power plot results for Subject 1's medium speeds (`arm003`, `arm007`, `arm017`).

Passive: For the passive case, the emulator functions primarily as a damper. With the actuator disabled, reaction forces created from backdriving the system largely reflect the system's Coulomb friction (Section 5.4.1). Peak power absorptions correlate well with peak elbow speeds. Zero crossings occur near the shoulder reversal, where elbow torque becomes zero, and at the elbow reversal, where the elbow velocity is zero. The zero crossings and small positive peaks near the shoulder reversal are a result of the emulator's armature and transmission inertias driving the system (Section 5.4.1). The precise locations of the crossings and peaks vary at different speeds and depend on the relative influence the drive train inertia had during the task. As in the elbow torque plots, the effect of the transmission inertia becomes more apparent at the faster speeds.

Impedance: The impedance controller provides power *to* the system throughout most of the cycles and provides a sharp contrast to the passive controller profiles. The amount of power transferred increases with speed and the magnitudes are significantly more than those found in the passive cases. Peak velocity *and* torque profiles coincide to form peak power curves. Zero crossings exist near the elbow reversal and at the beginnings and ends of the lifting cycles. Negative power flows just past the elbow reversals are a consequence of elbow torque transition delays exhibited by the subjects (Section 5.4.1). Negative powers near the tail ends of the cycles develop from the emulator's passive friction as the subject relaxes muscle activation and allows the emulator to be backdriven. For the fast cases, the controller's active damping can dominate the elbow torque (Section 3.2.3). This is evident in the elbow torque

profiles and can create power profiles that show resemblance to the passive power profiles. Subject 1's fast case, `arm010`, demonstrates the similarities (Appendix B).

NY Electric Elbow: Subject 1's medium speed case in Figure 5.21 serves as a good example of the base profile found for the NY Electric Elbow controller. During the first quarter of the cycle, the emulator absorbed a significant amount of power as the subject forced the prosthesis to flex faster than the controller desired. The controller's resistance to the subject's motion appears in the profiles as power absorption. For the second quarter of the cycle, the prosthesis provided power to the system. However, after the shoulder reversal, the prosthesis began to move too fast for subject. The subject's attempt to slow the prosthesis down stimulated the controller to provide higher flexion torques and output powers. The powers peaked at the elbow reversal. A discontinuity occurred at the reversal as the subject reversed elbow torques. The third quarter shows positive power flows that are not as dramatic as in the previous quarter. Low velocities resulting from subject resistance prevented high power flows from developing. Power absorption developed in the final quarter as the subject attempted to drive the prosthesis faster than the controller desired.

The base profile exists at all speeds. Higher speeds show less power absorption (negative values) relative to power dissipation (positive values) since the prosthesis is less likely to be moving too slowly for the subject. Subject 2's slow transitions through the controller's deadzone created dual discontinuities near the elbow reversal.

Boston Elbow: The Boston Elbow power flows are substantially different from the previous NY Electric Elbow cases by showing minimal power absorptions. Figure 5.22 shows Subject 3's medium speed (`arm003`). Two factors helped make Subject 3's results different from

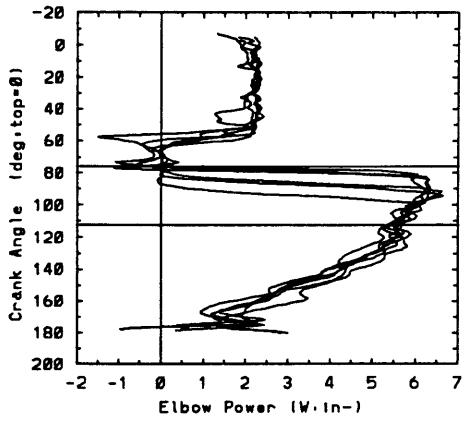

Figure 5.22 Elbow Power Plot for the Boston Elbow Controller

the rest. First, the subject did not try to overdrive the controller at the start and finish of the cycles. This prevented power absorptions normally found for the NY Electric Elbow controller at the bottom and top of the crank cycles. Second, the radial and tangential force plots show that the subject was very instrumental at implementing, to some degree, the preload strategy (Section 5.4.2) at *all* speeds. Since the preload strategy keeps the elbow torque in flexion through most of its flexion movement, only positive power flows developed.

Despite using the preload strategy, the subject's plots still show the abrupt transitions at the elbow reversal that have become characteristic of the high output impedance controllers. In the case of the NY Electric Elbow controller, which is an "on-off" controller (Section 3.2.1), the abrupt transitions resulted from a subject's inability to reduce the speed of the emulator. In contrast, the Boston Elbow provided a proportional speed control, MEA Window (Section 3.2.2). One might have expected that this controller would have produced substantially smoother elbow power transitions since the subject should have had better control of the emulator's speed. When comparing the two controllers, it is not obvious that the subject had better control or took advantage of the proportional control feature.

Summary: Combining elbow torque and elbow velocity into one measurement, elbow power draws a dramatic picture of the differences between individual controllers and strategies. Passive profiles remain largely negative throughout the task while impedance profiles are consistently positive. Velocity controllers contain a combination of both. Low output impedance devices show smooth power transitions while high output impedance controllers illustrate very abrupt changes. Subject 3's velocity controller profiles show that different strategies can produce substantially different results.

While very informative, the power plots must not be misinterpreted. Controllers that exhibit positive power profiles are not necessarily "good" controllers and controllers that reveal negative power profiles are not necessarily "bad" controllers. The NY Electric Elbow controller demonstrates that conflicts between the subject and the controller can *increase* the emulator's power output. The impedance controller contains examples of power dissipation that may be useful for controlling the emulator's speed.

The radial force profiles reveal different strategies implemented by the subjects. The power profiles indicate how successfully the chosen strategy worked in performing the task using a specific controller. While the best controller may not always produce positive power, the kinematic plots, dynamic plots, and subject comments suggest that the *time rate of change of power* may be a very informative measurement for quantifying synergistic coordination. All

four subjects demonstrated that rapid changes in elbow power are directly related to the conflicts existing between what the subject *appears* to desire and what the controller desires. Controllers that created fewer conflicts during the task appear to produce lower overall power gradients in the power plots.

5.4.5 FORCE MAGNITUDE

The vector sum of the radial and tangential forces produces a resultant force vector that acts on the crank handle. The *magnitude* of this vector is plotted in the force magnitude versus crank angle plots. The plots were constructed to find out if the crank handle's resultant force contained any patterns unique to a particular controller. After reviewing the plots, there appears to be very little information that can not be found and extracted more easily from the tangential and radial force plots.

Radial forces dominate the force magnitude plots. Force magnitudes peak at the shoulder reversal and increase as speed increases. When comparing the various controllers at the slow speed, the passive controller shows the highest force peaks since the subjects must compensate with passive dynamic or preload strategies (Section 5.4.2). As the crank speed increases, the impedance and velocity controllers' force peaks begin to approach the magnitudes of the passive controller's peaks. This reflects the previously discussed radial force results that suggested the passive dynamic strategy was used regardless of the controller architecture at the faster speeds (Section 5.4.2). When compared to the impedance controller, the velocity controllers usually show higher peaks at the slow and medium speeds. The higher peaks are caused by the conflicting desired speeds between the subject and controller (Section 5.3.6). At the fast speed, the velocity controllers can show *lower* peaks than the impedance controller. The lower peaks resulted from the high output impedance controllers limiting the flexion speed of the elbow joint. Limiting the speed of the elbow limited the speed at which crank could be turned. This, in turn, limited the acceleration forces experienced by the crank handle and recorded by the radial force sensor.

A possible usage of the force magnitude plots would be to monitor human learning and adaptation. As representative plots were selected for the subjects, it was observed that trials performed under the same crank conditions and controllers but at later times in the experiments showed lower peak magnitudes. Figure 5.23 shows an example of two such trials performed by Subject 3. For both trials, the subject was turning the crank using the passive controller at medium speed with no friction or weights. Trial `arm017` was initiated approximately one

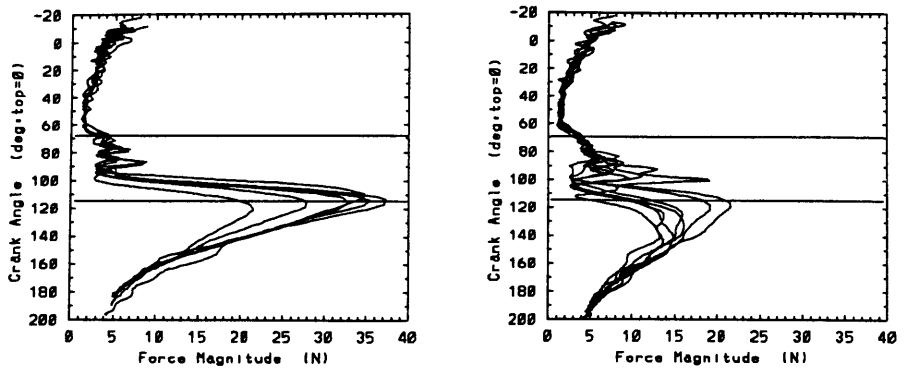

First Trial: `arm016` Second Trial: `arm017`

Figure 5.23 Comparing Force Magnitude Trials

minute after trial `arm016` was completed. During the one minute interval between trials, the subject was resting and not turning the crank.

As the subject performed the task, the force magnitudes of each trial began to decrease. Trial `arm016` shows peak magnitudes at approximately 35 N for most of the trial. But for the last two cycles, the peak forces began to reduce to 28 N and then to 21 N. For trial `arm017`, the trend continued until most of the cycles produced approximately 15 N peaks. The significant reduction in peaks as the subject continued to perform the task has the possible implication that the subject was *learning* how to perform the task. In the process of learning and adapting to the task, the subject began to minimize the task's force interactions.

If the trend found in the two trials is a result of a learning process, the 20 second trials performed by all subjects suggest that the process takes several minutes to become evident. Trends within a single trial are not obvious for most subjects and trends between trials can sometimes be contradictory by showing increases in force peaks. To properly document the "learning process" for the crank task, longer and more trials under the same crank conditions would be required.

5.4.6 TANGENTIAL VERSUS RADIAL FORCE

Like the force magnitude plots, the tangential versus radial force plots were created in hopes of finding additional differences between controllers. The results are not encouraging. All subjects show a circular pattern for the passive controller. The pattern is also present in the fast speeds for the remaining controllers. The velocity controllers display abrupt shifts pro-

duced by radial force discontinuities and small loops created from tangential and radial force fluctuations. The impedance controller largely preserves the passive controller's circular pattern for the medium speeds but becomes inconsistent and irregular for the slow speeds.

The cross-plots do serve as a useful check for cross-coupling between the tangential and radial force measurements. Both measurements were obtained from strain gages attached to perpendicular sides of the same cantilever beam (Section 2.4). The phase plots show a positive correlation (4%) between the measurements within the working ranges (under 65 N) of the transducers. A 10 N, positive radial force will produce a 0.4 N, positive tangential force. When the radial transducer becomes saturated, cross-coupling becomes very serious. This is clearly demonstrated in the fast impedance and fast passive cases. For this reason, any time the radial force transducer becomes saturated (above 65 N), the tangential force and any calculations based on tangential force should be discarded.

5.4.7 CRANK POWER

Crank power is defined as the product of estimated crank velocity and measured crank tangential force. Negative power means power is flowing into the crank; positive power means power is flowing out. The crank power plots are normally reversed images of the tangential force plots. Tangential force dominates the force-velocity product because of two reasons. First, the crank speed is relatively constant throughout a cycle, and second, when significant variations in crank velocities exist, near zero tangential forces eliminate the velocities' potential impact. Because of the similarities, one should refer to the discussion given for the tangential force plots (Section 5.4.3).

5.4.8 MYOELECTRIC ACTIVITY

The myoelectric activity (MEA) plots display amplified signals measured from the amputee's remnant biceps and triceps. Signal sites were identical to those used for the subject's personal prosthesis (Section 3.5). Figure 5.24 shows the MEA plots for Subject 1's medium speeds (`arm003`, `arm007`, `arm017`). The number beside the identified controller signifies the order at which the controller was given to the subject for the crank experiments. For Subject 1, the first set of trials was performed using the NY Electric Elbow controller, then the impedance controller, and finally the passive controller. The biceps signal is represented by a solid line and the triceps signal is represented by a dashed line. The signals are unprocessed in the sense that they are not normalized with respect to each other or with respect to their respec-

tive maximum voluntary contraction (MVC) measurements. Normalizing with respect to the MVC measurements was misleading because of the procedure used to obtain MVC values and because of gain adjustments made during the experiments (Section 3.2). As mentioned in Section 5.1, Subject 1's measured myoelectric activity for the biceps originates from a separated portion of his remnant triceps muscle.

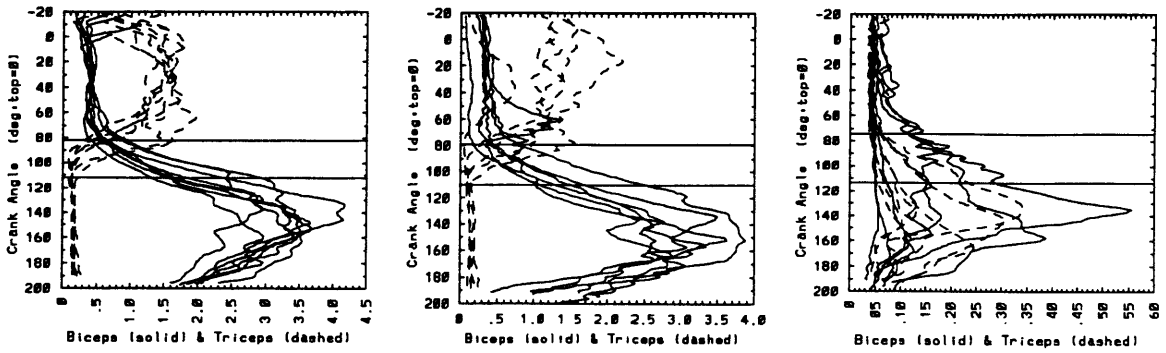

NY Electric Elbow (1st) Impedance (2nd) Passive (3rd)

Figure 5.24 MEA Plots for Subject 1's Medium Speeds

Except for Subject 4, all subjects show significant biceps *and* triceps MEA's. Biceps activation usually peaked before or at the shoulder reversal and triceps activation peaked after the elbow reversal. Coactivation often occurred near the elbow reversal. Signal amplitudes occasionally decreased at faster speeds. This result complements the radial force results: As the task became faster, less emphasis was put on providing input signals to control the prosthesis and more emphasis was put on the system's passive dynamics. When friction or weights were added, signal strength increased. Biceps MEA's dominate the lifting cycles. This agrees with the experimental results obtained from Russell for intact subjects [34] and stresses the importance of elbow flexion near the shoulder reversal if the task is to be completed at the slower speeds. All subjects produced significant MEA's for the passive case. Subject 2 and 3 show, even after accounting for gain adjustments, MEA amplitudes for the passive cases that are *higher* than their respective powered emulations.

Of the three controllers, only the velocity controller required triceps activation to complete the task. Insufficient triceps activity past the elbow reversal would cause the emulator to lock. This was not true for the impedance or passive controllers. Because the two controllers displayed a low output impedance, the subject could have used upper arm flexion to carry the emulator to the top of the cycle once the shoulder reversal was passed. Subject 4's plots demonstrate this by showing the absence of triceps activation in *all* of his trials and may ex-

plain why he was unsuccessful at using the velocity controller. Despite not being required, Subjects 1, 2, and 3 show strong triceps activation for the low output impedance controllers.

The MEA plots stress the importance of a controller's sensitivity to input signals. Controllers that are less responsive to a given set of MEA's have lower input gains. The passive controller is an example of a controller that has zero input gain. Because of the existing MEA deadzones for locking the prosthesis and the signal separation required to move the prosthesis, the velocity controllers have a lower input gain than the impedance controller. Subject 2's impedance cases demonstrate how the task can be performed using a high input gain controller with minimal signal separation. Subject 2's medium speed results are shown in Figure 5.25 (`arm009`, `arm001`, `arm016`).

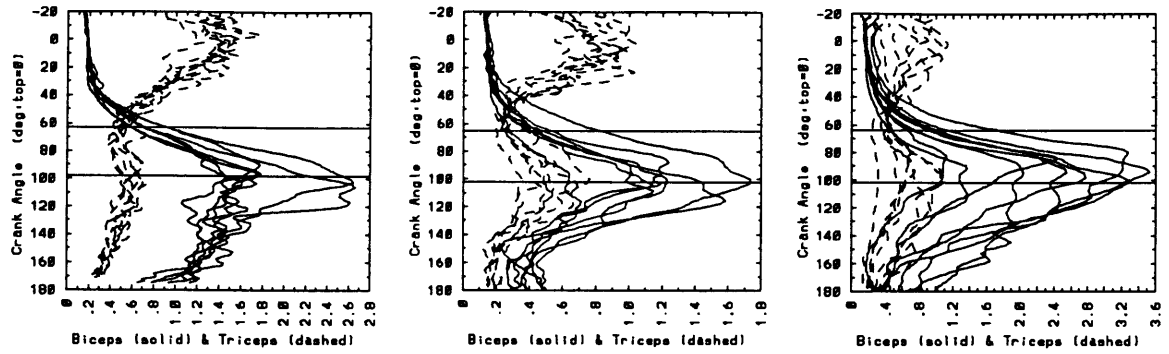

NY Electric Elbow (2nd) Impedance (1st) Passive (3rd)

Figure 5.25 MEA Plots for Subject 2's Medium Speeds

When the velocity controllers were used before the impedance controller, the subjects appeared to have become conditioned to the lower input gain required to activate the emulator. In the crank experiments, Subjects 1 and 3 used the velocity controller before the impedance controller. As can be seen in Figure 5.24, the MEA's created by Subject 1 for the different controllers are very similar despite the impedance controller not requiring: 1) large levels of signal separation to control the emulator and 2) triceps activation to complete the task. Subject 2 used the impedance controller before the velocity controller in his crank experiments. Figure 5.25 shows that triceps activation was still present for both controllers but the signal separation created for the impedance controller is noticeably less than the velocity controller.

The MEA plots show several surprising results. Even though the impedance and velocity controllers produce substantially different output impedances, the MEA inputs can be very similar. Some of the similarities, such as those found in signal separation, may be a result of

the subject becoming biased towards a particular input gain. Other similarities, such as triceps activation, muscle coactivation, and peak amplitude locations, appear *regardless* of the controller. The latter similarities, together with the presence of MEA's in the passive controller, may demonstrate how potentially useful and informative input signals can be underutilized due to improper controller input gains.

5.5 ADL TASKS

All subjects performed the activities of daily living (ADL) tasks using the impedance controller as one of their two given controllers. Subjects 1, 2, and 3 used the NY Electric Elbow as their second controller. The second controller for Subject 4 was the NY Electric Elbow for the cutting meat task and the Boston Elbow for the donning socks and the rolling pin tasks.

Time measurements (in seconds) taken to complete the tasks for each subject are listed in Tables 5.6 through 5.9. Each task was performed and recorded twice. All subjects performed the tasks and used the controllers in different orders to help eliminate biasing of results. The order of performance of the task or controller is shown in parentheses. Figures 5.26 through 5.28 show bar graphs comparing subjects and trial times for each task.

Timed measurements of a task's second trial were faster then a task's first trial 19 out of 24 times (79%). The subject's average task performance using the first controller was the same or slower than the second controller 10 out of 12 times (83%). The data suggests that subjects underwent learning and adaptation between trials and controllers. Video tapes confirm that

Table 5.6 Subject 1's ADL Times (seconds)

Controller	Rolling Pin (3)		Donning Socks (2)		Cutting Meat (1)	
	Trial 1	Trial 2	Trial 1	Trial 2	Trial 1	Trial 2
Impedance (2)	86	45	26	30	48	25
Velocity (1)	30	20	70	54	40	33

Table 5.7 Subject 2's ADL Times (seconds)

Controller	Rolling Pin (1)		Donning Socks (3)		Cutting Meat (2)	
	Trial 1	Trial 2	Trial 1	Trial 2	Trial 1	Trial 2
Impedance (1)	53	20	24	18	36	33
Velocity (2)	14	22	21	18	36	33

subjects changed strategies, sometimes dramatically, between trials which improved task speeds. The data shows no significant statistical differences between the timed performances of the impedance and velocity controllers [22].

An affiliated study compared ADL times with *changes* in elbow torques near the elbow reversal [21]. The results show positive canonical correlations: 0.77 for slow cases, 0.72 for medium cases, and 0.45 for fast cases. The weaknesses in correlations can easily be attributed to the inconsistent performances of the subjects during the ADL tasks. Correlations decreasing as speeds increase are most likely related to the subject's ability to use passive dynamics for the crank task. At the faster speeds, all subjects relied less on the emulator's controller architecture and more on the system's passive dynamics to turn the crank.

Qualitatively, the ADL tasks revealed several important aspects of the different controllers. In the cutting meat task, the impedance controller provided smoother elbow flexions and extensions for lifting and dropping the fork. The velocity controllers' lock improved the subject's ability to maintain fixed elbow positions for stabbing the meat and for supporting the fork when the prosthesis was fully flexed. For the donning socks task, the prosthesis remained fully extended throughout most of the task. The velocity controllers were normally locked. The low output impedance of the impedance controller showed some signs of permitting the subject to coordinate limbs to shimmy the sock up the leg. During the rolling pin task, the velocity controllers' lock permitted the subjects to better maintain a fixed elbow position while applying forces to the dough. This most likely explains why the average completion times for the velocity controllers were consistently less than the impedance controller. Most subjects

Table 5.8 Subject 3's ADL Times (seconds)

Controller	Rolling Pin (1)		Donning Socks (3)		Cutting Meat (2)	
	Trial 1	Trial 2	Trial 1	Trial 2	Trial 1	Trial 2
Impedance (2)	51	33	24	21	43	41
Velocity (1)	34	32	35	19	46	39

Table 5.9 Subject 4's ADL Times (seconds)

Controller	Rolling Pin (3)		Donning Socks (2)		Cutting Meat (1)	
	Trial 1	Trial 2	Trial 1	Trial 2	Trial 1	Trial 2
Impedance (1)	60	69	37	39	46	47
Velocity (2)	59	36	37	24	43	41

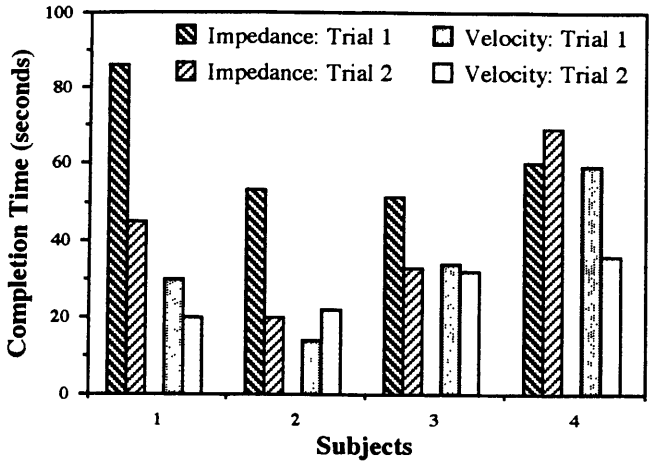

Figure 5.26 Time Comparisons for Rolling Pin Task

favored their intact arm for the rolling pin task. The pin handle held by the intact arm produced most of the pin's rolling motion and applied the forces required to displace the dough while the prosthesis's handle acted as a pivot and remained largely stationary throughout the task.

A common nuisance found in all tasks was the terminal device (TD). The TD was a standard hook device operated by a Bowden cable attached to the subject's shoulder harness. For the cutting meat task, the subjects often had difficulty holding the utensils with the hook. The reaching motion in the donning socks task forced the TD to open unintentionally several times and the compliant rubber bands limited the amount of force the prosthesis could apply in the rolling pin task. While not known by how much, the problems associated with the TD increased the recorded times of several of the ADL tasks.

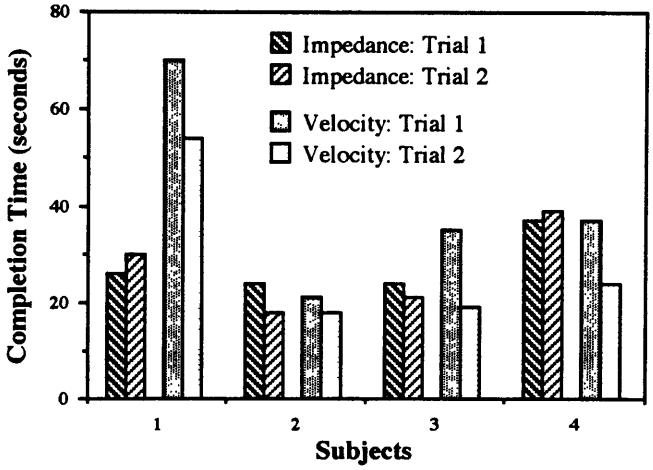

Figure 5.27 Time Comparisons for Donning Socks Task

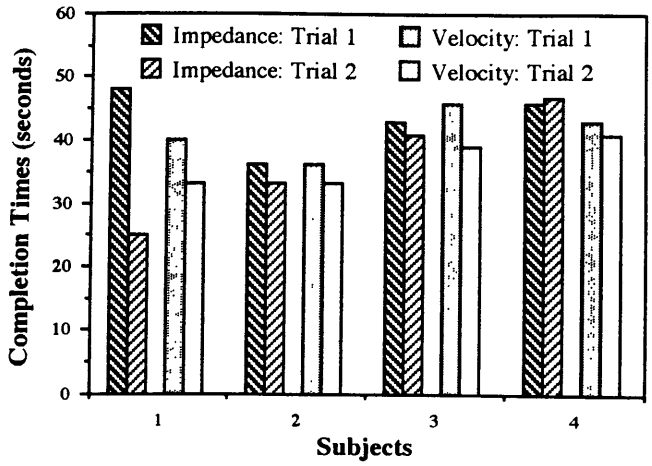

Figure 5.28 Time Comparisons for Cutting Meat Task

The performance of the ADL tasks was an attempt to relate these tasks, which are familiar but more abstract to quantify, to the more easily quantified crank task. Despite the difficulties of quantifying the tasks, all three proved to be very informative. Each showed the advantages of low output impedances for movement and contact control and high output impedances for postural stability and force applications. These results are strengthened by the crank task findings and the subject opinions. The crank and ADL tasks both demonstrated that time is a questionable measure of performance. Based on his comments, Subject 1 clearly preferred the impedance controller for the rolling pin task even though the task took over twice as long to complete. The subjects could easily describe *where* they were having problems during the ADL tasks but would have difficulties explaining *why* the problems existed. This was very similar to their descriptions of the shoulder and elbow reversals during the crank task. Postural shifts became extremely important to compensate for controller inadequacies. While measurable in the crank task, these shifts were often unnoticeable in the ADL tasks and made it very difficult to differentiate between controllers and to qualify or quantify performances. For better quantification of the ADL tasks, it is strongly recommended that time measurements be complemented with power and force measurements.

5.6 SUMMARY

The crank and ADL tasks have uncovered several interesting findings that are interspersed among the various plots, video tapes, and subject opinions. Included in these findings are the limitations of measurements for quantifying performance, the different *apparent* strategies used by the subjects to perform tasks at different speeds, and the importance of controller ar-

chitecture. This section highlights some of the more important findings common to all four subjects.

5.6.1 RELEVANT MEASUREMENTS

Results strongly argue that time and kinematic measurements are very limited in quantifying interactions and performance. The crank experiments show the task being performed over a broad range of times without providing any information on the subject's proficiency. ADL task results confirm that controllers preferred by the subjects did not necessarily produce the fastest performances. Relative angle measurements are only useful for defining the geometric state of the system. Relative velocity measurements begin to show differences between controllers but do not reveal why the differences exist. Without referencing the dynamic measurements, conclusions based on the time and kinematic measurements are speculative. Both the crank task and ADL tasks demonstrated that conclusions based solely on time and kinematic measurements can be deceiving or wrong.

The kinematic plots show nine measurements. Of the nine, the three most informative measurements are crank velocity, elbow velocity, and shoulder position. When compared to the dynamic measurements, the similar patterns shown in the velocity plots suggest that the subjects may be using a set of *kinematic objectives* to accomplish the task. Primary objectives span the performance of the entire task (e.g., constant crank velocity, minimum jerk, etc.) while secondary objectives address issues or portions of the task hindering the primary objectives from being achieved (e.g., controller architectures, reversal locations, etc.).

The elbow velocity plots are useful for categorizing controllers into different *output impedance families* and *input gain families*. Low output impedance controllers with high input gains show smoother velocity profiles when compared to high output impedance controllers with low input gains. High output impedance devices are less forgiving when interacting with the environment and low input gain thresholds crop useful information that would enable smooth elbow torque and speed transitions.

Shoulder position plots explain occasional anomalies found in both the kinematic and dynamic plots. Sudden shifts in force and position profiles can result from subtle shoulder movements. The movements are not noticeable while the subject is performing the task but are often detectable as small loops and deviations from the shoulder position's overall U-shaped profile. The other kinematic measurements proved to be too insensitive to detect such movements. More accurate and precise shoulder measurements may provide better insights

on synergistic coordination but the costs associated with obtaining such measurements may be impractical. The dynamic plots provide better and more economical alternatives.

The dynamic plots contain a wealth of information. Of the eight measurements, five are particularly useful for understanding the apparent objectives and strategies of the subjects and for monitoring the resulting interactions between the various subsystems. These measurements are elbow torque, elbow power, tangential force, radial force, and MEA's.

The power plots are by far the most informative of all the kinematic and dynamic plots. The plots show the largest differences between human strategies and controllers and provide insights on how the two complement or conflict with each other. "Good" controllers do not necessarily provide positive power flow. However, there is strong evidence suggesting controllers that complement the execution of the task minimize the *time rate of change of power* (the derivative of the power curves). The data and subject comments support this proposal. The time rate of change of power is also a very attractive measurement since it does not put any requirements on the direction or amount of energy transferred between subsystems. High output impedances, low input gains, and actuator limitations (e.g., the actuator limitations for the passive controller at slow speed force the subject to transfer large amounts of energy to the crank) can all cause unusual rates of change in power flows.

While the power plots reflect how well a strategy was executed, the radial force plots delineate which strategy was chosen. At slow speeds, the subjects appear to use a *preload strategy*. The strategy produces elbow and shoulder flexion torques before the shoulder reversal and makes the crank arm unstable at the reversal. Evidence of the preload strategy can also found in results obtained from intact subjects turning the crank [34]. At faster speeds, the subjects relied less on the actuator and the controller and more on the system's inertia. For the fast case, all subjects implemented a strategy that recruited the system's *passive dynamics* regardless of the controller architecture. The subjects needed no knowledge of the system's passive dynamics (including the emulator's "hidden" transmission dynamics described in Section 5.4.1) to take advantage of them.

The MEA plots stress the importance of a controller's input gain. While all other plots show the results of a controller's output impedance, the MEA plots are the only plots that show what the subject's inputs were and which ones were processed by the controller. Despite having zero input gain, the passive controller showed significant MEA's from the subjects. The velocity controller's input thresholds created tiered elbow velocities and dual elbow torque peaks near the elbow reversal. Because of the potential to misrepresent the subject's

intent, the input gain may become as important as the controller's output impedance in the overall performance of the task. Coactivation and the occurrence of MEA's for the passive case prove that there is more information in the MEA's than just the relative differences.

The elbow torque and crank tangential force are useful references for interpreting the data. By themselves, the radial force and power measurements can become confusing without referring to these two additional measurements. The tangential forces clearly demonstrate how the crank toggles passed the shoulder reversal when the preload strategy is implemented. The tangential force plots are also useful for confirming force interactions and crank velocities. The elbow torque plots separate the force contributions produced by the actuator and transmission from the rest of the system. When the system's geometric constraints prevent the elbow from moving in the desired direction, the elbow torques can be very revealing.

5.6.2 QUANTIFYING SYNERGY

A central theme of this work is to understand and quantify the interactions between humans, machines, and environments. If a task is to be accomplished, the three subsystems must interact and coordinate with each other. This is not only true for the crank task, but for any task requiring the usage of tools.

Of all the data acquired from the experiments, the rate of change of power shows the greatest potential for quantifying the system's synergistic coordination. The dynamic plots reveal that high rates of change of power produce unnecessary high levels of force interaction. While not as evident, the kinematic plots show high rates of change of power produce abrupt shifts in the position and velocity profiles. All plots suggest that high rates of change of power are a result of poor coordination between one or more of the subsystems. In addition, the consequences of sudden power shifts appear to be undesirable to the amputees. The subjects often compensated for the shifts by using superfluous postural movement. The sudden shifts may have also caused minor skin abrasions seen on an amputee's stump after performing the set of experiments. Besides the inconveniences directly experienced by the subject, the power shifts could also have a hidden cost. Sudden changes in power may make the performance of the task more inefficient by dissipating higher levels of energy. This will be discussed in greater detail in Chapter 7.

A reason why power may excel as a useful measurement for quantifying performance may be based on its definition. Power combines kinematic (velocity) and dynamic (force) measurements into one measurement. Velocity permits the power sensor to quantify local joint coor-

dination, the joint at which the sensor is attached. Force permits the sensor to quantify the coordination of adjacent joints. If the adjacent joints are not coordinating well, their interference forces are relayed back to the power sensor.

5.6.3 OBJECTIVES & STRATEGIES

While performing the tasks, each subject began to reveal his own personality. Subject 1 was a strong, young, rambunctious individual who was very aggressive with the crank task. Subject 1's forces were almost to the point of destroying the apparatus. Subjects 2 and 3 were older and more methodical. These subjects were less aggressive and put more forethought into each task. Having less experience and more difficulties with the tasks, Subject 4's attention span was shorter and he was less willing to try different variations of a task.

Despite their differences, the subjects showed similar kinematic profiles among controllers, speeds and themselves. When asked how they dealt with the difficult regions of the crank task, each subject described the problem (the shoulder reversal) in terms of crank position and their solution to the problem in terms of increased crank velocity. No mention was made of the task's force interactions or the problems associated with using substantially different controller architectures. All of these observations suggest that the subjects had a set of *kinematic objectives* in mind when performing the task. The data shows no obvious indications that the objectives might have been dynamic in nature. What the specific objectives were is not clear. The subjects may have been trying to turn the crank at a constant velocity or perhaps indirectly optimizing another kinematic variable such as acceleration or jerk.

The apparent strategies implemented by the subjects also proved to be very similar. At the slower speeds, a strategy described as the *preload strategy* created upper arm and elbow flexion torques before the subjects encountered the shoulder reversal. At the reversal, upper arm flexion made the crank arm unstable and elbow flexion ensured that the crank would pass through the reversal. As the speed became faster, the subjects relied less on the preload strategy and more on the *passive dynamic strategy* which used the system's momentum to carry the crank system through the reversal. The advantage of both strategies is that they do not require precise knowledge of the shoulder reversal location and permit errors in coordinating the upper arm with the prosthesis by as much as 30° in crank angle.

The transition between the two strategies is not well defined. Slow cases can show signs of the passive dynamic strategy while fast cases can show signs of the preload strategy. The fact that the transition occurs stresses the importance of the controller's output impedance. As the

system's passive dynamics begin to dominate the task, controllers that provide lower output impedances begin to excel since these controllers complement the subject's strategy. High output impedance devices hindered the subject by not permitting him to take full advantage of the system's passive dynamics.

5.6.4 INPUT GAINS & OUTPUT IMPEDANCES

At least three paradoxes occurred when the subjects operated the emulator with different input gains. First, when the input gain was zero, there was no reason for the subjects to activate their muscles since the controller did not process the MEA signals. Nevertheless, the passive controller, which had a zero input gain, showed significant MEA's. Second, the velocity controllers did not utilize muscle coactivation to operate the prosthesis. High levels of coactivation only locked the prosthesis and accelerated muscle fatigue. Despite the negative side effects, coactivation was still present in the velocity controllers. Third, the low output impedance controllers (impedance and passive) did not require triceps activation to complete the lifting cycle. Once past the shoulder reversal, the upper arm could have applied flexion torques to complete the cycle without *any* assistance from elbow flexion or elbow extension torques. Nevertheless, the MEA plots show strong levels of triceps activation after the shoulder reversal.

The contradictions in what MEA signals were *required* for the subjects to perform the task and what signals the subjects *provided* stresses the importance of designing a controller with proper myoelectric processing to take full advantage of the available signals. The apparent evidence of adaptation and memory as displayed in the MEA plots when the subjects changed controllers shows that the subjects do have some ability to adapt to different input gains when necessary. However, too much adjustment may become a mental burden to the subjects. The results obtained from the impedance controller suggest that the muscle separation required for the velocity controllers is not a natural phenomenon and necessitates significant adaptation.

A controller's output impedance can have a significant impact on the subject's overall performance of the task. High output impedance devices are useful for supporting and transferring high loads. Stabbing the meat in the cutting meat task and rolling the dough in the rolling pin task were examples where high output impedances allowed the subject to perform the task faster. Low output impedance devices were useful for partially constrained tasks requiring coordination and compliance between two or more subsystems. The performances of the

crank task and the donning socks task showed more graceful movements when using the low output impedance devices. Depending on the task, providing the wrong output impedance could result in unusually high interactive forces or insufficient forces.

Poorly designed input gains can be compensated by low output impedances. The passive case in the crank task is an extreme example. Although the passive controller's input gain was zero, the subject could still manipulate the crank system by using the muscles in his upper body to transfer the required energy to the low output impedance, emulator. This ability to recruit adjacent limbs to perform a task is often referred to as *Body-English*. While difficult to quantify, Body-English appeared to play a significant role in all tasks and controllers. For the crank task, Body-English was most prevalent in the slow cases when the subject was near the shoulder reversal.

Prostheses with high output impedances can accentuate input gain limitations. Subject 2's tiered, velocity profile (Section 5.3.6, Figure 5.6) results from the MEA thresholds established for the controller's input gains. Because of the controller's high output impedance, MEA signals passing through the thresholds abruptly stopped or started the prosthesis and created high reaction forces. High output impedances do not appear to facilitate the usage of Body-English or passive dynamics during task performance.

5.6.5 PROSTHESIS DESIGN

The experimental results provide several insights for future controller designs. There is strong evidence that MEA signals are underutilized in the velocity controllers. Velocity controllers operate primarily on the relative MEA differences between the biceps and triceps signals and do not encourage coactivation. The impedance controller, on the other hand, uses the relative MEA differences *and* accepts the sums of the two signals to simulate coactivation. Several subjects commented on how they thought their muscle signals were being processed by the different controllers and were surprisingly accurate with their assessments. Subjects thought that Controller B (impedance controller) provided a "more natural" feeling, especially when making transitions from biceps to triceps activation.

The velocity controllers monitor one MEA parameter; the impedance controller monitors two. There is no reason why other parameters related to MEA's (or some other input) could not be monitored, such as rates of changes or patterns, to supplement the controller's input gains. The cost of adding additional inputs in terms of hardware and software are minimal yet the potential impacts in terms of amputee acceptance could be substantial. In addition, the

positive results obtained from such investigations could quickly be implemented in current prosthesis designs and would be readily available for all amputees.

A variable output impedance controller with a lock appears to have several advantages over all four controllers used in the experiments. Low output impedances are useful when making contact with high output impedance environments to minimize force interactions and for taking advantage of the system's passive dynamics and the amputee's Body-English. A lock is useful for providing the amputee with a high output impedance for supporting loads and for transferring high forces. The lock is also energy efficient: an important design constraint for self-contained prostheses.

Interestingly enough, the body powered prosthesis is very similar to the recommended externally powered prosthesis design. The prosthesis has a high output impedance in lock phase and displays a low output impedance in swing phase. In addition, the prosthesis is relatively simple to use and is very responsive to the amputee's inputs. These advantages may very well explain why the body powered prosthesis is still so popular and why the externally powered prostheses have had only limited success.

Properly designed, the externally powered prosthesis can provide all the listed attributions of the body powered prosthesis plus take advantage of the subject's MEA signals and supply the subject with an active elbow. The extra command inputs provided by the MEA signals can help relay the subject's objectives and strategies to the prosthesis without requiring superfluous body movements. An active elbow is particularly useful when passive dynamics are minimal in tasks requiring slow elbow movements.

One disadvantage of the emulator's impedance controller is its inefficiency. With the current emulator design, high levels of energy dissipation occur when high levels of output impedance are desired. If a self-contained prosthesis is to have a variable output impedance, new prosthesis designs have to be investigated. Simple designs that implement real springs and dampers could be instrumental in creating the proper output impedances in a lightweight prosthesis without requiring a large amount of energy. Such a prosthesis runs counter to most design philosophies since one is trying to enhance instead of minimize the mechanism's intrinsic dynamics.

5.6.6 ROBOTICS & TELEROBOTICS

Several of the results obtained from the amputee experiments are applicable to the fields of telerobotics and robotics. While proprioceptive and exteroceptive feedback are important for

telerobotics, input signal transfer from the human to the robot's controller is pivotal if the human's objectives and strategies are to be conveyed and executed as expected. The crank task results suggest that appropriate input gains and signal processing can enhance the transfer of information between the human and machine interface and therefore make the two subsystems more compatible. Of the four controllers used for the experiments, the controller that possessed the highest input gains and which extracted the most information from the MEA signals, the impedance controller, was the best accepted. The emulator system demonstrated that improving information transfer from the human to the robot does not necessarily require additional sensors. In fact, controllers that can recognize and manipulate input signal patterns relative to themselves and to other signals could reduce the number of required sensors.

The controllers that exhibited low output impedances demonstrated at least two advantages over the high output impedance controllers during the experiments. When the low output impedance controllers interacted and contacted the high output impedance environments, the amputees showed lower interactive forces and no signs of chattering. High interactive forces and chattering are two common problems found in current robot designs [31]. With the low output impedance controllers, the subjects were able to make larger endpoint position errors and did not require precise timings of the input command signals to successfully perform the tasks. The errors did not appear to have any associated costs or penalties while the tasks were being performed.

Some robot designs are not physically suited to produce a low output impedance. Robots that must be structurally strong enough to support heavy loads are an example. In such circumstances, micro-macro manipulators may be the solution [35]. A set of micro manipulators can create the low output impedance interface between the environment and the macro manipulator and still permit the macro manipulator to support the required loads. Such a design is similar to the human arm where the fingers act as the micro manipulators and the upper arm is the macro manipulator.

During partially constrained tasks, low output impedances permitted the crank system's passive dynamics to assist the subject in performing the task. This result has two implications. First, when a robot participates in a dynamic interaction, the intrinsic passive characteristics of a robot should not be underestimated. Instead of minimizing friction and maximizing stiffness, which are two common design goals, one may want to design a flexible, damped, inertial system to take advantage of the robot's passive dynamics. Pumps actuated by electrical solenoids are simple examples of designs that can be very efficient if the intrinsic dynamics

of the hardware are properly selected. Second, properly designed passive dynamics could easily reduce the demands on the implemented controller. This could in turn increase the system's stability, reduce the demands on the system's actuators, and prove to be a lighter, more economical choice over the rigid, under-damped alternative.

Finally, the experiments demonstrated that high output impedances proved to be useful when no interactions occurred or after making contact and controlling a force. During the absence of interaction, amputees were very effective at using the lock to support the prosthesis's posture or to carry a static load. After contact, the lock permitted the subject to transfer high and variable loads to the environment with little concern over the elbow's position. These results agree with the experiences gained from robotics. Robots are commonly high output impedance devices and have proven useful for performing unconstrained positioning tasks, such as in spray-painting and welding. Robots have also been used for measuring and controlling forces, such as in assembling torque nuts and varying grasping pressures.

CHAPTER
SIX

MODELING

6.1 INTRODUCTION

This thesis discusses the investigation of the fundamental requirements for effective tool use by an amputee; in particular, this research sought to find what factors are important for humans to *effectively* interact with tools and the environment to accomplish a broad range of tasks. A set of experiments was designed and implemented to measure different task performances of above-elbow amputees. The description of the experiments and their results were discussed in the first part of this thesis, Chapters 2 through 5.

One of the more striking results obtained from the experiments was exemplified in the power plots. When compared to the other measurements, power disclosed the greatest contrasts between controllers and ostensibly quantified the success of a chosen strategy. Although controllers that were better accepted by the amputees did not always produce positive power throughout the task, the accepted controllers consistently produced lower *time rates of change of power* (the time derivative of power) when compared to other, less accepted controllers. Why a subject would prefer a controller that produces lower time rates of change of power is not obvious. One possible reason is that the subjects were trying to implement a fundamental task strategy that favors lower rates of change of power. Other reasons may be

related to minimizing socket slippage, reducing joint force interactions, muscle fatigue, or simply be a matter of preference.

The second part of this thesis, Chapters 6 through 8, discusses two hypotheses regarding the amputee preference for controllers with smoother power transitions. Each hypothesis is based on a thermodynamic argument [10, 37]. The first hypothesis states: Subjects *minimize* the system's *power dissipation.* Minimizing the system's power dissipation is equivalent to minimizing the amount of energy leaving the task. For example, a subject may prefer to minimize the amount energy leaving the crank task as a result of the system's bearing friction or some other energy absorbing mechanism. The amount of energy leaving the system is not necessarily the same as the amount of energy provided by the system's actuators since energy may be stored in one or more of the system's elements.

The second hypothesis states: Subjects maximize the utilization of their *available energy* while performing a task. For the model that will be presented, maximizing the utilization of available energy will be equivalent to *minimizing* the system's *entropy generation.* The second hypothesis assumes that as energy leaves a system, an irreversible process develops as heat transfer and temperature gradients form between the system and the surrounding environment. The process will generate entropy and reduce the amount of work available from the energy leaving the system for performing future tasks. If a temperature gradient does not develop between the system and the environment, no entropy will be generated and the second hypothesis converges to the first.

To test the applicability of each hypothesis, computer simulations were performed using simplified mechanical and thermodynamic models. This chapter defines the models and assumptions used for the simulations. Chapters 7 and 8 discuss the simulation results for the minimum power dissipation hypothesis and the minimum entropy generation hypothesis respectively.

6.2 GENERAL MODEL

To investigate both hypotheses, a general model of a human-machine-environment system for constrained motions was developed and is shown in Figure 6.1. The model consists of a series of masses interconnected with springs and dampers. Each mass represents a separate entity while the springs and dampers permit power to be transferred between the various masses. The human, machine, and environment each represent a mass but only the human has

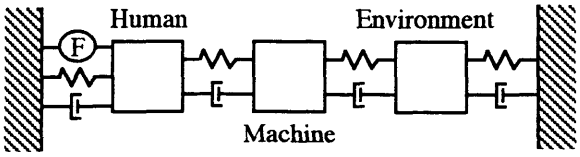

Figure 6.1 Human-Machine-Environment Model

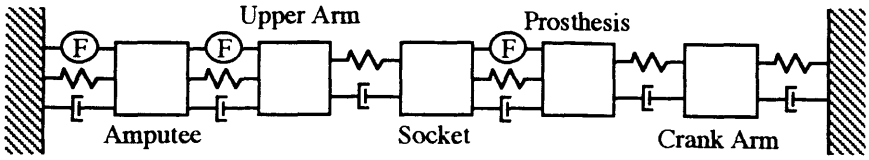

Figure 6.2 Human-Prosthesis-Crank Model

access to a force generator (e.g., a set of muscles). The damper can represent a wide range of irreversible processes and, depending on the method of energy transfer, can result in high levels of entropy generation and power dissipation. To show how the general model can be applied to a specific task, Figure 6.2 shows a detailed model representing the crank task.

No penalty is given for the *form* of energy stored in the models. Thus, while a task is being performed, energy can be stored without cost as either kinetic or potential energy. A penalty is associated with *how* energy is transferred between masses. During the crank task, the amputee was quite proficient at exchanging *forms* of stored energy to accomplish the task. This was particularly obvious at the shoulder reversal where the system's stored kinetic energy was transformed into potential energy to aid the subject in lifting the crank.

6.3 MECHANICAL MODEL

Because the human-machine-environment model consists of a series of masses, springs, and dampers whose interaction is difficult to visualize, the simplified model shown in Figure 6.3 will be used for analysis. The mechanical model consists of one mass, a linear spring, and a linear, viscous damper and has a velocity source as the input. The model's bond graph is shown in Figure 6.4.

The simplified mechanical model contains the *minimal type* and *number* of elements necessary to represent a generalized mechanical linkage that can transmit power. Transformers and gyrators could have been included in the model; but since they do not store or remove en-

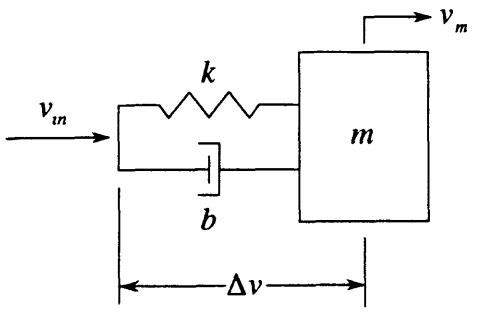

Figure 6.3 Simplified Mass-Spring-Damper Model

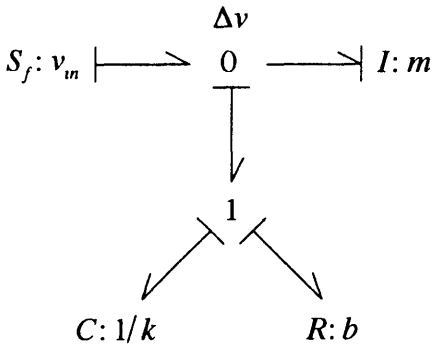

Figure 6.4 Mass-Spring-Damper Bond Graph

ergy, their inclusion or exclusion will not affect the results. The model produces relative results (as opposed to absolute results) since there is no specific reference to ground. Absolute results can be obtained by assuming an infinite mass to represent ground. Complex linkages can be created using different combinations of the simplified model. Since an effort (force) source could produce infinite compression or extension accelerations of the spring (e.g., step input), a flow (velocity) source was chosen.

The state equations for the mechanical model are:

$$\dot{v}_m = -\left(\frac{b}{m}\right)v_m + \left(\frac{1}{m}\right)F_k + \left(\frac{b}{m}\right)v_{in}$$

$$\dot{F}_k = -k\,v_m + k\,v_{in}$$

For the upcoming optimizations, the model's task will be to move the mass, m, a specified distance, d, in a fixed amount of time, T. This will require knowledge of the mass's position, x_m. Thus, one additional state equation will be necessary:

$$\dot{x}_m = v_m$$

The mechanical model, the bond graph, and the three state equations will form the basis for all future analyses and discussions. For the first hypothesis, subjects minimize the system's power dissipation, the analyses will focus on the amount of power being transmitted to the mechanical model's damper. Minimizing the power being absorbed by the damper is equivalent to minimizing the power being dissipated by the simplified system.

6.4 THERMODYNAMIC MODEL

The damper in the mechanical model provides a path for energy to leave the simplified system. The first hypothesis assumes that energy leaving a system while a task is being performed is undesirable. However, if all the energy leaving the system could be used for future tasks, minimizing a particular task's power dissipation may not be a very attractive or useful cost function.

The second hypothesis, subjects maximize the utilization of their available energy, focuses on what happens to the energy after it is absorbed by the mechanical model's damper. If the energy is absorbed by the damper and then transferred to the environment under isothermal or other reversible conditions, the amount of energy available to perform future work remains the same. On the other hand, if the damper absorbs the energy and then transfers the energy to the environment through a temperature gradient or some other irreversible process, entropy will be generated, and the amount of energy available for future work will be less then that available under the isothermal (reversible) conditions.

The second hypothesis assumes that energy being absorbed by the mechanical model's damper is not transferred to the environment under isothermal conditions. Thus, the amount of work available for performing future tasks will depend on how the energy absorbed by the damper is transferred to the environment. Energy transfer processes that create less entropy will provide greater levels of available work for future tasks. To study the consequences of the second hypothesis's assumption, a simple thermodynamic model was created and is shown in Figure 6.5.

It will be assumed that energy absorbed by the damper will be transferred to the environment as heat and that the heat transfer process will not be instantaneous. The power, P, represents the power absorbed by the damper as power is transferred between the velocity source and the mass. The absorbed power increases the stored energy of the damper. A constant heat ca-

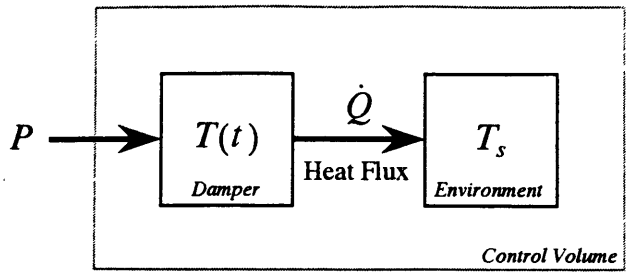

Figure 6.5 Thermodynamic Model of Power Dissipater

pacitance, C, of the damper is assumed so that a linear relationship exists between the damper's temperature, T, and the damper's stored energy.

$$P - \dot{Q} = \dot{E}_b = C\dot{T}$$

As the damper temperature increases above the surrounding environment's temperature, T_S, heat transfer will develop. The damper's thermal resistance, R, will represent an assumed linear relationship between the heat flux and the temperature difference.

$$\dot{Q} = \frac{1}{R}(T - T_s)$$

Combining equations, the state equation for the system's temperature becomes

$$\dot{T} + \left(\frac{1}{RC}\right)T = \left(\frac{1}{C}\right)P + \left(\frac{1}{RC}\right)T_s$$

With no device present (e.g., a Carnot heat engine) to extract the useful work available during the heat transfer process, the entropy generation of the control volume is

$$\dot{S}_{gen} = \frac{\dot{Q}}{T_s} - \frac{\dot{Q}}{T}$$

Substituting temperature differences for the heat flux,

$$\dot{S}_{gen} = \frac{(T - T_s)^2}{RTT_s}$$

The temperature equation and the entropy generation equation represent the thermodynamic model's state equations. Although the thermodynamic model may appear to be abstract and unrelated to the damper, applications of the model can easily be found whenever power dis-

sipation is present. Frictional effects in devices moving relative to each other, such as door hinges and wheels; stress effects encountered when bending materials, such as credit cards; and the effects of electrical resistance are just a few examples of processes that tend to "heat up" as energy is absorbed by the dissipative elements. This energy is normally transferred to the surrounding environment as heat while the various dissipative systems attempt to "cool down". With no devices present to take advantage of the heat transfer processes, the overall entropy of the control volume must increase.

6.5 SUMMARY

As an amputee is performing a task, the amputee may be attempting to implement one or more underlying strategies. To execute a strategy, the amputee may rely on using several objectives; one of which appears to be kinematic. If the prosthesis controller complements the strategies and objectives desired by the amputee, there is an improved chance that the controller will be better accepted by the amputee.

The two hypotheses and models presented in this chapter attempt to capture the strategies and therefore the reasons why one controller would be preferred over another. The hypotheses were formulated from observations made from the crank task's experimental results and from comments made by the subjects. The first hypothesis suggests that the subjects prefer to perform tasks and to use controllers that minimize power dissipation while the second hypothesis suggests that subjects prefer to minimize entropy generation. Both hypotheses indirectly require the rates of change of power to be minimal. Chapter 7 will investigate the probable usefulness and applicability of the first hypothesis using the mechanical model while Chapter 8 will look at the second hypothesis using the thermodynamic model.

CHAPTER
SEVEN

MINIMIZING POWER

7.1 INTRODUCTION

This chapter analyzes how a system can minimize power dissipation while performing a task. The system consists of the mechanical model discussed in Chapter 6 (Figure 6.3). The task will be to move the model's mass a specified distance in a finite amount of time using a velocity input. During the task, the amount of power being absorbed by the model's damper will be minimized. As will be shown, the optimal power dissipation solution for the mechanical model can be found analytically. After obtaining a solution for a particular set of modeling parameters, simulations of the task were performed to observe the behavior of the system. The results are compared to the experimental results obtain from the crank turning task.

7.2 CALCULUS OF VARIATIONS

Finding the minimal amount of power absorbed by the mechanical model's damper (Section 6.3) as the mass moves a specified distance is a problem that can be solved with the calculus of variations. No attempt is made to explain the supporting theory. Several text books are available that cover the method in detail. The text by Bryson and Ho is one primary source of information [9]. This section will briefly define some of the method's terminology

and outline how the power optimization problems were set up and solved. The sections that follow discuss specific solutions found for variations of the mechanical model.

Constraint Relations:

The constraint relations are a set of nonlinear differential equations that describe the system:

$$\dot{\mathbf{x}} = f[\mathbf{x}(t),\mathbf{u}(t),t]; \qquad \mathbf{x}(t_o) \text{ given}, \qquad t_o \le t \le t_f$$

Quite often the relations are the system's state equations. $\mathbf{x}(t)$ is an n-vector state function and $\mathbf{u}(t)$ is an m-vector input function.

Performance Index:

The performance index is the function that is to be minimized (or maximized) with respect to the input function, $\mathbf{u}(t)$:

$$J = \varphi[\mathbf{x}(t_f),t_f] + \int_{t_o}^{t_f} L[\mathbf{x}(t),\mathbf{u}(t),t]dt$$

Unless stated, no cost will be associated with the system's end states,

$$\varphi[\mathbf{x}(t_f),t_f] = 0$$

Thus, the performance index will be of the form:

$$J = \int_{t_o}^{t_f} L[\mathbf{x}(t),\mathbf{u}(t),t]dt$$

Lagrange Multipliers:

An additional set of variables and differential equations are established to minimize the performance index. The variables are called the *Lagrange multipliers*:

$$\Lambda^T(t) = [\lambda_1(t) \quad \lambda_2(t) \quad \cdots \quad \lambda_n(t)]$$

Hamiltonian:

For convenience, a scalar function called the *Hamiltonian* is defined as follows

$$H[\mathbf{x}(t),\mathbf{u}(t),\Lambda(t),t] = L[\mathbf{x}(t),\mathbf{u}(t),t] + \Lambda^T(t)\,\dot{\mathbf{x}}[\mathbf{x}(t),\mathbf{u}(t),t]$$

The partial derivatives of the Hamiltonian with respect to the state and input vectors are

$$\frac{\partial H}{\partial \mathbf{x}} = \frac{\partial L}{\partial \mathbf{x}} + \Lambda^T \frac{\partial \dot{\mathbf{x}}}{\partial \mathbf{x}}$$

$$\frac{\partial H}{\partial \mathbf{u}} = \frac{\partial L}{\partial \mathbf{u}} + \Lambda^T \frac{\partial \dot{\mathbf{x}}}{\partial \mathbf{u}}$$

Euler-Lagrange Equations:

The *Euler-Lagrange equations* are the key set of equations that must be solved if the performance index is to be minimized under the given constraint relations:

$$\dot{\Lambda}^T = -\frac{\partial H}{\partial \mathbf{x}}$$

$$0 = \frac{\partial H}{\partial \mathbf{u}}$$

The *Euler-Lagrange equations* provide $n + m$ equations while the constraint relations provide an additional n equations. Since there are $2n + m$ unknowns (n states, n multipliers, and m inputs), solutions can be found for the complete set of differential equations.

Boundary Conditions:

Since there are $2n$ differential equations, the solutions require $2n$ boundary conditions. This does not imply that one boundary condition must be assigned to each equation. For example, if the mass is going to travel a specified distance, the state equation for the mass's position will have an initial *and* final boundary condition. Equations that do not have a boundary condition were assigned unknown constants that acted as *pseudo*-boundary conditions. As the equations were solved, the *pseudo*-boundary conditions were replaced by functions of the actual boundary conditions. For the solutions found for the mechanical model, initial and final boundary conditions were assigned to the constraint relations. Unknown constants were assigned to the Euler-Lagrange equations as final *pseudo*-boundary conditions.

Definitions:

To help simplify the results obtained, several additional variables were defined and substituted into the final solutions. The variables and their respective definitions are shown in Table 7.1. The mechanical model's mass, m, was constrained to travel a *net* distance, d, in a finite amount of time, T. The model is assumed to have a linear spring, k, and a linear viscous damper, b.

Results and Discussion:

No details are shown on how the results were obtained. After a system's set of differential equations and boundary conditions are defined, only the model's final set of equations, simulations, and discussion are presented. *Mathematica*™, an algebraic software package, was employed to expedite the process of finding solutions for a system's set of differential equations and for plotting the final simulation results [40]. A value of one was assigned to all constants used in the simulations *except for the damping coefficient, b.* The damping coeffi-

Table 7.1 Variable Definitions

Variable	Symbol	Definition
Time Ratio	τ	t/T
Average Velocity	v_{ave}	d/T
Average Acceleration	a_{ave}	d/T^2
Average Jerk	j_{ave}	d/T^3
Natural Frequency	ω_n	$\sqrt{k/m}$
Damping Ratio	ζ	$b/2\sqrt{1/km}$

cient was assigned a value of two so that the system would be critically damped (i.e., the system's damping ratio was one).

7.3 MINIMIZING TIME DERIVATIVES

Before optimizing power absorption for the mechanical model, it will be informative to understand some of the characteristics found when one tries to minimize the time derivative of an integrand. The general results obtained will be useful for the forthcoming discussions.

Constraint Relations:

Assume the existence of an integrand, N, which is a function of time. The constraint relations are:

$$\dot{N}(t) = u(t)$$

$$\dot{I}(t) = N(t)$$

Performance Index:

In a finite time, T, the integral, I, of the integrand may or may not change by a finite value. Over the given time span, it is desired that the time derivative of the integrand be minimum. Thus, the performance index becomes:

$$J = \int_0^T u^2 \, dt$$

where

$$L = u^2$$

Lagrange Multipliers:

$$\Lambda^T(t) = [\lambda_N(t) \quad \lambda_I(t)]$$

Partial Derivative Evaluations:

$$\frac{\partial L}{\partial \mathbf{x}} = \begin{bmatrix} \frac{\partial L}{\partial N} & \frac{\partial L}{\partial I} \end{bmatrix} = \begin{bmatrix} 0 & 0 \end{bmatrix}$$

$$\frac{\partial L}{\partial \mathbf{u}} = \frac{\partial L}{\partial u} = 2u$$

$$\frac{\partial \dot{\mathbf{x}}}{\partial \mathbf{x}} = \begin{bmatrix} \frac{\partial \dot{N}}{\partial N} & \frac{\partial \dot{N}}{\partial I} \\ \frac{\partial \dot{I}}{\partial N} & \frac{\partial \dot{I}}{\partial I} \end{bmatrix} = \begin{bmatrix} 0 & 0 \\ 1 & 0 \end{bmatrix}$$

$$\frac{\partial \dot{\mathbf{x}}}{\partial \mathbf{u}} = \begin{bmatrix} \frac{\partial \dot{N}}{\partial u} & \frac{\partial \dot{I}}{\partial u} \end{bmatrix}^T = \begin{bmatrix} 1 & 0 \end{bmatrix}^T$$

Euler-Lagrange Equations:

$$\dot{\lambda}_N = -\lambda_I$$

$$\dot{\lambda}_I = 0$$

$$0 = 2u + \lambda_N$$

Boundary Conditions:

The general characteristics of interest will be independent of the chosen boundary conditions. For this reason, no specific boundary conditions will be listed.

Minimization Results:

$$u = 6\alpha t + 2\beta$$

$$N = 3\alpha t^2 + 2\beta t + \gamma$$

$$I = \alpha t^3 + \beta t^2 + \gamma t + \delta$$

where α, β, γ, and δ are constants that depend on the boundary conditions.

Discussion:

Minimizing the integrand's time derivative results in an *integrand* that is *quadratic* and a *time derivative* that is *linear* with respect to time. This result is independent of the system's boundary conditions and is true for any set of functions that display the above constraint relationships.

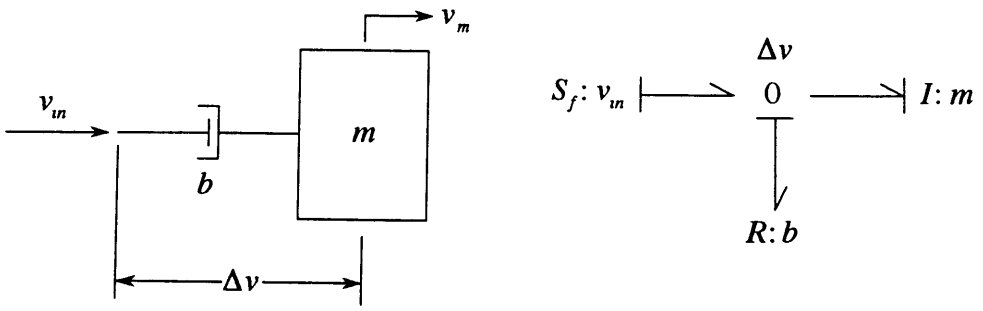

Mass-Damper Model Bond Graph

Figure 7.1 Mass-Damper Model and Bond Graph

7.4 MASS-DAMPER MODEL

Some of the results that will be obtained from the complete mass-spring-damper model are counterintuitive. To help explain these results, it will be useful to observe the behavior of the mechanical model when only the spring or the damper participates in the task. The first model to be analyzed is the mass-damper model. The model and bond graph are shown in Figure 7.1.

Constraint Relations:

$$\dot{v}_m = \left(\frac{b}{m}\right)(v_{in} - v_m) = \left(\frac{b}{m}\right)\Delta v$$

$$\dot{x}_m = v_m$$

Performance Index:

It is desired to minimize the power absorbed in the damper as the task is being performed. For a linear viscous damper, the power absorbed is

$$P_b = F_b v_b = b(\Delta v)^2$$

The performance index becomes

$$J = \int_0^T b(\Delta v)^2 \, dt$$

where

$$L = b(\Delta v)^2$$

Lagrange Multipliers:

$$\Lambda^T(t) = [\lambda_{v_m}(t) \quad \lambda_{x_m}(t)]$$

Partial Derivative Evaluations:

$$\frac{\partial L}{\partial \mathbf{x}} = \begin{bmatrix} \frac{\partial L}{\partial v_m} & \frac{\partial L}{\partial x_m} \end{bmatrix} = [0 \quad 0]$$

$$\frac{\partial L}{\partial \mathbf{u}} = \frac{\partial L}{\partial \Delta v} = 2b(\Delta v)$$

$$\frac{\partial \dot{\mathbf{x}}}{\partial \mathbf{x}} = \begin{bmatrix} \frac{\partial \dot{v}_m}{\partial v_m} & \frac{\partial \dot{v}_m}{\partial x_m} \\ \frac{\partial \dot{x}_m}{\partial v_m} & \frac{\partial \dot{x}_m}{\partial x_m} \end{bmatrix} = \begin{bmatrix} 0 & 0 \\ 1 & 0 \end{bmatrix}$$

$$\frac{\partial \dot{\mathbf{x}}}{\partial \mathbf{u}} = \begin{bmatrix} \frac{\partial \dot{v}_m}{\partial \Delta v} & \frac{\partial \dot{x}_m}{\partial \Delta v} \end{bmatrix}^T = \begin{bmatrix} \frac{b}{m} & 0 \end{bmatrix}^T$$

Euler-Lagrange Equations:

$$\dot{\lambda}_{v_m} = -\lambda_{x_m}$$

$$\dot{\lambda}_{x_m} = 0$$

$$0 = 2(\Delta v) + \left(\frac{1}{m}\right)\lambda_{v_m}$$

Table 7.2 Mass-Damper Boundary Conditions

Initial Conditions	Final Conditions	
$v_m(0) = 0$	$v_m(T) = 0$	$\lambda_{v_m}(T) = c_{v_m}$
$x_m(0) = 0$	$x_m(T) = d$	$\lambda_{x_m}(T) = c_{x_m}$

Mass-Damper Results:

Table 7.2 lists the boundary conditions used for the mass-damper model. Table 7.3 lists the equations obtained from minimizing the task's power dissipation for the model. Figure 7.2 shows the simulation results.

Discussion:

Unlike the mass trajectory equations found for a mass-spring-damper responding to a step input in displacement, the minimization results reveal that the mass-damper's trajectory equations are not dependent on the values chosen for the mass and damper coefficients. At

Table 7.3 Mass-Damper Minimization Results

TRAJECTORY EQUATIONS

$$x_m(t) = d\left(3\tau^2 - 2\tau^3\right)$$
$$v_m(t) = v_{ave}\left(6\tau - 6\tau^2\right)$$
$$a_m(t) = a_{ave}(6 - 12\tau)$$
$$j_m(t) = -12 j_{ave}$$

RELATIVE EQUATIONS

$$\Delta x(t) = d\left(\frac{6m}{bT}\right)\left(\tau - \tau^2\right)$$
$$\Delta v(t) = v_{ave}\left(\frac{6m}{bT}\right)(1 - 2\tau)$$
$$\Delta a(t) = -a_{ave}\left(\frac{12m}{bT}\right)$$
$$\Delta j(t) = 0$$

INPUT EQUATIONS

$$x(t) = d\left[\left(\frac{6m}{bT}\right)\left(\tau - \tau^2\right) + \left(3\tau^2 - 2\tau^3\right)\right]$$
$$v(t) = v_{ave}\left[\left(\frac{6m}{bT}\right)(1 - 2\tau) + \left(6\tau - 6\tau^2\right)\right]$$

$\tau = 1/2$, the mass will always be at a position of $d/2$ with a maximum velocity of $1.5 v_{ave}$ and zero acceleration. At $\tau = 1$ the mass fulfills the final boundary conditions by traveling a distance d and having zero velocity. The relative equations are dependent of the mass and damper values chosen. As expected, the input equations are the summation of the relative and trajectory equations.

The optimization results show that minimizing the power absorbed by the damper also minimizes the damper's relative position time derivative, the relative velocity, and the mass's

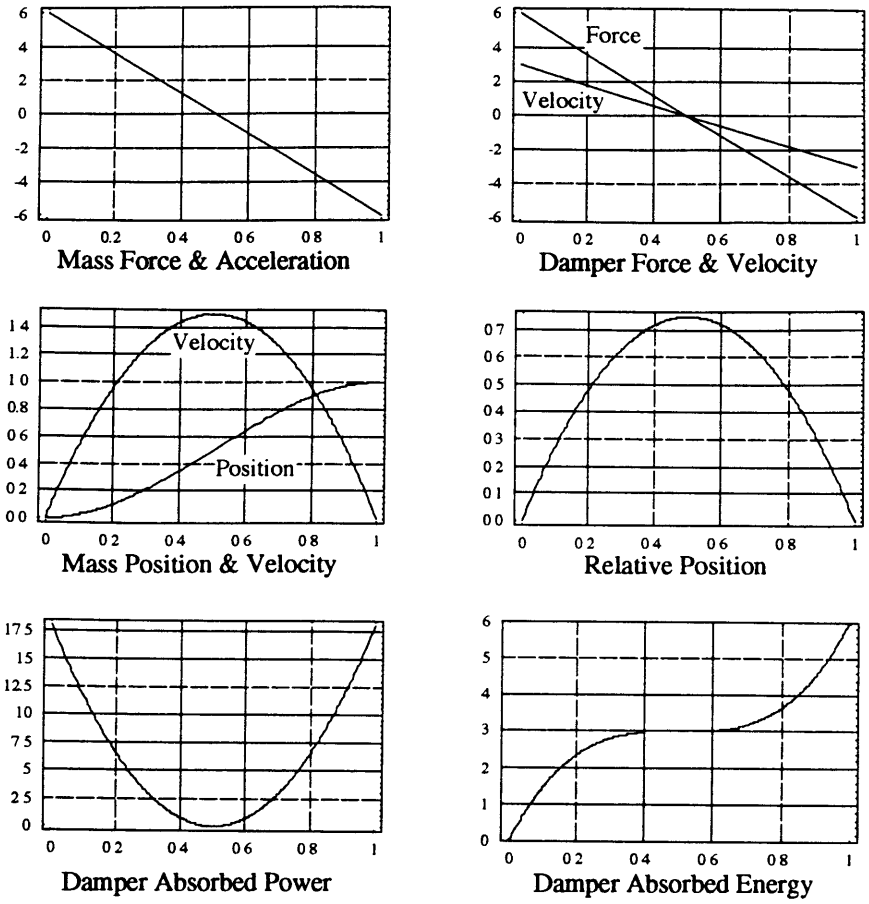

Figure 7.2 Mass-Damper Simulations

velocity time derivative, the mass acceleration. All minimizations are not mutually exclusive. The relative velocity is minimized because of the proportional relationship that exists between the damper's power absorption and the system's relative velocity squared. Mass acceleration is minimized because of the proportional relationship that exists between the damper's relative velocity and the force applied to the mass. Under proportional relationships, minimizing one variable will minimize the second. Instead of minimizing power dissipation, the performance index could have been defined to minimize relative velocity and the results would have been identical:

$$J = \int_0^T (\Delta v)^2 \, dt$$

The independence of parameter values found in the trajectory equations is also a result of proportional relationships. Although power absorption is the *direct* variable being minimized, the proportional relationships *indirectly* minimize the mass's acceleration. Minimizing the

mass's acceleration as the mass travels a distance d in T seconds becomes a minimization problem that is independent of the forces used to accelerate the mass. Thus, the parameters that determine the interactive forces for the mass-damper system, specifically the mass value, m, and the damper value, b, are not required to describe the mass kinematics.

Since the trajectory equations are independent of the mass and damper values, the remaining equations must account for the missing parameters. The input and relative equations reflect this by having the mass parameter in the numerator and the damping parameter in the denominator. Increasing the mass requires higher forces and velocities to accelerate the mass in the same amount of time while increasing the damping permits the same level of forces to be applied at smaller velocities.

The description of the mass-damper simulations is straightforward. The force applied to the mass is equal to the damper force. Immediate compression of the damper permits a finite acceleration force to be applied to the mass despite the relative position of the damper being zero. The mass velocity increases while moving the mass closer to its final destination. At $\tau = 1/2$, *the damper is at maximum compression and does not apply any additional acceleration forces to the mass.* The mass velocity has reached a maximum value and the mass is half way to its final destination. After maximum compression, the damper begins to extend and decelerate the mass. At $\tau = 1$, the mass reaches its final destination with zero velocity and the damper's relative position returns to zero. During the entire task, the mass accelerates and decelerates once. Additional accelerations and decelerations are possible but this would result in excessive damper motion and additional power absorption.

It can be shown that the damper *must* return to its initial zero relative position if the final mass velocity is to be zero. Since the mass acceleration is proportional to the damper force,

$$a_m = \frac{F_b}{m} = \left(\frac{b}{m}\right)\Delta v$$

one can integrate this equation to show that the mass velocity is proportional to the damper's relative position:

$$v_m = \left(\frac{b}{m}\right)\Delta x$$

The trajectory and relative equations can be used to confirm the above equation. Thus, when the system starts from rest, *the only time the mass velocity will be zero is when the damper*

relative position is zero. This is true regardless of the task duration and the velocity input profile selected for the task.

This last result will have important consequences for the mass-spring-damper model to be discussed in Section 7.6. For the mass-damper model, all the energy transmitted to the mass by the damper during the first half of the simulation is *completely* removed by the damper during the second half of the simulation. *Any time the relative position of the damper is zero, the damper's net contribution to the mass's total kinetic energy must be zero.*

7.5 MASS-SPRING MODEL

Figure 7.3 shows the model and bond graph for the mass-spring system. The damper has been replaced by a linear spring.

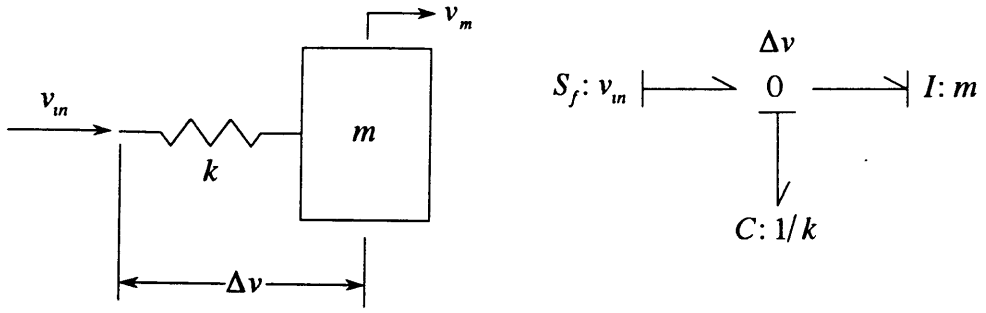

Mass-Spring Model Bond Graph

Figure 7.3 Mass-Spring Model and Bond Graph

Constraint Relations:

$$\dot{v}_m = \left(\frac{1}{m}\right) F_k$$

$$\dot{x}_m = v_m$$

$$\dot{F}_k = k\left(v_{in} - v_m\right) = k\,\Delta v$$

Performance Index

Without a damper, minimizing the system's power absorption becomes meaningless. However, the mass-damper model revealed that minimizing power absorption is equivalent to minimizing the square of the system's relative velocity. Since the spring will be in parallel with the damper in the complete mass-spring-damper model and will experience the same

relative velocities as the damper, a performance index that minimizes the relative velocity will be implemented for the mass-spring model. This index will preserve the initial intent of minimizing power absorption while permitting the spring characteristics to be analyzed separately.

$$J = \int_0^T (\Delta v)^2 \, dt \qquad \text{where} \qquad L = (\Delta v)^2$$

Lagrange Multipliers

$$\Lambda^T(t) = [\lambda_{v_m}(t) \quad \lambda_{x_m}(t) \quad \lambda_{F_k}(t)]$$

Partial Derivative Evaluations

$$\frac{\partial L}{\partial \mathbf{x}} = \left[\frac{\partial L}{\partial v_m} \quad \frac{\partial L}{\partial x_m} \quad \frac{\partial L}{\partial F_k}\right] = [0 \quad 0 \quad 0]$$

$$\frac{\partial L}{\partial \mathbf{u}} = \frac{\partial L}{\partial \Delta v} = 2(\Delta v)$$

$$\frac{\partial \dot{\mathbf{x}}}{\partial \mathbf{x}} = \begin{bmatrix} \frac{\partial \dot{v}_m}{\partial v_m} & \frac{\partial \dot{v}_m}{\partial x_m} & \frac{\partial \dot{v}_m}{\partial F_k} \\ \frac{\partial \dot{x}_m}{\partial v_m} & \frac{\partial \dot{x}_m}{\partial x_m} & \frac{\partial \dot{x}_m}{\partial F_k} \\ \frac{\partial \dot{F}_k}{\partial v_m} & \frac{\partial \dot{F}_k}{\partial x_m} & \frac{\partial \dot{F}_k}{\partial F_k} \end{bmatrix} = \begin{bmatrix} 0 & 0 & 1/m \\ 1 & 0 & 0 \\ 0 & 0 & 0 \end{bmatrix}$$

$$\frac{\partial \dot{\mathbf{x}}}{\partial \mathbf{u}} = \left[\frac{\partial \dot{v}_m}{\partial \Delta v} \quad \frac{\partial \dot{x}_m}{\partial \Delta v} \quad \frac{\partial \dot{F}_k}{\partial \Delta v}\right]^T = [0 \quad 0 \quad k]^T$$

Euler-Lagrange Equations

$$\dot{\lambda}_{v_m} = -\lambda_{x_m}$$

$$\dot{\lambda}_{x_m} = 0$$

$$\dot{\lambda}_{F_k} = -(1/m)\lambda_{v_m}$$

$$0 = 2(\Delta v) + k\lambda_{F_k}$$

Mass-Spring Results:

Table 7.4 lists the boundary conditions used for the mass-spring model. Table 7.5 lists the equations obtained from minimizing the task's power dissipation for the model. Figure 7.4 shows the simulation results.

Table 7.4 Mass-Spring Boundary Conditions		
Initial Conditions	**Final Conditions**	
$v_m(0) = 0$	$v_m(T) = 0$	$\lambda_{v_m}(T) = c_{v_m}$
$x_m(0) = 0$	$x_m(T) = d$	$\lambda_{x_m}(T) = c_{x_m}$
$F_k(0) = 0$	$F_k(T) = 0$	$\lambda_{F_k}(T) = c_{F_k}$

Discussion

Some of the results found for the mass-spring model are similar to those found for the mass-damper model: 1) the trajectory equations do not depend on the parameter values chosen for the mass and spring, 2) at $\tau = 1/2$, the mass will always be at a position of $d/2$ with a maximum velocity of $1.875 v_{ave}$ and zero acceleration, 3) at $\tau = 1$ the mass fulfills the final boundary conditions by traveling a distance d and having zero velocity, 4) the input equations are a summation of the relative and trajectory equations, 5) the mass accelerates and decelerates only once. Any additional accelerations or decelerations would produce excessive relative velocities and increase the performance index.

Because a proportional relationship exists between the relative velocity and the time rate of change of force applied to the mass, minimizing the relative velocity also minimizes the mass's jerk. The trajectory and relative equations in Table 7.5 show that the mass jerk and the relative velocity have parabolic profiles and their respective time derivatives are linear. Thus, while minimizing the relative velocity, the results from Section 7.3 reveal that the model's relative acceleration and the mass's *snap* have also been minimized. Looking back to the mass-damper equations in Table 7.3, it can be seen that the higher derivatives of the relative velocity and mass acceleration were minimized to a constant. The following observation can be made from the mass-damper and mass-spring results: Minimizing a task's power dissipation could constrain other system variables to being minimized. This observation, by itself, may explain why controllers that produced lower time derivatives in Chapter 5's experimental results were preferred by the amputees.

The lack of spring and mass parameters in the mass-spring trajectory equations is an indirect result of minimizing the mass's jerk. As in the mass-damper model, this indirect minimization decouples the trajectory equations from the forces required to obtain the mass time responses. The required forces are accounted for in the relative and input equations by having the mass parameter in the equations' numerators and the stiffness parameter in the denomina-

Table 7.5 Mass-Spring Minimization Results

TRAJECTORY EQUATIONS

$$x_m(t) = d\left(10\tau^3 - 15\tau^4 + 6\tau^5\right)$$

$$v_m(t) = 30v_{ave}\left(\tau^2 - 2\tau^3 + \tau^4\right)$$

$$a_m(t) = 60a_{ave}\left(\tau - 3\tau^2 + 2\tau^3\right)$$

$$j_m(t) = 60j_{ave}\left(1 - 6\tau + 6\tau^2\right)$$

RELATIVE EQUATIONS

$$\Delta x(t) = d\left(\frac{60}{T^2\omega_n^2}\right)\left(\tau - 3\tau^2 + 2\tau^3\right)$$

$$\Delta v(t) = v_{ave}\left(\frac{60}{T^2\omega_n^2}\right)\left(1 - 6\tau + 6\tau^2\right)$$

$$\Delta a(t) = a_{ave}\left(\frac{720}{T^2\omega_n^2}\right)\left(\tau - \frac{1}{2}\right)$$

$$\Delta j(t) = j_{ave}\left(\frac{720}{T^2\omega_n^2}\right)$$

INPUT EQUATIONS

$$x(t) = d\left[\left(10\tau^3 - 15\tau^4 + 6\tau^5\right) + \left(\frac{60}{T^2\omega_n^2}\right)\left(\tau - 3\tau^2 + 2\tau^3\right)\right]$$

$$v(t) = v_{ave}\left[30\left(\tau^2 - 2\tau^3 + \tau^4\right) + \left(\frac{60}{T^2\omega_n^2}\right)\left(1 - 6\tau + 6\tau^2\right)\right]$$

tors. Increasing the mass will necessitate higher changes in position to create higher spring forces. Increasing the spring stiffness will permit lower changes in position to create the same force profiles.

The mass-spring simulations show that the mass accelerates and decelerates once as it travels the distance *d*. The acceleration comes from the compressed spring during the first half of the

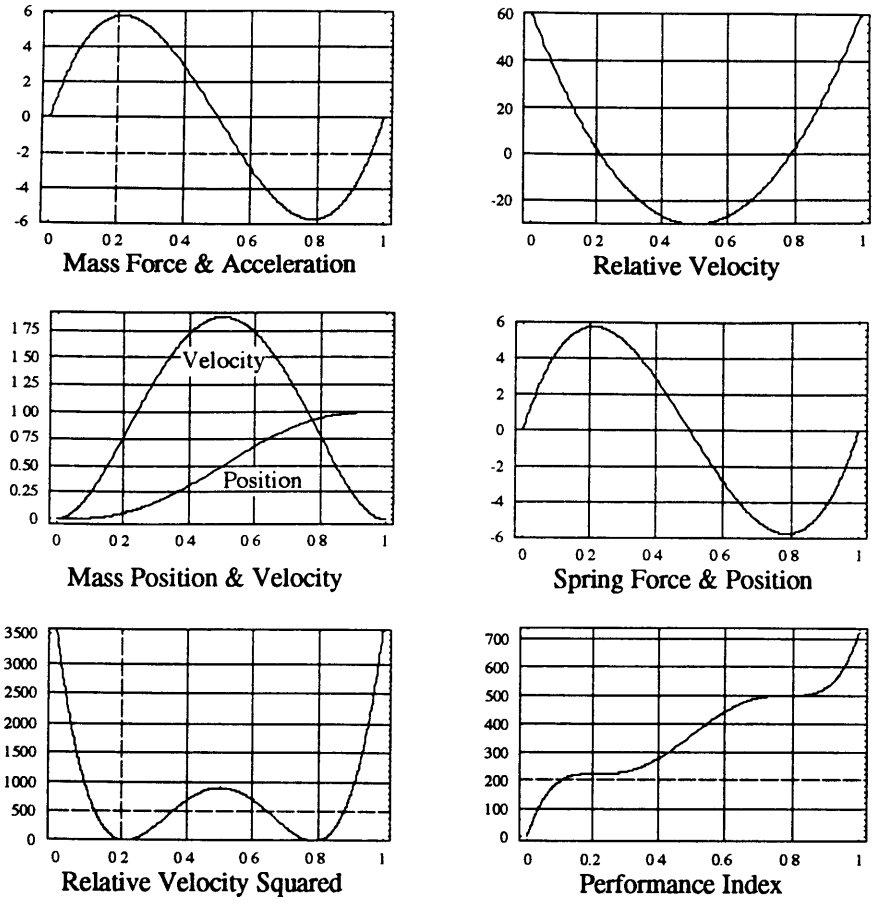

Figure 7.4 Mass-Spring Simulations

cycle as the spring adds energy to the mass; the deceleration occurs during the latter half of the cycle as the spring extends and removes energy from the mass. The mass's acceleration can be shown to be a function of the model's relative velocity:

$$a_m = \left(\frac{k}{m}\right)\int_0^T \Delta v \, dt$$

Integrating mass acceleration with respect to time, mass velocity becomes a function of the relative position:

$$v_m = \left(\frac{k}{m}\right)\int_0^T \Delta x \, dt$$

The above equation shows that *if the mass is to start and stop with zero velocity, the time integral of the spring's relative position must be zero.* Thus, the spring's contribution to the mass's total energy will only be zero when the time integral of the spring's compression pe-

riod (positive relative values) is equal to the time integral of its extension period (negative relative values). This constraint for starting and stopping the mass with zero velocity is more restrictive than the mass-damper's constraint; the mass-damper model only requires the damper's relative position to be zero. No constraints are put on the damper's relative position profile during the task.

In the upcoming mass-spring-damper model (Section 7.6), the spring and damper are in parallel with the mass and their respective energy contributions to the mass's total energy can be treated independently. If the mass is to start and stop with zero velocity for the mass-spring-damper system, both the spring's and damper's individual energy constraints must be satisfied despite any associated costs of dissipating energy. As Section 7.6 will show, satisfying both elements' constraints produce some unexpected results.

7.6 MASS-SPRING-DAMPER MODEL

The mass-damper and the mass-spring model results have shown some interesting relationships between the relative and trajectory equations. More importantly, the models have shown what characteristics the individual elements, the damper and the spring, must display if the task is going to be completed under the given boundary conditions. With what has been learned from the two models, the results that will be obtained from the complete mass-spring-damper model will be easier to understand. For convenience, the model and bond graph are repeated in Figure 7.5.

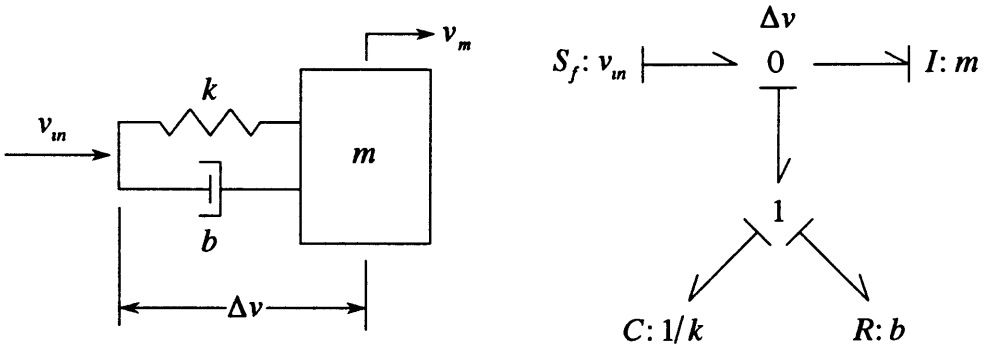

Mass-Spring-Damper Model Bond Graph

Figure 7.5 Mass-Spring-Damper Model and Bond Graph

Constraint Relations

$$\dot{v}_m = \left(\frac{1}{m}\right)F_k + \left(\frac{b}{m}\right)\Delta v$$
$$\dot{x}_m = v_m$$
$$\dot{F}_k = k\,\Delta v$$

Performance Index

Since the objective is to minimize the power absorbed by the damper, the mass-spring-damper model's performance index is the same as the mass-damper's index:

$$J = \int_0^T b(\Delta v)^2\,dt \qquad \text{where} \qquad L = b(\Delta v)^2$$

Defined Lagrange Multipliers

$$\Lambda^T(t) = [\lambda_{v_m}(t) \quad \lambda_{x_m}(t) \quad \lambda_{F_k}(t)]$$

Partial Derivative Evaluations

$$\frac{\partial L}{\partial \mathbf{x}} = \left[\frac{\partial L}{\partial v_m} \quad \frac{\partial L}{\partial x_m} \quad \frac{\partial L}{\partial F_k}\right] = [0 \quad 0 \quad 0]$$
$$\frac{\partial L}{\partial \mathbf{u}} = \frac{\partial L}{\partial \Delta v} = 2b(\Delta v)$$

$$\frac{\partial \dot{\mathbf{x}}}{\partial \mathbf{x}} = \begin{bmatrix} \frac{\partial \dot{v}_m}{\partial v_m} & \frac{\partial \dot{v}_m}{\partial x_m} & \frac{\partial \dot{v}_m}{\partial F_k} \\ \frac{\partial \dot{x}_m}{\partial v_m} & \frac{\partial \dot{x}_m}{\partial x_m} & \frac{\partial \dot{x}_m}{\partial F_k} \\ \frac{\partial \dot{F}_k}{\partial v_m} & \frac{\partial \dot{F}_k}{\partial x_m} & \frac{\partial \dot{F}_k}{\partial F_k} \end{bmatrix} = \begin{bmatrix} 0 & 0 & 1/m \\ 1 & 0 & 0 \\ 0 & 0 & 0 \end{bmatrix}$$

$$\frac{\partial \dot{\mathbf{x}}}{\partial \mathbf{u}} = \left[\frac{\partial \dot{v}_m}{\partial \Delta v} \quad \frac{\partial \dot{x}_m}{\partial \Delta v} \quad \frac{\partial \dot{F}_k}{\partial \Delta v}\right]^T = \left[b/m \quad 0 \quad k\right]^T$$

Euler-Lagrange Equations

$$\dot{\lambda}_{v_m} = -\lambda_{x_m}$$
$$\dot{\lambda}_{x_m} = 0$$
$$\dot{\lambda}_{F_k} = -\left(1/m\right)\lambda_{v_m}$$

$$0 = 2b(\Delta v) + \left(b/m\right)\lambda_{v_m} + k\lambda_{F_k}$$

Table 7.6 Mass-Spring-Damper Boundary Conditions		
Initial Conditions	**Final Conditions**	
$v_m(0) = 0$	$v_m(T) = 0$	$\lambda_{v_m}(T) = c_{v_m}$
$x_m(0) = 0$	$x_m(T) = d$	$\lambda_{x_m}(T) = c_{x_m}$
$F_k(0) = 0$	$F_k(T) = 0$	$\lambda_{F_k}(T) = c_{F_k}$

Mass-Spring-Damper Results:

Table 7.6 lists the boundary conditions used for the mass-spring-damper model. Table 7.7 lists the equations obtained from minimizing the task's power dissipation for the model. Figure 7.6 shows the simulation results.

Discussion

Figure 7.6 shows two unexpected results. First, in the process of achieving the defined boundary conditions, the mass *overshoots* its final destination. Second, the amount of energy absorbed by the damper is *240 times* the levels absorbed in the mass-damper simulations. With such counterintuitive results, is the optimization correct, and if it is, why does the mass overshoot and why is the level of power absorption so high?

To confirm the optimization results and to ensure that the equations produce a minimum solution, *Leibnitz's rule* can be used to take the derivative of the performance index with respect to the relative velocity [13]:

$$\frac{dJ}{d\Delta v} = 2b\int_0^T \Delta v\, dt = 2b\,\Delta x\Big|_0^T$$

Using the relative position equation obtained from the optimization results, it can be shown:

$$\frac{dJ}{d\Delta v} = 0$$

Thus, the optimization equations produce a *stationary* function. Taking the index's second derivative,

$$\frac{d^2J}{d\Delta v^2} = 2bT > 0$$

Since the second derivative is always positive, the optimization results prove to be the performance index's sole minimum.

Table 7.7 Mass-Spring-Damper Minimization Results

TRAJECTORY EQUATIONS

$$x_m(t) = d\left[\left(10\tau^3 - 15\tau^4 + 6\tau^5\right) + \left(\frac{60\zeta}{T\omega_n}\right)\left(\tau^2 - 2\tau^3 + \tau^4\right)\right]$$

$$v_m(t) = v_{ave}\left[30\left(\tau^2 - 2\tau^3 + \tau^4\right) + \left(\frac{120\zeta}{T\omega_n}\right)\left(\tau - 3\tau^2 + 2\tau^3\right)\right]$$

$$F_k(t) = 60(ma_{ave})\left(\tau - 3\tau^2 + 2\tau^3\right)$$

RELATIVE EQUATIONS

$$\Delta x(t) = d\left(\frac{60}{T^2\omega_n^2}\right)\left(\tau - 3\tau^2 + 2\tau^3\right)$$

$$\Delta v(t) = v_{ave}\left(\frac{60}{T^2\omega_n^2}\right)\left(1 - 6\tau + 6\tau^2\right)$$

$$\Delta a(t) = a_{ave}\left(\frac{720}{T^2\omega_n^2}\right)\left(\tau - \frac{1}{2}\right)$$

$$\Delta j(t) = j_{ave}\left(\frac{720}{T^2\omega_n^2}\right)$$

INPUT EQUATIONS

$$x(t) = d\left[\left(10\tau^3 - 15\tau^4 + 6\tau^5\right) + \left(\frac{60}{T^2\omega_n^2}\right)\left(\tau - 3\tau^2 + 2\tau^3\right) + \left(\frac{60\zeta}{T\omega_n}\right)\left(\tau^2 - 2\tau^3 + \tau^4\right)\right]$$

$$v(t) = v_{ave}\left[30\left(\tau^2 - 2\tau^3 + \tau^4\right) + \left(\frac{60}{T^2\omega_n^2}\right)\left(1 - 6\tau + 6\tau^2\right) + \left(\frac{120\zeta}{T\omega_n}\right)\left(\tau - 3\tau^2 + 2\tau^3\right)\right]$$

Why does the mass overshoot its final destination? This question can be answered by looking at the system's boundary conditions and the individual characteristics of the spring and damper. The system's boundary conditions require the mass to start and end with zero velocity (i.e., zero kinetic energy). Because the spring and damper are linear elements connected in

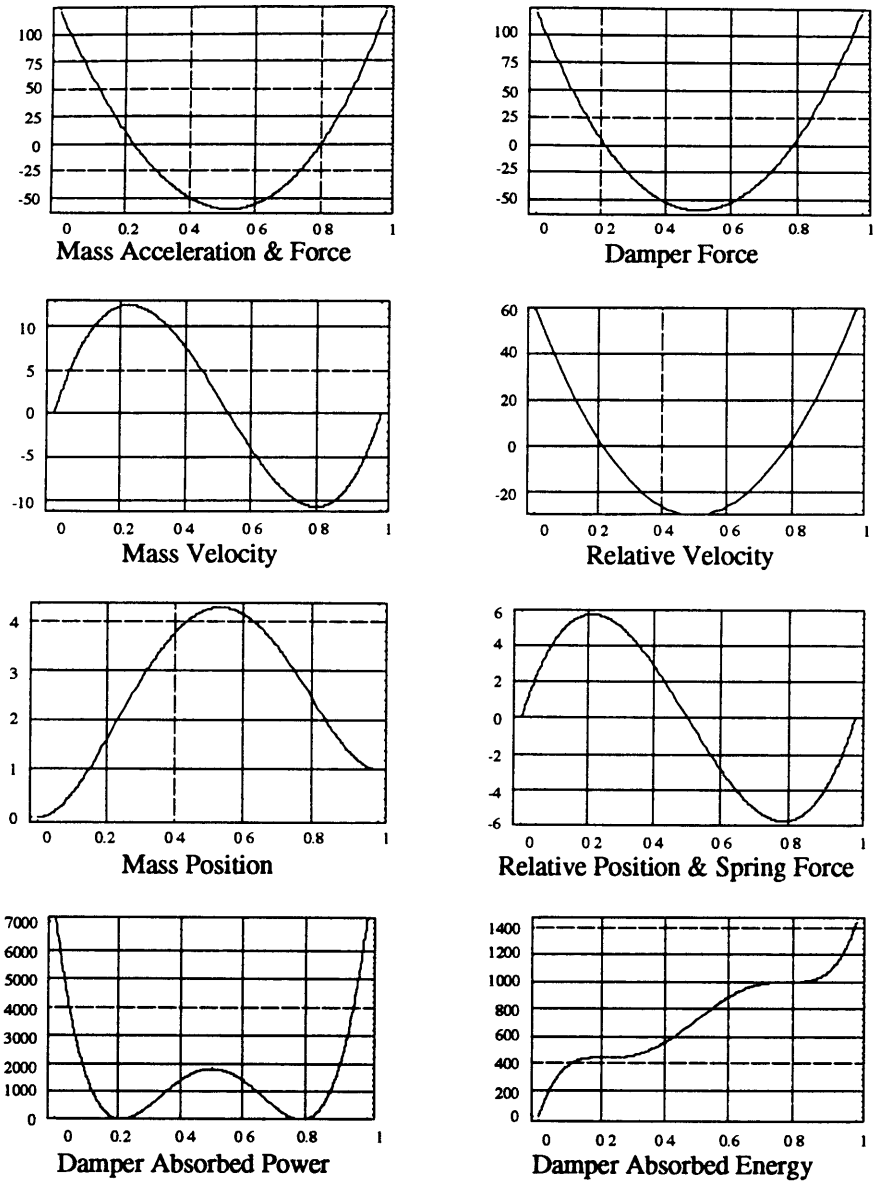

Figure 7.6 Mass-Spring-Damper Simulations

parallel to the mass, the principle of superposition can be used to describe each element's contribution to the mass's total energy.

$$E_{m_{total}} = E_{m_{damper}} + E_{m_{spring}}$$

Written in terms of kinetic co-energy, the spring and damper can be thought of as contributing to the mass's total velocity:

$$v^2_{m_{total}} = v^2_{m_{damper}} + v^2_{m_{spring}}$$

The mass-damper model in Section 7.4 showed that the damper's net energy contribution to the mass will only be zero when the system's relative position is zero. A non-zero relative position will always produce a mass with finite velocity. Thus, one constraint for the mass-spring-damper model is for the system to start and stop with zero relative position if the mass is to have a zero net velocity contribution from the damper. The mass-spring model in Section 7.5 showed that the integral of the system's relative position profile must be zero if the spring's net energy contribution to the mass is to be zero. This constraint forces the relative position profile of the mass-spring-damper model to contain at least one period of positive relative position values followed by a zero crossing and then one period of negative relative position values. Notice that satisfying the zero boundary conditions for the spring automatically satisfies the damper's energy transfer constraints. Starting and stopping the task with zero spring force (zero relative position) ensures that the damper's net energy contribution to the mass is zero.

During the task, the spring's zero integral constraint (see Section 7.5),

$$v_{m_{spring}} = \left(\frac{k}{m}\right)\int_0^T \Delta x \, dt = 0$$

requires the damper to pass through one cycle of positive relative positions (like those required to displace the mass in the mass-damper model) and then one cycle of negative relative positions (not necessary in the mass-damper model). In fact, satisfying the spring's zero integral constraint for producing zero mass velocity indirectly makes the damper's contribution to the mass's net displacement in the mass-spring-damper model zero. This is easily shown by integrating the damper's contribution to the mass's velocity:

$$v_{m_{damper}} = \left(\frac{b}{m}\right)\Delta x$$

$$x_{m_{damper}} = \left(\frac{b}{m}\right)\int_0^T \Delta x \, dt = 0$$

Thus, the spring contributes to *all* the mass's *net* displacement, d, in the mass-spring-damper model. The damper's *net* contribution in moving the mass the distance d in time T is *zero*.

Although the damper does not contribute to the mass's *net* displacement, the damper can play a major role in moving the mass *during* the task. Figure 7.7 shows the contributions of the spring and damper towards the mass's overall position. The contributions were calculated using the relative position equation, Δx, listed in Table 7.7 and the following integrals:

$$x_{m_{damper}}(t) = \left(\frac{b}{m}\right)\int \Delta x \, dt$$

$$x_{m_{spring}}(t) = \left(\frac{k}{m}\right)\iint \Delta x \, dt$$

It can be shown that the sum of the integrals is equivalent to the mass position trajectory equation listed in Table 7.7.

$$x_{m_{damper}}(t) + x_{m_{spring}}(t) = x_m(t)$$

As can be seen from the plot, the damper contributes significantly to the mass's position during the task and is the sole element responsible for the mass's overshoot. The spring's contribution to the mass's position is identical to the results obtained from the mass-spring simulations.

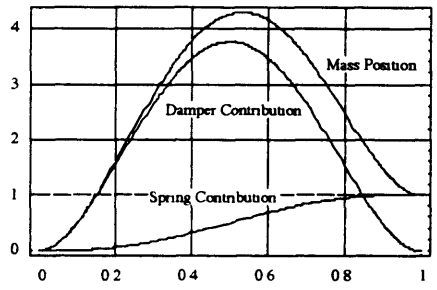

Figure 7.7 Mass Position Contributions

The relative contributions made by each element to the mass's overall position will depend on the values selected for the spring and damper. *As the damping ratio increases, the mass's overshoot will increase.* As the damping ratio decreases, the mass-spring-damper results will approach the mass-spring model results. Regardless of the size of the damping ratio, there will always be one overshoot. The overshoot is a consequence of the damper constrained to the spring's requirements for satisfying the system's boundary conditions. Overshoot will only be absent when either the spring or damper are missing.

With the damper providing zero contribution to the task's final displacement, the power absorbed by the damper becomes dictated by the parameter values chosen for the spring. Figure 7.8 shows the levels of energy absorbed by the damper at task completion for different values of spring stiffness. For stiff springs, very little energy is absorbed by the damper since small changes in relative position and velocity will create the forces necessary to move the mass. The mass overshoot will be very small. As the spring stiffness becomes smaller, larger

changes in relative position and velocity are required to create the appropriate spring forces necessary to move the mass a given distance in a fixed amount of time. This indirectly creates higher levels of power dissipation and increased overshoot. Very small spring stiffnesses will produce very high levels of power dissipation. The levels of power dissipation are unavoidable *if* the system's boundary conditions are to be satisfied.

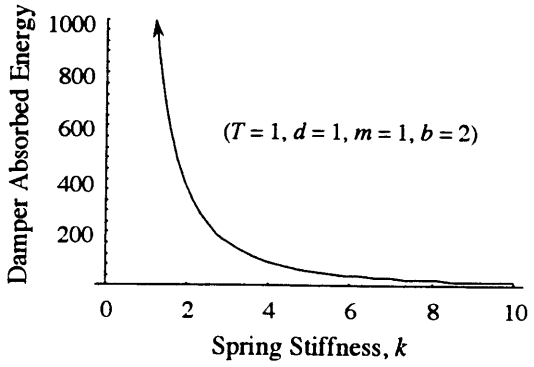

Figure 7.8 Absorbed Energy Versus Spring Stiffness

The concept of *increasing* a system's *damping* to *increase overshoot* is not an expected occurrence for most simple second-order systems. The primary difference between the "typical" mass-spring-damper system, which has the parallel spring and damper attached to a fixed reference frame rather than a velocity input, and the model presented are the system's boundary conditions. The normal step response to a critically damped (or overdamped) second-order system (relative to a fixed reference frame) is a mass displacement with no overshoot. However, the initial boundary conditions for the system are usually a mass with a zero velocity and a spring that is compressed. The system does not overshoot because the energy stored in the spring is completely absorbed by the damper by the time the mass reaches its final position. In the second-order model presented, the system starts at rest with no stored energy in the spring or the mass. A step input to the system compresses the spring but it also provides a force impulse to the mass because of the infinite velocity experienced by the damper. The system contains both potential energy in the form of a compressed spring and kinetic energy in the form of mass velocity. To achieve the system's final boundary conditions while minimizing the task's power absorption requires the damper to absorb *all* the system's stored energy in a fixed amount of time. This, as the optimization results show, will always produce one overshoot in mass position regardless of the damping ratio.

7.7 CONCLUSIONS

The purpose of this chapter was to investigate the possibility that humans minimize power dissipation while performing tasks. As part of the investigation, a simple mass-spring-damper model was developed and analyzed to perform a task. The task was to move the mass, using the spring and damper in parallel, a given distance in a fixed amount of time while minimizing the system's power dissipation.

An intriguing result develops when the damping ratio in the mass-spring-damper model's mass position equation approaches zero (Table 7.7). At a damping ratio of zero, the equation becomes:

$$x_m(t) = d\left(10\tau^3 - 15\tau^4 + 6\tau^5\right)$$

This equation is equivalent to the minimum jerk model developed by Flash and Hogan to successfully predict both the qualitative features and the quantitative details observed experimentally in planar, multijoint arm movements [12]. To make the coincidence in equations even more compelling, Flash and Hogan's experimental results occasionally show humans making a slight overshoot as their arm approaches the final destination. While this overshoot can not be predicted with Flash and Hogan's model, it can be predicted with the minimum power model. Minimum power dissipation may be an underlying reason for performing tasks in a minimum jerk fashion. The preliminary results are at least promising.

The experimental results in Chapter 5 showed that subjects did not prefer controllers that produced rapid power transitions. The rapid transitions were often the result of sudden changes in relative velocity or torque between the upper arm and the prosthesis. Chapter 7's minimum power dissipation simulations show that rapid changes in relative velocity during a task can produce unnecessary damper forces and higher levels of power dissipation. These results would suggest that the subjects preferred controllers that minimized power dissipation during the task. While there is no strong evidence supporting this claim, there is no reason to refute it based on Chapter 7's results. Minimizing power dissipation still has to be considered a possible motive during task performance.

At first passing, minimizing power dissipation does not appear to explain why the elbow power measurement in Chapter 5's experiments has been such an informative variable. In practice, measuring power dissipation for a task only requires one kinematic measurement – a joint's relative velocity. Total power dissipation of a system could be inferred from measuring the relative velocities of each of the system's dissipative joints, and then taking the

weighted sum of the joint velocities squared (assuming linear dampers). Minimum power dissipation would produce the lowest summation. Notice that minimizing the system's summation is not the same as minimizing the power dissipation at each joint. An individual joint could be very inefficient throughout the task as long as the other system joints compensated for the incurred losses. Under such situations, *synergistic coordination* can play a vital role in minimizing total energy losses.

There are many situations where the desired kinematic quantity can not be measured. Under such conditions, it may still be possible to indirectly infer the measurement. While a kinematic measurement can be the ideal variable for direct quantification of a joint, the same variable can be futile in indirectly measuring quantities from adjacent joints. Figure 7.9 illustrates this in a simple example.

Figure 7.9 shows one joint from a system consisting of a series of mass-spring-damper joints. The joint contains three elements: an active force source, F, a spring, and a damper. Each element experiences the same relative joint velocity, v. The relative joint velocity, v, is the only variable being measured. For simplicity, the series of adjacent elements attached to the shown masses are represented by the external forces, F_1 and F_2. For measuring the power absorption of the damper at the joint shown, measuring the joint's relative velocity, v, is sufficient. When the relative velocity is minimized, one knows that the joint's power absorption will also be minimized. On the other hand, a velocity sensor's ability to measure the efficiencies of the adjacent joints is limited. To take an extreme example, suppose that Figure 7.9's force source, F, is able to perfectly counter the effects of very erratic external forces, F_1 and F_2. Figure 7.9's relative joint velocity, v, will remain zero while the fluctuating external forces will drive large amounts of energy into the mass's adjacent dampers not shown. The joint shown in Figure 8.9 will measure zero power dissipation even though the adjacent joints are suffering tremendous power losses. Unless the adjacent joints have velocity sensors, the total losses of the entire system will be greatly underestimated.

A sensor that could indirectly measure a joint's adjacent power losses from the external forces F_1 and F_2 is a force sensor at the shown joint. This *dynamic* sensor would be able to

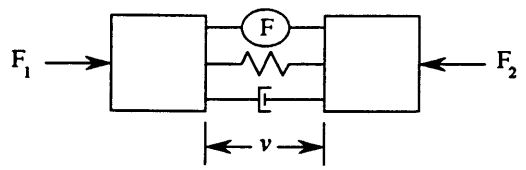

Figure 7.9 Limitations of Kinematic Measurements

measure the high external force fluctuations even though its own joint may show a zero relative velocity. Interestingly enough, while the force sensor is useful for indirect measurement of adjacent efficiencies, the sensor is limited in direct measurement of efficiencies at its own joint. The previous simulations demonstrated that a zero force measurement does not imply zero power absorption. The *kinematic* measurement from the velocity sensor still excels as the best measurement for monitoring power loss at the particular joint in question.

The velocity and force sensors are capable of complementing each other at any particular joint. When the number and location of velocity sensors are limited for a system, a joint that combines a force and velocity sensor can provide information on the joint to which the sensor is attached and of the neighboring joints by revealing how well the joints are coordinating to minimize the overall power absorption of the task. Indeed, the above conclusions may very well explain why the power variable, which combines a joint's velocity and force measurements, has been such an informative variable in Chapter 5's crank turning experiments.

Minimizing power flow is not the same as minimizing power absorption. When minimizing power flow, one is assigning a cost to the total amount of energy that is being transferred through a joint to complete a task. As stated in Chapter 6, the concern is not in the amount of energy being transferred between masses but *how* the energy is being transferred. This is why the time rate of change of power becomes so attractive. Using the definition of power,

$$P = Fv$$

the rate of change of power is

$$\frac{dP}{dt} = \dot{F}v + F\dot{v}$$

The rate of change of power accounts for sudden changes in forces or abrupt changes in velocities. Minimizing the terms that contain these variables may help minimize the inefficiencies at the power sensor's attached joint and the sensor's neighboring joints. It must be stressed that minimizing the rate of change of power is still not the same as minimizing power absorption. While minimizing power absorption has been the major thrust of the analysis, the results show that quantifying a complete system will require a kinematic sensor at every joint of interaction. Minimizing the rate of change of power helps reduce the number of required sensors while still stressing the importance of how energy is being transferred at the sensor's attached joint and how efficient the surrounding joints are coordinating in the transfer process. Unlike minimizing power flow, no penalty is incurred for transferring large amounts of energy when the rate of change of power is minimized as long as the rates of change of force and velocity are kept to a minimum.

CHAPTER
EIGHT

MINIMIZING ENTROPY

8.1 INTRODUCTION

Chapter 6 presented two hypotheses regarding amputee task strategies and the amputee's preference for controllers that yielded lower rates of change of power during task performance. The first hypothesis was the minimum power hypothesis and the second hypothesis was the minimum entropy generation hypothesis. Chapter 6 also presented two models. The first model, the mechanical model, concentrated on the amount of power that was being dissipated by its damper as energy was transferred from the velocity source to the mass during task performance. Chapter 7 used the mechanical model to investigate the applicability of the minimum power dissipation hypothesis. The second model, the thermodynamic model, expanded on the mechanical model to include entropy generation as energy was transferred from the damper to the environment under non-isothermal conditions. This chapter uses the thermodynamic model to examine the second hypothesis, the minimum entropy hypothesis, and assess the probable usefulness and applicability of the hypothesis for modeling human task strategies.

Chapter 7 implemented calculus of variations to determine the optimal power dissipation profile for the mechanical model's damper during the performance of a task. The task was to move the mechanical model's mass (m) a distance (d) in a specified amount of time (T) with

an input velocity source (v_{in}). Unfortunately, the same technique could not be used to find the task's optimal entropy generation profile when the thermodynamic model was included. The difficulty lies in trying to solve the thermodynamic model's set of *nonlinear* differential equations *algebraically*. Mathematical software packages (Mathematica™, Maple™, and Theorist™) were employed to assist and expedite deriving a unique solution but no such solution was found. Despite the inability to find a general solution, several characteristics of the optimal solution were deduced by exploring the relationships among entropy generation, temperature, and power absorption. Sections 8.2 and 8.3 discuss these relationships.

8.2 CONSEQUENCES OF TEMPERATURE

In section 6.4, the state equation for the temperature of the damper was:

$$\dot{T}+\left(\frac{1}{RC}\right)T=\left(\frac{1}{C}\right)P+\left(\frac{1}{RC}\right)T_s$$

where R represents the damper's thermal resistance to the surrounding environment and C is the damper's heat capacitance. Essentially, the temperature of the damper is the output of the absorbed energy created by the input power, P, passing through a low pass filter.

As the temperature of the damper changes, heat transfer develops and the total entropy generated inside the thermodynamic model's control volume (Figure 6.5) is

$$S_{gen}=\int\frac{(T-T_s)^2}{RTT_s}\,dt$$

Making the substitution

$$T=T_s+\Delta T$$

the integral becomes

$$S_{gen}=\frac{1}{R}\int\frac{\Delta T^2}{T_s^2+T_s\Delta T}\,dt$$

Figure 8.1 shows plots of the entropy's integrand and the derivative of the integrand with respect to ΔT. The integrand is positive for *all* values of ΔT and closely approximates a parabola for the first 50 K. The integrand's derivative is always positive and *increasing for increasing values of* ΔT. This fact becomes important in Section 8.2.1's discussion. For both plots, the surrounding temperature was assumed to be 298.15 K (standard atmospheric conditions).

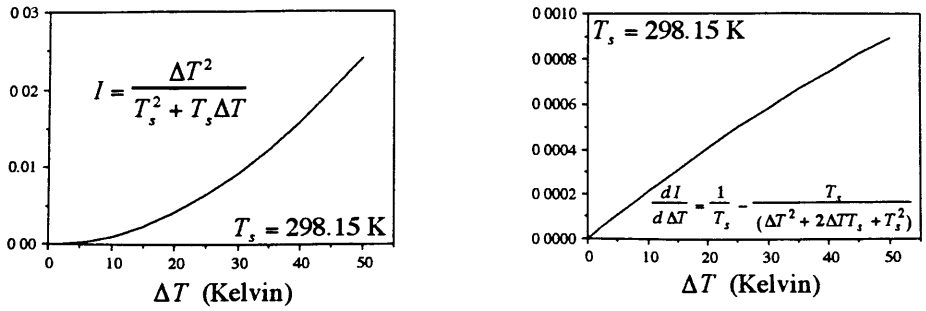

Integrand versus ΔT $\qquad$ $dI/d\Delta T$ versus ΔT

Figure 8.1 Entropy Generation with respect to ΔT

8.2.1 DISCUSSION

To understand the consequences of the integrand plots, a simple example of two possible heat transfer processes will be discussed for the thermodynamic model. Let's assume that in a fixed amount of time, say T seconds, a fixed amount of energy, E, must be transferred from the damper to the environment in the form of heat. Two possible time profiles of the energy transfer are shown in Figure 8.2.

Case 1 shows the energy being transferred at a constant damper temperature, T_0, and Case 2 shows the same amount of energy being transferred at two different temperatures, T_H and T_L which represent higher and lower temperatures relative to T_0. For Case 2, assume the change in temperature occurs at time $T/2$. For the same amount of energy to be transferred in the same amount of time, it can be shown that the following is true:

$$\Delta T_H = \Delta T_L$$

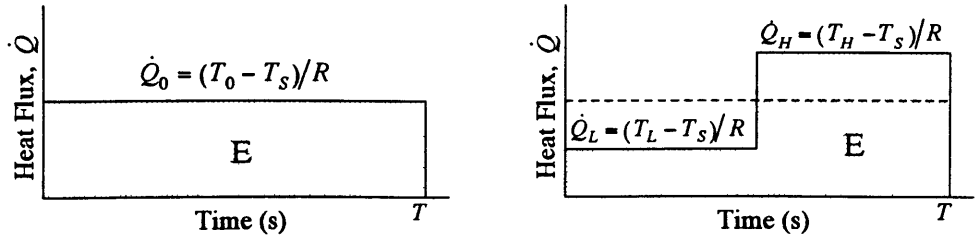

Case 1 $\qquad$ **Case 2**

Figure 8.2 Two Possible Heat Transfer Profiles

where

$$\Delta T_H = T_H - T_0$$
$$\Delta T_L = T_0 - T_L$$

Let's assume for the moment that the integrand is a linear function of the temperature difference:

$$I = m\Delta T$$

where m is the slope of the line. For Case 1, the entropy generated becomes

$$S_1 = \left(\frac{T}{R}\right) I_0$$

For Case 2,

$$S_2 = \left(\frac{1}{2}\right)\left(\frac{T}{R}\right)(2I_0 + \Delta I_H - \Delta I_L)$$

where

$$\Delta I_H = I_H - I_0$$
$$\Delta I_L = I_0 - I_L$$

The difference in entropy created is

$$S_2 - S_1 = \left(\frac{1}{2}\right)\left(\frac{T}{R}\right)(\Delta I_H - \Delta I_L)$$

However, since a linear relation exists between the integrand and the temperature difference and because the temperature differences for Case 2 must be equal if the same quantity of energy is to be transferred, the entropy difference becomes zero.

$$S_2 - S_1 = 0 \quad \text{(linear case)}$$

For the nonlinear case, the integrand plots show

$$\Delta I_H > \Delta I_L \qquad \forall\, \Delta T$$

$$\therefore \quad S_2 - S_1 > 0 \quad \text{(nonlinear case)}$$

The following conclusion can be drawn from the example: To minimize entropy generation for a given quantity of heat transferred in a fixed amount of time, the temperature difference, $T - T_s$, must be minimized during the entire process. In the example, Case 1 contains the

optimal temperature profile, a constant temperature difference, and permits the minimal amount of entropy to be generated.

Notice that the example does not assume a specific quantity of either energy or time. Thus, the values of time and energy can be arbitrary in size. In the limit, this permits a continuous, fluctuating temperature profile to be approximated as a series of discrete step changes in temperature. Smaller step changes in temperature for the same amount of heat transferred will result in less entropy generation. *For the continuous case with a fixed amount of heat to be transferred, minimizing entropy generation becomes synonymous to minimizing the temperature gradient* ***during*** *the heat transfer process.* The word "during" is stressed since step changes in temperature that produce infinite gradients are permissible just before and after the heat transfer process. The ideal situation is one of transferring the required amount of heat while using the smallest, single step-input temperature profile possible for the given time constraint.

8.3 CONSEQUENCES OF POWER ABSORPTION

Section 8.2 discussed the relationship between the temperature of the damper and the entropy generated. This section discusses the more complex relationship between the power absorbed by the damper and entropy generated. Making the substitution

$$T = T_s + \Delta T$$

the relationship between the power absorbed by the damper and the damper's temperature becomes

$$\Delta\dot{T} + \left(\frac{1}{RC}\right)\Delta T = \left(\frac{1}{C}\right)P$$

Given the first order relationship between power and temperature, one can see that higher power gradients can produce higher temperature gradients. It appears that if one minimizes the power gradient for a fixed amount of energy absorbed, one will also minimize the temperature gradient *and* the entropy generated for the system. It will be shown that *this statement is not necessarily true.* But first, it will be helpful to review a simple example that demonstrates the relations between absorbed power and entropy generation.

Figure 8.3 shows three examples of possible power input profiles for the damper. All three add the same amount of energy to the damper in the same amount of time. Case 1 maintains a

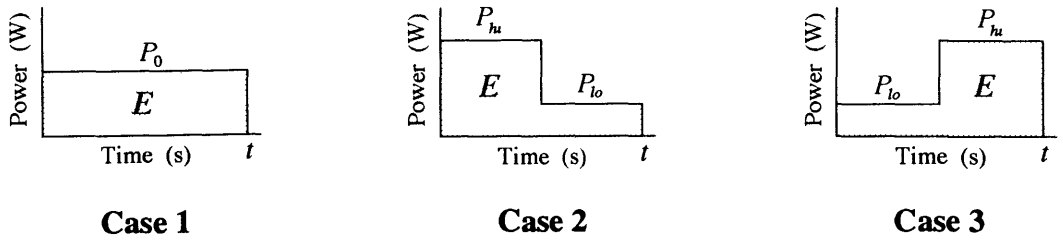

Figure 8.3 Three Possible Power Profiles

constant level of input power while Case 2 and Case 3 contain step decreases and increases respectively.

Figure 8.4 shows simulations (based on the thermodynamic model discussed in Section 6.4) of the temperature and entropy profiles for the respective power input profiles. All simulations transferred 100 Joules of energy in one time constant to the damper. Power transitions occurred at 0.5 time constants. The surrounding temperature was set to 298.15 K (standard atmospheric conditions). Table 8.1 ranks the entropy generation results for the three cases after each achieved stable equilibrium. Stable equilibrium was reached when the damper temperature returned to the surrounding temperature (roughly six time constants) and prevented additional entropy from being generated. A process that produced less entropy was ranked higher.

The damper's temperature profile for Case 1 shows the classic exponential rise and fall of a first order system to a step input:

$$\Delta T = PR\left(1 - e^{-(1/RC)t}\right)$$

The temperature peaks at 63.21 K in one time constant. Cases 2 and 3 show the fastest and slowest temperature rises because of their respective higher and lower initial levels of power absorption. At 0.5 time constants, Case 2's temperature drops while Case 3's temperature increases at a higher rate because of the relative changes in power. After one time constant, all temperatures show an exponential decay since no additional power is absorbed.

Table 8.1 reveals that after all cases have reached stable equilibrium, Case 1 generates the least entropy while Cases 2 and 3 generate essentially the same amount. The additional entropy generated by Cases 2 and 3 results from the higher temperature and/or temperature gradients created during the periods of higher power input.

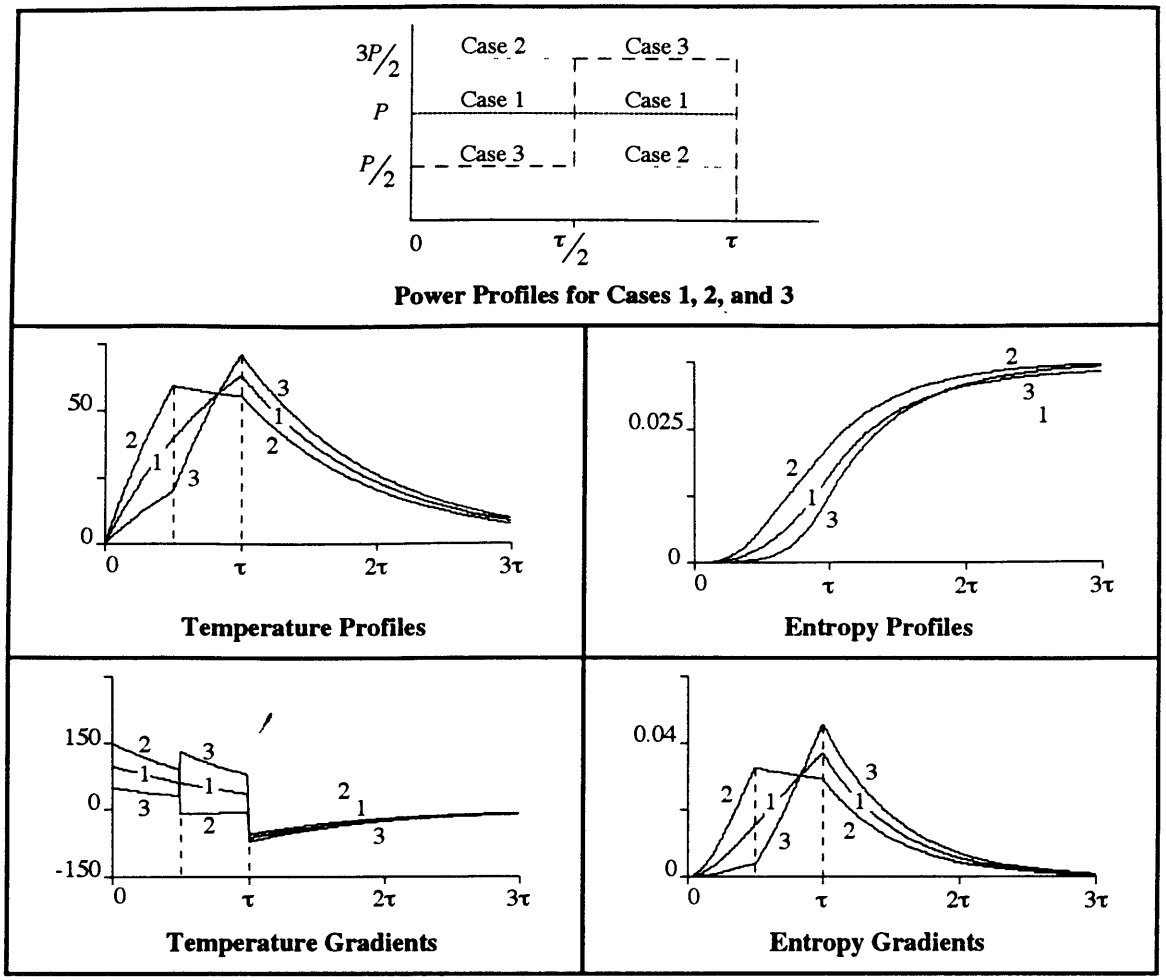

Figure 8.4 Simulation Results for Cases 1, 2, and 3

8.3.1 DISCUSSION

Three points are worth stressing from the example: 1) Case 1 proves to have the lowest entropy generation despite not having the lowest temperature peak. Overall, Case 2 produces the lowest temperature peak yet it creates the most entropy. 2) One must account for the en-

Table 8.1 Entropy Summary

Ranking	Case	Entropy Generated
Best	1	0.03595
	3	0.03700
Worst	2	0.03723

tropy generation of a system's *entire* thermodynamic process and not just the power absorption process. The thermodynamic process consists of starting and stopping at equivalent equilibrium states whereas the power absorption process ends after the first time constant. After the first time constant, Case 3 creates the least amount of entropy despite being the furthest from a stable equilibrium state. 3) After the first time constant, Case 2 has a lower temperature than Case 1 and produces less entropy for the remaining thermodynamic process. However, the overall entropy generation of Case 2 is higher than Case 1 because of Case 2's higher entropy generation levels during the first half of the power absorption process.

Case 1 produces the least entropy of the three cases by taking advantage of the nonlinear relations between temperature and entropy generation. The integrand plots (Figure 8.1) show that an increase in temperature generates a larger increase in entropy and its corresponding gradient. High temperature gradients at low temperatures have less of a cost associated with them than high gradients at high temperatures. Case 1's high temperature gradients occurring at low temperatures followed by low gradients occurring at higher temperatures enable it to produce the least entropy of the three cases. Case 2's high gradients during the initial phase of the power absorption process prove costly in the long run while Case 3's high temperatures occurring later in the thermodynamic process offset any advantages it gains from having low initial temperatures.

8.3.2 ADDITIONAL SIMULATIONS

Given a *fixed* amount of energy to be absorbed by the damper, what is the minimum or maximum entropy generation for the thermodynamic model? As previously mentioned, analytical solutions could not be found because of the system's nonlinearities. Since entropy is still generated after the power absorption process, the solution is not only a function of the input

Table 8.2 Power Inputs

Case	Power Curve (W)	Initial Temperature (K)
Case 4	$P = 50$	$\Delta T(0) = 50$
Case 5	$P = 600(t - t^2)$	$\Delta T(0) = 0$
Case 6	$P = 78.44$	$\Delta T(0) = 21.56$
Case 7	$P = 40 + 60t + 30t^2$	$\Delta T(0) = 20$
Case 8	$P = 0$	$\Delta T(0) = 100$

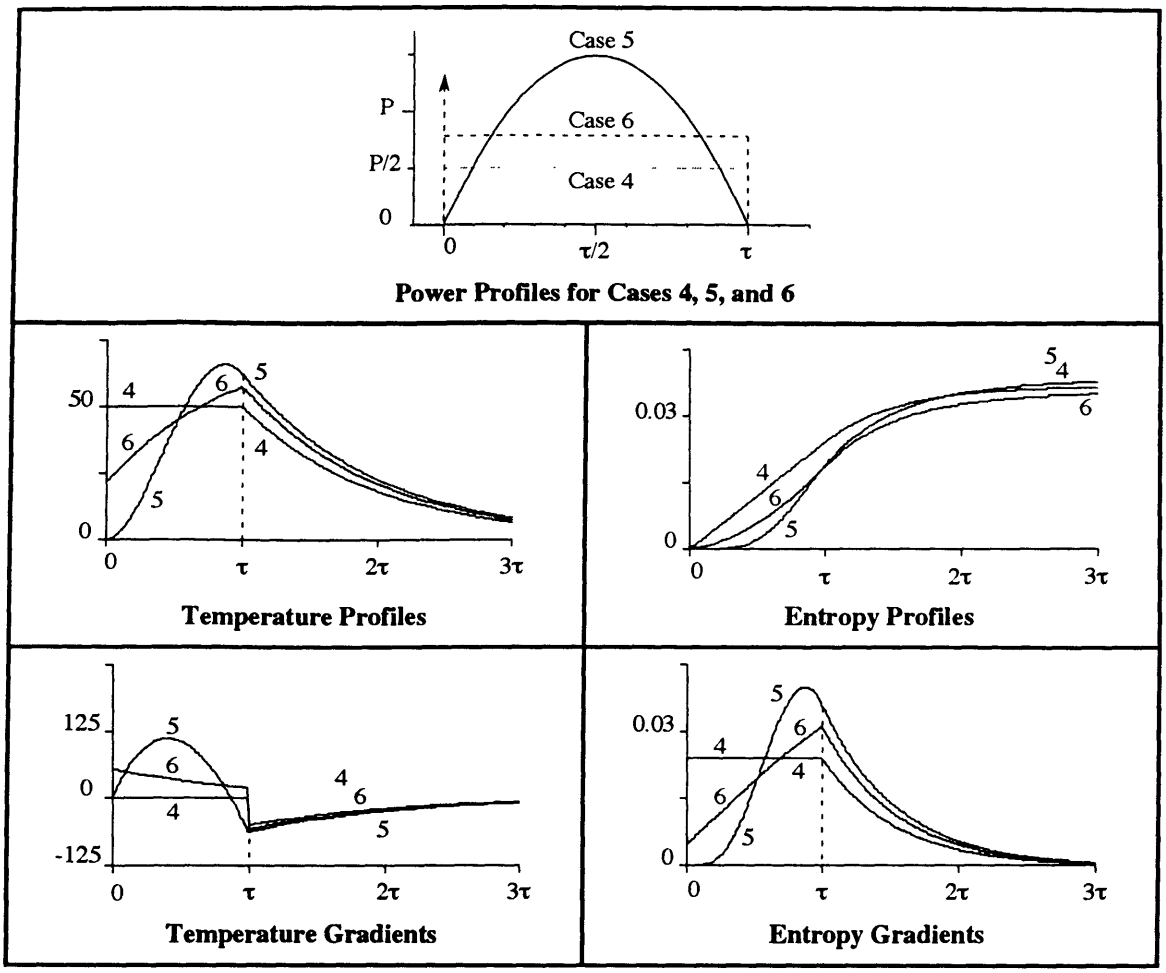

Figure 8.5 Simulation Results for Cases 4, 5, and 6

power but also a function of the model's method of transferring heat during the *entire* thermodynamic process. To see what characteristics the solutions may have, several additional simulations were performed using different power inputs. Figures 8.5 and 8.6 show five of the simulations. The power input and initial temperature used for each case is listed in Table 8.2. All parameter values were set equal to one.

Case 4 is the minimal temperature solution. That is, for a fixed amount of energy to be absorbed by the damper, Case 4 is the lowest temperature that the damper can sustain for the entire power absorption process. Case 4's power input consists of a 50 J impulse that instantly raises the temperature of the dissipator to a predetermined level of 50° and is immediately followed by a 50 W step input which maintains the temperature. For one second, Case 4's total energy absorption is 100 J. The case produces a useful temperature reference since any other power absorption process that produces temperatures lower (higher) than

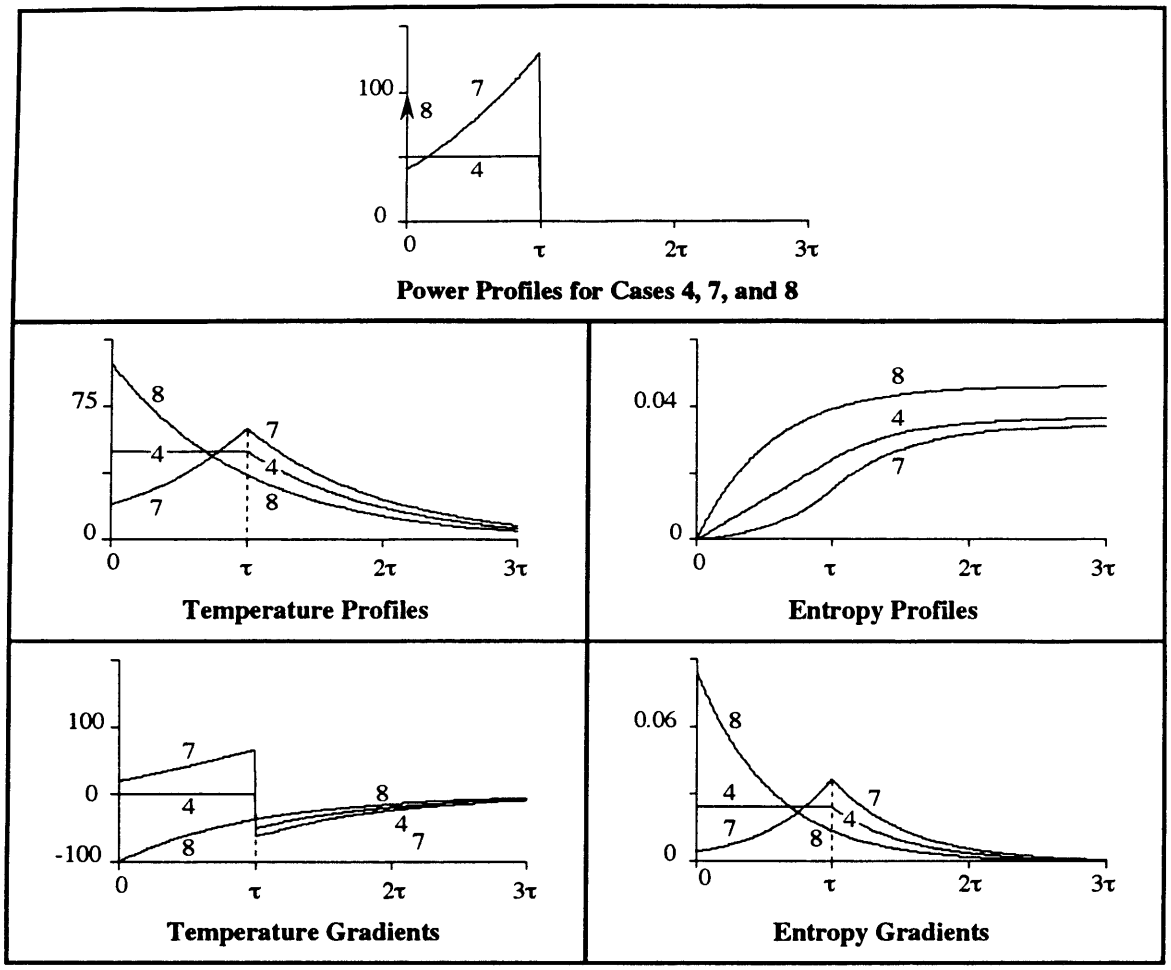

Figure 8.6 Simulation Results for Cases 4, 7, and 8

Case 4 must be accompanied by higher (lower) temperatures within the same power process if the same amount of energy is to be transferred in the same amount of time.

Case 5 shows a power input which transfers the same amount of energy while *minimizing the time derivative* of the absorbed power (Section 7.3). The entropy summary table, Table 8.3, reveals that Case 5 generates one of the highest levels of entropy. Case 6 shows the minimum entropy generation solution for a class of power processes that consist of an impulse followed by a step input. Case 6's power input consists of a 21.56 J impulse that instantly raises the temperature of the dissipator to a predetermined level of 21.56° and is immediately followed by a 78.44 W step input. For one second, Case 6's total energy absorption is 100 J. Using Case 4 as a reference, Case 6 demonstrates the tradeoff between having lower temperatures with high gradients and high temperatures with low gradients to obtain an optimal solution. It is interesting that Case 6's temperature gradient at t = 0 seconds is the negative of the gradi-

Table 8.3 Entropy Summary

Ranking	Case	Entropy Generated
Best	Case 7	0.0345
	Case 6	0.0351
	Case 1	0.0360
	Case 4	0.0368
	Case 3	0.0370
	Case 2	0.0372
	Case 5	0.0380
Worst	Case 8	0.0462

ent at $t = \tau$ seconds. Although no conclusions can be drawn from this fact, all simulations supported the following guideline: Entropy generation is reduced when the maximum temperature gradient produced during the power absorption process closely approximates the temperature gradient of the exponential decay function at $t = \tau$ sec.

The simulations uphold the argument that entropy generation will be minimized if the *power absorption process* minimizes the temperature gradient of the *entire thermodynamic process.* Unfortunately, the absorption process can only control a portion of thermodynamic process. Once the absorption process is complete, the damper's temperature gradient becomes a function of the current temperature (which acts as an initial condition), the intrinsic properties of the thermodynamic model, and the method of heat transfer. Under such conditions, two guidelines can be used to help minimize entropy. First, create an absorption process that possesses time constants that are much longer than the damper's thermodynamic time constant. This permits the absorption process to overlap and control a larger portion of the thermodynamic process. When the absorption process is complete, any additional entropy created from the remaining thermodynamic process will be minimal. In most instances, however, this is an impractical solution.

Second, match the *maximum* temperature gradient found in the thermodynamic process with those created in the absorption process. Case 6 is an example of this guideline where the initial temperature gradient of the power absorption process at $t = 0$ seconds matches the temperature gradient of the thermodynamic process at $t = \tau$ seconds. Absorption processes whose

maximum gradients are greater or less than the associated thermodynamic gradients tend to produce higher temperatures too early or late in the absorption process and eventually lead to greater levels of entropy generation.

Figure 8.6 shows another example of this second guideline. In these simulations, Case 4 is the same minimum temperature case previously discussed. Case 7 attempts to match maximum temperature gradients at $t = \tau$ seconds while producing a temperature rise in the absorption process that is a mirror image of the temperature's exponential fall in the thermodynamic process. Table 8.3 shows that Case 7 produces the least amount of entropy of all the cases. Although Case 7 is not the minimum entropy generation solution, it is believed to contain several of the characteristics that would exist in the optimal case. Case 8's power absorption simply consists of a 100 J impulse at $t = 0$ seconds. Because of its high initial temperatures and grossly mismatched temperature gradients between the absorption and thermodynamic processes, Case 8 is believed to be one of the worst cases possible for the model.

8.4 CONCLUSIONS

The minimum entropy hypothesis is one candidate for the explanation of why amputees prefer prosthesis controllers that create lower power gradients. The hypothesis states that the power gradients of a task are minimized if the entropy generation is minimized. After developing a simplified thermodynamic model and a set of state equations, defining a general relationship between entropy generation and power gradients during the performance of a task was found to be complicated by three issues: the *inherent nonlinearities* associated with the definition of entropy, the *method of power absorption*, and the *method of heat transfer*. To define an entropy-power gradient relationship for a task requires each issue to be addressed. Unfortunately, the methods of power absorption and heat transfer are task specific, so a general entropy relationship for all tasks does not exist.

Despite not finding a general relationship, simulations of the simplified model showed several interesting characteristics. During the performance of a task, entropy generation contains two processes: the power absorption process consists of the period when power is absorbed by the system's irreversible elements; the thermodynamic process consists of the period when the system is not at stable equilibrium. For the simplified model, the thermodynamic process starts at the same time the power absorption process starts but continues beyond the completion of the absorption process. The amount of overlap between the two processes depends on how energy is being absorbed by the damper and the model's heat transfer parameters.

Except for Case 8, all absorption processes last one time constant while the thermodynamic process last roughly three time constants. Thus, the length of the power process is about 33% of the thermodynamic process. Shorter absorption processes that transfer the same amount of energy create higher temperature and entropy levels. Case 8 is an extreme example of this where the absorption process is 0% of the thermodynamic process. Longer absorption processes usually produce less entropy. For the longer processes, the *method* of power absorption becomes critical since the amount of entropy generated after the absorption process is less significant. Methods that create *unnecessarily* high temperatures prove to be inferior to those that produce low, consistent temperatures like those found in the heat flux analysis (Section 8.2).

Minimizing energy loss to a system's irreversible elements is not sufficient to minimize the system's entropy generation. While each simulation in the simplified model uses a different power absorption profile for the damper, all simulations absorb the same amount of energy. If this energy represented the minimum energy loss required for task completion, the simulations show that the level of entropy generation can vary depending on the *method* of absorption (the power profile). An absorption process that does not minimize a system's energy loss but possesses a better *method* of absorption can produce less entropy.

Case 5 demonstrates that minimizing the time derivatives of absorbed power does not necessarily minimize entropy generation. But how does Case 5 compare to the following "optimal" case: Let's assume that the damper's absorbed energy is transferred to the environment using the optimal heat flux profile found in Section 8.2. Since all simulations generate the majority of their entropy in three time constants, let's also assume that the absorbed energy is transferred as heat in the same amount of time. Transferring 100 J of energy to the environment at a constant temperature difference of 33.33 K produces 0.0337 J/K of entropy. The minimum power gradient profile produces 12.8% more entropy than this optimal case. Given that the minimum power gradient profile is not a function of either the system's parameters or method of heat transfer, the results are surprisingly close.

To minimize a system's entropy generation, detailed knowledge of the system's state equations, boundary conditions, and time duration of the task are required. Low levels of entropy generation *during* task performance do not guarantee overall minimum levels for the task since larger levels of entropy can be generated long after the task has been completed. Even for the simplified model, obtaining and retaining the knowledge required to minimize the system's entropy would be a very demanding task for most humans. This is why Case 5, the

minimal power gradient case, is still an attractive alternative. While the case did not produce minimal entropy for the chosen model, it did produce levels that were reasonably close to the "optimal" case without requiring detailed knowledge of the system's parameters. The benefits gained from not requiring knowledge of the system's thermodynamic process could easily overshadow Case 5's costs associated with increasing the system's entropy.

Entropy generation can become a delicate balance between the *amount* of energy absorbed by the system's irreversible elements and the *method* in which the energy is absorbed (i.e., the power absorption profile). While both can contribute to minimizing entropy, the thermodynamic model suggests that priority should be given to minimizing the *amount* of energy absorbed. After all, if no energy is absorbed by the damper, no net entropy can be generated by the system; both power absorption and entropy generation are minimized. As an example, simulations for the thermodynamic model showed a 40% entropy range between the "worst" (Case 8) and the "optimal" cases when a fixed amount of energy was absorbed (100 J). This 40% range is a relatively small entropy window. Minimizing power absorption places a ceiling on the amount of entropy that can be generated. Once a ceiling has been established, alternative power absorption profiles could be used to reduce the system's entropy generation; however, this assumes that alternative profiles are viable for the given set of system elements and task constraints.

CHAPTER
NINE

CONCLUSIONS

9.1 REVIEW

This thesis has covered many topics and it is worth reviewing how these topics relate to the thesis's objectives and conclusions. To date, very little is known about how humans interact with the environment to perform tasks. To assist in performing a task, a human will often use a tool. If the human feels that the tool improves the performance of the task, the human will most likely continue to use the tool. However, if task performance degrades, the tool will most likely be replaced by an alternative tool or means.

Understanding how humans interact with the environment is imperative if one is to understand how humans perform tasks and use tools. Once a better understanding of the interactions is obtained, one can then begin to assess task performance and determine why one task is performed "better" than another. This leads to improving task performance and has several long term contributions. First, there is the self-satisfaction of the humans performing the task. Improving task performance can give the human a better sense of accomplishment and boost his self-esteem. Second, improved task performance can improve productivity and growth. From an economic perspective, this has all the traits for improving one's standard of living. Third, this better understanding of human interactions can be incorporated into future ma-

chine design for performing both similar and unrelated tasks. Robots, for example, would not only become more diverse but also more able to perform tasks that are not currently possible.

Human interaction and task performance are very complex problems. To make any headway on solving the problem requires division of the problem into several issues that can be addressed separately. This thesis concentrated on interactions during constrained motions and more specifically, it concentrated on a relatively simple constrained motion task – turning a crank. Two approaches can be taken to study the interactions involved in turning a crank. The first approach is to hypothesize a method humans use to turn the crank and then test the validity of the hypothesis. This approach has been done in the past with limited success. While the approach lends itself to being well defined, choosing a constructive hypothesis can be futile given the limited amount of information known about the problem. A second approach is to launch a general investigation of the task and to establish a basis for future, more educated hypotheses. Since there is no specific attribute to be highlighted, this exploratory approach is likely to raise more questions than it answers.

Given the infancy of understanding human interactions, this thesis delineates an exploratory approach. It was believed that keeping an open mind to all the possible forms of task performance and interaction would be more informative and productive than concentrating on only a few speculative forms. A set of experiments was defined to take advantage of a unique interface existing among a human, a machine, and the environment by way of an amputee using the emulator to turn the crank. The emulator system allowed the characteristics of the *tool* to be changed while controlling the remaining experimental variables and it also enabled the experiments to be highly quantified. From the experiments and the selected analysis, several conclusions and suggestive results have been uncovered that were not previously known or understood.

9.2 CONCLUSIONS

Three conclusions have been extracted from Chapter 5's experimental results and are the thesis's most significant contributions:

1) During task performance, **high output impedance** devices **produced adverse effects.** This finding is supported by three facts. First, the power plots consistently show higher rates of change of power for the high output impedance controllers (Boston Elbow and NY Electric Elbow) when compared to the low output impedance controllers (Impedance and Passive). The differences are so dramatic that additional data processing is not neces-

sary. Second, the high output impedance controllers are the only controllers to show significant amounts of power absorption. Recording power absorption during task performance means that the controllers are *hindering* the subject from performing the task. Third, high output impedance controllers consistently produced higher peak force interactions during the task. These higher forces are extrinsic and cannot be justified; especially when the low output impedance controllers proved that the task could be performed with significantly lower force levels.

The conclusion is that the **low output impedance** controllers **complement** tasks requiring **constrained interaction** and **synergistic coordination**. Unlike the high output impedance controllers, the low output impedance controllers enable the passage of energy among the various subsystems without reducing the system's kinematic degrees of freedom. This conclusion points to a serious limitation of current, above-elbow, externally powered prosthesis designs and to some telerobotic and robotic designs.

2) The **different controllers** and task constraints used in the crank task **produced similar kinematics** in terms of positions and velocities but **dissimilar dynamics** in terms of force interactions and power flows. This is clearly demonstrated in the comparison of the kinematic plots with the dynamic plots. The kinematic plots contain similar profiles among the different controllers, subjects, and crank speeds and therefore make the understanding of task performance and interactions difficult. The dynamic plots show dramatically different power and force profiles even when the respective kinematic plots are quite similar.

   The kinematic plots are supportive that **humans use kinematic objectives** when performing a task. The plots suggest that dynamic objectives are secondary objectives, more complicated to understand and execute, and require learning and adaptation. The results also support the claim that **humans have a hierarchical organization of motor behavior**: Tasks are approached first in terms of their kinematics before considering the type of force interactions.

3) When compared to the kinematic plots, the **dynamic measurements** readily **segregate** prosthesis **controllers** and human **strategies**. Not only do the power plots show obvious differences between low and high output impedance controller *families*, the plots also show significant differences between controllers within the same family. The radial force plots reveal at *least* two different strategies used by the subjects to turn the crank. One strategy, the *preload strategy*, makes the crank unstable at the shoulder reversal while the

second strategy, the *passive dynamics strategy*, takes advantage of the system's momentum to pass through the shoulder reversal.

The experimental results have shown that **dynamic measurements** are *extremely* useful for understanding how humans interact with the environment and how humans use tools to effectively perform a task. This strongly suggests that force interactions and power flows should be measured whenever possible to **quantify** and assess **task performance.**

9.3 SUGGESTIVE FINDINGS

The amputee experiments are saturated with tantalizing findings that are very suggestive but should not be considered conclusive without further investigation. Only a few of the most compelling results are listed.

1) Controllers that produced rapid changes in power flow created high reaction forces and were not as well accepted by the amputees. The dynamic plots show that controllers with lower rates of change of power have lower elbow torques and lower radial and tangential forces. When asked which controllers the subjects preferred, the subjects would unknowingly describe the controllers that produced lower rates of change of power. All of these results suggest that the **rate of change of power** may be used as a measure for **quantifying synergistic coordination and amputee acceptance.** The strong correlations were the prime motivation for hypothesizing that humans may be minimizing entropy generation or power dissipation during task performance and that the observed reduction in power fluctuations is the product of achieving one of the two minimization processes.

2) A system's *passive dynamics* can play a significant role in task performance. The strongest proof of this finding is based on the apparent ease amputees could perform the crank task without an active prosthesis. Both the kinematic and dynamic measurements show crank momentum aiding the amputees at the shoulder reversal. The plots also reveal the emulator's design permitting the amputees to take advantage of the emulator's "hidden" transmission dynamics. The crank-emulator system demonstrates that **mechanical designs with** appropriate **passive dynamics** will **enhance task performance** while reducing controller demands.

3) Depending on the task, **amputees benefited** from controllers **with different output impedances.** High output impedances permitted the amputees to maintain a rigid elbow position during the rolling pin and cutting meat tasks. Rigid elbow position appeared to

allow the subjects to have better force control of the prosthesis's terminal device when cutting the meat and rolling the dough and enabled faster completion times. Low output impedance controllers appeared to excel in contact tasks and constrained motion interactions. Subjects were less likely to hesitate when making contact with the environment during the ADL tasks with a low output impedance device and lower force interactions were recorded during the constrained motion, crank task.

The results **emphasize** the importance of a ***variable*** **output impedance design** for task performance. The results may also explain the limited acceptance of all, commercially available, externally powered, above-elbow prostheses. All current designs can only produce an elbow with high output impedance during task performance. In addition, the results may also explain the surprisingly stanch acceptance of the body-powered prosthesis that provides the amputee with a low or high output impedance elbow.

4) The **radial force plots reveal** transitions in an amputee's **strategies** when turning the crank. At slower speeds, the amputees adopted the *preload strategy* and compressed the crank arm at the shoulder reversal. As the crank speed became faster, the *passive dynamic strategy* was more apparent. Not only does this suggest that strategies for task performance are speed dependent, but the unstable crank arm at the slower speeds also suggests that the amputee's strategies can be **relatively ingenious for the task**. Similar to humans walking, which is inherently unstable, the crank task shows that humans are willing and able to create an unstable situation as a means to accomplish a task.

5) When performing a task, limb recruitment was often used by the amputee. The most noticeable times occurred when the subject turned the crank with the passive controller or when the subject had difficulty with the shoulder reversal. When using the passive controller, the amputee would use upper-body motion to transfer additional kinetic energy to the crank system. If the crank was decelerating too fast at the shoulder reversal, the amputee would often move his shoulder to pass through the reversal quicker. Although present with all controllers, body motion, or Body-English, can be very subtle and is often detectable only through the dynamic measurements. Observations based only on video tapes can be impossible. Despite its elusiveness, **Body-English** can play an **important** role **during** constrained motion **tasks**.

6) An amputee's myoelectric activity (MEA) shows similar gross features among the substantially different controllers. Triceps activation showed up in all controllers despite only being necessary in the high output impedance controllers. Significant biceps activa-

tion was recorded for the passive controller even though the signals were not processed. Except for regions of coactivation near the reversals, the impedance and velocity controllers showed similar profiles. The amputee results support the possibility that **MEA's** are **primarily "preprogrammed"** but do have some capability of being modified. The extent to which modification can occur and the level of burden put on the amputee to modify his signals is not obvious. The limited results suggest that of the active controllers, the impedance controller, which recognizes coactivation, requires the least amount of modification from the amputee.

9.4 MODELING & ANALYSIS

The exploratory approach has provided a wealth of information on amputees performing a constrained motion task. One of the interesting results obtained from the experiments was the *negative* correlation between controllers that produced higher rates of change of power and controllers that were more likely to be preferred by the amputees. Using the experimental results as a foundation, two thermodynamic hypotheses were investigated to determine if there was a fundamental motive supporting the amputee's preference. The first hypothesis stated that amputees attempted to minimize a task's power dissipation during task performance. The second hypothesis stated that amputees minimized entropy generation. An indirect consequence of achieving either objective would be to minimize the task's rates of change of power. Controllers that permitted the amputee's to achieve their optimization goals would be deemed more favorable.

1) Using calculus of variations, a mass-spring-damper model's power dissipation was minimized for a simple task. The model demonstrated that **minimizing power dissipation** does not create rapid or unnecessary changes in power flow. For low damping coefficients, the minimization results approach a minimum jerk profile. Minimum jerk models have previously been documented and experimentally verified for planar, multijoint arm movements. The power profiles obtained from the power optimization results do not resemble those obtained for minimizing entropy generation. Thus, it is not obvious that minimizing a task's power dissipation indirectly minimizes a task's entropy generation.

   Minimizing power dissipation does not require prediction of future system characteristics like those required for entropy minimization. Since minimizing power dissipation does not encourage rapid changes in power, there is no evidence to suggest that the amputees were not trying to minimize power dissipation when performing the crank task. The

minimization results may also provide motivation for why humans perform planar, multi-joint arm movements in a minimum jerk fashion. Preliminary investigations show that the minimum power dissipation hypothesis is **promising**.

2) A simple thermodynamic model demonstrated that **minimizing entropy generation** does not necessarily minimize rates of change of power for a task. Simulations revealed that minimizing entropy generation requires knowledge or assumption of several modeling parameters and can be a process that continues far beyond task completion. To minimize entropy generation also requires foreknowledge of the control volume's heat transfer characteristics. Unforeseen heat transfer effects would prevent a minimization from being achieved. The model and simulation findings suggest that it is **unlikely** that minimizing entropy generation is a fundamental motive for task performance or for effectively interacting with the environment. There is no evidence from the experimental results that would suggest that the crank task's reduced rates of change of power are a consequence of minimizing the system's entropy.

9.5 FUTURE WORK

The experimental results, along with the modeling and analysis, suggest several directions that can be taken to advance the current work and to gain a better understanding of how humans interact with the environment. Future work can be divided into two categories: short term and long term. The short term work primarily deals with performing additional data processing and analysis using the current experimental results. The long term work extrapolates the research to future experiments and analysis.

9.5.1 SHORT TERM

If one is going evaluate task performance and claim one controller is "better" than another, a systematic means of comparing the experimental results is necessary. One advantage in using the passive controller during the experiments was that it provided a basis for comparing the active controller results. One disadvantage of the passive controller was that it still contained many of the non-quantifiable measurements that may play an important role in task performance. A specific example of a measurement that is difficult to quantify is the shoulder movement.

A possible solution to the comparison and quantification problem is to establish a theoretical, interactive model of the crank task using a computer simulated, four-bar linkage. Similar models have already been constructed for gait analysis [27]. The model would accept theoret-

ical or empirical inputs and would analyze the force interactions and power flows required to perform the task. The model's results could then be used to normalize the experimental results for purposes of comparison. Quantifying the similarities of the kinematic measurements and the differences in the dynamic measurements would be one possible application for the model. The model does not have to be *identical* to the actual system since all controllers would be compared to the same model. The computer model would also provide an avenue for exploring the various strategies observed during the task. Immediate possibilities could be to define a minimum jerk or minimum power model and compare the results or to test the validity of the preload or passive dynamic strategies.

If general conclusions are to be extrapolated from the crank task, the method of relating the crank task's results to other unrelated, ADL tasks becomes an important issue. The experimental results show that measuring rates of change of power can be very informative and appears to be a very promising, quantifiable measurement. The next step would then be to determine how the measurement should be quantified. Two of the many possible methods are: normalizing with respect to the aforementioned computer model, or taking the *integral* of a crank cycle's rate of change of power (squared) over a fixed range of crank angles (which includes both reversals). Once a method of quantification has been established, one can then correlate the results to the amputee's acceptance and to the performances of different ADL tasks.

If statements about human interaction are to be made from the amputee results, the results need to be compared with those obtained from intact humans. Russell's results provide some preliminary intact, crank data that could be immediately compared with the amputee's raw results [34]. In addition, Russell's hypothesis on virtual trajectories could be compared to the amputee's preload strategy found at the slower crank speeds.

9.5.2 LONG TERM

The most obvious long term work is to collect more data from amputees and intacts. The current set of data only reflects four amputees. Several of the suggestive results can become conclusive if more amputees and permutations of the crank task's constraints are performed.

One of the more interesting results found from the experiments was the importance of a variable output impedance elbow. This result could very well explain why the body-powered prosthesis, which can provide limited but different output impedances, has a 5:1 acceptance ratio over the externally powered prostheses, which all exhibit a high output impedance. To gain a better understanding of the dispersion in acceptance, it would be well worth taking a

step backward in technology to better quantify the benefits of the body-powered prosthesis. While weight and simplicity have always been the prosthesis's strong point, there is evidence suggesting that its ability to transfer energy through its passive dynamics may be under-appreciated.

A variable output impedance design appears not only to be useful for elbow prostheses, but it also has applications in robotics and telerobotics as a diverse tool for performing unrelated tasks. A common method of achieving a variable output impedance design is to make the transmission backdrivable and use a high position feedback gain to simulate a high stiffness. Unfortunately, such a design is energy inefficient. This opens the doors for finding a new, variable output impedance design that is significantly more efficient. The design may contain passive elements, such as springs and dampers, to reduce the design's controller demands and the actuator's energy consumption. This not only adds passive dynamics the system, which is counter to most common engineering design philosophies, but it also suggests an innovative, nonconventional design.

With the advancements in digital signal processing, there should be continuing exploration of more advanced algorithms for processing the myoelectric signals. The high output impedance controllers operate on the difference of MEA's while the impedance controller uses both differences and sums. More sophisticated algorithms could recognize patterns and trends in the MEA's so that the input command signals better reflect the amputee's intentions. Since the hardware required to implement the new algorithms could easily consist of adding only a few new IC chips to the prosthesis's electronic package, a successful algorithm could quickly be implemented in current prosthesis and enjoyed by the amputee population.

Finally, the positive results obtained from the minimum power hypothesis are very compelling. Having the mass-spring-damper model approach the successfully demonstrated minimum jerk model when the damping ratio decreases may simply be a coincidence or it be the corner stone for describing a fundamental process used by humans when interacting with the environment. At the very minimum, the hypothesis would explain the motivation behind performing tasks in a minimum jerk fashion. Additional analysis and experiments are strongly urged to further test the validity of the hypothesis.

BIBLIOGRAPHY

[1] Product Literature: *The NY Electric Elbow*. Hosmer Dorrance Corporation, Campell, CA, 1992.

[2] Product Literature: *The Utah Artificial Arm*. Motion Control, Inc., Salt Lake City, Utah, 1992.

[3] Abul-Haj, C.J., *The Design of an Upper-Arm Prosthesis Simulator with Variable Mechanical Impedance*. Master of Science, Massachusetts Institute of Technology, Department of Mechanical Engineering, 1981.

[4] Abul-Haj, C.J., *Elbow-Prosthesis Emulation: A Technique for the Quantitative Assessment of an Assistive Device*. Doctor of Science in Mechanical Engineering, Massachusetts Institute of Technology, Department of Mechanical Engineering, 1987.

[5] Abul-Haj, C.J. and N. Hogan, *An Emulator System for Developing Improved Elbow-Prosthesis Designs*. IEEE Trans. Biomed. Eng., 1987. **34**(9): p. 724-737.

[6] Abul-Haj, C.J. and N. Hogan, *Functional Assessment of Control Systems for Cybernetic Elbow Prostheses-Part I: Description of the Technique*. IEEE Trans. Biomed. Eng., 1990. **37**(11): p. 1025-1036.

[7] Abul-Haj, C.J. and N. Hogan, *Functional Assessment of Control Systems for Cybernetic Elbow Prostheses-Part II: Application of the Technique*. IEEE Trans. Biomed. Eng., 1990. **37**(11): p. 1037-1047.

[8] Angliss, V., *et al. Evaluation of the Voluntary Closing "TRS" Terminal device.* in *Proceedings of 7th World Congress of the International Society for Prosthetics and Orthotics (ISPO).* 1992. Chicago, IL: p. 65.

[9] Bryson, A.E. and Y.-C. Ho, *Applied Optimal Control: Optimization, Estimation, and Control.* 2nd ed. 1975, New York: John Wiley & Sons.

[10] Cravalho, E.G. and J.L. Smith, *Engineering Thermodynamics.* 1981, Cambridge, MA: Massachusetts Institute of Technology.

[11] Dohrmann, C.R., H.R. Busby, and D.M. Trujillo, *Smoothing Noisy Data Using Dynamic Programming and Generalized Cross-Validation.* ASME Journal of Biomechanical Engineering, 1988. **110**(February): p. 37-41.

[12] Flash, T. and N. Hogan, *The Coordination of Arm Movements: An Experimentally Confirmed Mathematical Model.* The Journal of Neuroscience, 1985. **5**(7): p. 1688-1703.

[13] Hildebrand, F.B., *Advanced Calculus for Applications.* 2nd ed. 1976, Englewood Cliffs, New Jersey: Prentice-Hall, Inc.

[14] Hogan, N., *Impedance Control: An Approach to Manipulation.* Journal of Dynamic Systems, Measurement, and Control, 1985. **107**(March): p. 1-24.

[15] Hogan, N., *Planning and Execution of Multijoint Movements.* Can. J. Physiol. Pharmacol, 1988. **66**: p. 508-517.

[16] Hogan, N. and R.W. Mann, *Myoelectric Signal Processing: Optimal Estimation Applied to Electromyography-Parts 1 and 2.* IEEE Trans. Biomed. Eng., 1980. **27**(7): p. 382-410.

[17] Jeannerod, M., *The Interaction of Visual and Proprioceptive Cues in Controlling Reaching Movements,* in *Motor Control: Concepts and Issues,* D.R. Humphrey and H.J. Freund, Editor. 1991, John Wiley & Sons, Ltd.: p. 277-291.

[18] Johansen, P., M. Breiholts, and R. Cavrini, *Prosthetic Rehabilitation in Bilateral High Above Elbow Amputation.* Scand. J. Rehab. Med., 1986. (19): p. 85-87.

[19] Kay, H.W. and E. Peizer, *Studies of the Upper-Extremity Amputee; Prosthetic Usefulness and Wearer Performance,* in *Artificial Limbs.* 1958, p. 31-87.

[20] Kennison, D., *NCAR Graphics: Autograph-A Graphing Utility.* Version 2.00, vol. NCAR/TN-245+IA. National Center for Atmospheric Research, Boulder, CO, 1987.

[21] Kishinchandani, R.S., *Quantitative Assessment of Above-Elbow Prosthetic Control.* Master of Science in Physical Therapy, MGH Institute of Health Professions, Graduate Program in Physical Therapy, 1991.

[22] Kishinchandani, R.S., *et al. Assessment of Multiple-Joint Coordination and ADL Tasks Performed by Above-Elbow Amputees.* in *1991 APTA Annual Conference.* 1991. Boston, MA, Vol. 71: p. S110.

[23] Kurtz, I., M. Mifsud, and S. Naumann. *Emulation and Evaluation of Strategies for Controlling Powered Upper Extremity Prostheses.* in *Proceedings of the ISPO Seventh World Congress.* 1992. Chicago, IL: p. 314.

[24] Lamb, D., T. Dick, and W. Douglas, *A New Prosthesis for the Upper Limb.* Journal of Bone Joint Surgery, 1988. **70-B**(1): p. 140-144.

[25] Lawrence, J.H. and C.J. De Luca, *Myoelectric Signal Versus Force Relationship in Different Human Muscles.* Journal of Applied Physiology: Respiratory, Environmental, and Exercise Physiology, 1983. **54**(6): p. 1653-1659.

[26] Leblanc, M.A. *Making the Case for Body-Powered Upper-Limb Prostheses.* in *Proceedings of the 10th Annual Conference on Rehabilitation Technology.* 1987. San Jose, CA, Vol. 1: p. 196-198.

[27] Lord, P.J., *3D_Gait: A Three Dimensional Computer Graphic Display for Human Motion Analysis from TRACK Gait Data.* Bachelor Thesis, Dept. of Mech. Eng., Massachusetts Institute of Technology, 1987.

[28] Lozach, Y., *et al. On the Evaluation of a Multifunctional Prosthesis.* in *Proceedings of the ISPO Seventh World Congress.* 1992. Chicago, IL: p. 185.

[29] Meredith, J.M. *Comparison of Three Myoelectrically-Controlled Prehensors and the Voluntary-Opening Cable-Operated Split Hook.* in *Proceedings of the ISPO Seventh World Congress.* 1992. Chicago, IL: p. 313.

[30] Miller, C.M., *A Method for Assessing the Importance of Elbow Dynamic Behavior in Manual Tasks.* Master of Science in Mechanical Engineering, Massachusetts Institute of Technology, Department of Mechanical Engineering, 1987.

[31] Paul, R.P. *Problems and Research Issues Associated with the Hybrid Control of Force Displacement.* in *IEEE International Conference on Robotics and Automation.* 1987: p. 1966-1971.

[32] Philipson, L. and R. Sorbye, *Myoelectric Elbow and Hand Prosthesis Controlled by Signals from Two Muscles Only in a Nine Year Old Girl.* Prosthetics and Orthotics International, 1981. (5): p. 29-32.

[33] Russell, D.L., *Arm Motion in Crank Turning.* Master of Science in Mechanical Engineering, Massachusetts Institute of Technology, Department of Mechanical Engineering, 1986.

[34] Russell, D.L., *An Analysis of Constrained Motions in Manipulation.* Doctor of Philosophy in Mechanical Engineering, Massachusetts Institute of Technology, Department of Mechanical Engineering, 1990.

[35] Sharon, A., N. Hogan, and D.E. Hardt. *High Bandwidth Force Regulation and Inertia Reduction Using a Macro/Micro Manipulator System.* in *IEEE Conference on Robotics and Automation.* 1988. Philadelphia, PA, Vol. 1: p. 126-132.

[36] Stein, R. and M. Walley, *Functional Comparison of Upper Extremity Amputees Using Myoelectric and Conventional Prostheses.* Arch. Phys. Med. Rehab., 1983. (64): p. 243-248.

[37] Wark, K., *Thermodynamics*. 3rd ed. Editors: B.J. Clark and J.W. Maisel. 1977, New York, NY: McGraw-Hill Book Company. 909.

[38] Williams, T.W., III, *The Boston Elbow,* in *SOMA*. 1986, p. 30-33.

[39] Williams, T.W., III, Liberty Mutual Research Center, Hopkinton, MA, Personal Communication, November 19, 1991.

[40] Wolfram, S., *Mathematica: A System for Doing Mathematics by Computer*. 2nd ed. 1991, RedWood City, CA: Addison-Wesley Publishing Co., Inc.

APPENDIX A

KINEMATIC PLOTS

SUBJECT 1

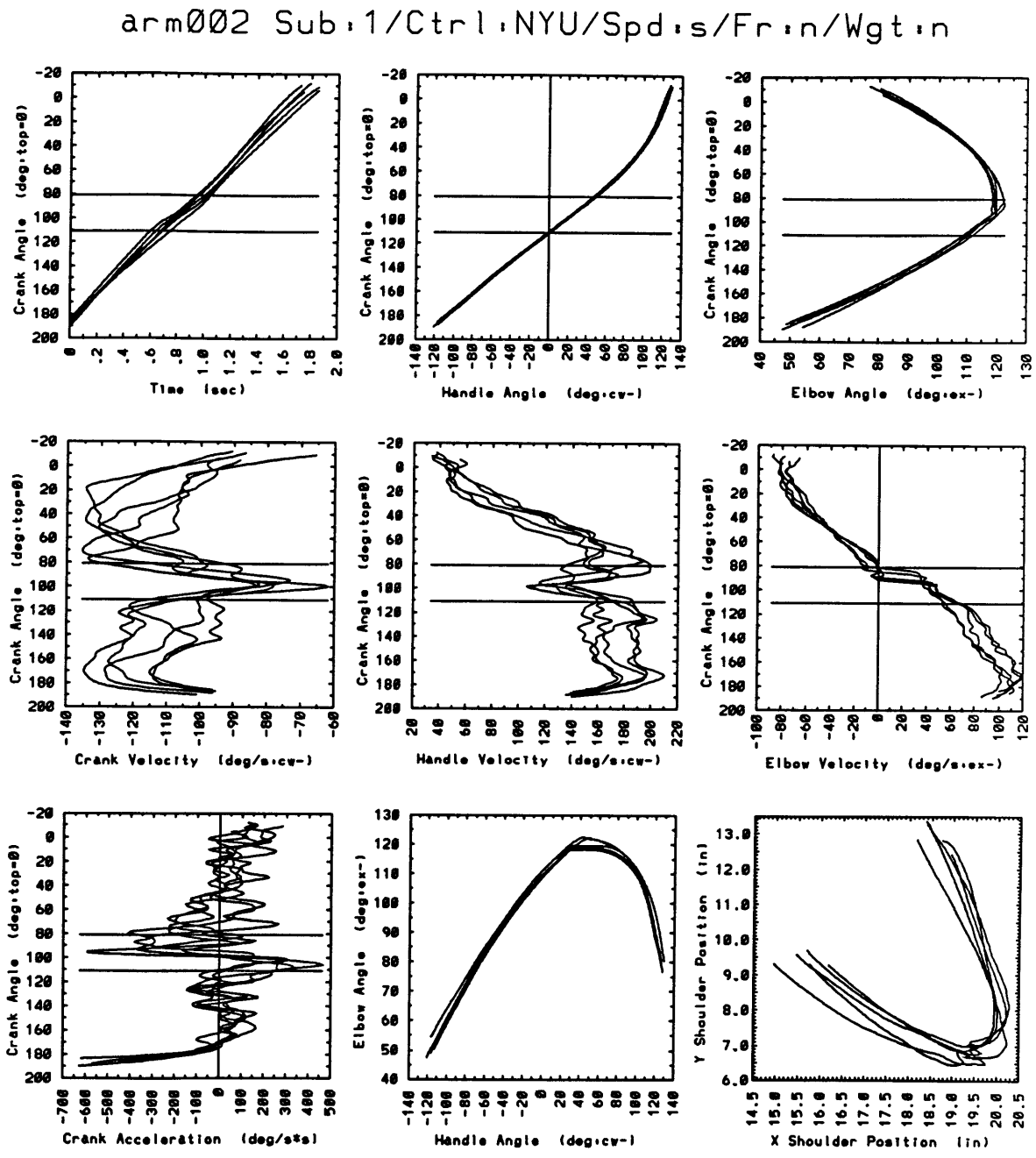
arm002 Sub:1/Ctrl:NYU/Spd:s/Fr:n/Wgt:n
Crank Angle (deg:top=0)
Time (sec)
Handle Angle (deg:cw-)
Elbow Angle (deg:ex-)
Crank Velocity (deg/s:cw-)
Handle Velocity (deg/s:cw-)
Elbow Velocity (deg/s:ex-)
Crank Acceleration (deg/s*s)
Y Shoulder Position (in)
X Shoulder Position (in)

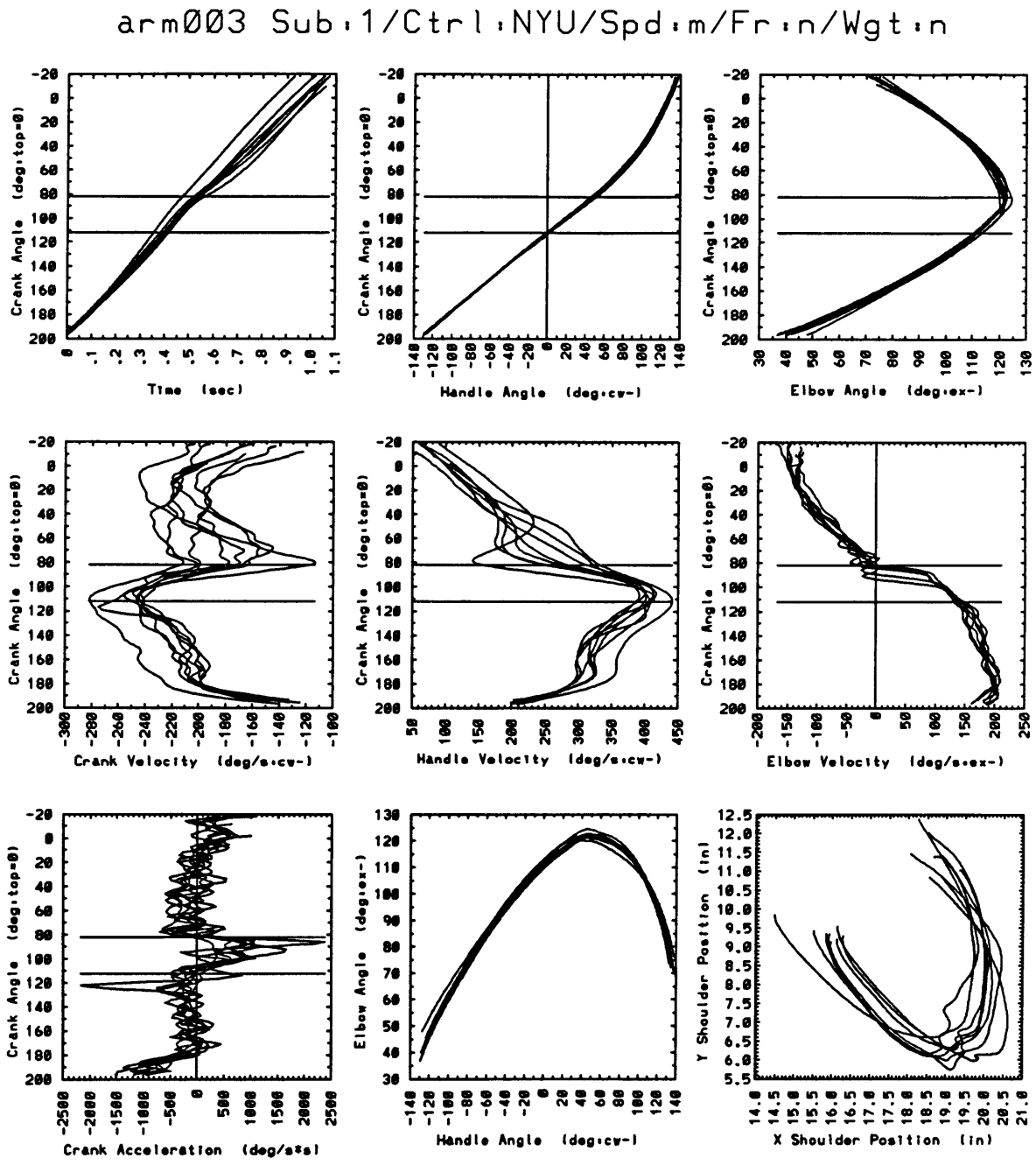
arm003 Sub:1/Ctrl:NYU/Spd:m/Fr:n/Wgt:n
Crank Angle (deg:top=0)
Time (sec)
Handle Angle (deg:cw-)
Elbow Angle (deg:ex-)
Crank Velocity (deg/s:cw-)
Handle Velocity (deg/s:cw-)
Elbow Velocity (deg/s:ex-)
Crank Acceleration (deg/s*s)
Elbow Angle (deg:ex-)
Handle Angle (deg:cw-)
Y Shoulder Position (in)
X Shoulder Position (in)

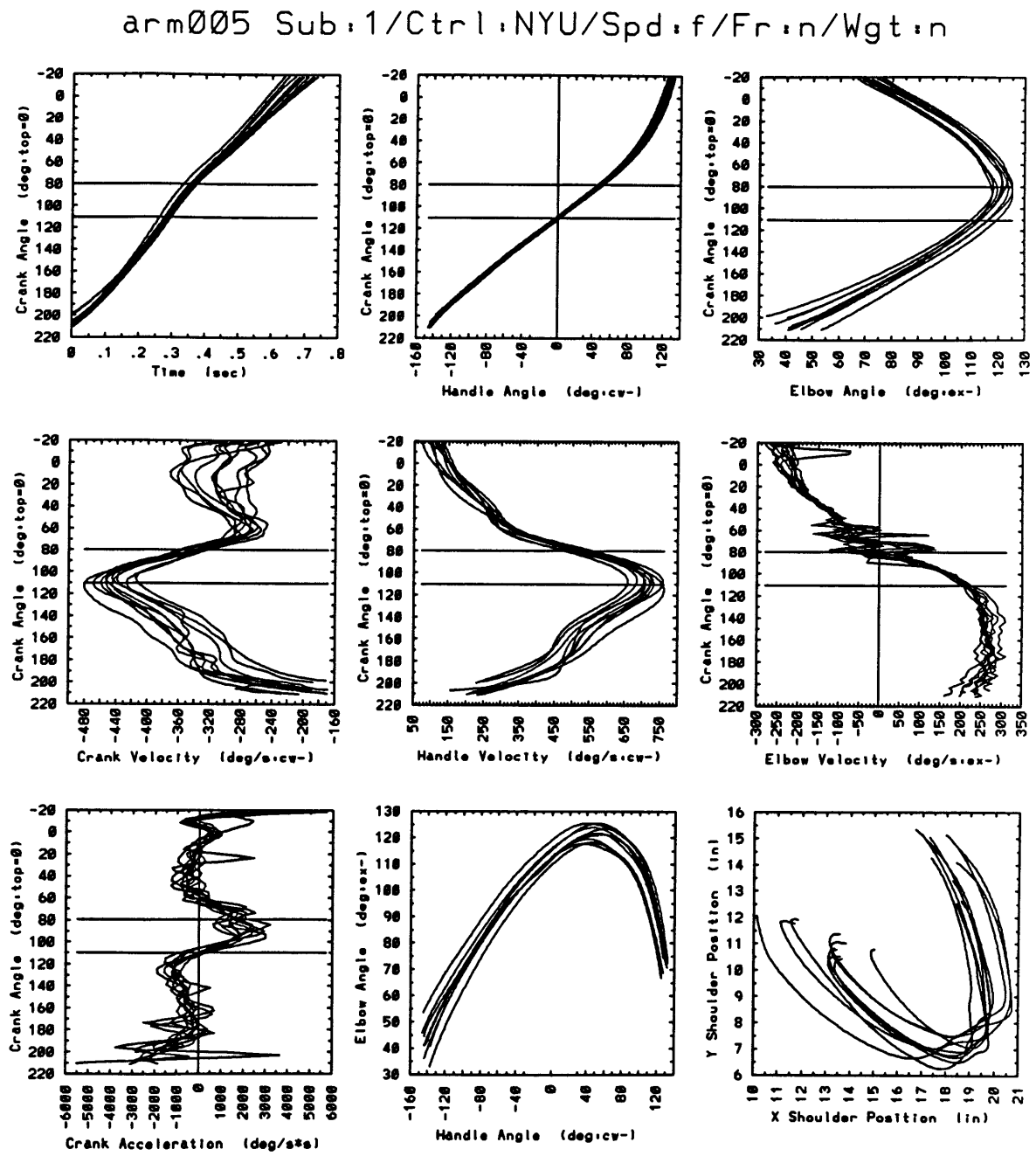
arm005 Sub:1/Ctrl:NYU/Spd:f/Fr:n/Wgt:n
Crank Angle (deg:top=0)
Time (sec)
Handle Angle (deg:cw-)
Elbow Angle (deg:ex-)
Crank Velocity (deg/s:cw-)
Handle Velocity (deg/s:cw-)
Elbow Velocity (deg/s:ex-)
Crank Acceleration (deg/s*s)
Elbow Angle (deg:ex-)
Handle Angle (deg:cw-)
Y Shoulder Position (in)
X Shoulder Position (in)

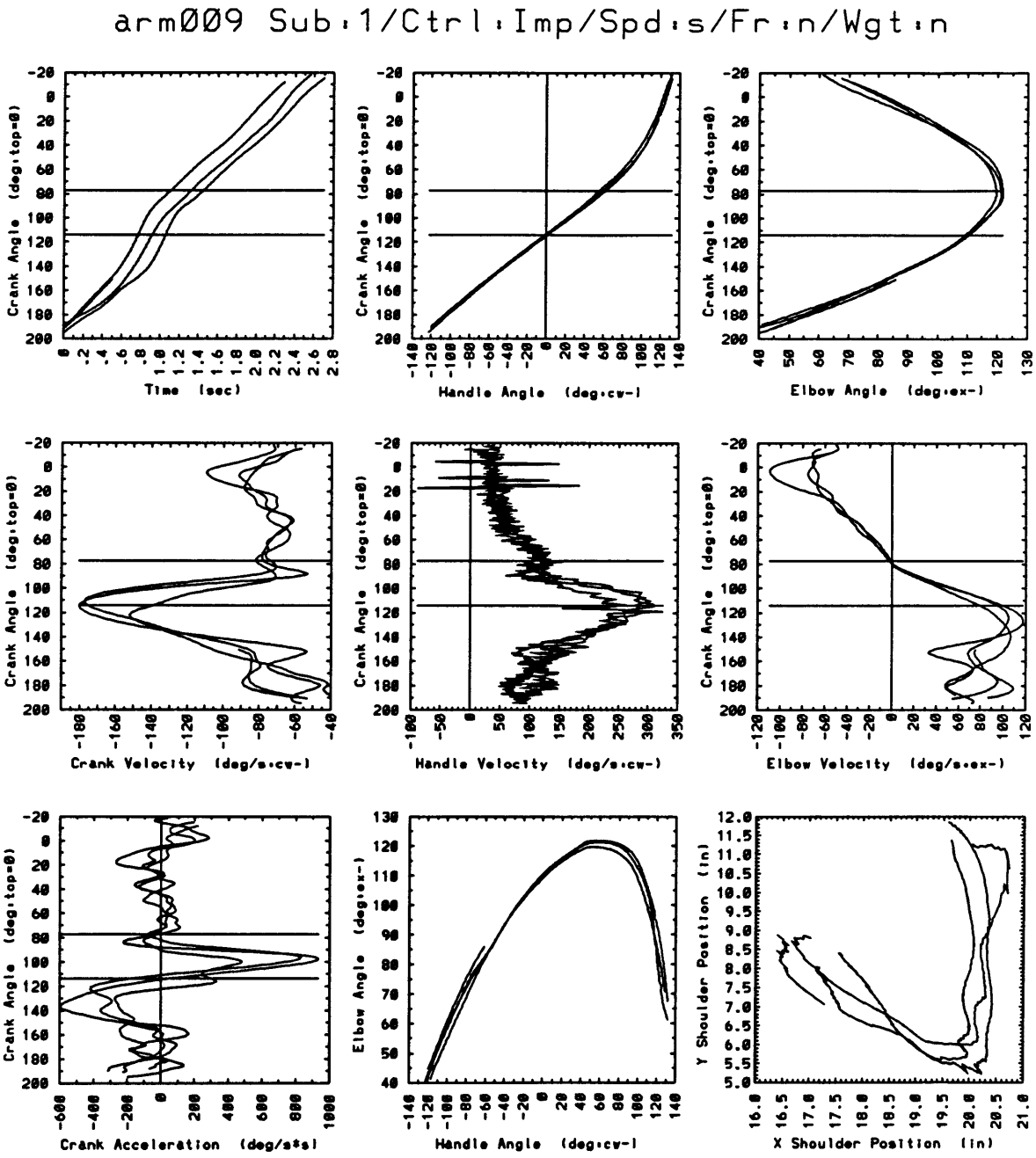
arm009 Sub:1/Ctrl:Imp/Spd:s/Fr:n/Wgt:n
Crank Angle (deg:top=0)
Time (sec)
Handle Angle (deg:cw-)
Elbow Angle (deg:ex-)
Crank Velocity (deg/s:cw-)
Handle Velocity (deg/s:cw-)
Elbow Velocity (deg/s:ex-)
Crank Acceleration (deg/s*s)
Elbow Angle (deg:ex-)
Handle Angle (deg:cw-)
Y Shoulder Position (in)
X Shoulder Position (in)

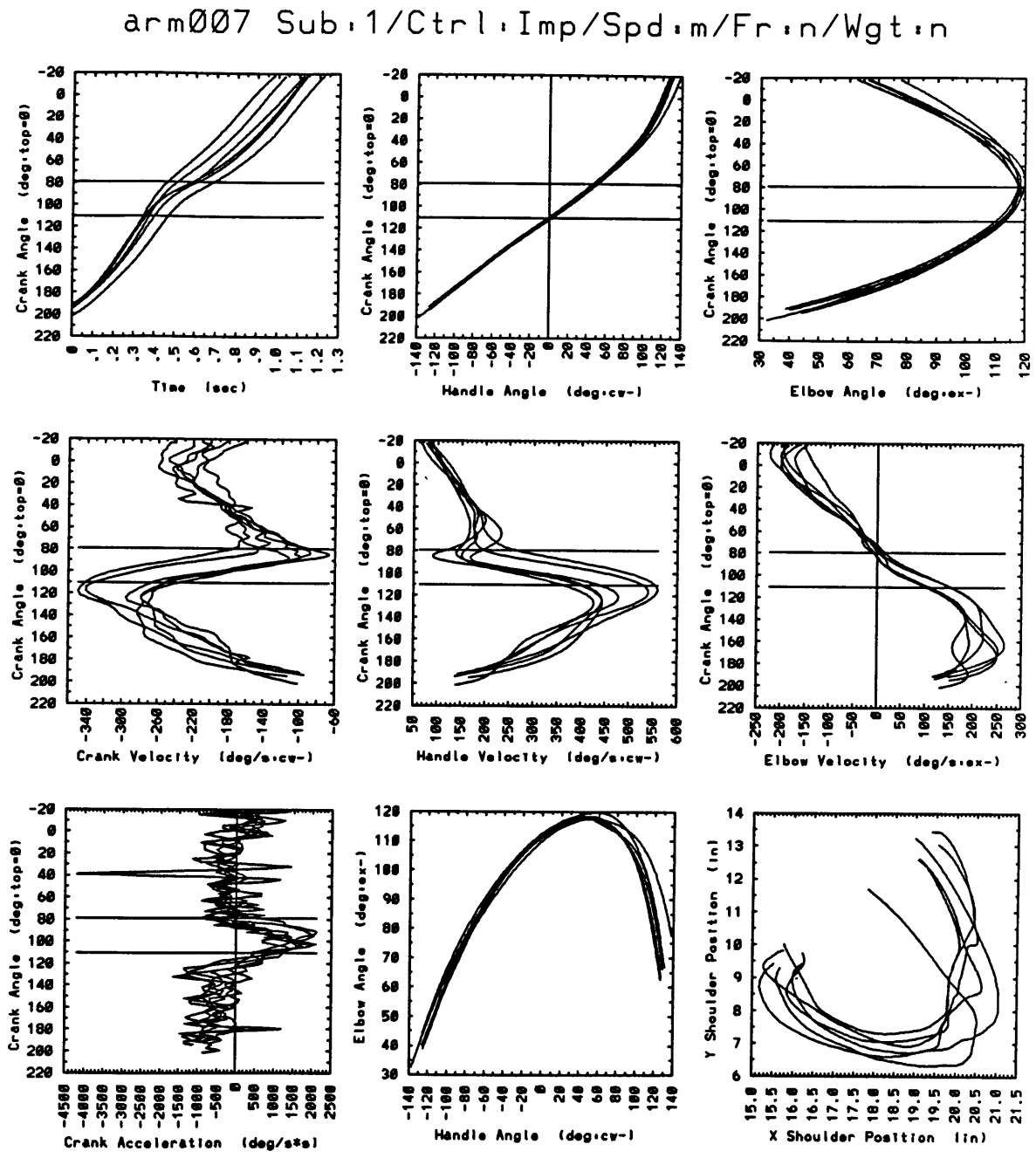
arm007 Sub:1/Ctrl:Imp/Spd:m/Fr:n/Wgt:n
Crank Angle (deg:top=0)
Time (sec)
Handle Angle (deg:cw-)
Elbow Angle (deg:ex-)
Crank Velocity (deg/s:cw-)
Handle Velocity (deg/s:cw-)
Elbow Velocity (deg/s:ex-)
Crank Acceleration (deg/s**s)
Elbow Angle (deg:ex-)
Handle Angle (deg:cw-)
Y Shoulder Position (in)
X Shoulder Position (in)

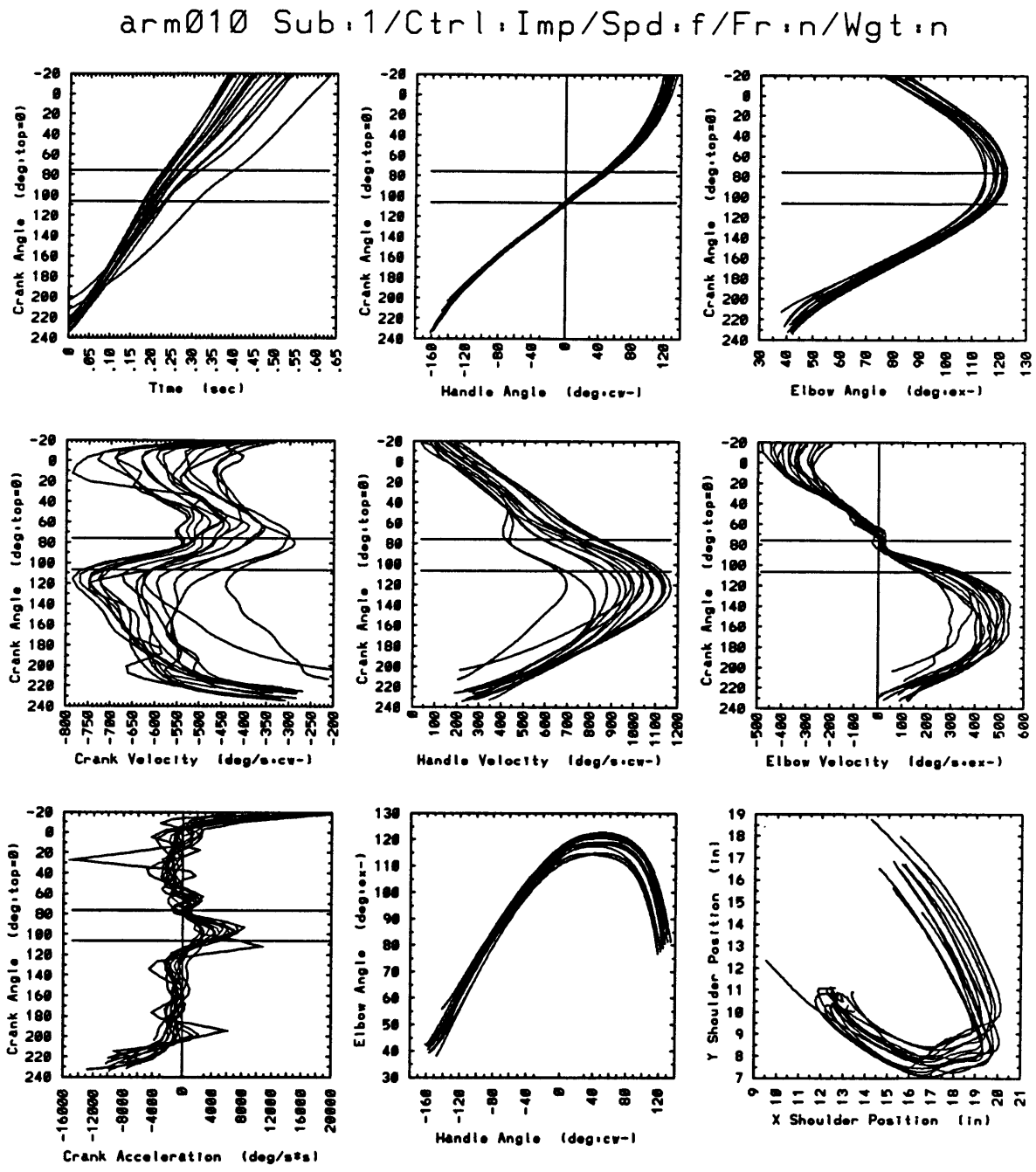
arm010 Sub:1/Ctrl:Imp/Spd:f/Fr:n/Wgt:n
Crank Angle (deg:top=0)
Time (sec)
Handle Angle (deg:cw-)
Elbow Angle (deg:ex-)
Crank Velocity (deg/s:cw-)
Handle Velocity (deg/s:cw-)
Elbow Velocity (deg/s:ex-)
Crank Acceleration (deg/s**2)
Y Shoulder Position (in)
X Shoulder Position (in)

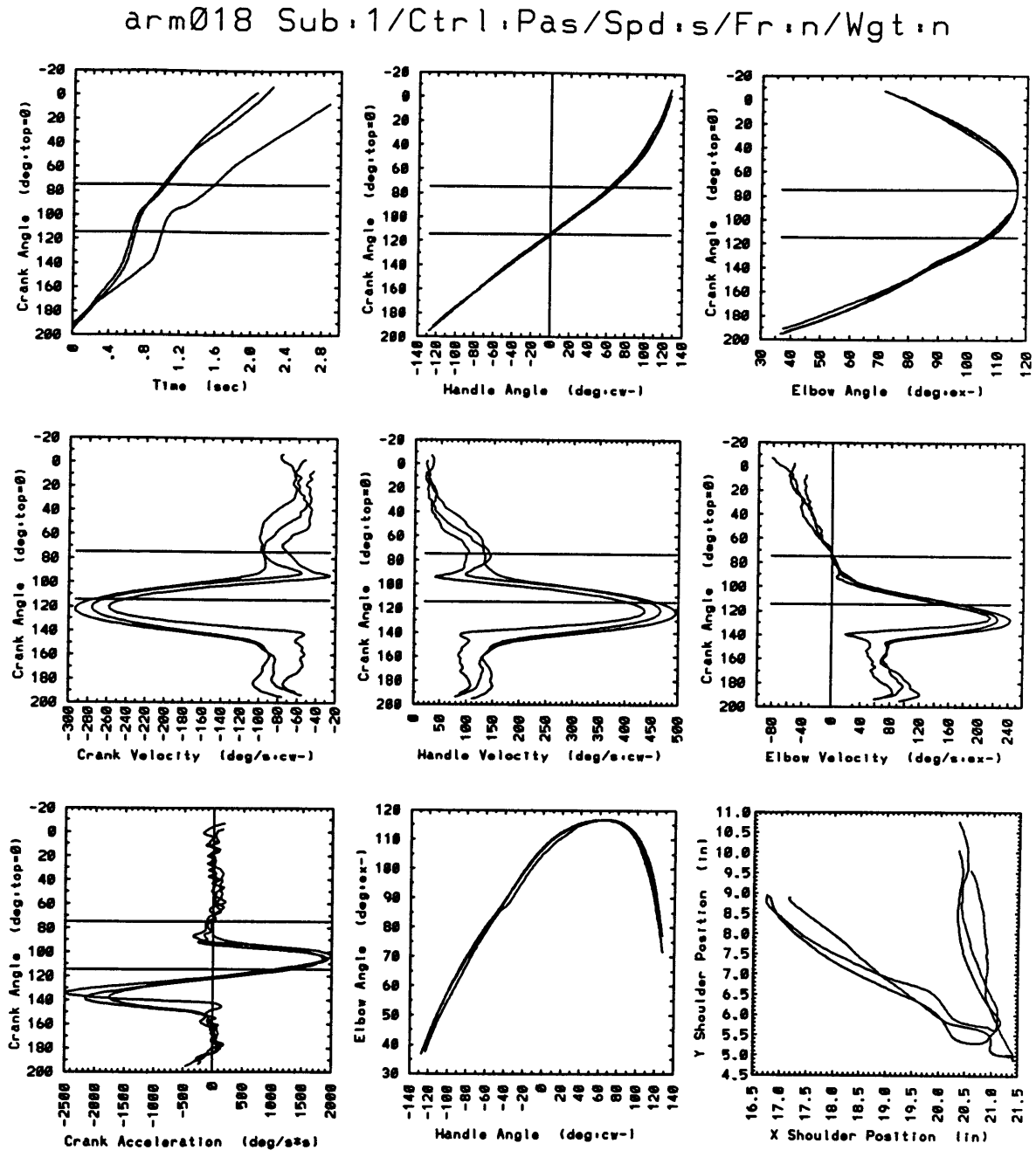
arm018 Sub:1/Ctrl:Pas/Spd:s/Fr:n/Wgt:n
Crank Angle (deg:top=0)
Time (sec)
Handle Angle (deg:cw-)
Elbow Angle (deg:ex-)
Crank Velocity (deg/s:cw-)
Handle Velocity (deg/s:cw-)
Elbow Velocity (deg/s:ex-)
Crank Acceleration (deg/s^2)
Y Shoulder Position (in)
X Shoulder Position (in)

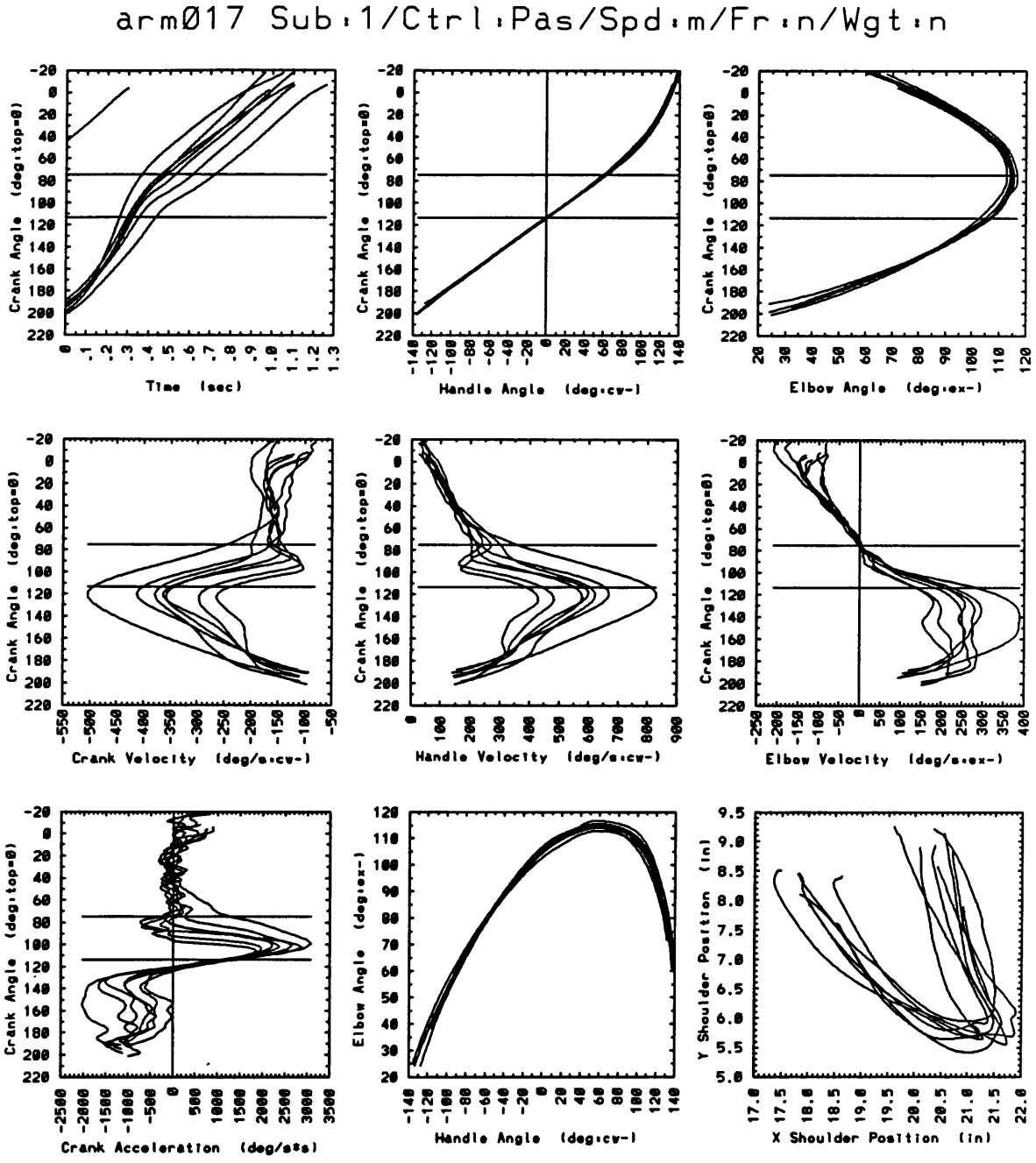
arm017 Sub:1/Ctrl:Pas/Spd:m/Fr:n/Wgt:n
Crank Angle (deg:top=0)
Time (sec)
Handle Angle (deg:cw-)
Elbow Angle (deg:ex-)
Crank Velocity (deg/s:cw-)
Handle Velocity (deg/s:cw-)
Elbow Velocity (deg/s:ex-)
Crank Acceleration (deg/s^2)
Y Shoulder Position (in)
X Shoulder Position (in)

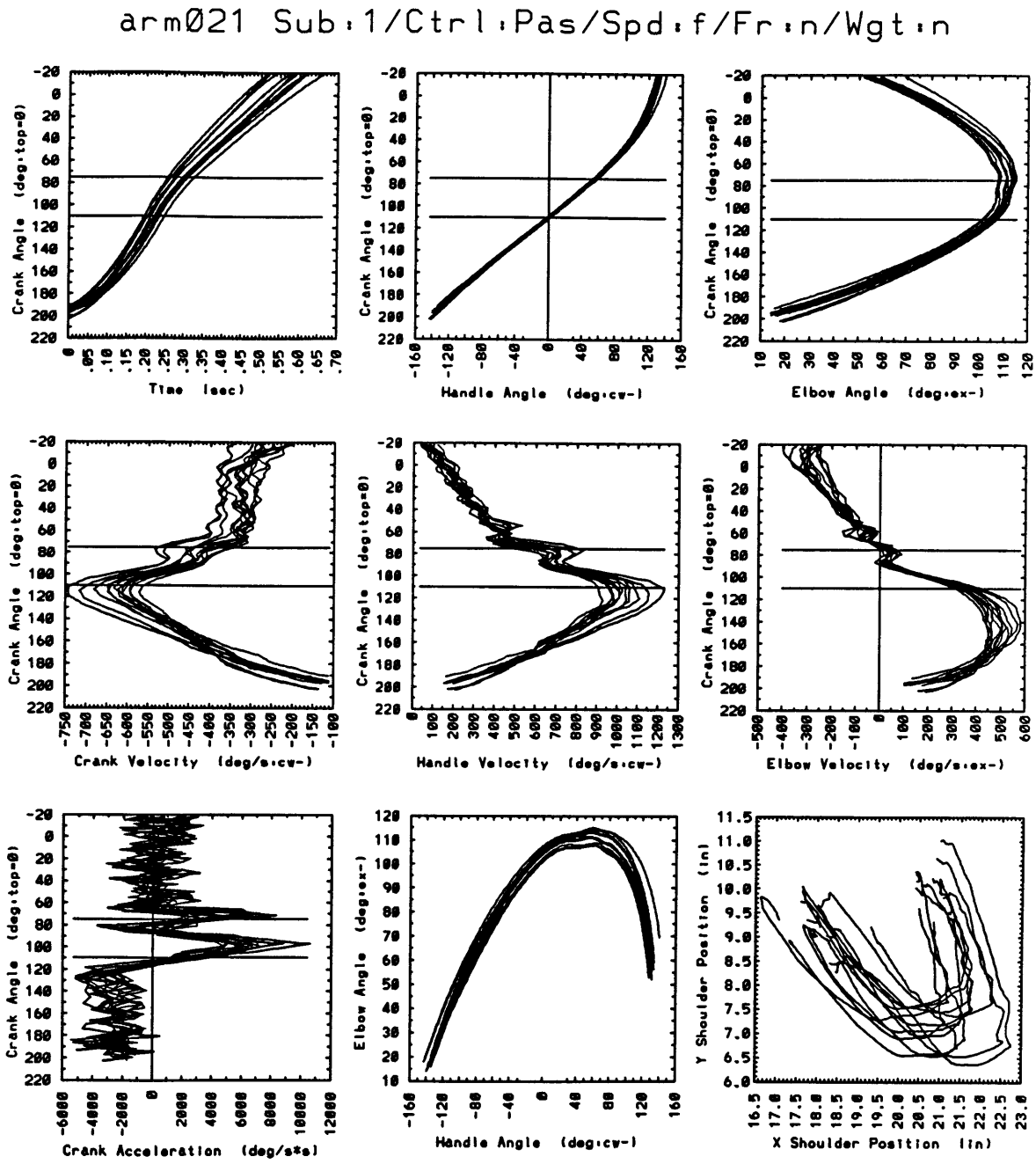
arm021 Sub:1/Ctrl:Pas/Spd:f/Fr:n/Wgt:n
Crank Angle (deg:top=0)
Time (sec)
Handle Angle (deg:cw-)
Elbow Angle (deg:ex-)
Crank Velocity (deg/s:cw-)
Handle Velocity (deg/s:cw-)
Elbow Velocity (deg/s:ex-)
Crank Acceleration (deg/s*s)
Elbow Angle (deg:ex-)
Y Shoulder Position (in)
X Shoulder Position (in)

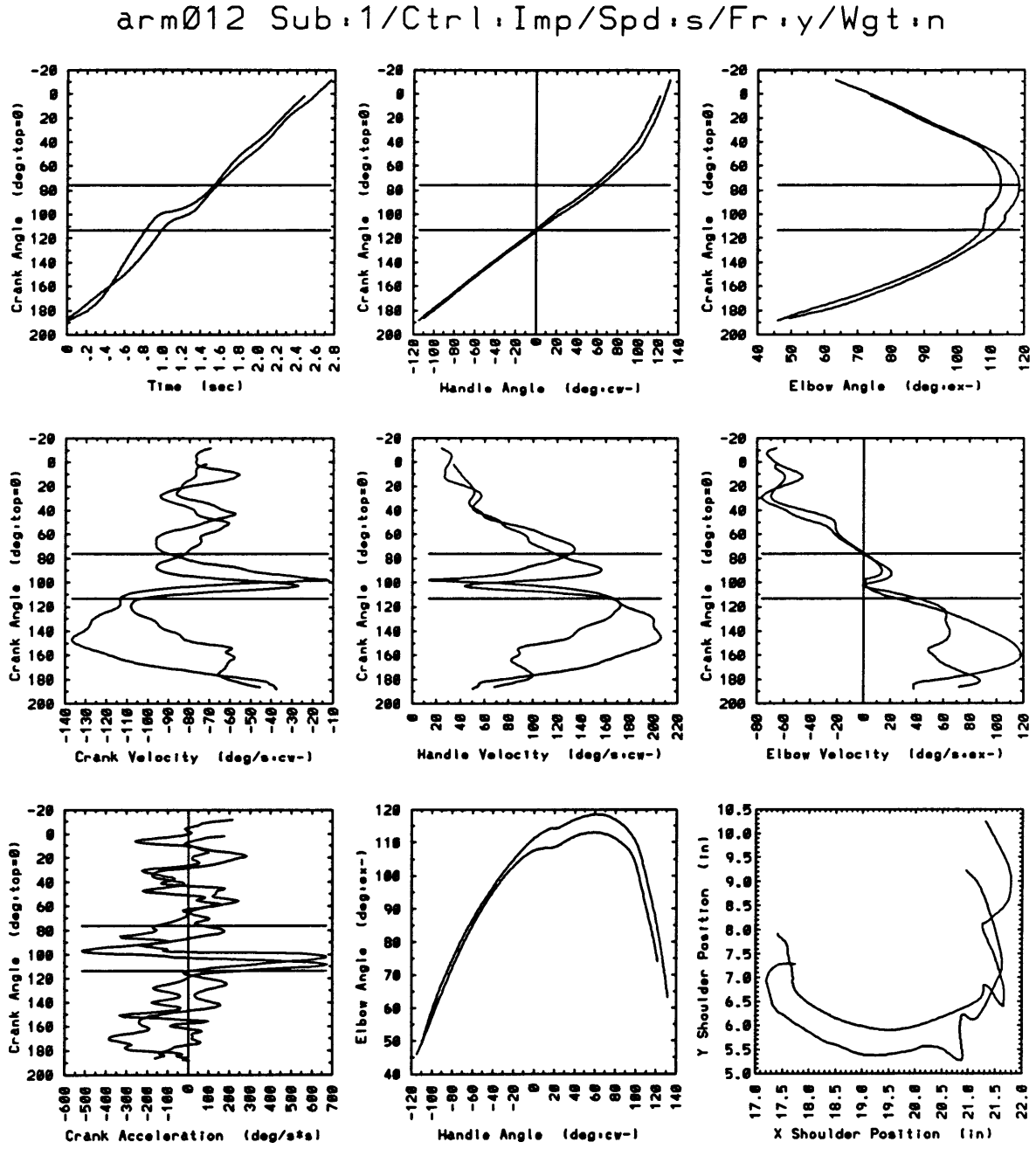
arm012 Sub:1/Ctrl:Imp/Spd:s/Fr:y/Wgt:n
Crank Angle (deg:top=0)
Time (sec)
Handle Angle (deg:cw-)
Elbow Angle (deg:ex-)
Crank Velocity (deg/s:cw-)
Handle Velocity (deg/s:cw-)
Elbow Velocity (deg/s:ex-)
Crank Acceleration (deg/s*s)
Elbow Angle (deg:ex-)
Handle Angle (deg:cw-)
Y Shoulder Position (in)
X Shoulder Position (in)

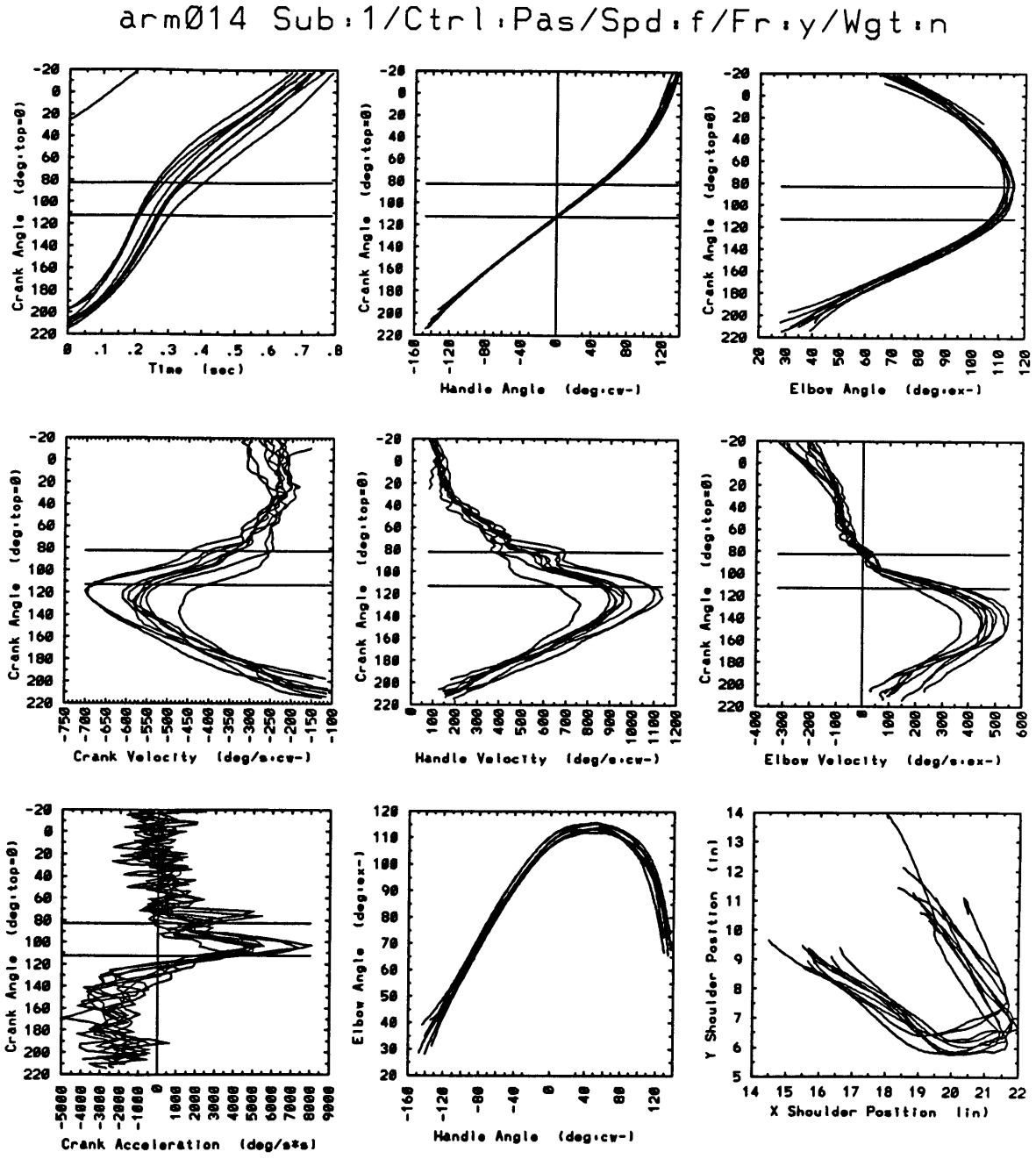
arm014 Sub:1/Ctrl:Pas/Spd:f/Fr:y/Wgt:n
Crank Angle (deg:top=0)
Time (sec)
Handle Angle (deg:cw-)
Elbow Angle (deg:ex-)
Crank Velocity (deg/s:cw-)
Handle Velocity (deg/s:cw-)
Elbow Velocity (deg/s:ex-)
Crank Acceleration (deg/s*s)
Elbow Angle (deg:ex-)
Handle Angle (deg:cw-)
Y Shoulder Position (in)
X Shoulder Position (in)

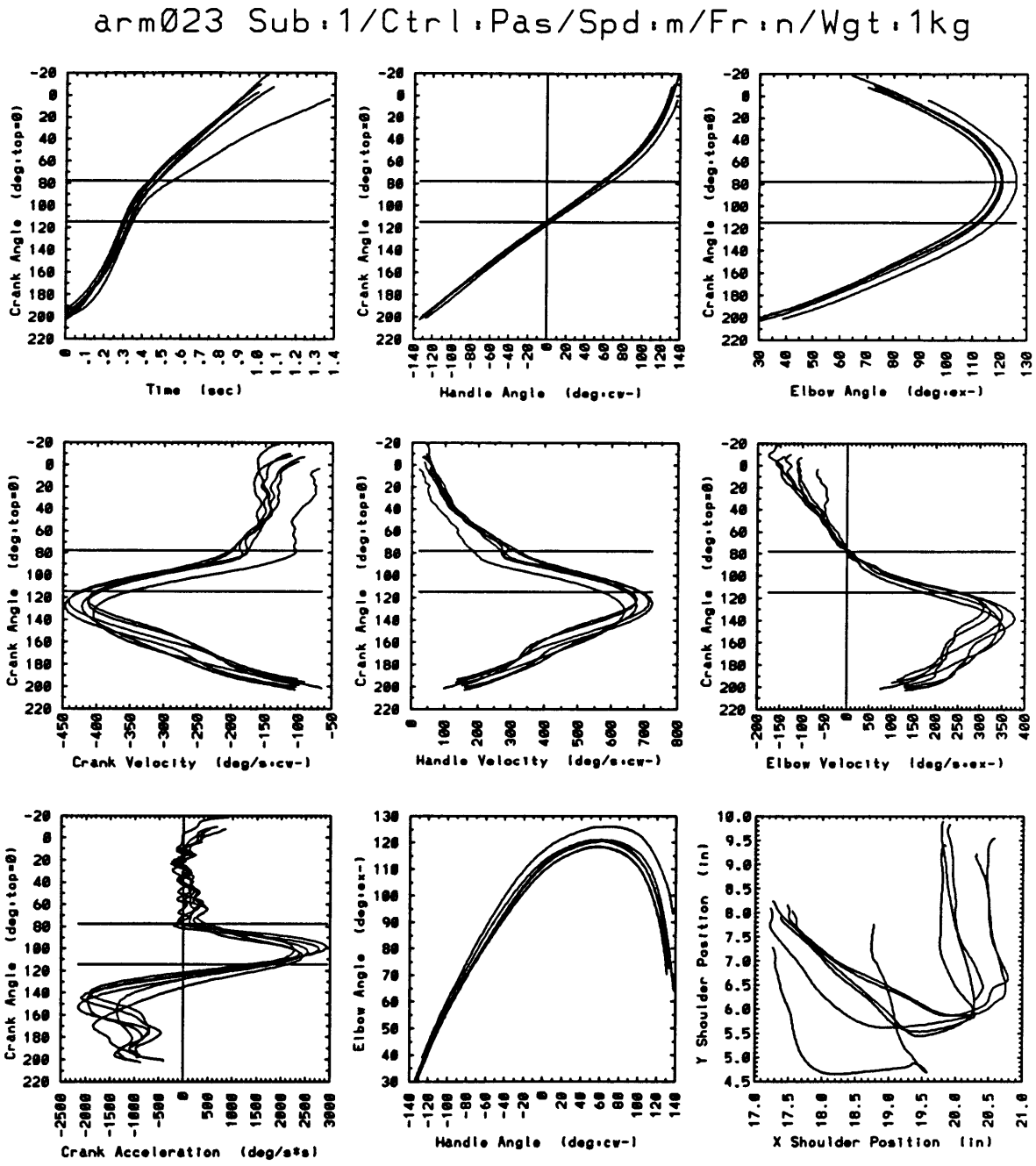
arm023 Sub:1/Ctrl:Pas/Spd:m/Fr:n/Wgt:1kg
Crank Angle (deg:top=0)
Time (sec)
Handle Angle (deg:cw-)
Elbow Angle (deg:ex-)
Crank Velocity (deg/s:cw-)
Handle Velocity (deg/s:cw-)
Elbow Velocity (deg/s:ex-)
Crank Acceleration (deg/s*s)
Y Shoulder Position (in)
X Shoulder Position (in)

SUBJECT 2

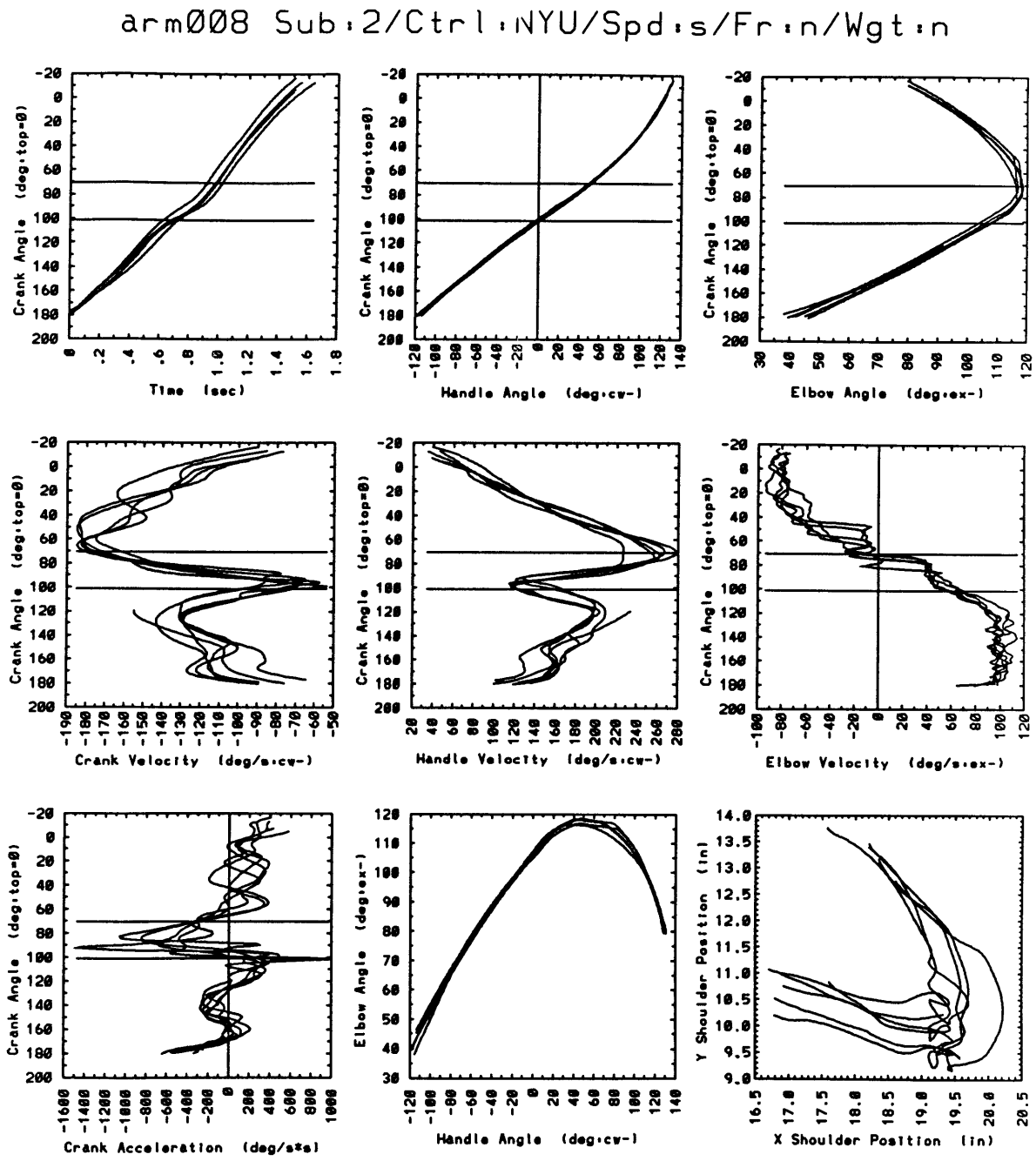
arm008 Sub:2/Ctrl:NYU/Spd:s/Fr:n/Wgt:n
Crank Angle (deg:top=0)
Time (sec)
Handle Angle (deg:cw-)
Elbow Angle (deg:ex-)
Crank Velocity (deg/s:cw-)
Handle Velocity (deg/s:cw-)
Elbow Velocity (deg/s:ex-)
Crank Acceleration (deg/s*s)
Y Shoulder Position (in)
X Shoulder Position (in)

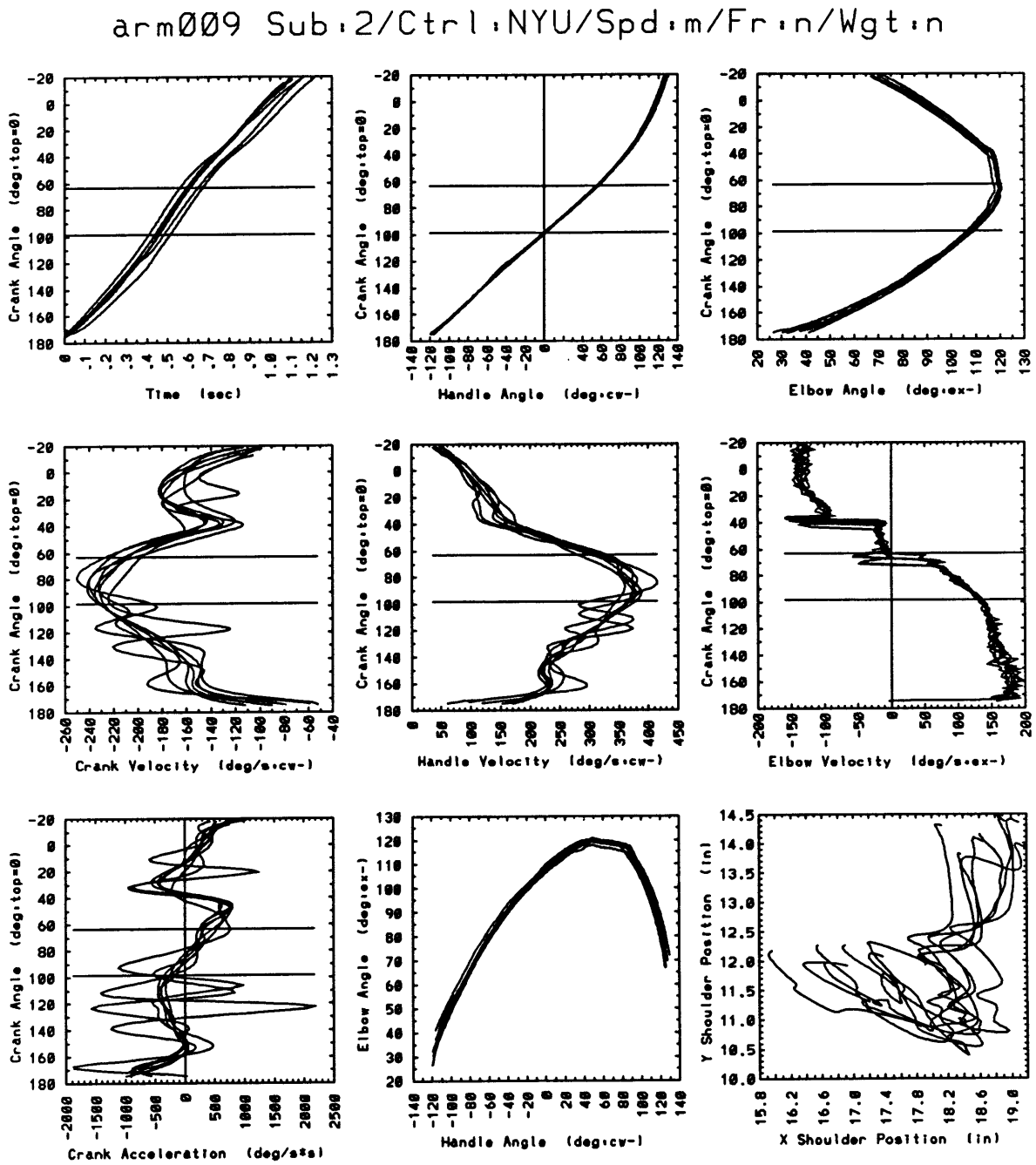
arm009 Sub:2/Ctrl:NYU/Spd:m/Fr:n/Wgt:n
Crank Angle (deg:top=0)
Time (sec)
Handle Angle (deg:cw-)
Elbow Angle (deg:ex-)
Crank Velocity (deg/s:cw-)
Handle Velocity (deg/s:cw-)
Elbow Velocity (deg/s:ex-)
Crank Acceleration (deg/s*s)
Y Shoulder Position (in)
X Shoulder Position (in)

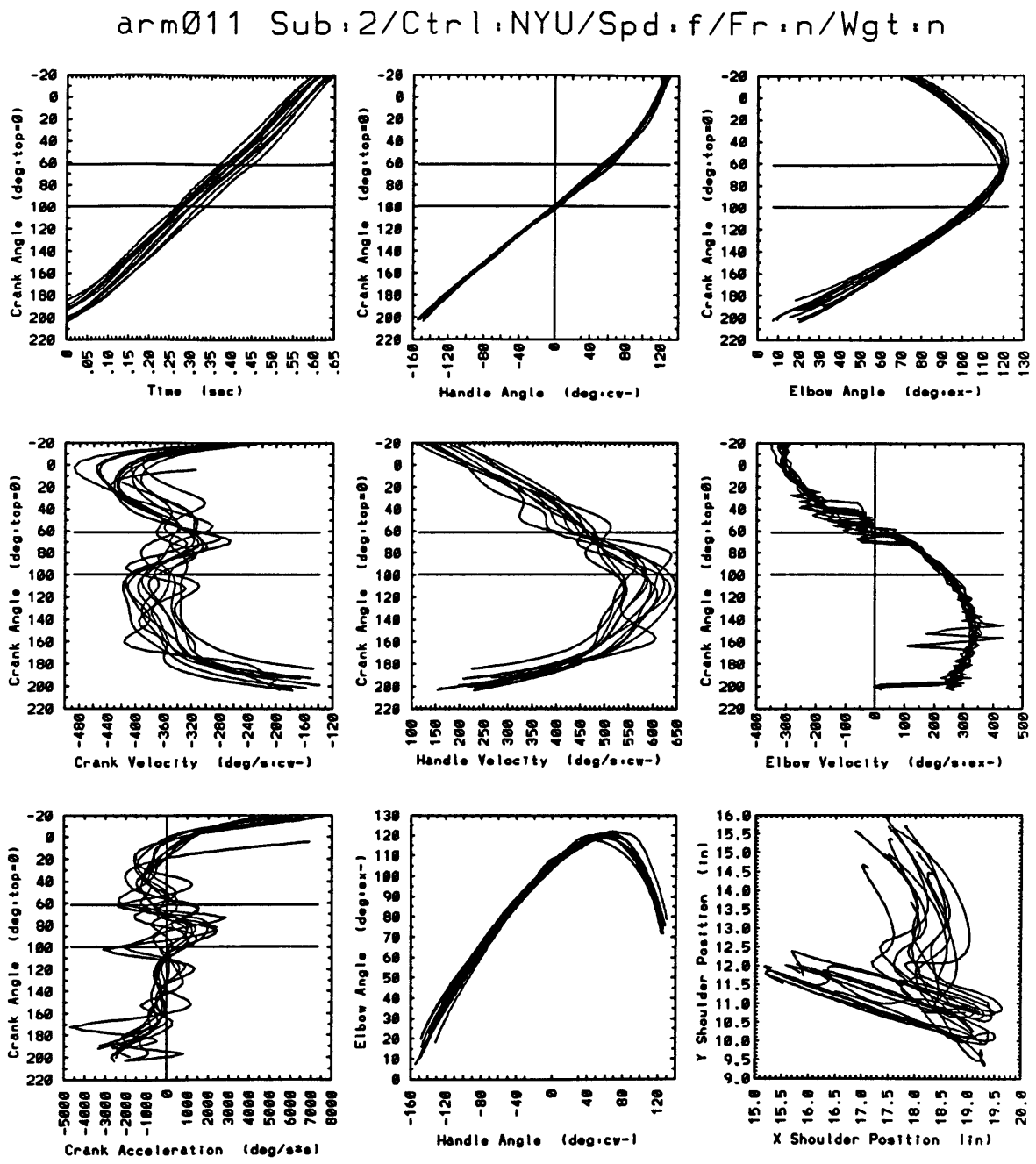
arm011 Sub:2/Ctrl:NYU/Spd:f/Fr:n/Wgt:n
Crank Angle (deg:top=0)
Time (sec)
Handle Angle (deg:cw-)
Elbow Angle (deg:ex-)
Crank Velocity (deg/s:cw-)
Handle Velocity (deg/s:cw-)
Elbow Velocity (deg/s:ex-)
Crank Acceleration (deg/s*s)
Elbow Angle (deg:ex-)
Y Shoulder Position (in)
X Shoulder Position (in)

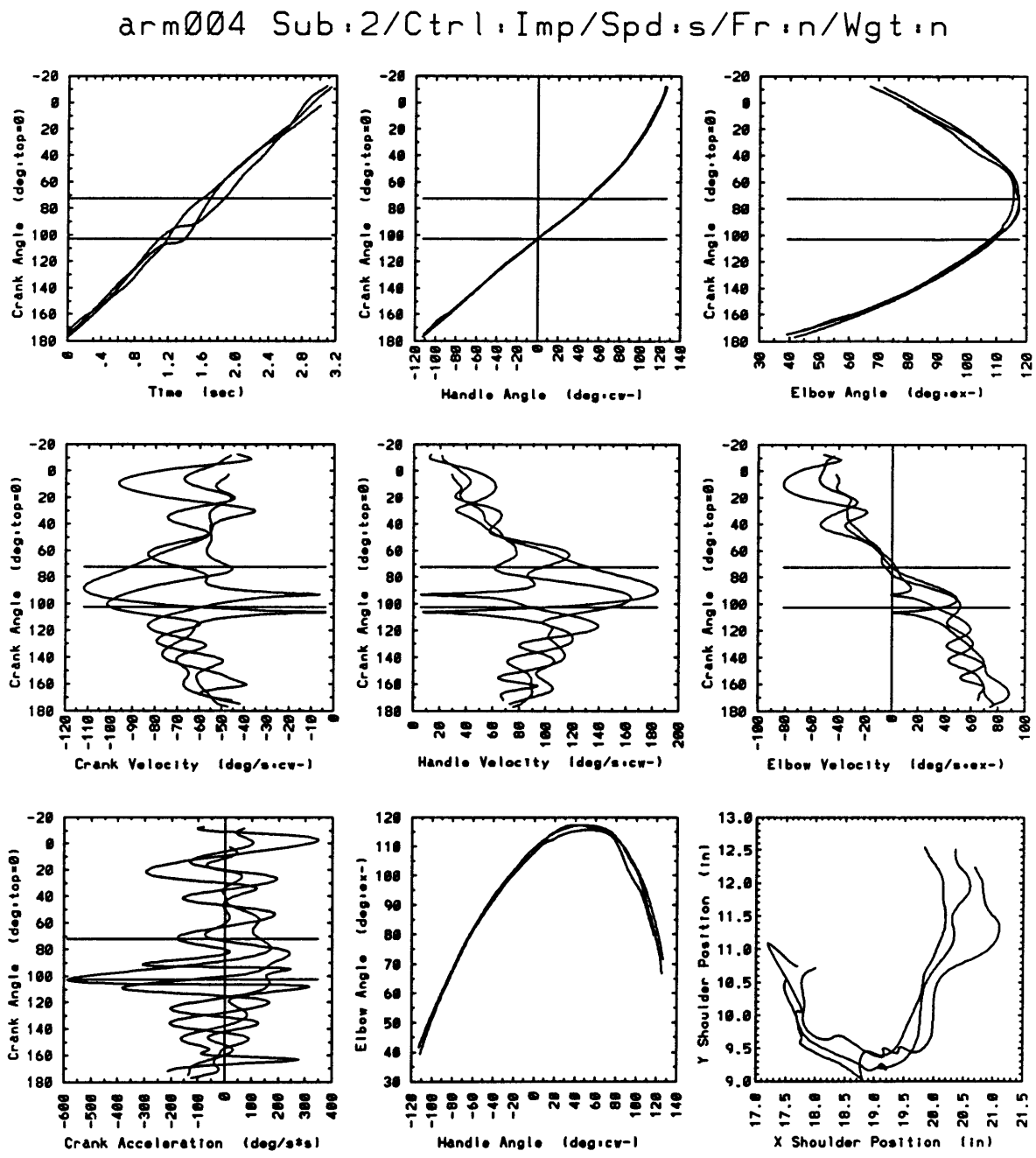
arm004 Sub:2/Ctrl:Imp/Spd:s/Fr:n/Wgt:n
Crank Angle (deg:top=0)
Time (sec)
Handle Angle (deg:cw-)
Elbow Angle (deg:ex-)
Crank Velocity (deg/s:cw-)
Handle Velocity (deg/s:cw-)
Elbow Velocity (deg/s:ex-)
Crank Acceleration (deg/s*s)
Y Shoulder Position (in)
X Shoulder Position (in)

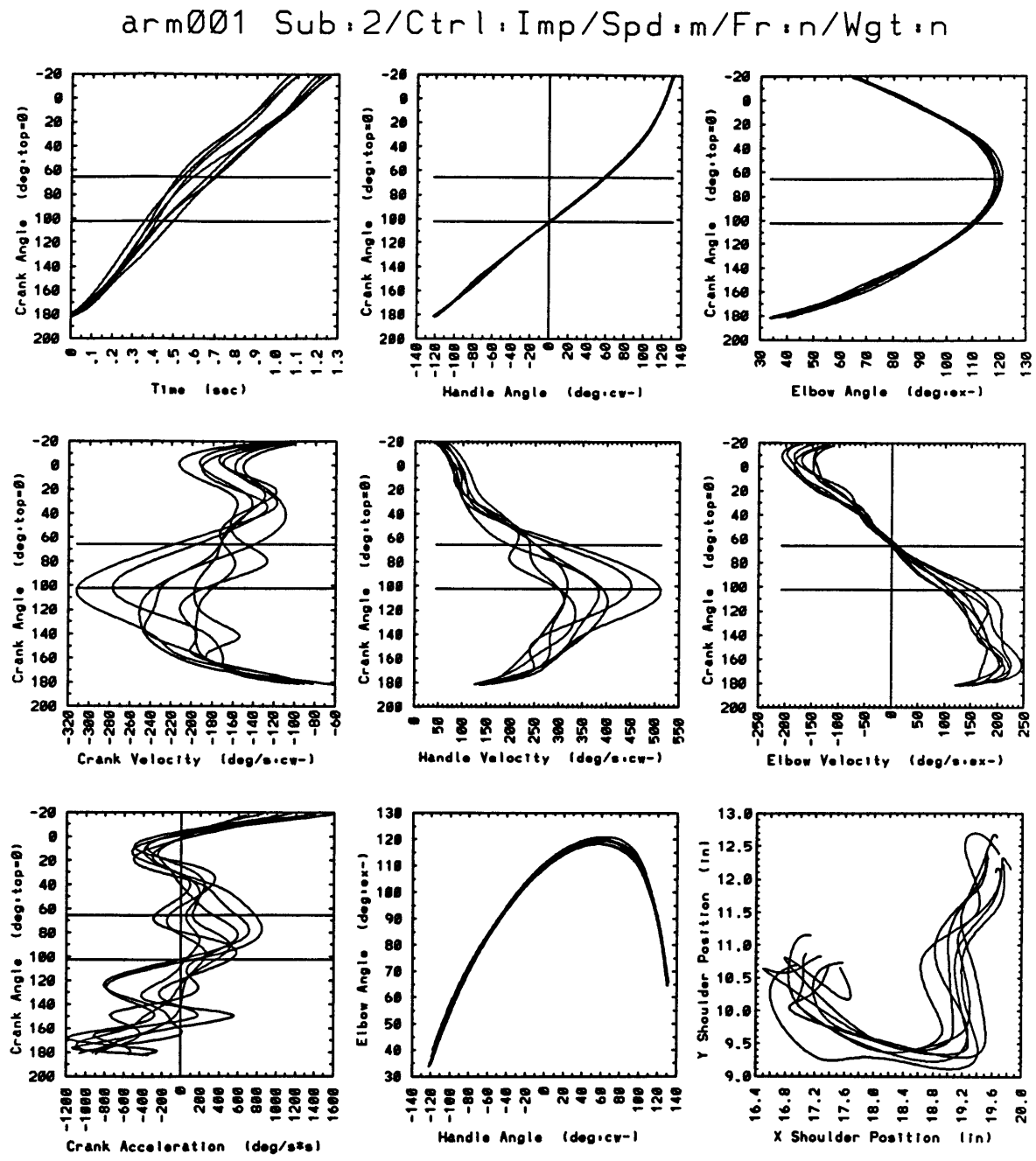
arm001 Sub:2/Ctrl:Imp/Spd:m/Fr:n/Wgt:n
Crank Angle (deg:top=0)
Time (sec)
Handle Angle (deg:cw-)
Elbow Angle (deg:ex-)
Crank Velocity (deg/s:cw-)
Handle Velocity (deg/s:cw-)
Elbow Velocity (deg/s:ex-)
Crank Acceleration (deg/s**s)
Elbow Angle (deg:ex-)
Handle Angle (deg:cw-)
Y Shoulder Position (in)
X Shoulder Position (in)

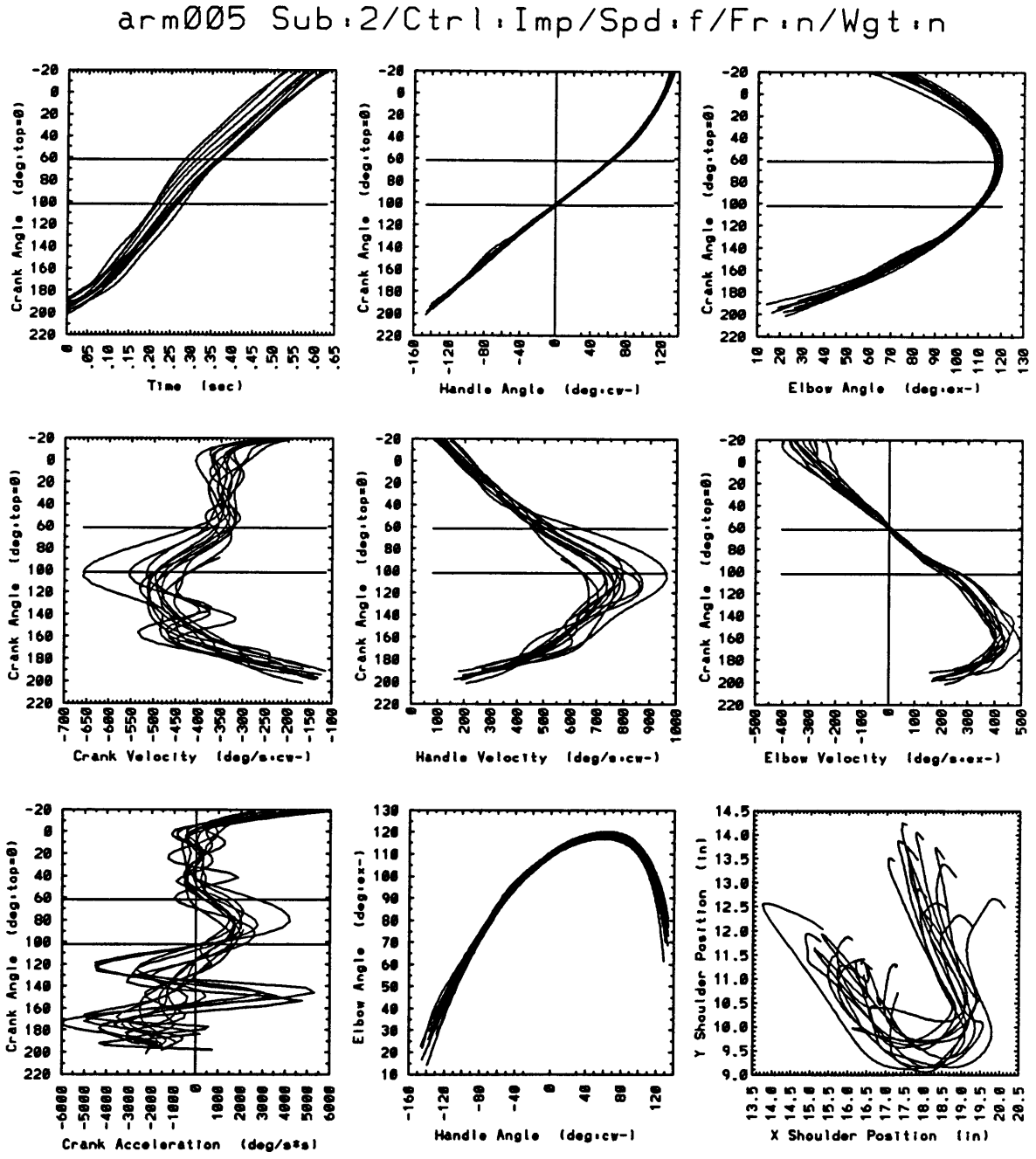
arm005 Sub:2/Ctrl:Imp/Spd:f/Fr:n/Wgt:n
Crank Angle (deg:top=0)
Time (sec)
Handle Angle (deg:cw-)
Elbow Angle (deg:ex-)
Crank Velocity (deg/s:cw-)
Handle Velocity (deg/s:cw-)
Elbow Velocity (deg/s:ex-)
Crank Acceleration (deg/s*s)
Elbow Angle (deg:ex-)
Y Shoulder Position (in)
X Shoulder Position (in)

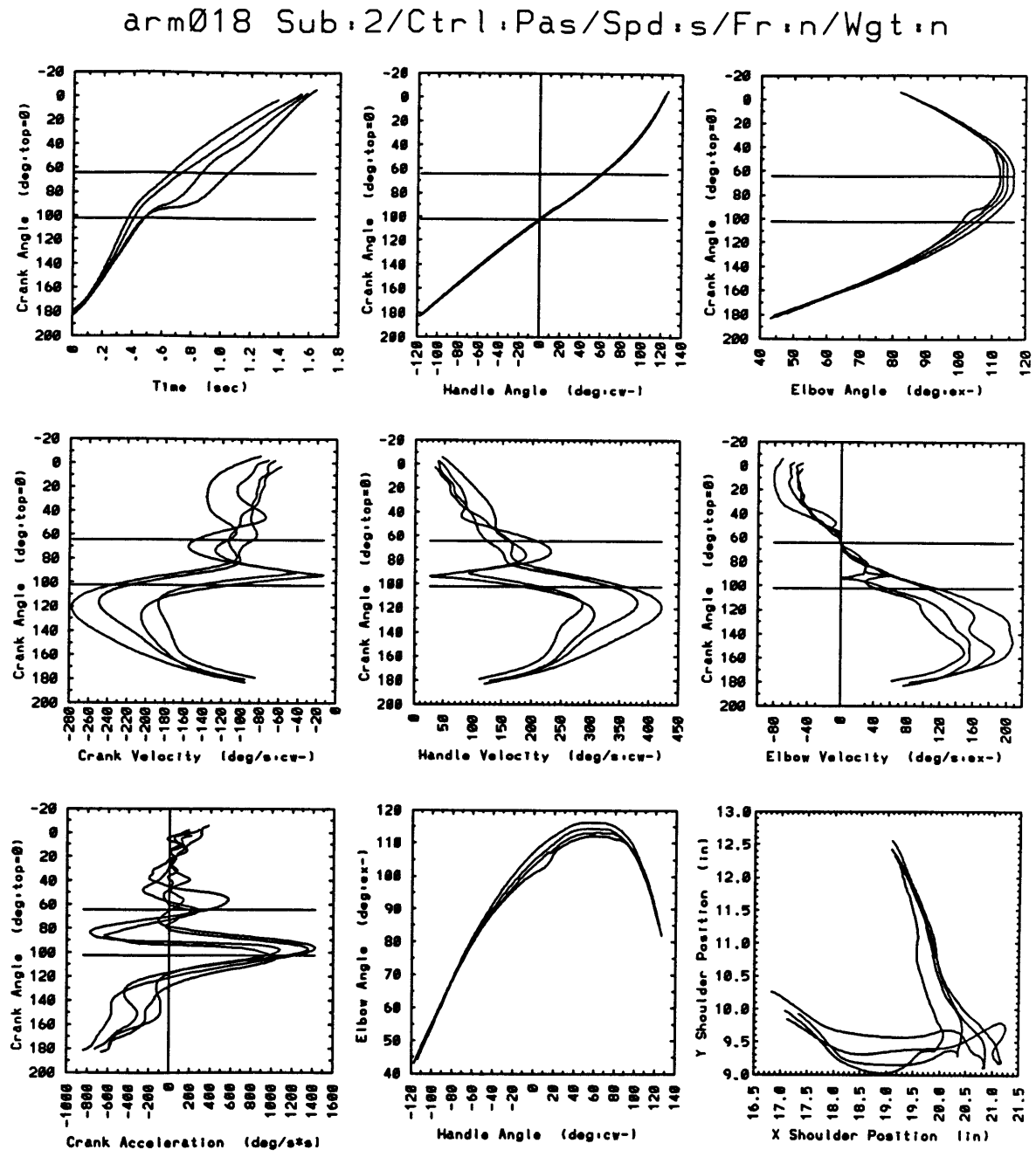
arm018 Sub:2/Ctrl:Pas/Spd:s/Fr:n/Wgt:n
Crank Angle (deg:top=0)
Time (sec)
Handle Angle (deg:cw-)
Elbow Angle (deg:ex-)
Crank Velocity (deg/s:cw-)
Handle Velocity (deg/s:cw-)
Elbow Velocity (deg/s:ex-)
Crank Acceleration (deg/s*s)
Elbow Angle (deg:ex-)
Handle Angle (deg:cw-)
Y Shoulder Position (in)
X Shoulder Position (in)

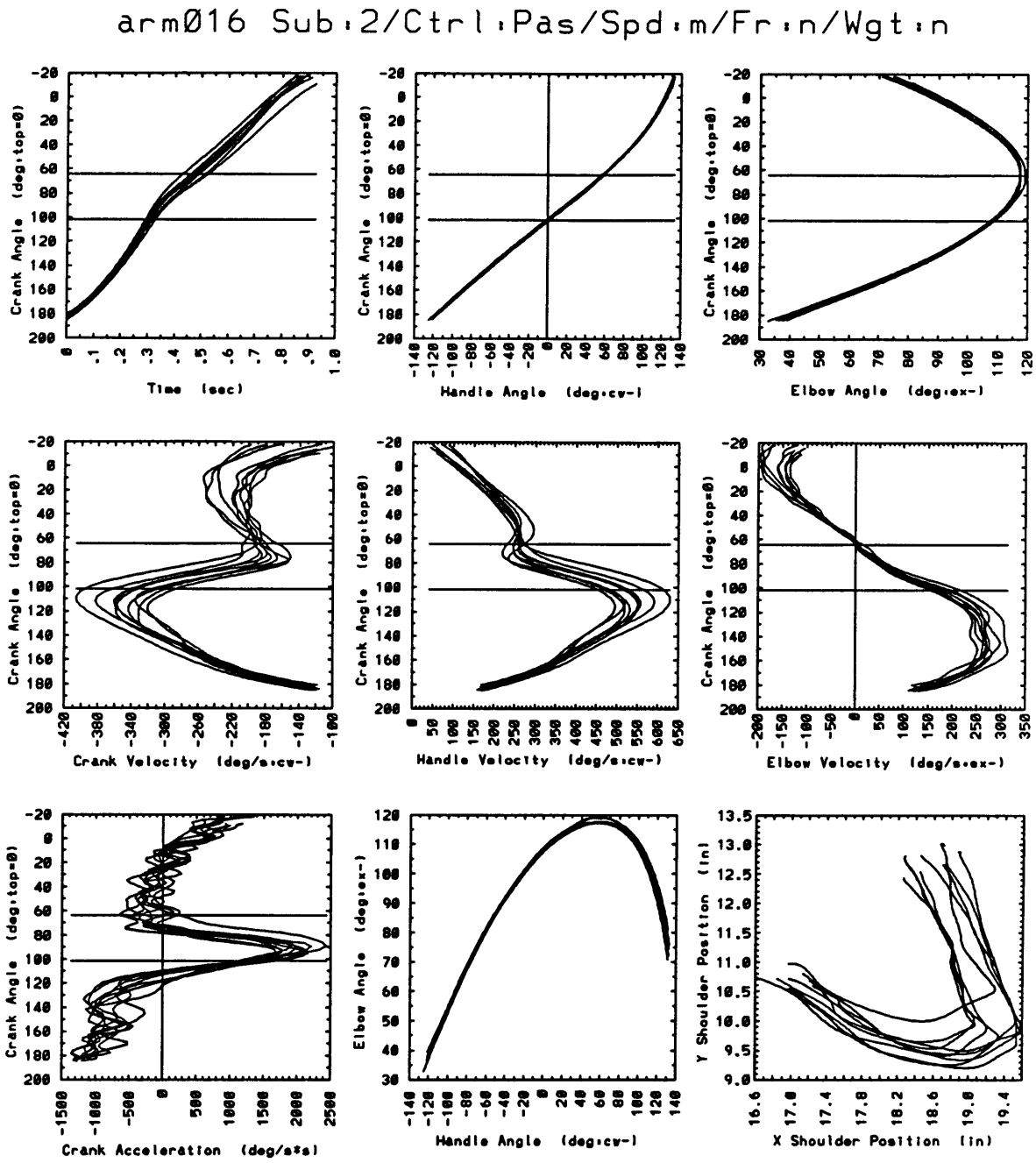
arm016 Sub:2/Ctrl:Pas/Spd:m/Fr:n/Wgt:n
Crank Angle (deg:top=0)
Time (sec)
Handle Angle (deg:cw-)
Elbow Angle (deg:ex-)
Crank Velocity (deg/s:cw-)
Handle Velocity (deg/s:cw-)
Elbow Velocity (deg/s:ex-)
Crank Acceleration (deg/s*s)
Y Shoulder Position (in)
X Shoulder Position (in)

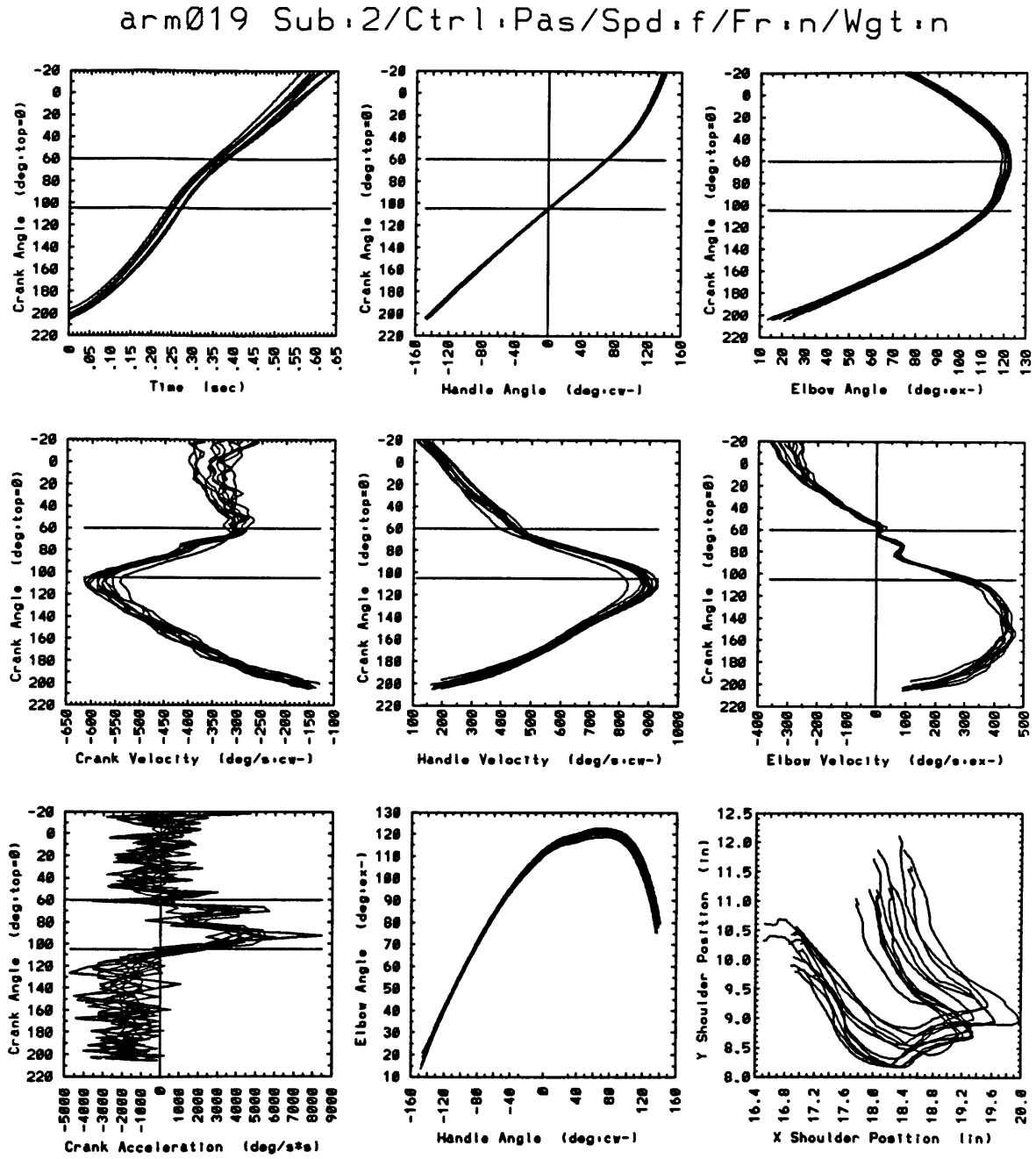
arm019 Sub:2/Ctrl:Pas/Spd:f/Fr:n/Wgt:n
Crank Angle (deg:top=0)
Time (sec)
Handle Angle (deg:cw-)
Elbow Angle (deg:ex-)
Crank Velocity (deg/s:cw-)
Handle Velocity (deg/s:cw-)
Elbow Velocity (deg/s:ex-)
Crank Acceleration (deg/s*s)
Elbow Angle (deg:ex-)
Y Shoulder Position (in)
X Shoulder Position (in)

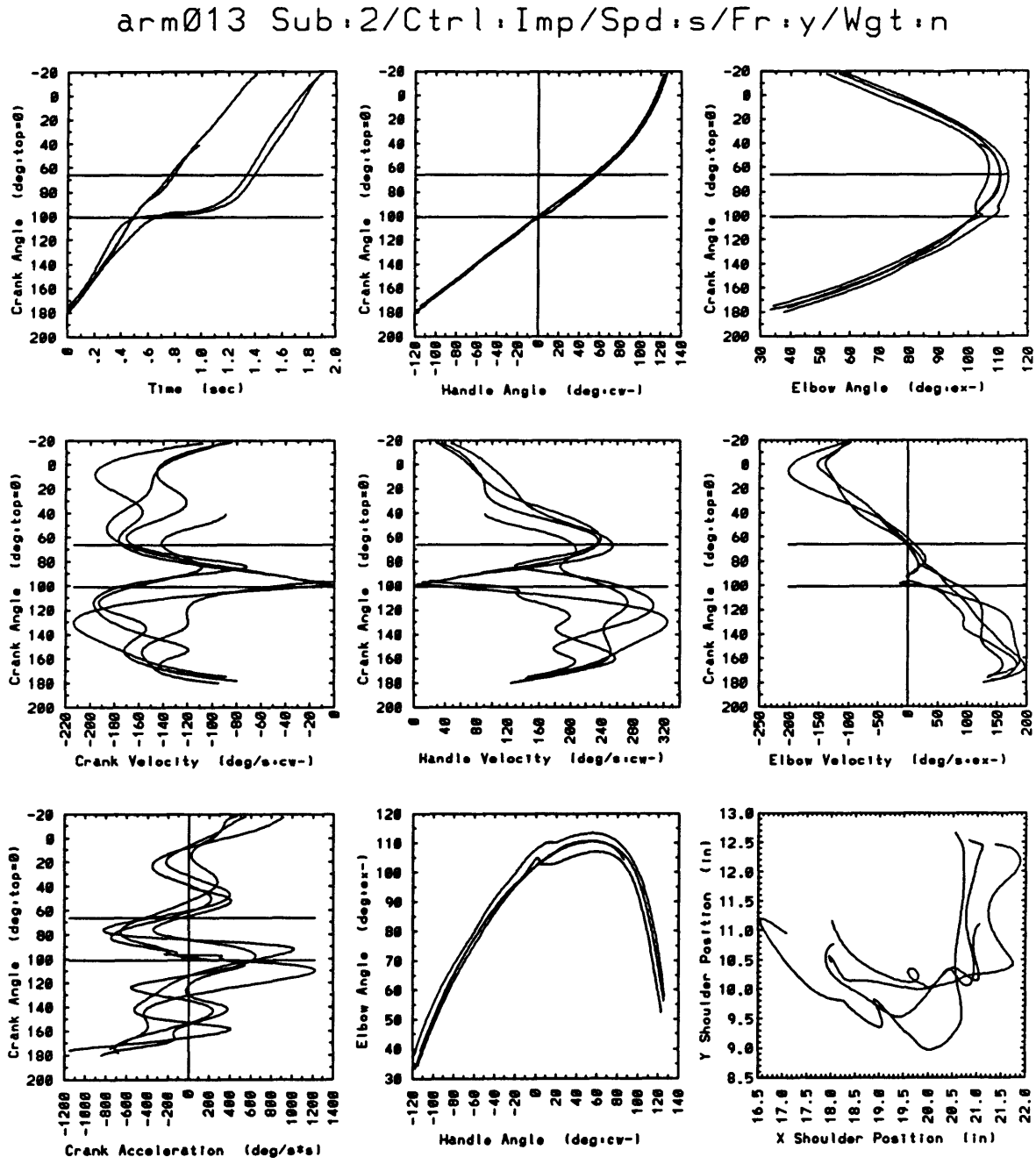
arm013 Sub:2/Ctrl:Imp/Spd:s/Fr:y/Wgt:n
Crank Angle (deg:top=0)
Time (sec)
Handle Angle (deg:cw-)
Elbow Angle (deg:ex-)
Crank Velocity (deg/s:cw-)
Handle Velocity (deg/s:cw-)
Elbow Velocity (deg/s:ex-)
Crank Acceleration (deg/s*s)
Elbow Angle (deg:ex-)
Handle Angle (deg:cw-)
Y Shoulder Position (in)
X Shoulder Position (in)

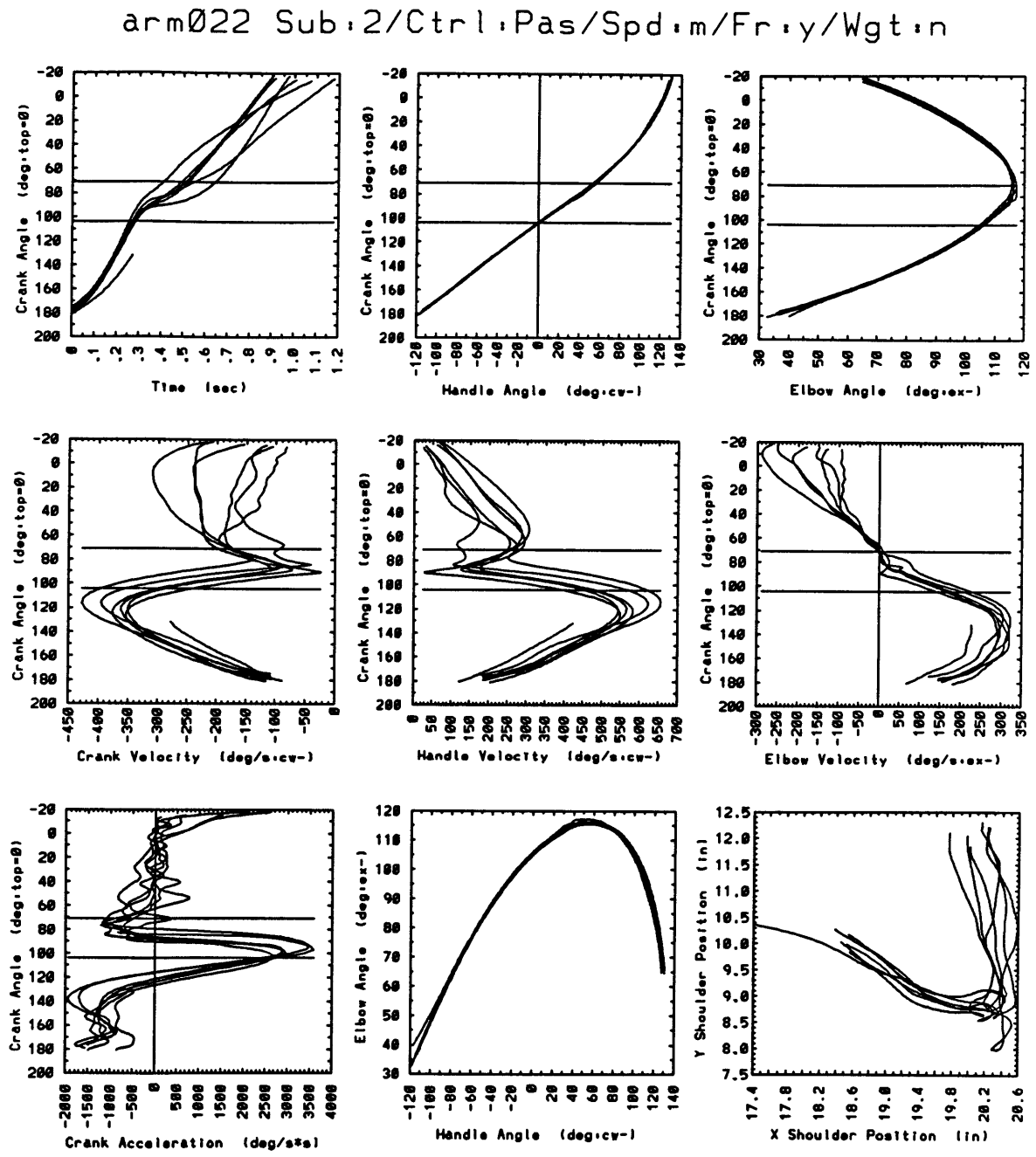
arm022 Sub:2/Ctrl:Pas/Spd:m/Fr:y/Wgt:n
Crank Angle (deg:top=0)
Time (sec)
Handle Angle (deg:cw-)
Elbow Angle (deg:ex-)
Crank Velocity (deg/s:cw-)
Handle Velocity (deg/s:cw-)
Elbow Velocity (deg/s:ex-)
Crank Acceleration (deg/s*s)
Y Shoulder Position (in)
X Shoulder Position (in)

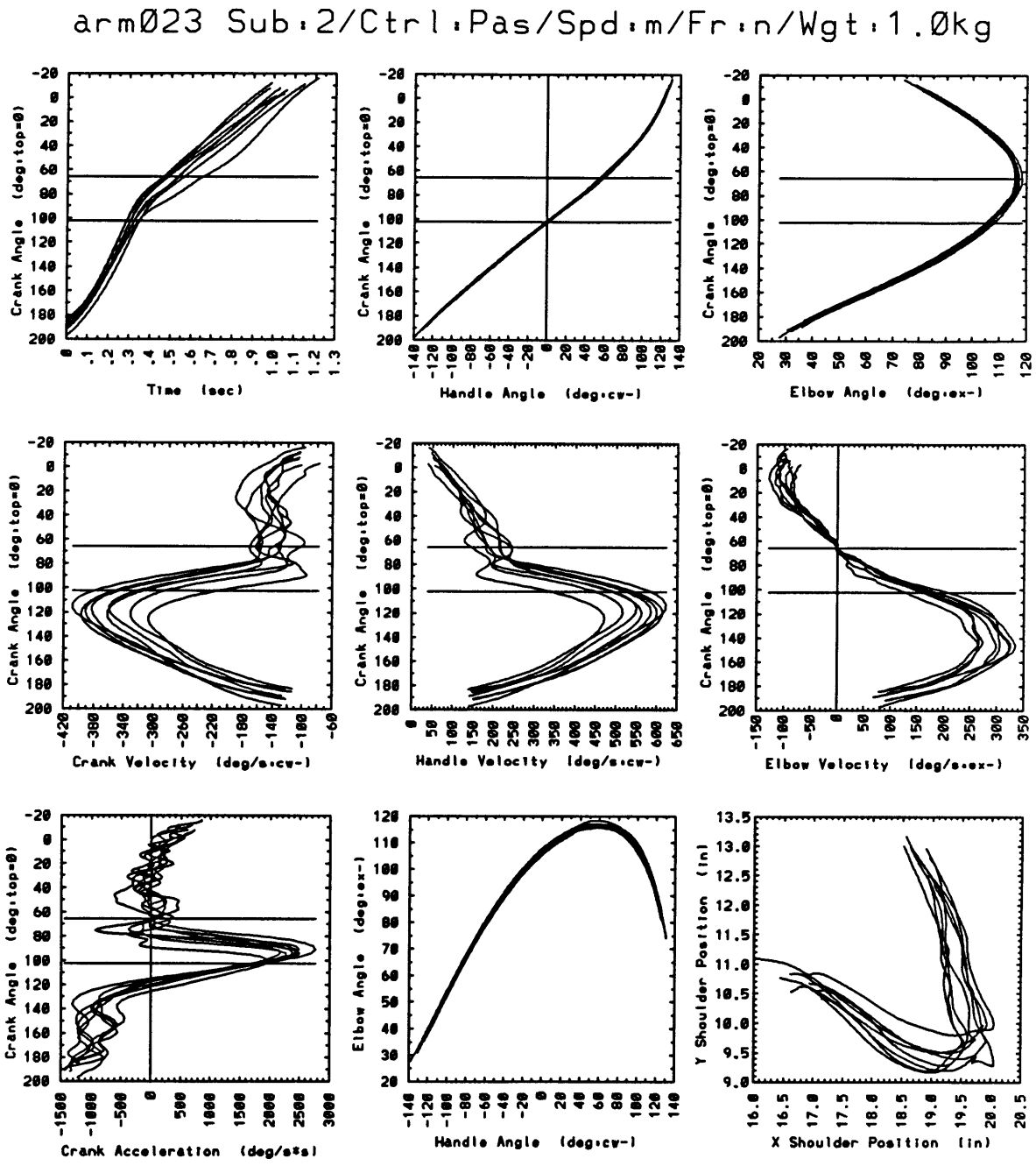
arm023 Sub:2/Ctrl:Pas/Spd:m/Fr:n/Wgt:1.0kg
Crank Angle (deg:top=0)
Time (sec)
Handle Angle (deg:cw-)
Elbow Angle (deg:ex-)
Crank Velocity (deg/s:cw-)
Handle Velocity (deg/s:cw-)
Elbow Velocity (deg/s:ex-)
Crank Acceleration (deg/s*s)
Elbow Angle (deg:ex-)
Handle Angle (deg:cw-)
Y Shoulder Position (in)
X Shoulder Position (in)

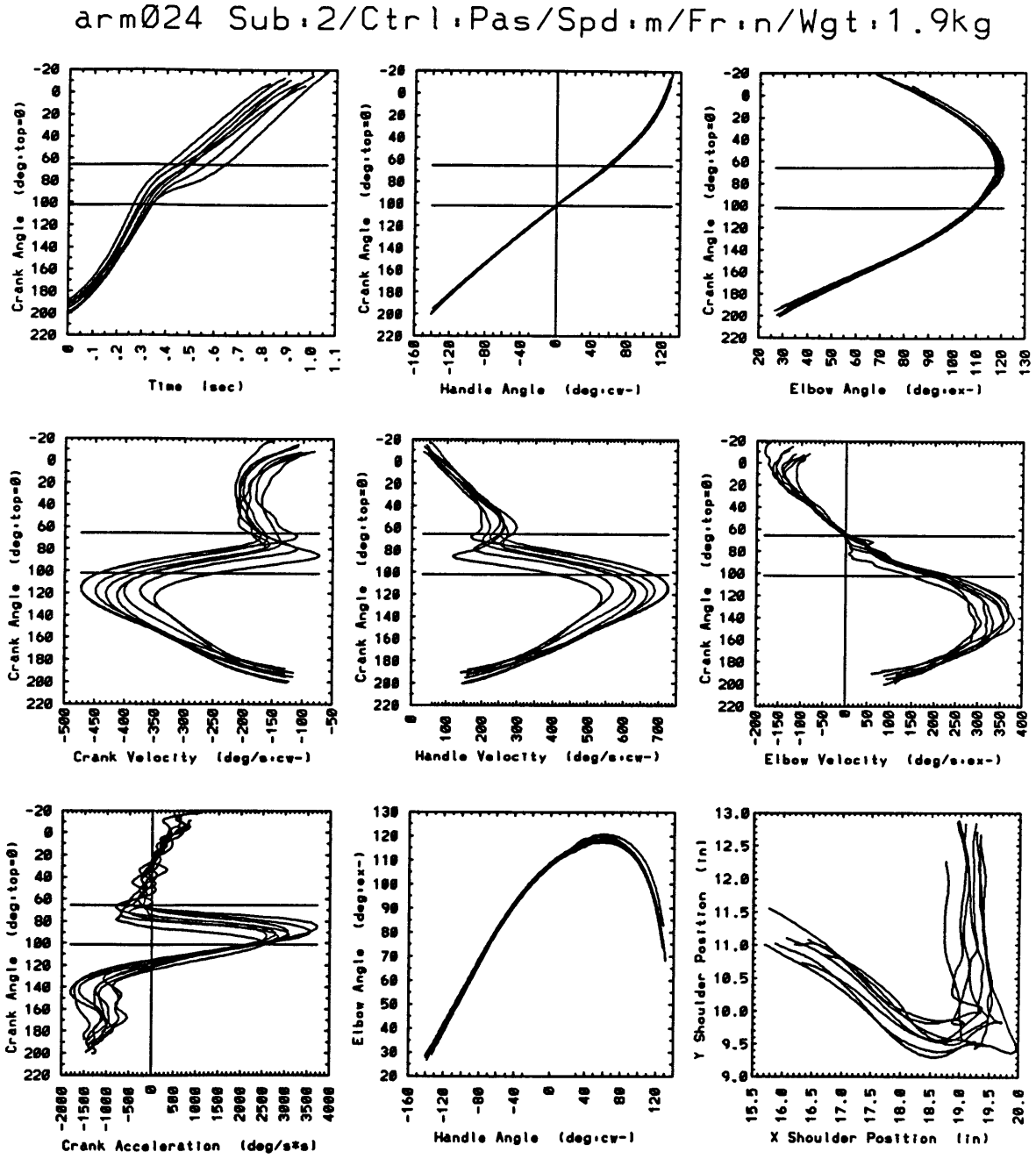
arm024 Sub:2/Ctrl:Pas/Spd:m/Fr:n/Wgt:1.9kg
Crank Angle (deg:top=0)
Time (sec)
Handle Angle (deg:cw-)
Elbow Angle (deg:ex-)
Crank Velocity (deg/s:cw-)
Handle Velocity (deg/s:cw-)
Elbow Velocity (deg/s:ex-)
Crank Acceleration (deg/s*s)
Elbow Angle (deg:ex-)
Handle Angle (deg:cw-)
Y Shoulder Position (in)
X Shoulder Position (in)

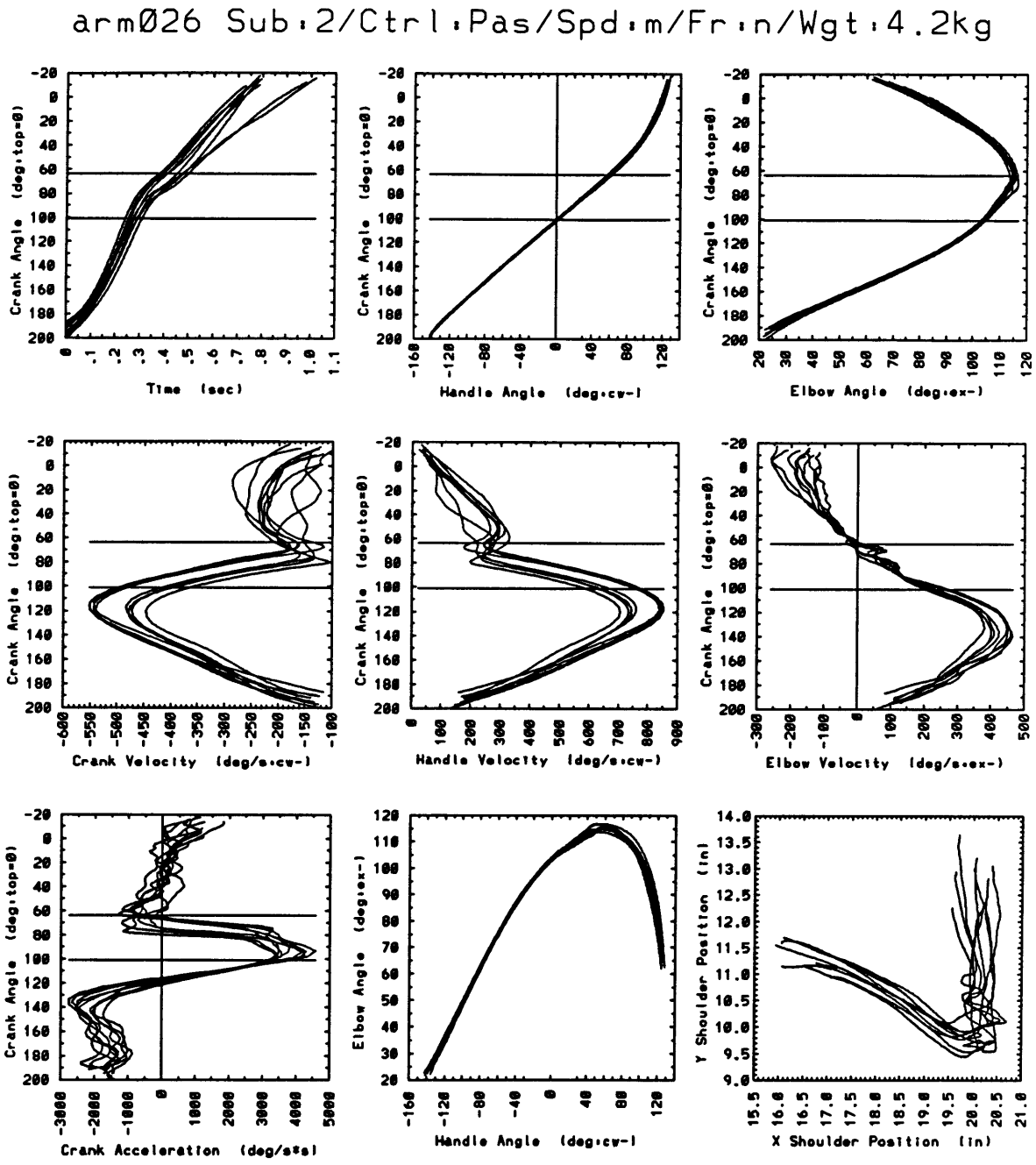
arm026 Sub:2/Ctrl:Pas/Spd:m/Fr:n/Wgt:4.2kg
Crank Angle (deg:top=0)
Time (sec)
Handle Angle (deg:cw-)
Elbow Angle (deg:ex-)
Crank Velocity (deg/s:cw-)
Handle Velocity (deg/s:cw-)
Elbow Velocity (deg/s:ex-)
Crank Acceleration (deg/s**2)
Y Shoulder Position (in)
X Shoulder Position (in)

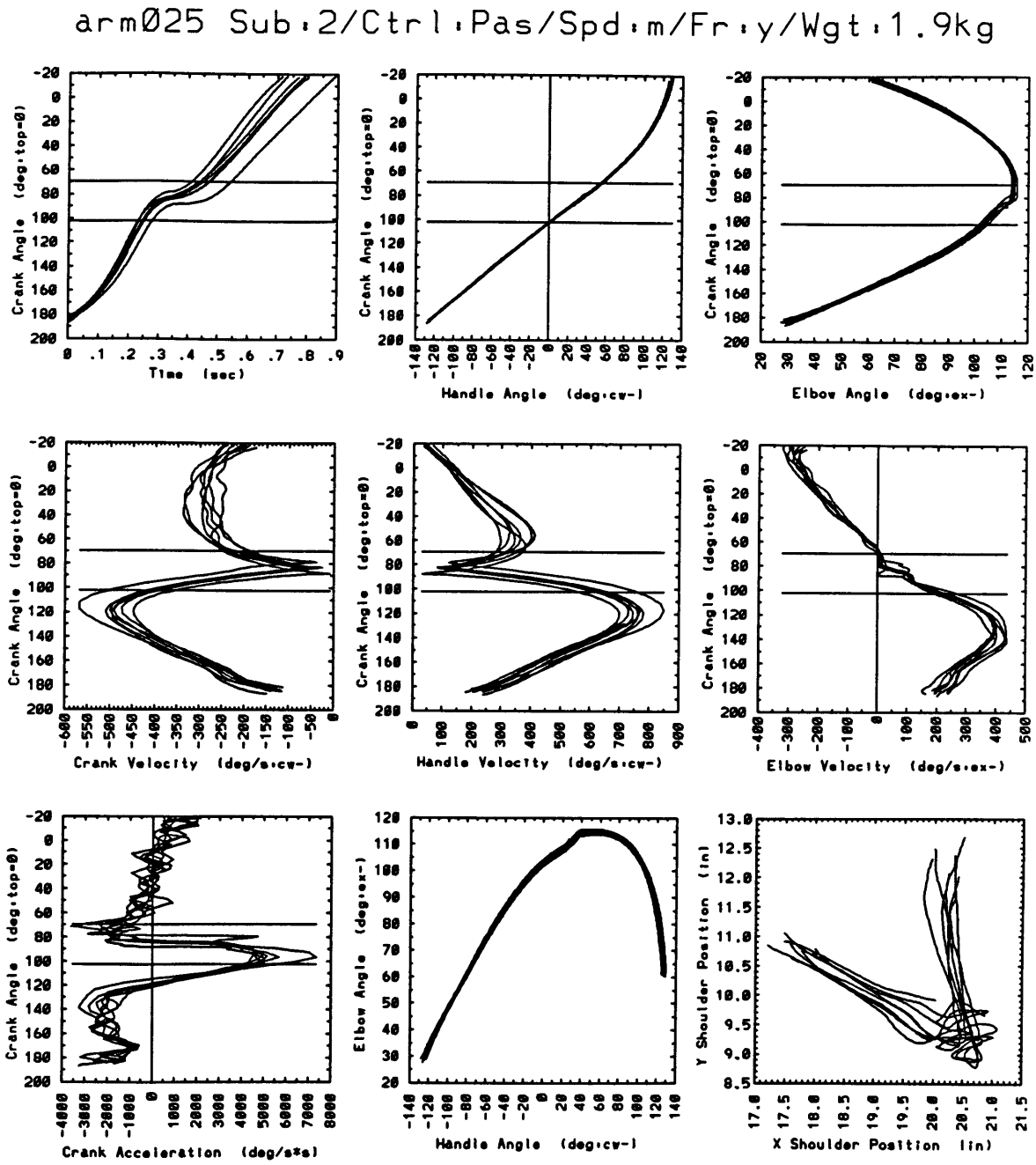
arm025 Sub:2/Ctrl:Pas/Spd:m/Fr:y/Wgt:1.9kg
Crank Angle (deg:top=0)
Time (sec)
Handle Angle (deg:cw-)
Elbow Angle (deg:ex-)
Crank Velocity (deg/s:cw-)
Handle Velocity (deg/s:cw-)
Elbow Velocity (deg/s:ex-)
Crank Acceleration (deg/s*s)
Elbow Angle (deg:ex-)
Handle Angle (deg:cw-)
Y Shoulder Position (in)
X Shoulder Position (in)

SUBJECT 3

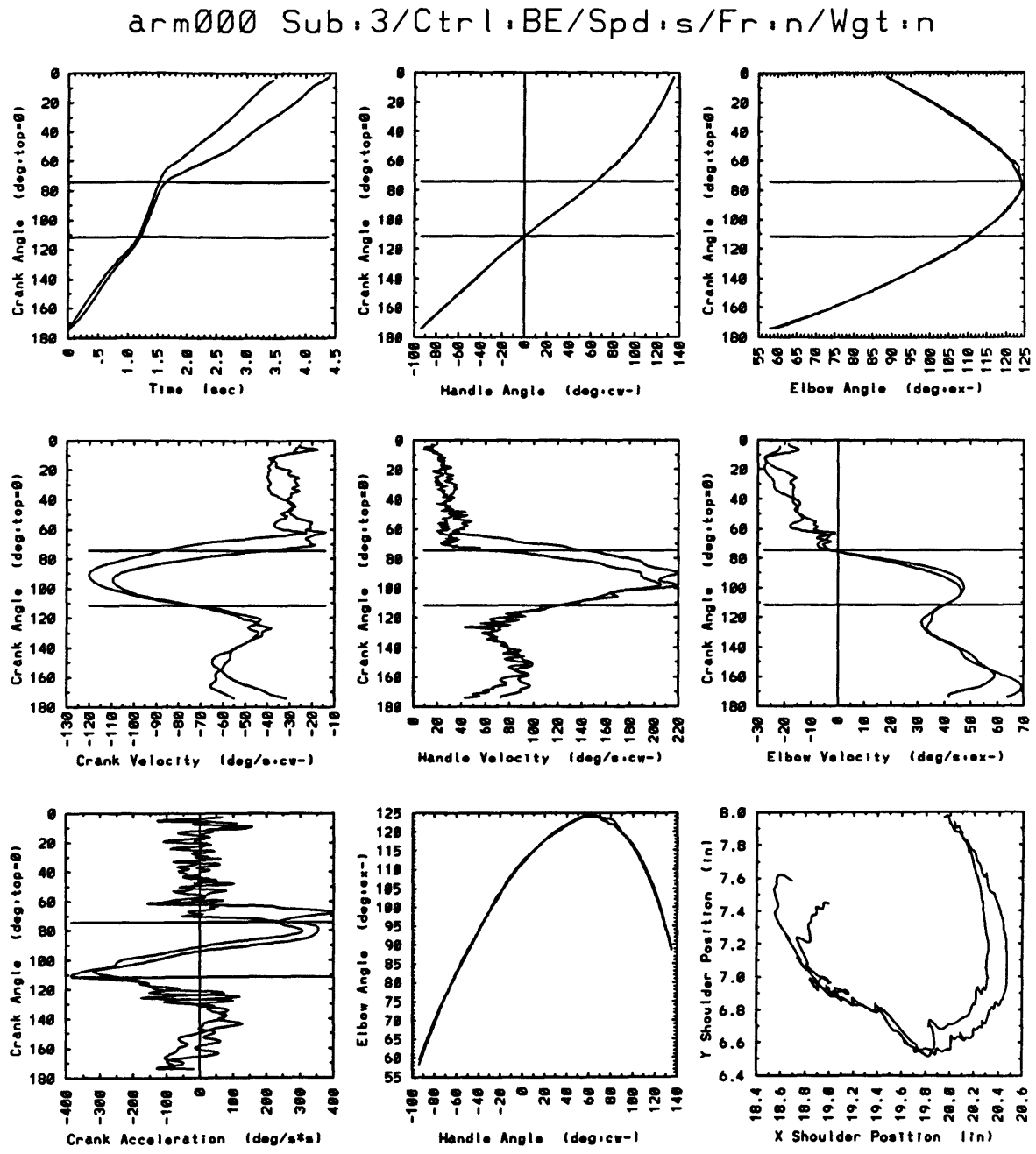
arm000 Sub:3/Ctrl:BE/Spd:s/Fr:n/Wgt:n
Crank Angle (deg:top=0)
Time (sec)
Handle Angle (deg:cw-)
Elbow Angle (deg:ex-)
Crank Velocity (deg/s:cw-)
Handle Velocity (deg/s:cw-)
Elbow Velocity (deg/s:ex-)
Crank Acceleration (deg/s*s)
Y Shoulder Position (in)
X Shoulder Position (in)

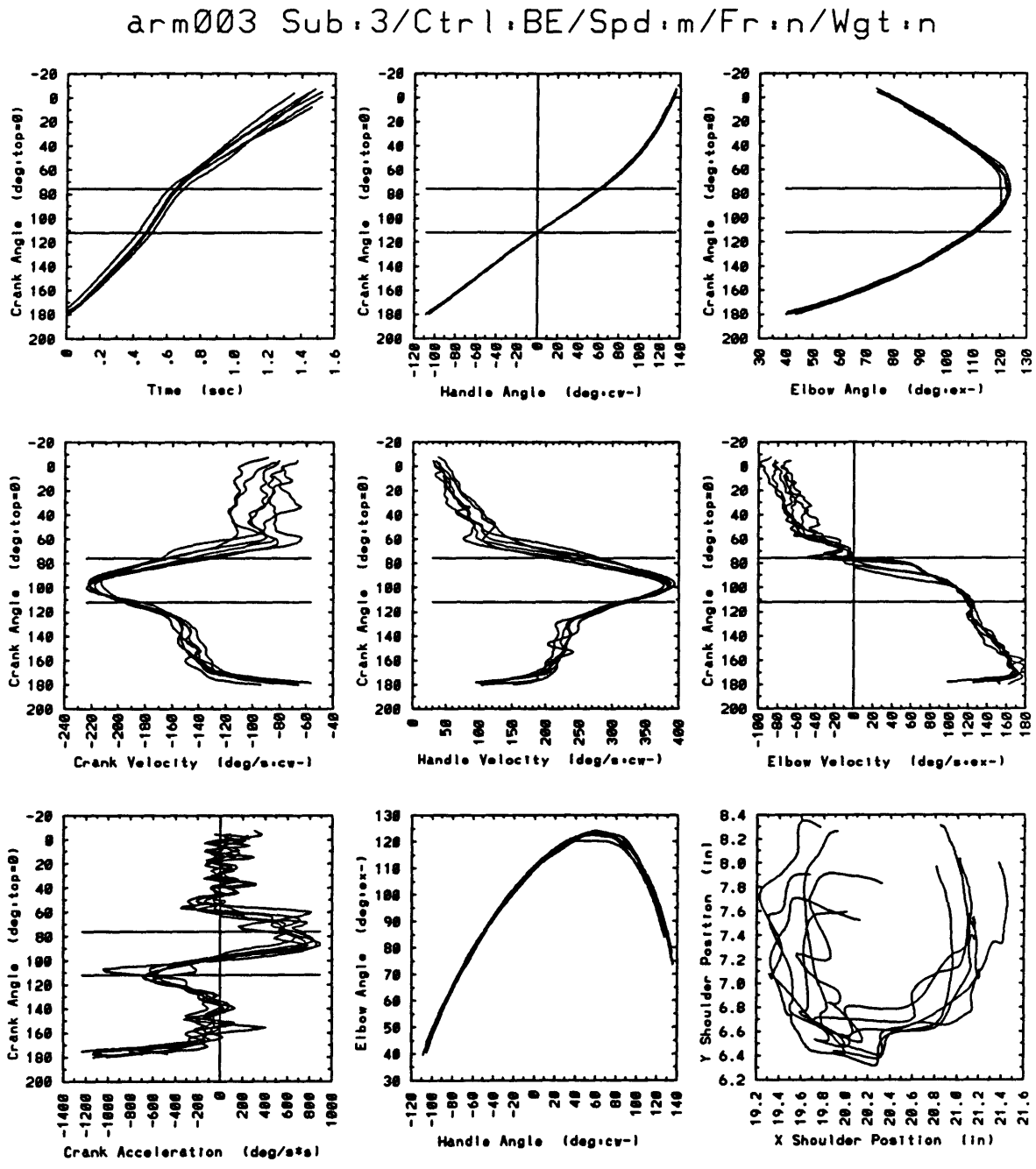
arm003 Sub:3/Ctrl:BE/Spd:m/Fr:n/Wgt:n
Crank Angle (deg:top=0)
Time (sec)
Handle Angle (deg:cw-)
Elbow Angle (deg:ex-)
Crank Velocity (deg/s:cw-)
Handle Velocity (deg/s:cw-)
Elbow Velocity (deg/s:ex-)
Crank Acceleration (deg/s*s)
Elbow Angle (deg:ex-)
Handle Angle (deg:cw-)
Y Shoulder Position (in)
X Shoulder Position (in)

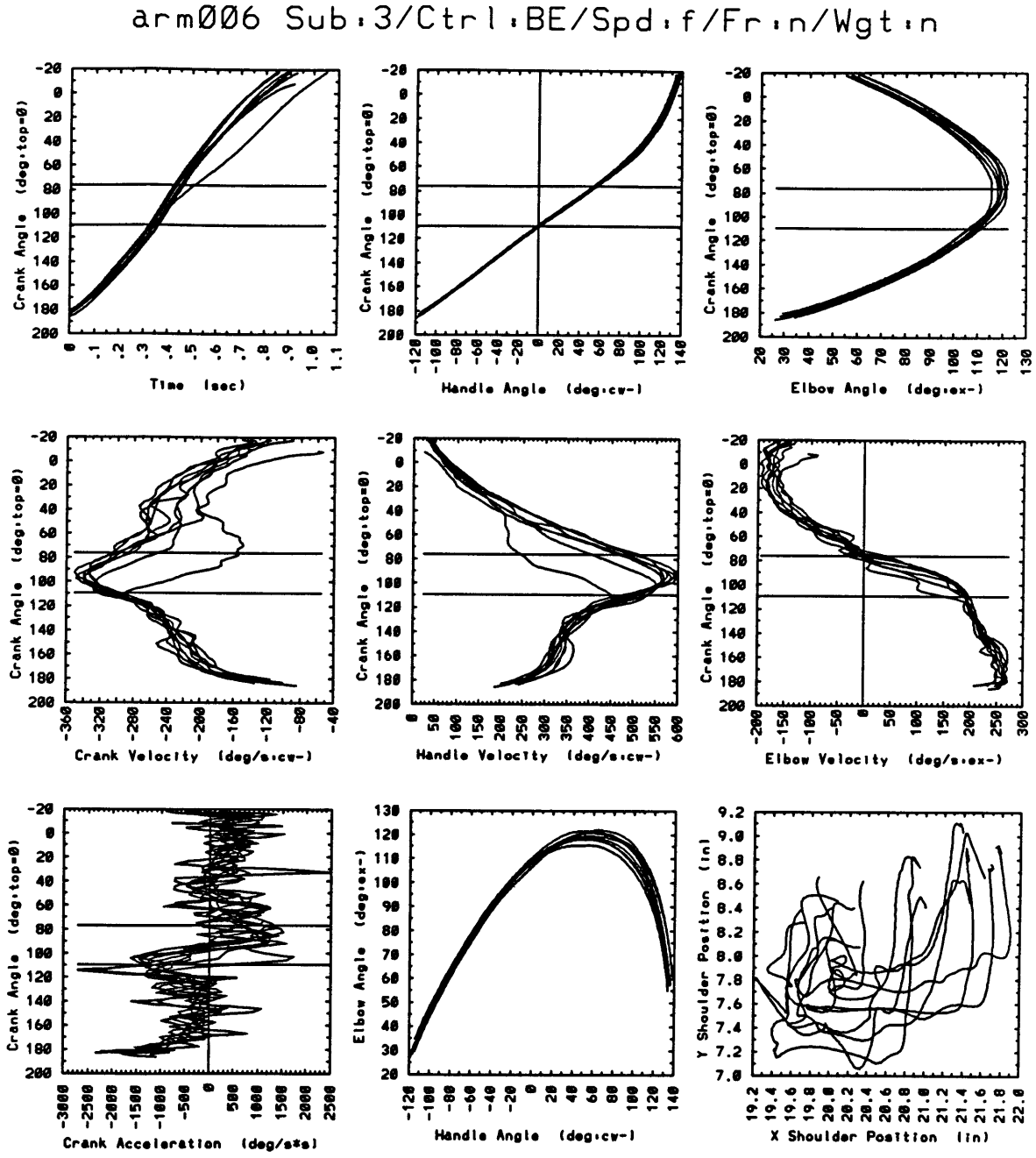
arm00b Sub:3/Ctrl:BE/Spd:f/Fr:n/Wgt:n
Crank Angle (deg:top=0)
Time (sec)
Handle Angle (deg:cw-)
Elbow Angle (deg:ex-)
Crank Velocity (deg/s:cw-)
Handle Velocity (deg/s:cw-)
Elbow Velocity (deg/s:ex-)
Crank Acceleration (deg/s**2)
Elbow Angle (deg:ex-)
Y Shoulder Position (in)
X Shoulder Position (in)

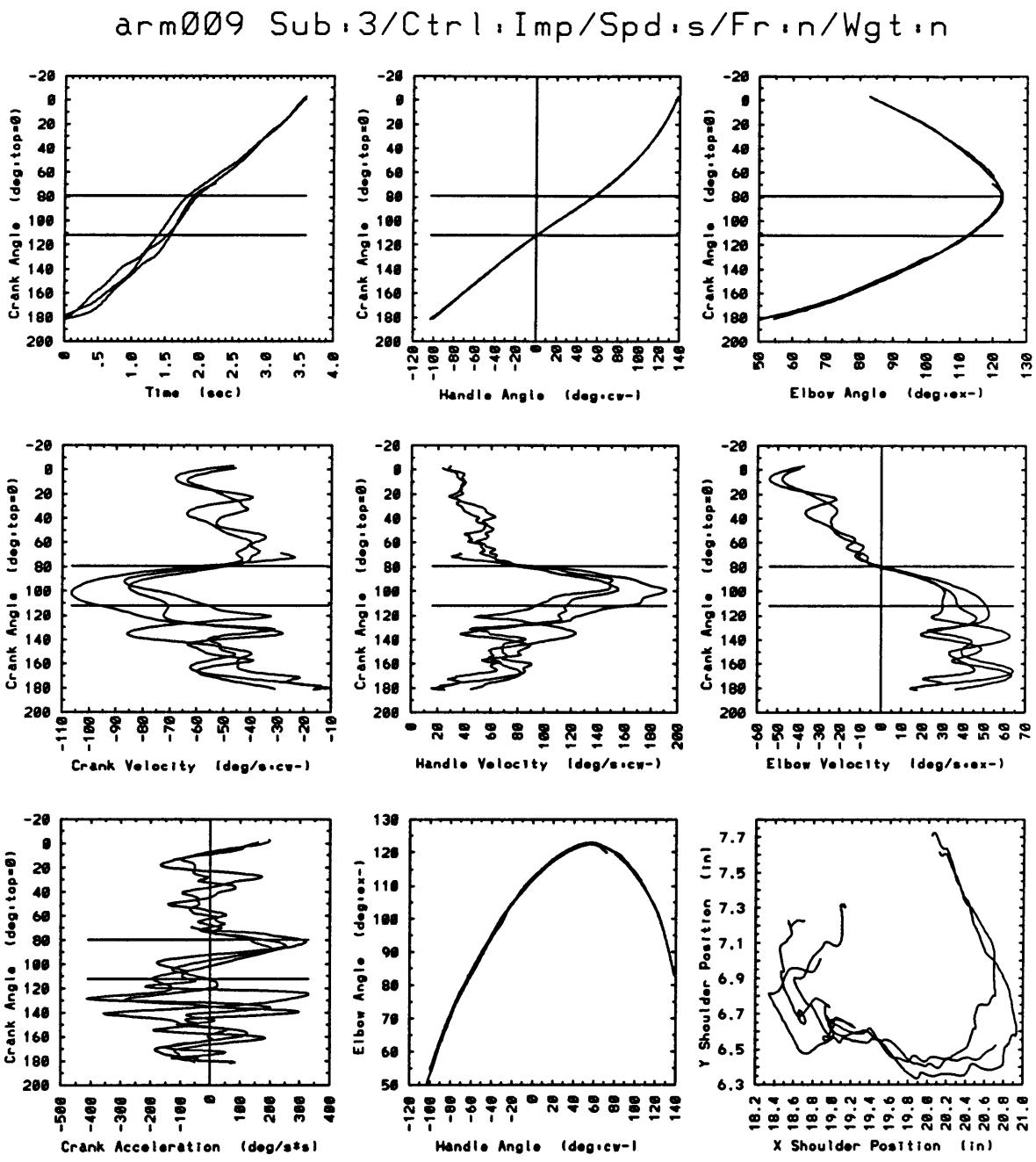
arm009 Sub:3/Ctrl:Imp/Spd:s/Fr:n/Wgt:n
Crank Angle (deg:top=0)
Time (sec)
Handle Angle (deg:cw-)
Elbow Angle (deg:ex-)
Crank Velocity (deg/s:cw-)
Handle Velocity (deg/s:cw-)
Elbow Velocity (deg/s:ex-)
Crank Acceleration (deg/s*s)
Elbow Angle (deg:ex-)
Handle Angle (deg:cw-)
Y Shoulder Position (in)
X Shoulder Position (in)

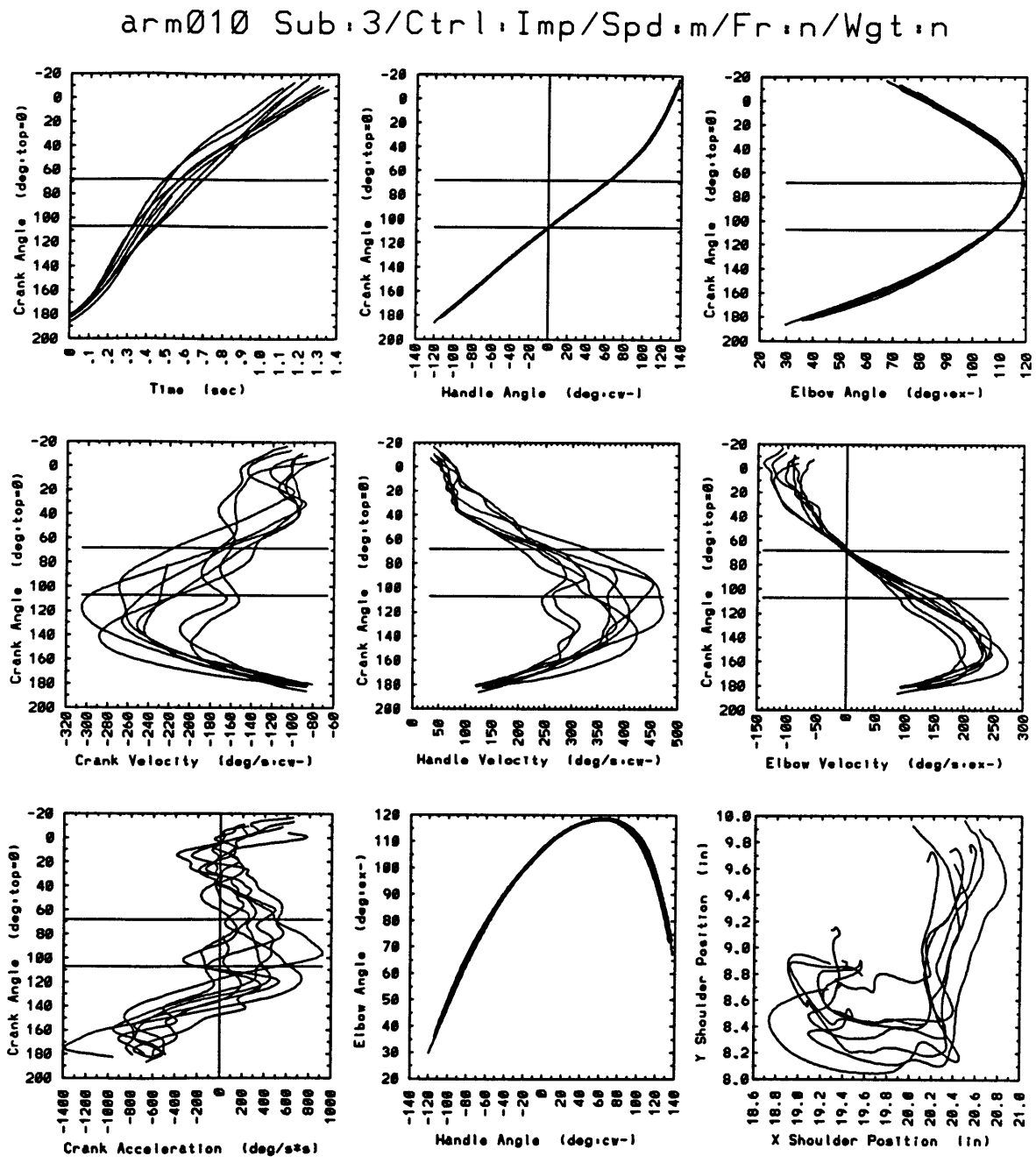
arm010 Sub:3/Ctrl:Imp/Spd:m/Fr:n/Wgt:n
Crank Angle (deg:top=0)
Time (sec)
Handle Angle (deg:cw-)
Elbow Angle (deg:ex-)
Crank Velocity (deg/s:cw-)
Handle Velocity (deg/s:cw-)
Elbow Velocity (deg/s:ex-)
Crank Acceleration (deg/s**s)
Elbow Angle (deg:ex-)
Handle Angle (deg:cw-)
Y Shoulder Position (in)
X Shoulder Position (in)

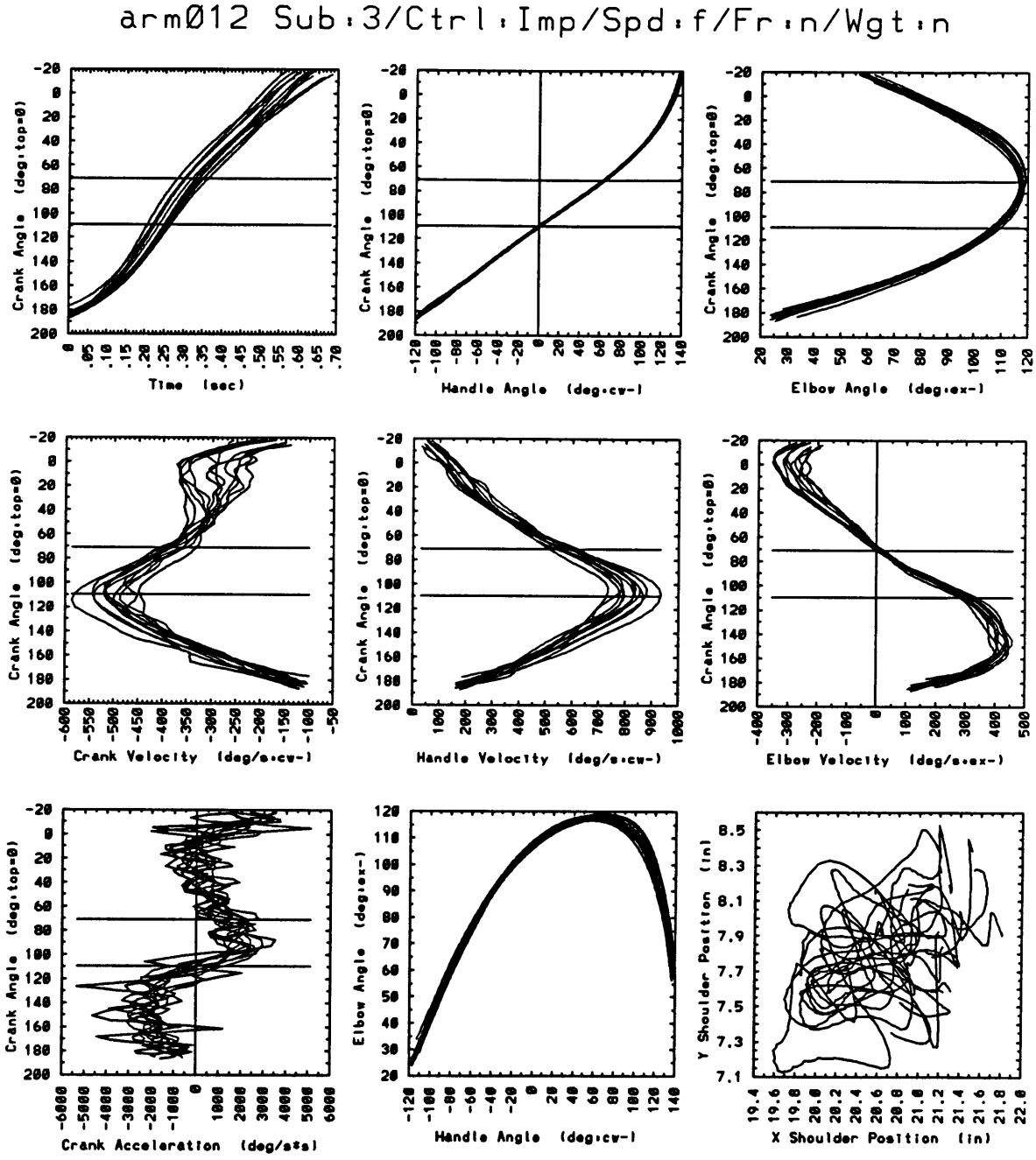
arm012 Sub:3/Ctrl:Imp/Spd:f/Fr:n/Wgt:n
Crank Angle (deg:top=0)
Time (sec)
Handle Angle (deg:cw-)
Elbow Angle (deg:ex-)
Crank Velocity (deg/s:cw-)
Handle Velocity (deg/s:cw-)
Elbow Velocity (deg/s:ex-)
Crank Acceleration (deg/s^2)
Handle Angle (deg:cw-)
Y Shoulder Position (in)
X Shoulder Position (in)

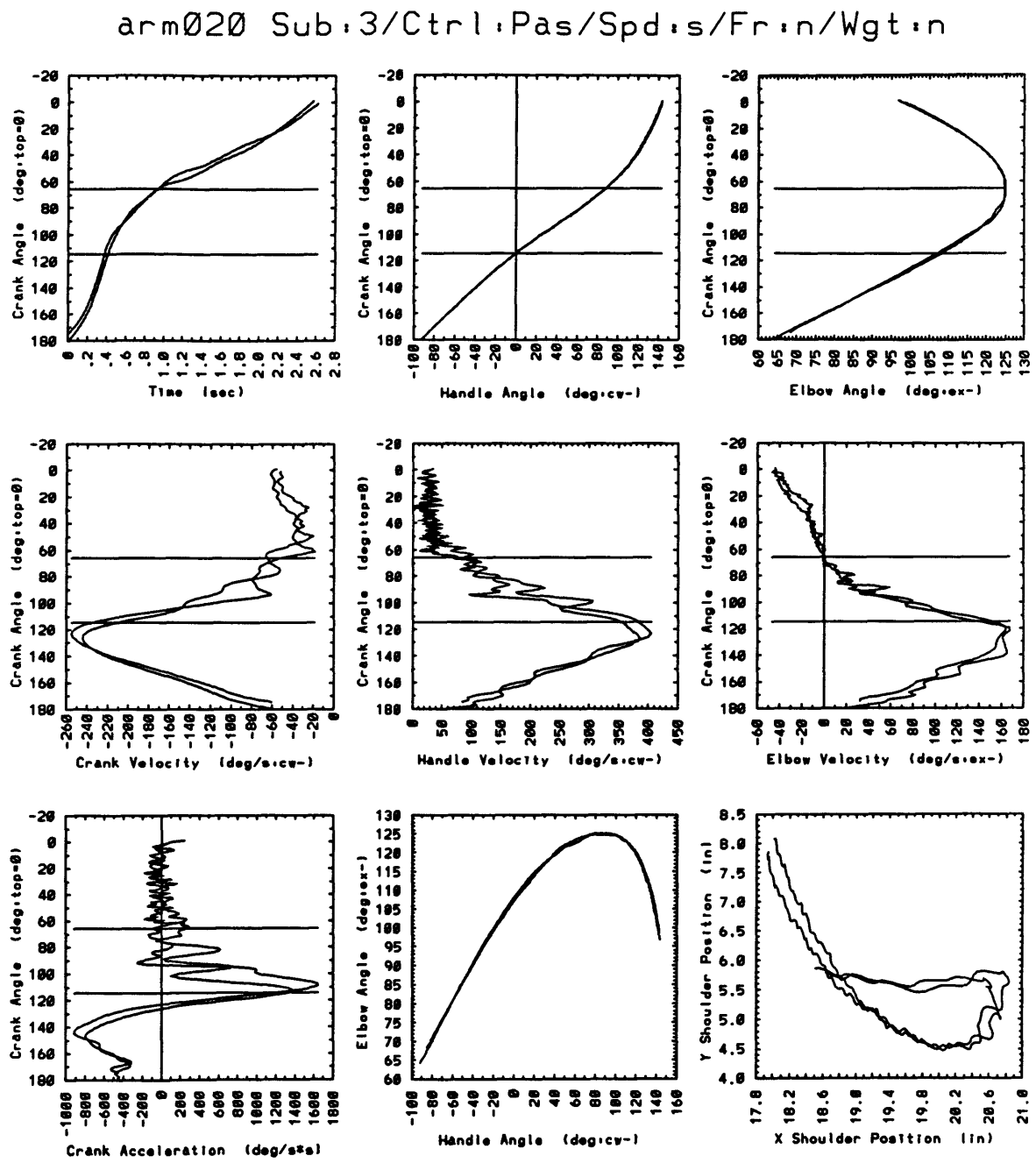
arm020 Sub:3/Ctrl:Pas/Spd:s/Fr:n/Wgt:n
Crank Angle (deg:top=0)
Time (sec)
Handle Angle (deg:cw-)
Elbow Angle (deg:ex-)
Crank Velocity (deg/s:cw-)
Handle Velocity (deg/s:cw-)
Elbow Velocity (deg/s:ex-)
Crank Acceleration (deg/s**2)
Y Shoulder Position (in)
X Shoulder Position (in)

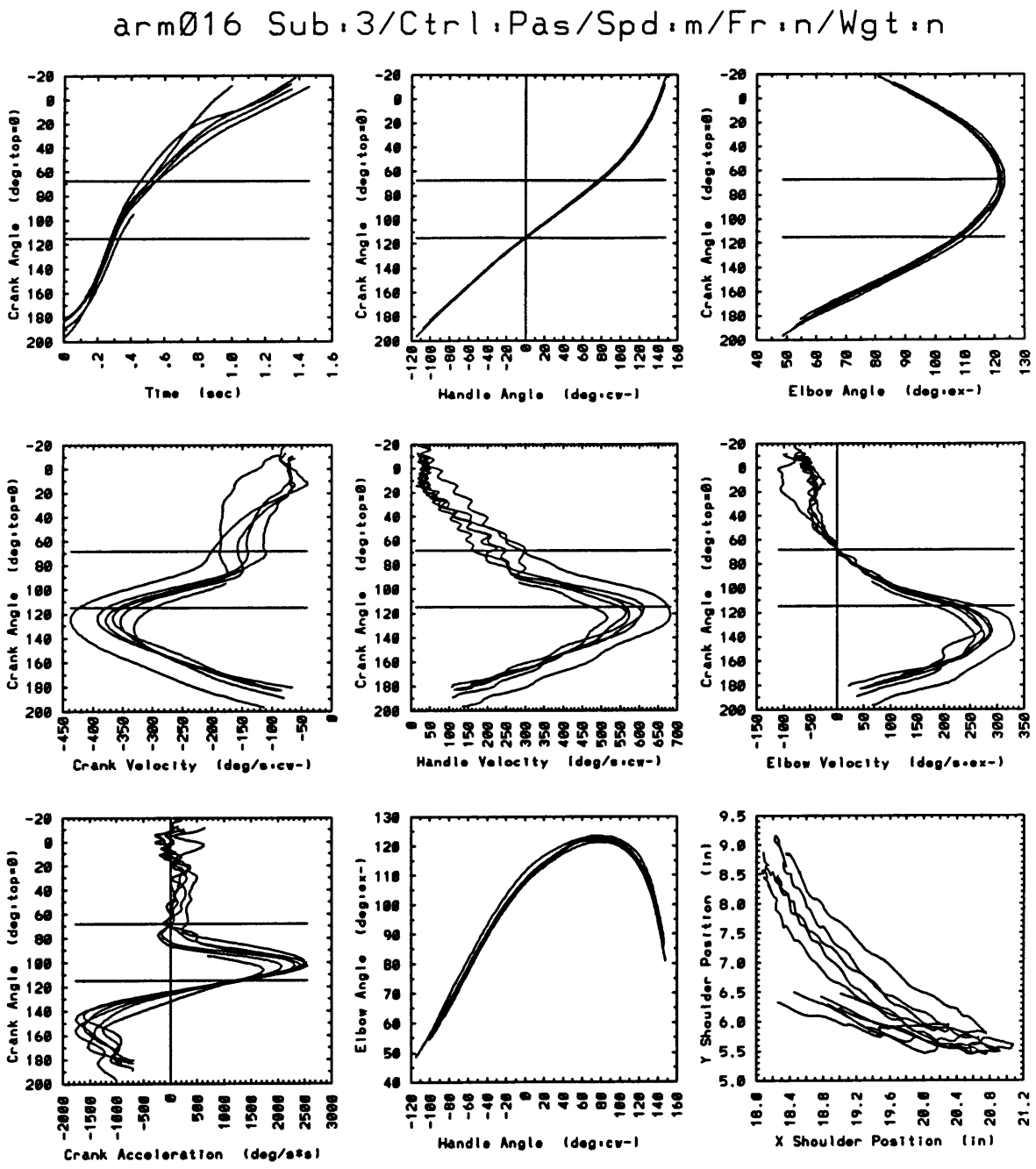
arm016 Sub:3/Ctrl:Pas/Spd:m/Fr:n/Wgt:n
Crank Angle (deg:top=0)
Time (sec)
Handle Angle (deg:cw-)
Elbow Angle (deg:ex-)
Crank Velocity (deg/s:cw-)
Handle Velocity (deg/s:cw-)
Elbow Velocity (deg/s:ex-)
Crank Acceleration (deg/s*s)
Elbow Angle (deg:ex-)
Handle Angle (deg:cw-)
Y Shoulder Position (in)
X Shoulder Position (in)

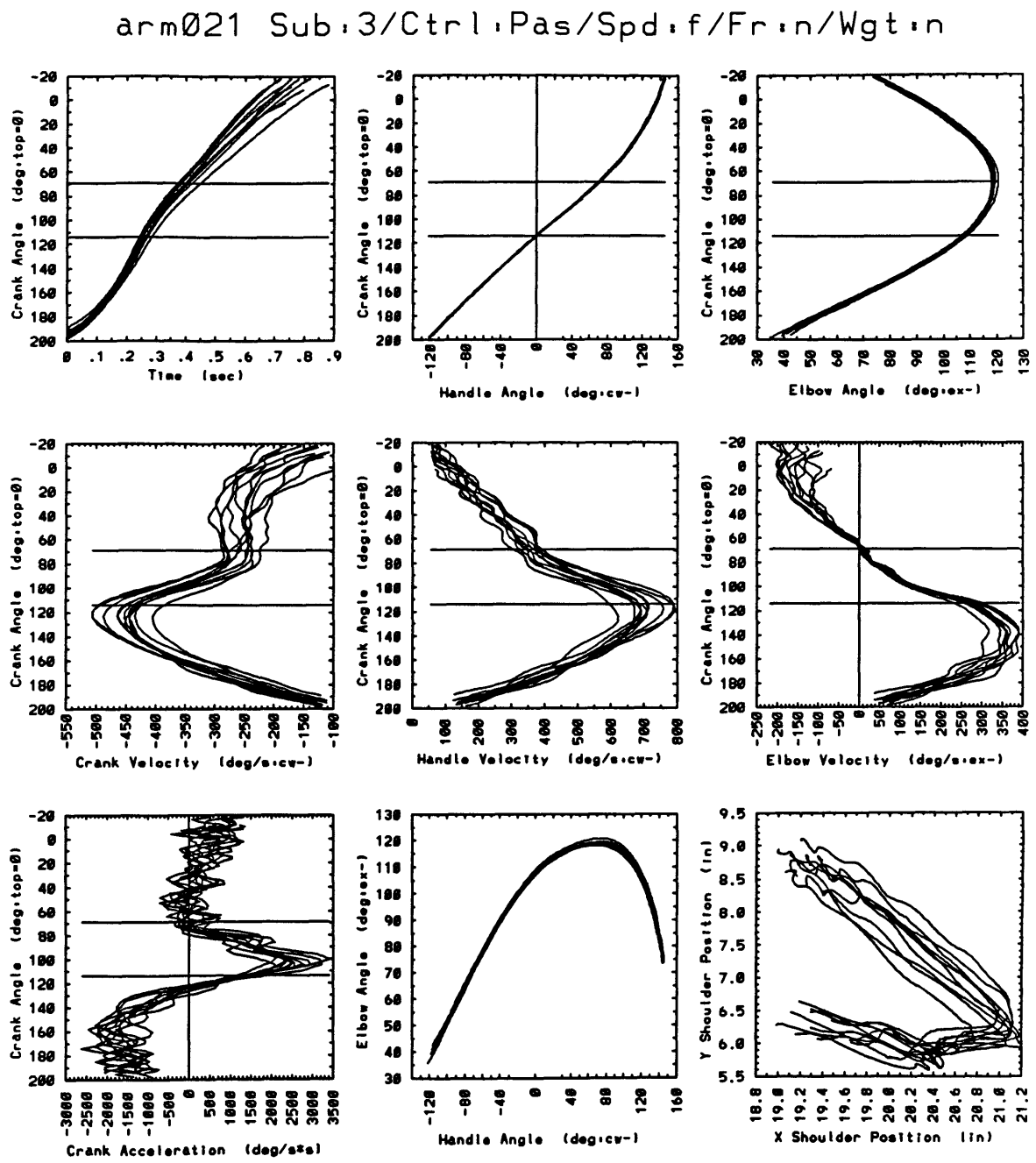
arm021 Sub:3/Ctrl:Pas/Spd:f/Fr:n/Wgt:n
Crank Angle (deg:top=0)
Time (sec)
Handle Angle (deg:cw-)
Elbow Angle (deg:ex-)
Crank Velocity (deg/s:cw-)
Handle Velocity (deg/s:cw-)
Elbow Velocity (deg/s:ex-)
Crank Acceleration (deg/s**2)
Y Shoulder Position (in)
X Shoulder Position (in)

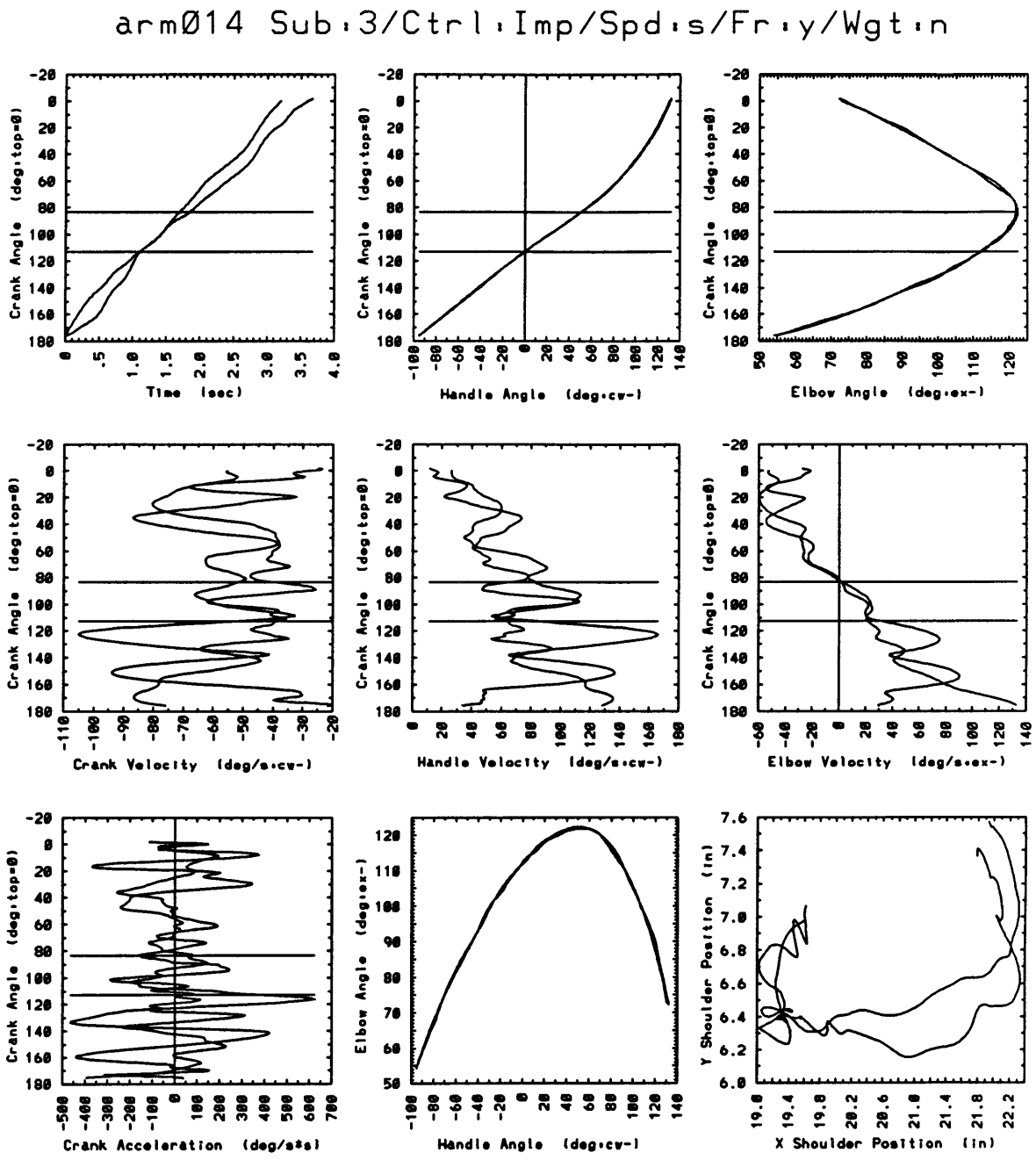
arm014 Sub:3/Ctrl:Imp/Spd:s/Fr:y/Wgt:n
Crank Angle (deg:top=0)
Time (sec)
Handle Angle (deg:cw-)
Elbow Angle (deg:ex-)
Crank Velocity (deg/s:cw-)
Handle Velocity (deg/s:cw-)
Elbow Velocity (deg/s:ex-)
Crank Acceleration (deg/s*s)
Elbow Angle (deg:ex-)
Handle Angle (deg:cw-)
Y Shoulder Position (in)
X Shoulder Position (in)

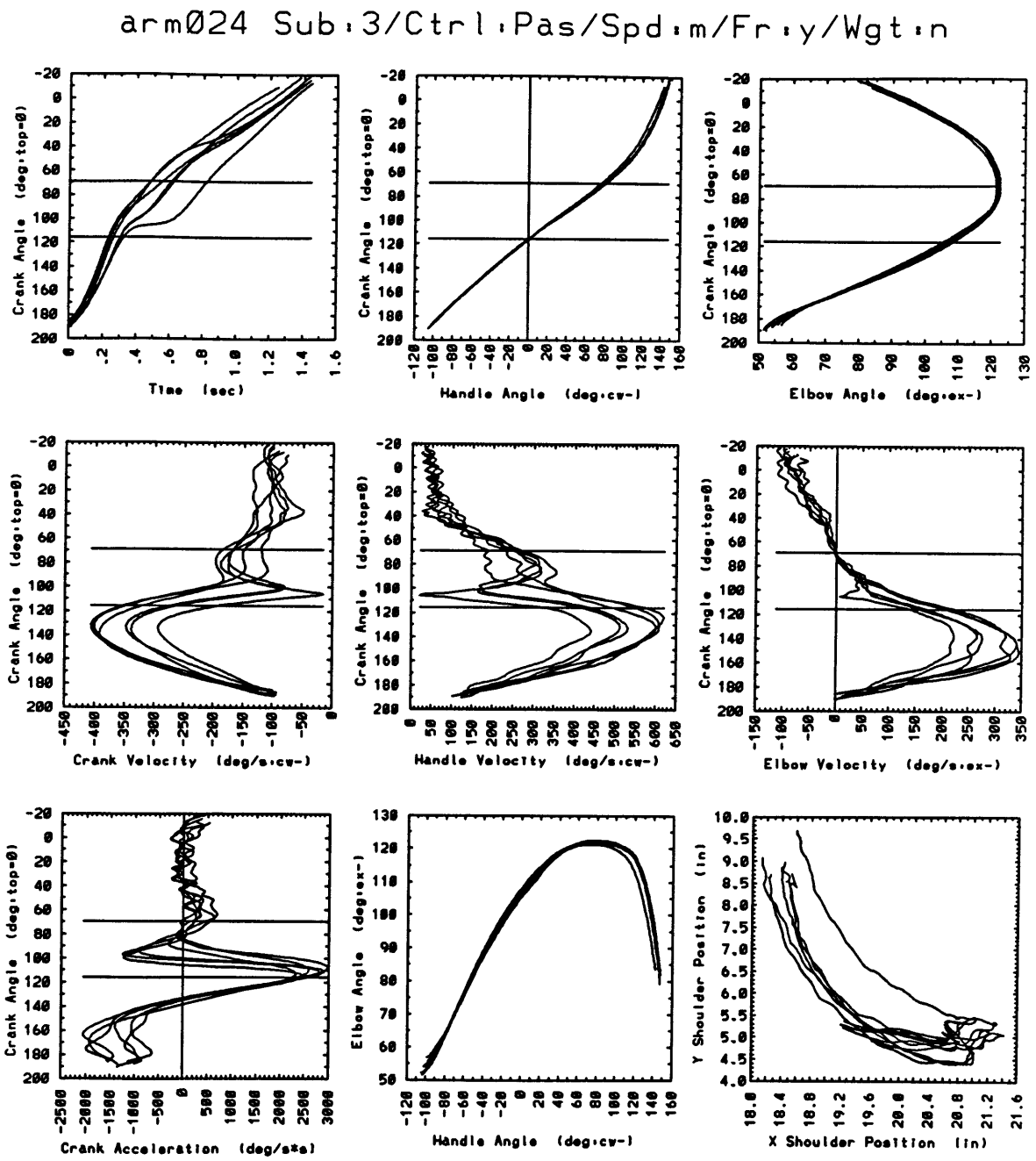
arm024 Sub:3/Ctrl:Pas/Spd:m/Fr:y/Wgt:n
Crank Angle (deg:top=0)
Time (sec)
Handle Angle (deg:cw-)
Elbow Angle (deg:ex-)
Crank Velocity (deg/s:cw-)
Handle Velocity (deg/s:cw-)
Elbow Velocity (deg/s:ex-)
Crank Acceleration (deg/s*s)
Elbow Angle (deg:ex-)
Handle Angle (deg:cw-)
Y Shoulder Position (in)
X Shoulder Position (in)

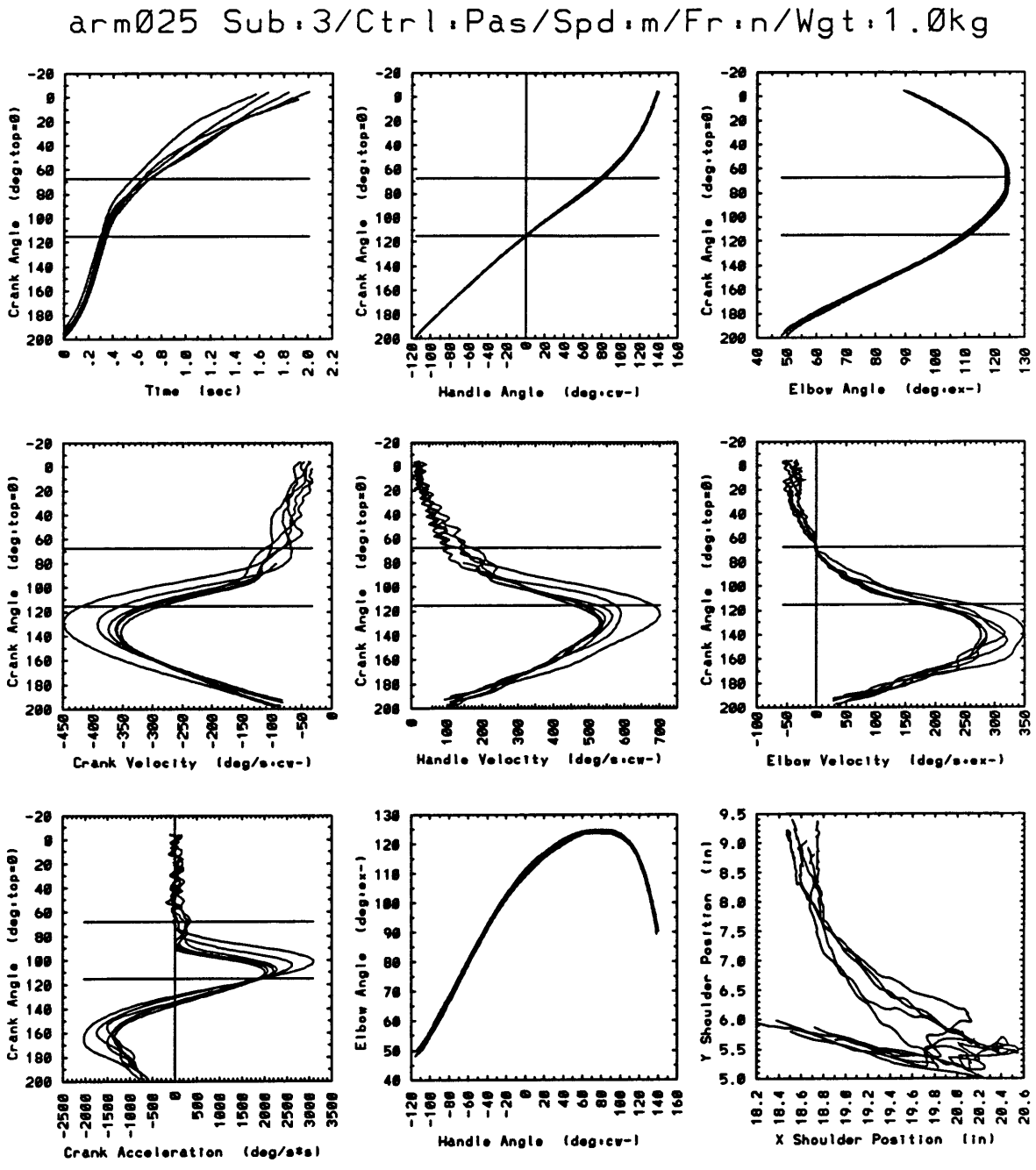
arm025 Sub:3/Ctrl:Pas/Spd:m/Fr:n/Wgt:1.0kg
Crank Angle (deg:top=0)
Time (sec)
Handle Angle (deg:cw-)
Elbow Angle (deg:ex-)
Crank Velocity (deg/s:cw-)
Handle Velocity (deg/s:cw-)
Elbow Velocity (deg/s:ex-)
Crank Acceleration (deg/s^2)
Y Shoulder Position (in)
X Shoulder Position (in)

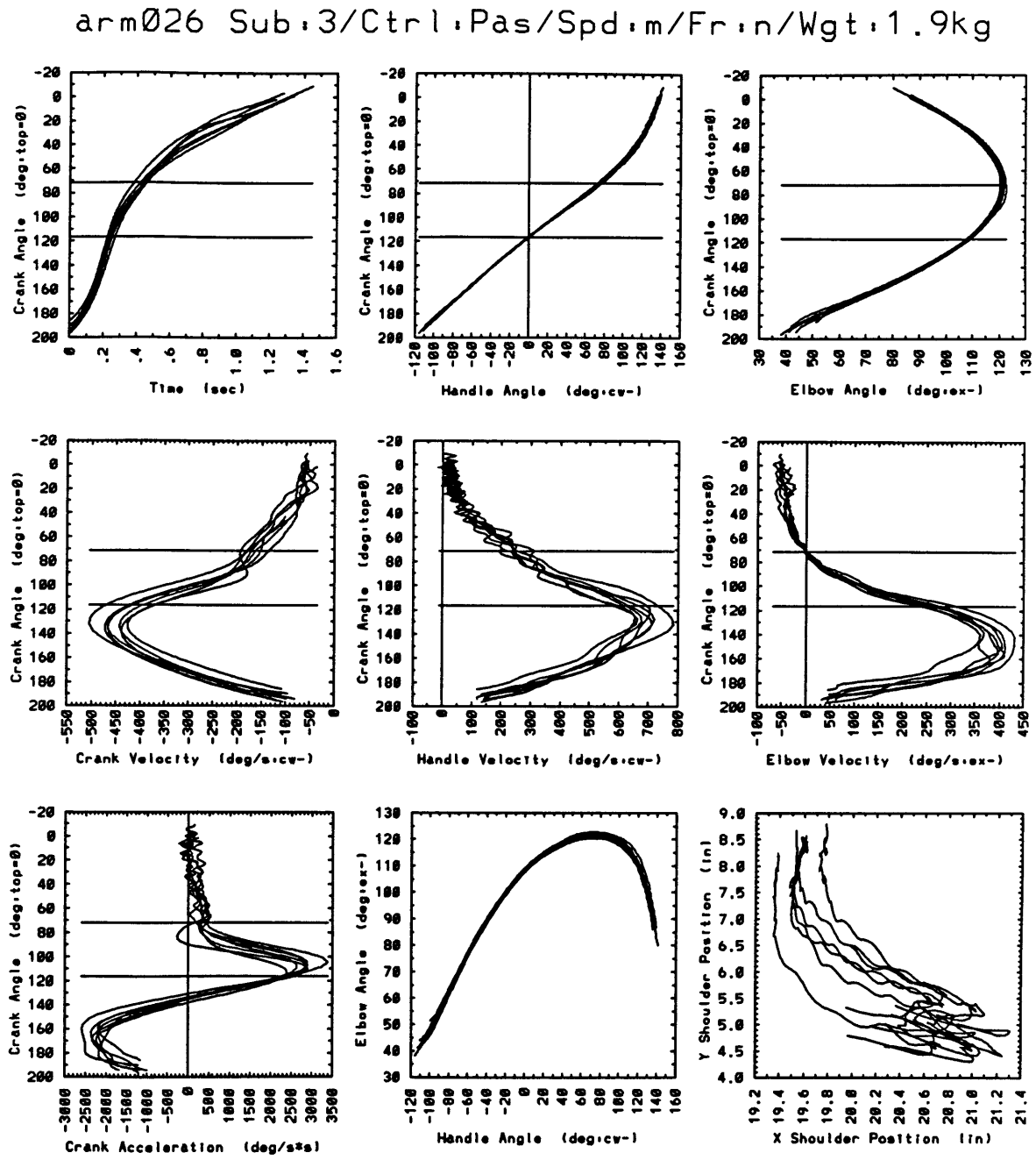
arm026 Sub:3/Ctrl:Pas/Spd:m/Fr:n/Wgt:1.9kg
Crank Angle (deg:top=0)
Time (sec)
Handle Angle (deg:cw-)
Elbow Angle (deg:ex-)
Crank Velocity (deg/s:cw-)
Handle Velocity (deg/s:cw-)
Elbow Velocity (deg/s:ex-)
Crank Acceleration (deg/s*s)
Elbow Angle (deg:ex-)
Handle Angle (deg:cw-)
Y Shoulder Position (in)
X Shoulder Position (in)

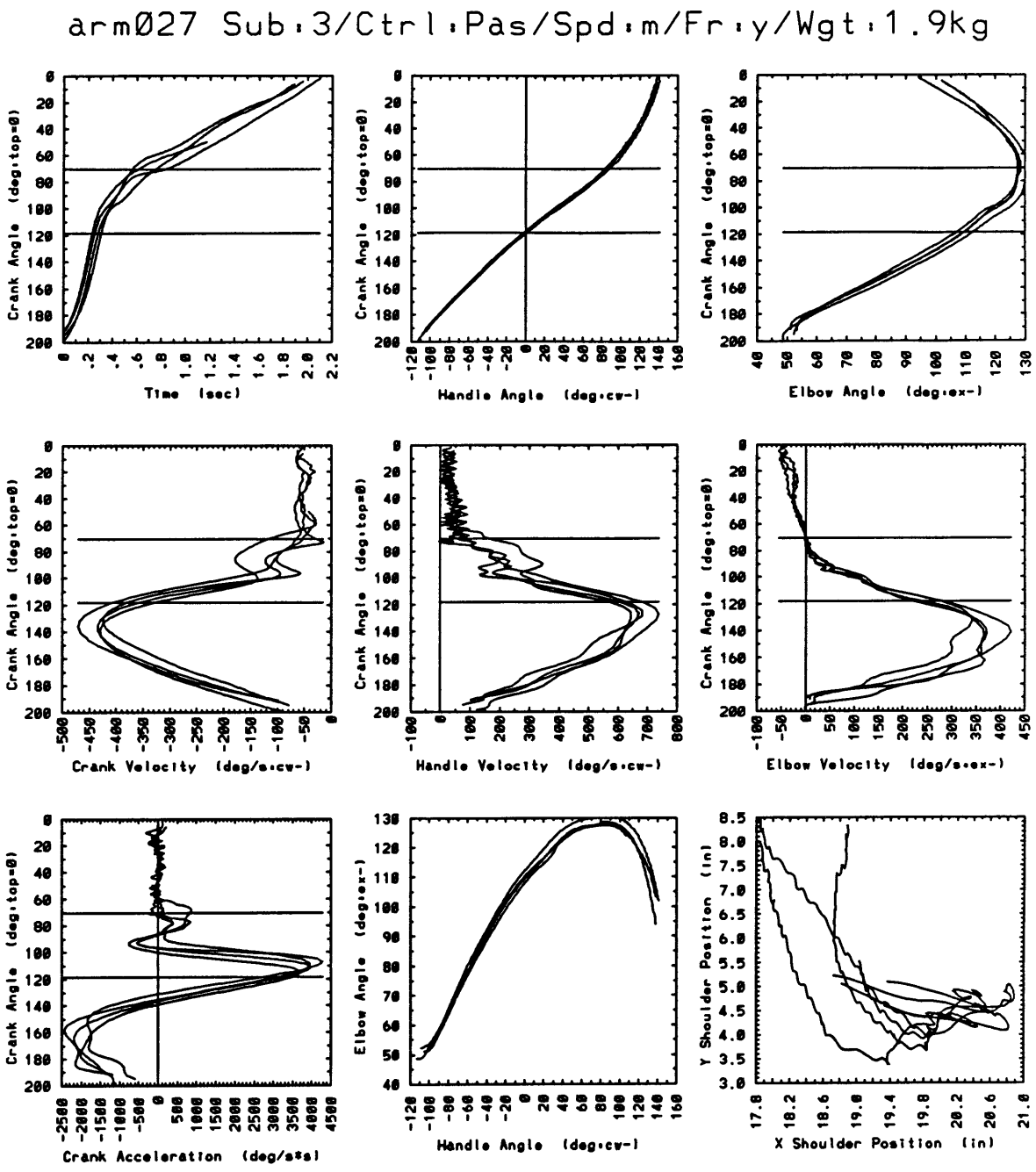
arm027 Sub:3/Ctrl:Pas/Spd:m/Fr:y/Wgt:1.9kg
Crank Angle (deg:top=0)
Time (sec)
Handle Angle (deg:cw-)
Elbow Angle (deg:ex-)
Crank Velocity (deg/s:cw-)
Handle Velocity (deg/s:cw-)
Elbow Velocity (deg/s:ex-)
Crank Acceleration (deg/s*s)
Y Shoulder Position (in)
X Shoulder Position (in)

SUBJECT 4

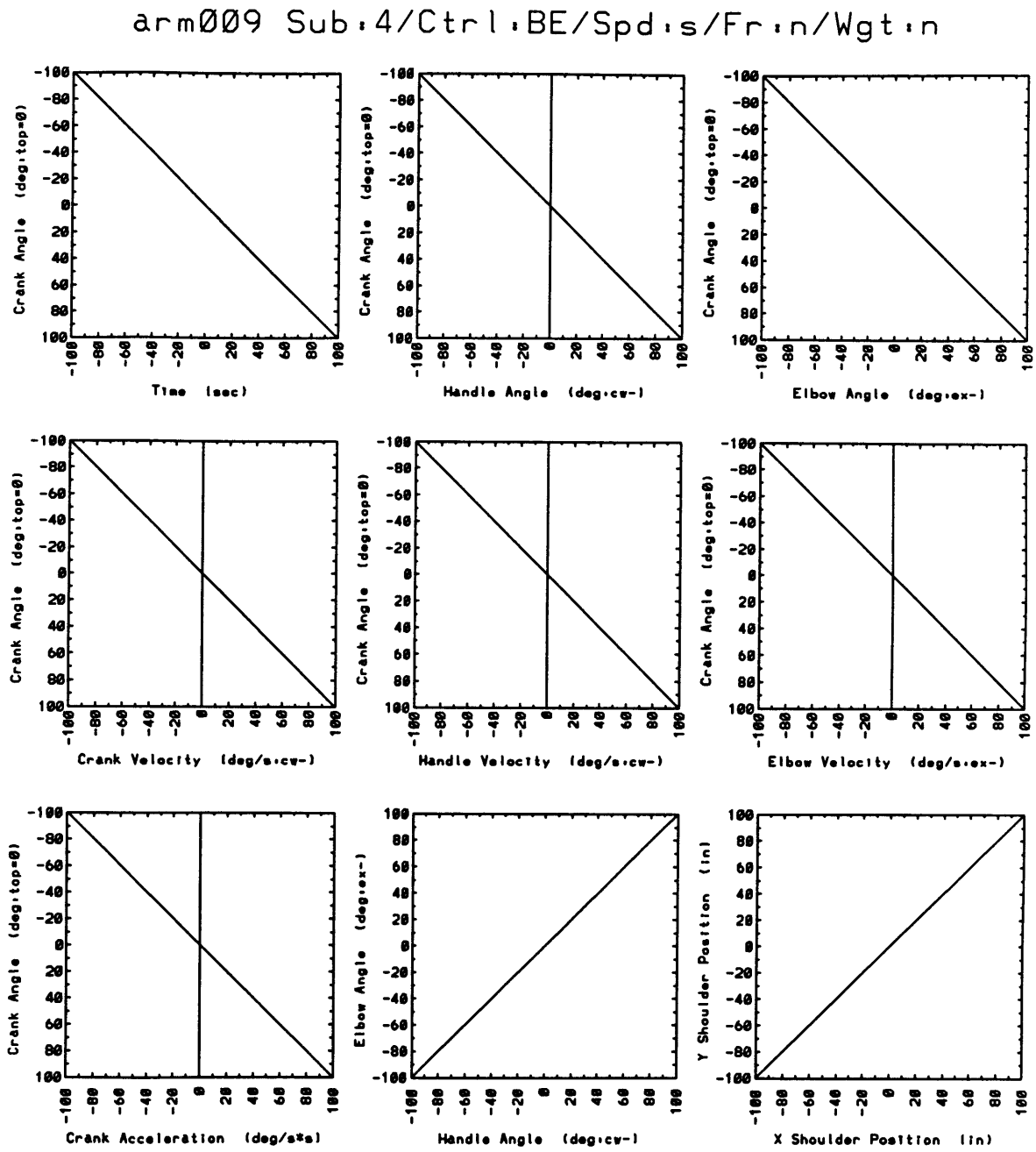
arm009 Sub:4/Ctrl:BE/Spd:s/Fr:n/Wgt:n
Crank Angle (deg:top=0)
Time (sec)
Handle Angle (deg:cw-)
Elbow Angle (deg:ex-)
Crank Velocity (deg/s:cw-)
Handle Velocity (deg/s:cw-)
Elbow Velocity (deg/s:ex-)
Crank Acceleration (deg/s*s)
Elbow Angle (deg:ex-)
Handle Angle (deg:cw-)
Y Shoulder Position (in)
X Shoulder Position (in)

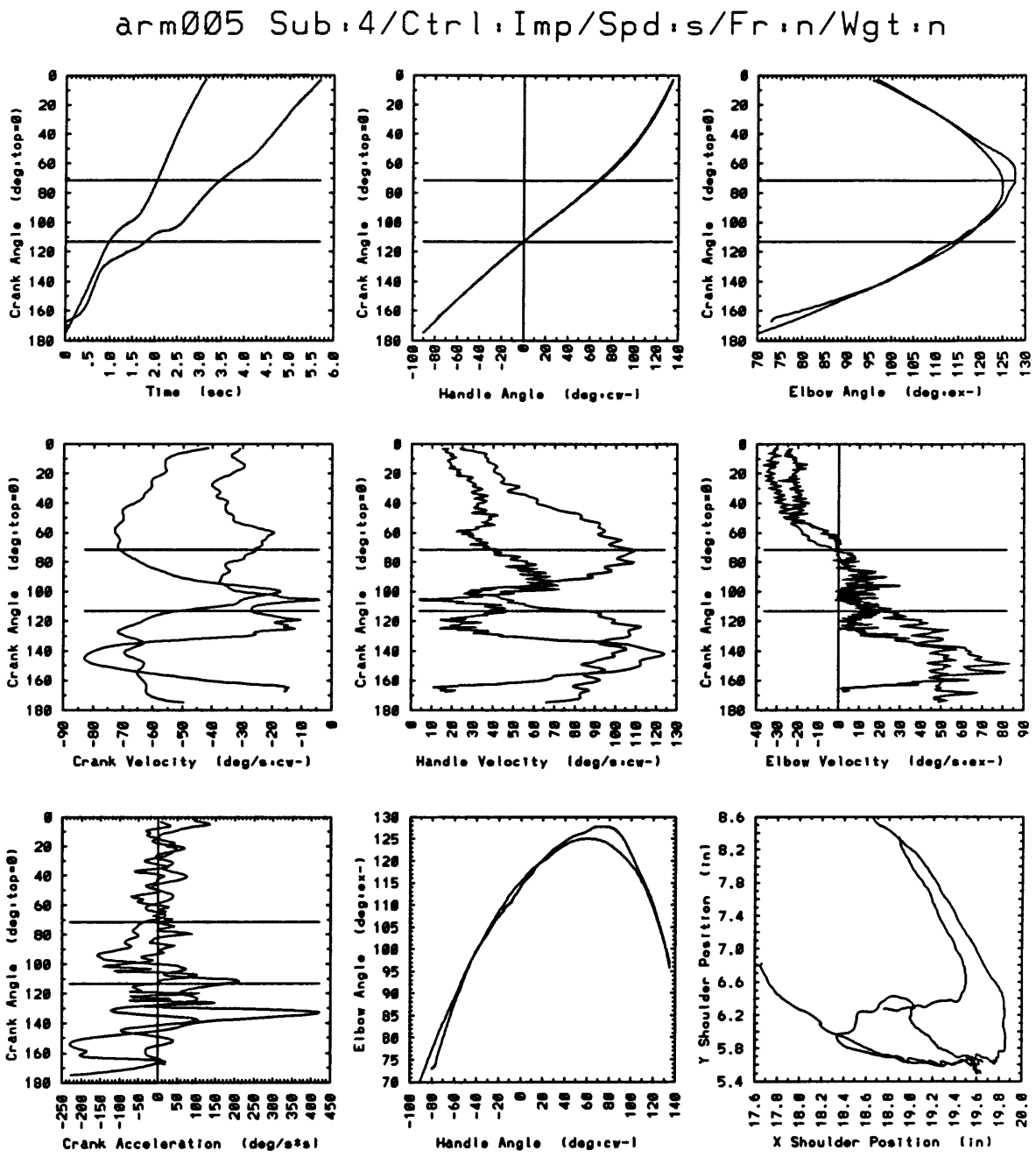
arm005 Sub:4/Ctrl:Imp/Spd:s/Fr:n/Wgt:n
Crank Angle (deg:top=0)
Time (sec)
Handle Angle (deg:cw-)
Elbow Angle (deg:ex-)
Crank Velocity (deg/s:cw-)
Handle Velocity (deg/s:cw-)
Elbow Velocity (deg/s:ex-)
Crank Acceleration (deg/s*s)
Y Shoulder Position (in)
X Shoulder Position (in)

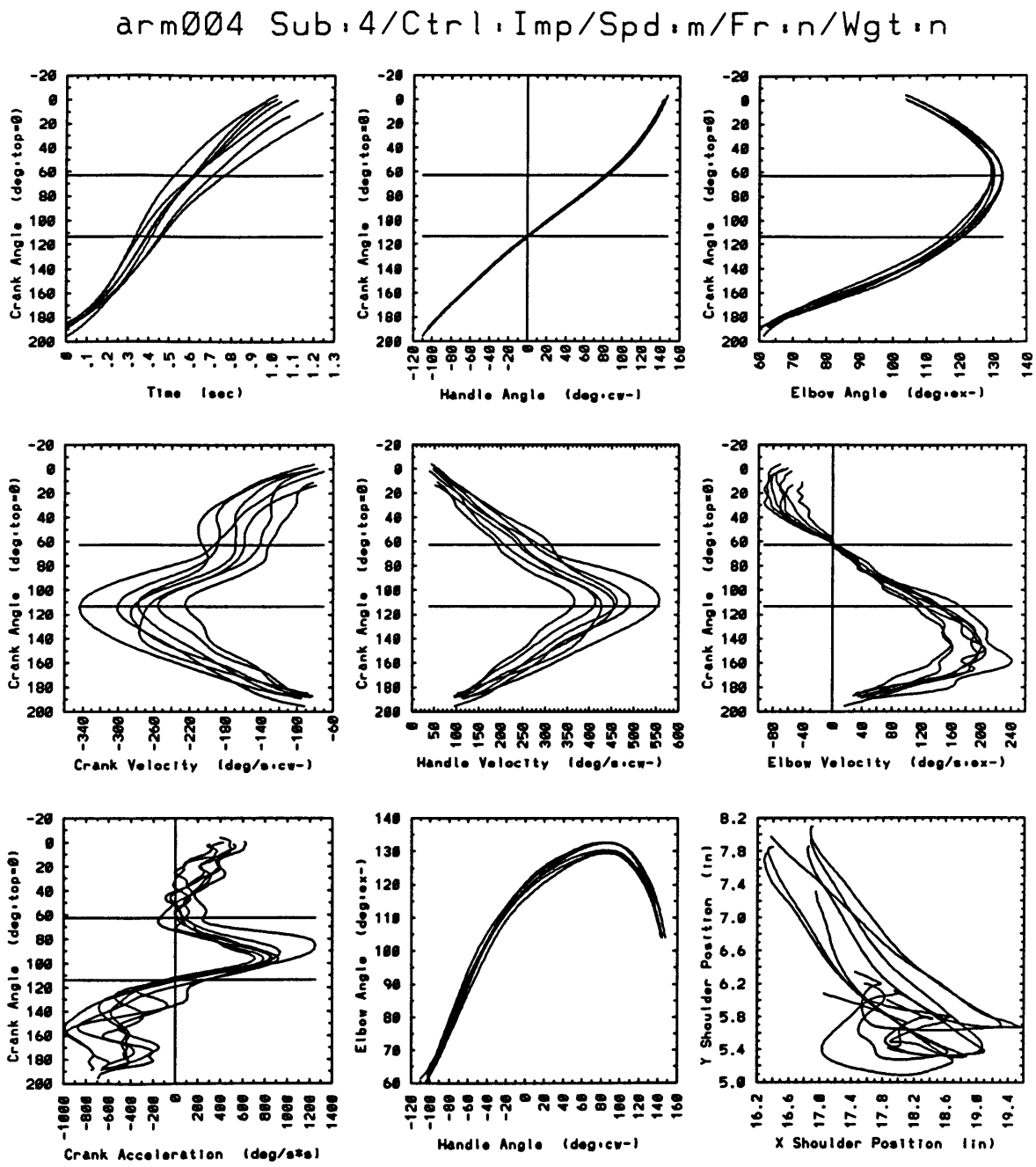
arm004 Sub:4/Ctrl:Imp/Spd:m/Fr:n/Wgt:n
Crank Angle (deg:top=0)
Time (sec)
Handle Angle (deg:cw-)
Elbow Angle (deg:ex-)
Crank Velocity (deg/s:cw-)
Handle Velocity (deg/s:cw-)
Elbow Velocity (deg/s:ex-)
Crank Acceleration (deg/s**2)
Elbow Angle (deg:ex-)
Handle Angle (deg:cw-)
Y Shoulder Position (in)
X Shoulder Position (in)

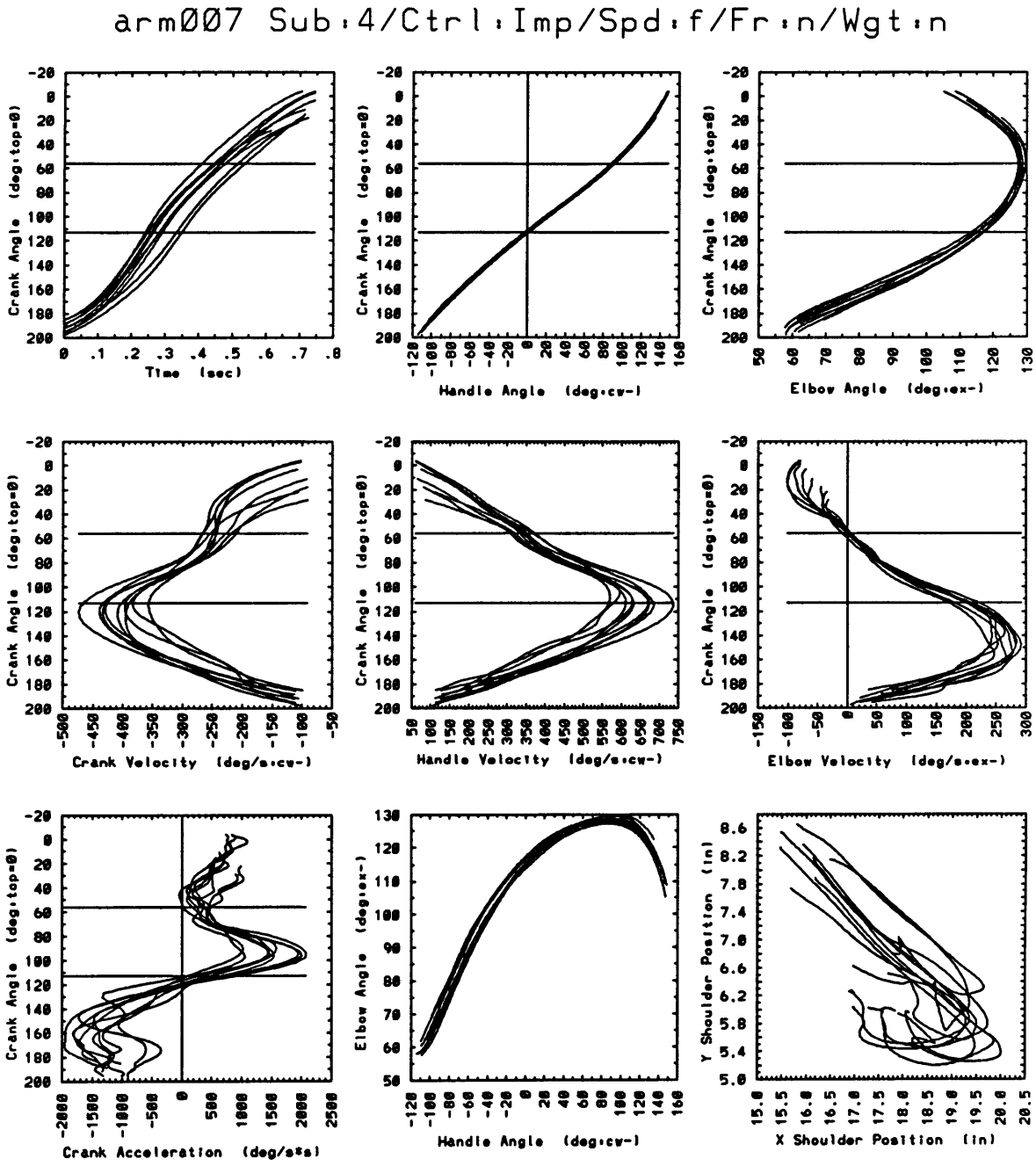
arm007 Sub:4/Ctrl:Imp/Spd:f/Fr:n/Wgt:n
Crank Angle (deg:top=0)
Time (sec)
Handle Angle (deg:cw-)
Elbow Angle (deg:ex-)
Crank Velocity (deg/s:cw-)
Handle Velocity (deg/s:cw-)
Elbow Velocity (deg/s:ex-)
Crank Acceleration (deg/s**2)
Elbow Angle (deg:ex-)
Handle Angle (deg:cw-)
Y Shoulder Position (in)
X Shoulder Position (in)

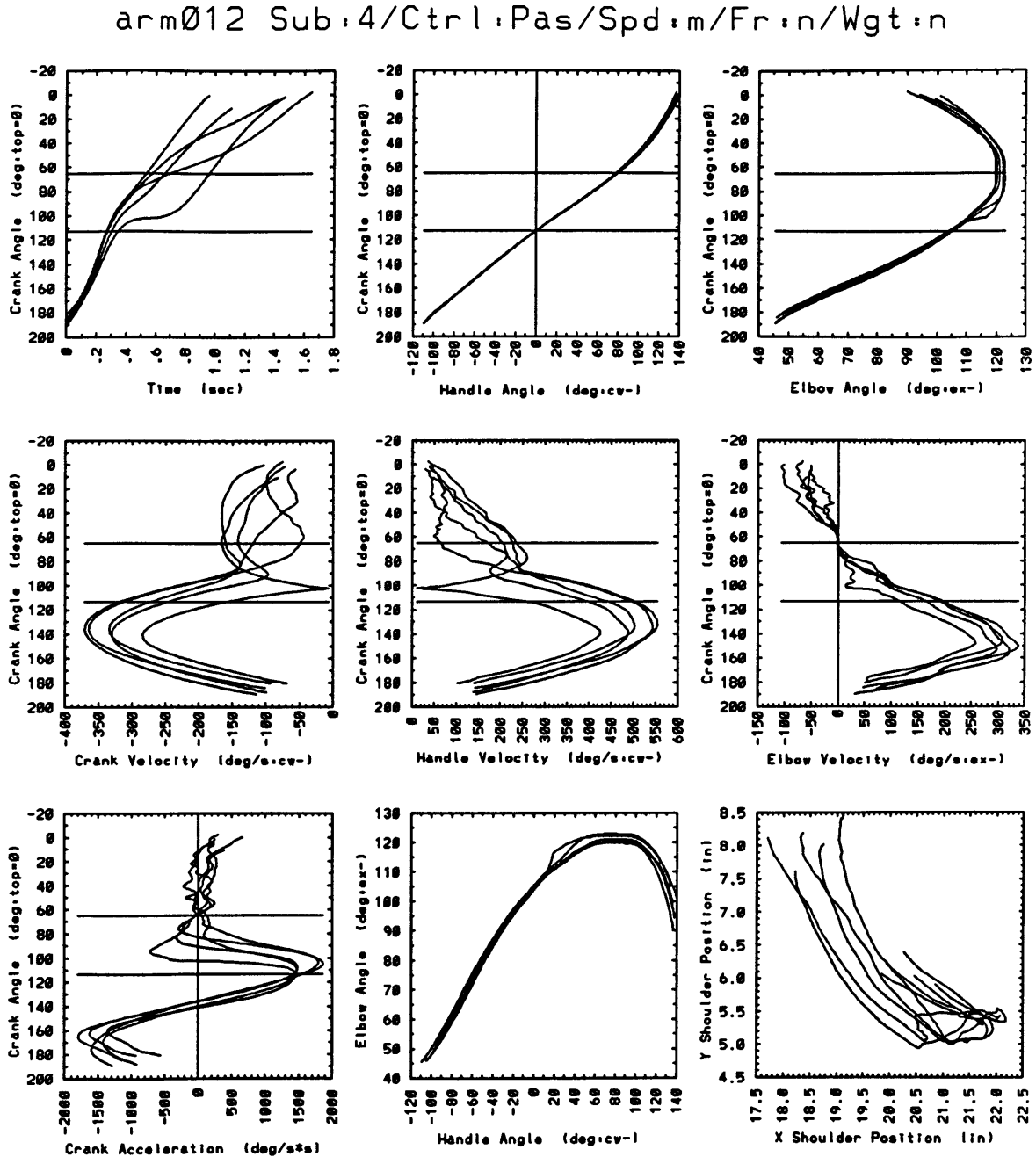
arm012 Sub:4/Ctrl:Pas/Spd:m/Fr:n/Wgt:n
Crank Angle (deg:top=0)
Time (sec)
Handle Angle (deg:cw-)
Elbow Angle (deg:ex-)
Crank Velocity (deg/s:cw-)
Handle Velocity (deg/s:cw-)
Elbow Velocity (deg/s:ex-)
Crank Acceleration (deg/s*s)
Elbow Angle (deg:ex-)
Handle Angle (deg:cw-)
Y Shoulder Position (in)
X Shoulder Position (in)

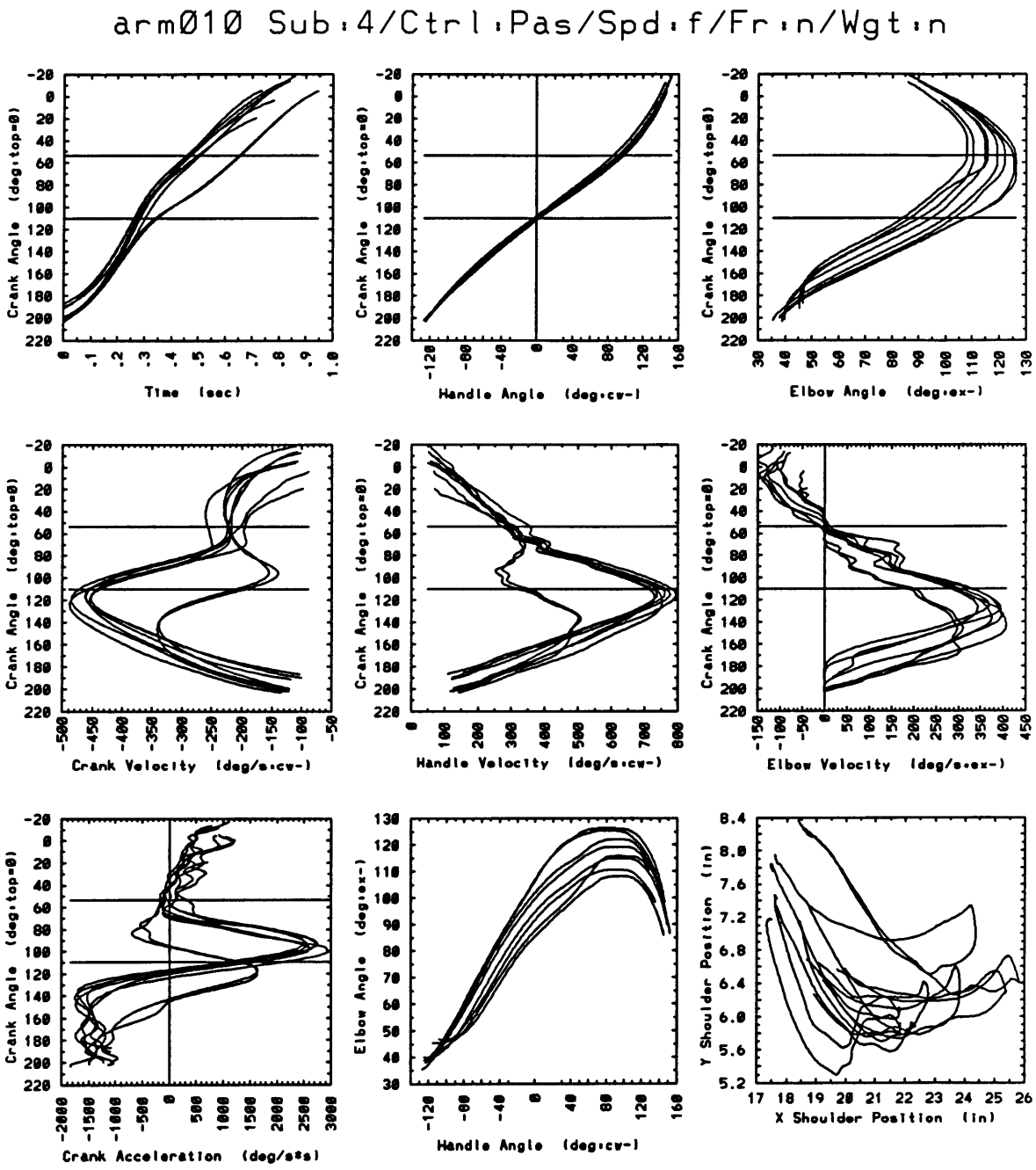
arm010 Sub:4/Ctrl:Pas/Spd:f/Fr:n/Wgt:n
Crank Angle (deg:top=0)
Time (sec)
Handle Angle (deg:cw-)
Elbow Angle (deg:ex-)
Crank Velocity (deg/s:cw-)
Handle Velocity (deg/s:cw-)
Elbow Velocity (deg/s:ex-)
Crank Acceleration (deg/s^2)
Elbow Angle (deg:ex-)
Handle Angle (deg:cw-)
Y Shoulder Position (in)
X Shoulder Position (in)

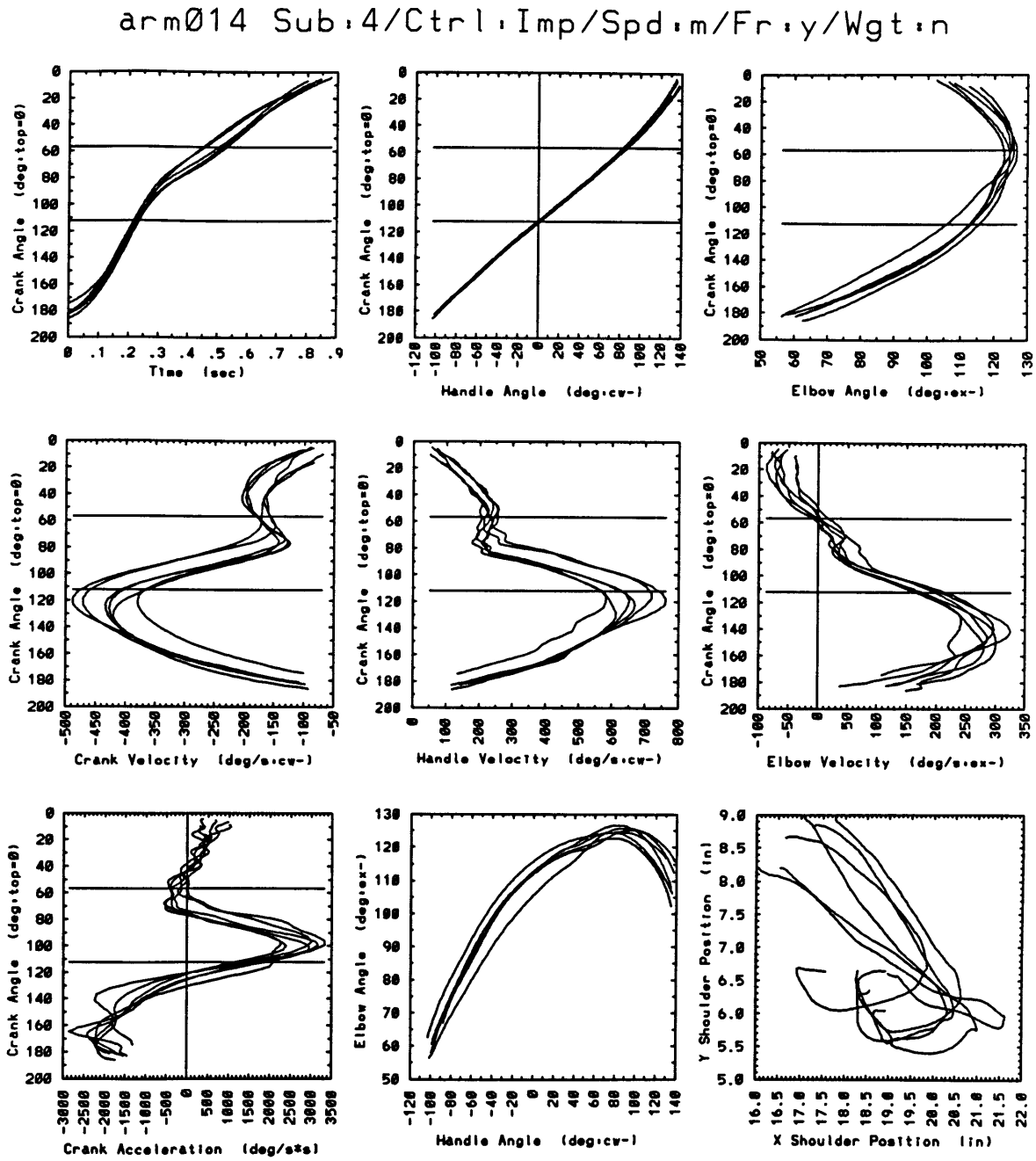
arm014 Sub:4/Ctrl:Imp/Spd:m/Fr:y/Wgt:n
Crank Angle (deg:top=0)
Time (sec)
Handle Angle (deg:cw-)
Elbow Angle (deg:ex-)
Crank Velocity (deg/s:cw-)
Handle Velocity (deg/s:cw-)
Elbow Velocity (deg/s:ex-)
Crank Acceleration (deg/s*s)
Elbow Angle (deg:ex-)
Handle Angle (deg:cw-)
Y Shoulder Position (in)
X Shoulder Position (in)

APPENDIX B

DYNAMIC PLOTS

SUBJECT 1

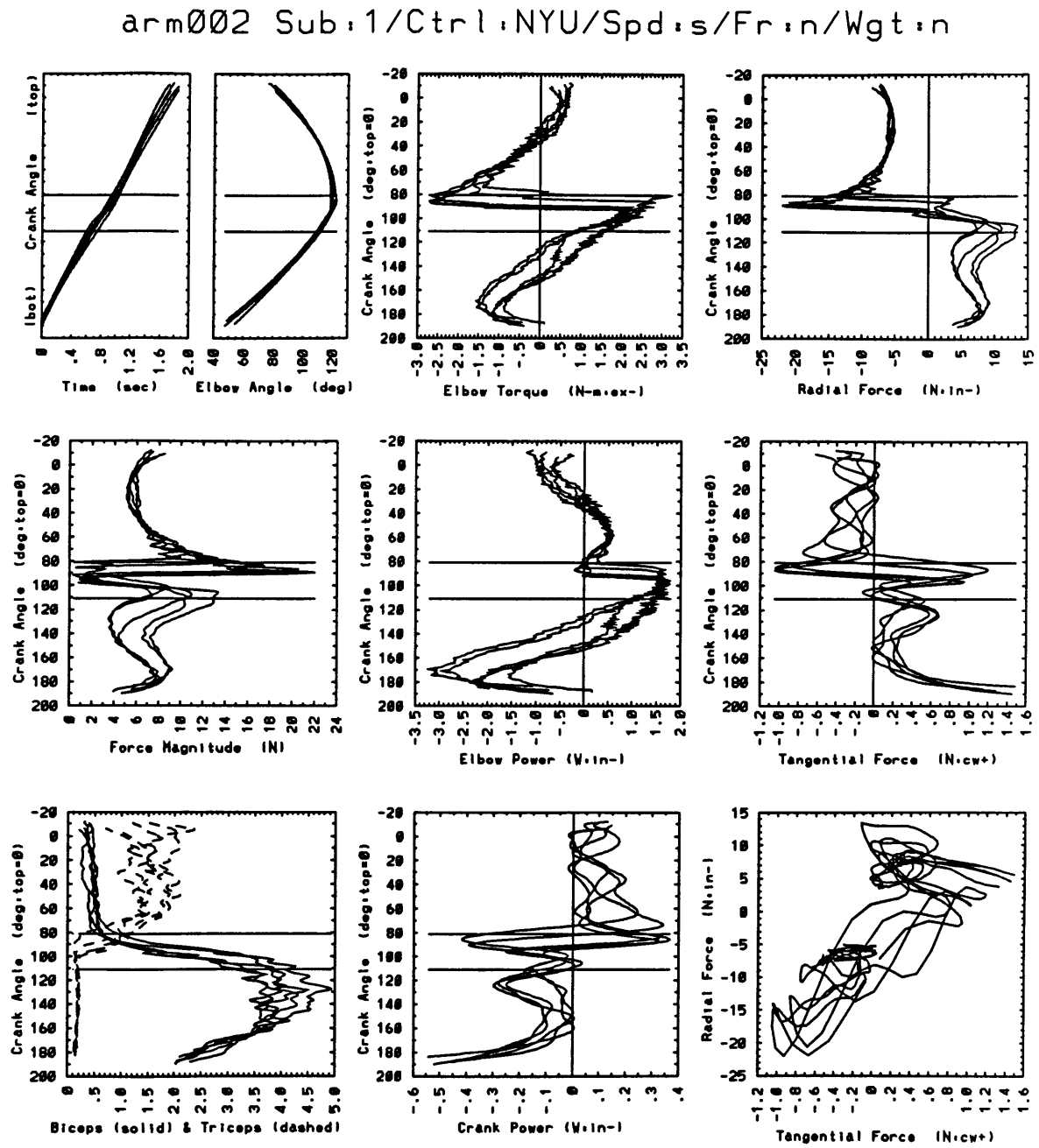
arm002 Sub:1/Ctrl:NYU/Spd:s/Fr:n/Wgt:n
Crank Angle (top) (bot)
Time (sec)
Elbow Angle (deg)
Crank Angle (deg:top=0)
Elbow Torque (N-m:ex-)
Radial Force (N:in-)
Force Magnitude (N)
Elbow Power (W:in-)
Tangential Force (N:cw+)
Biceps (solid) & Triceps (dashed)
Crank Power (W:in-)

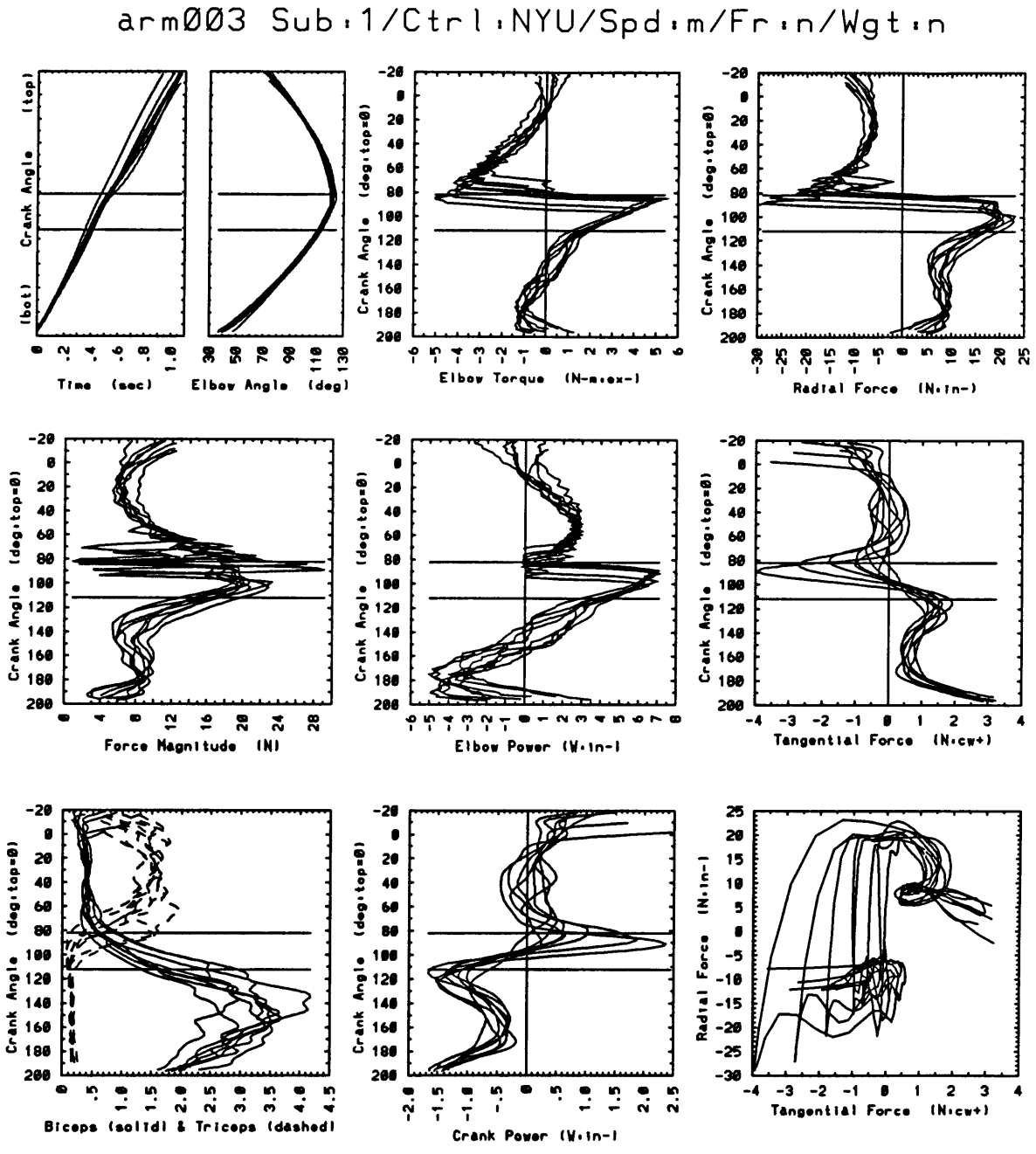
arm003 Sub:1/Ctrl:NYU/Spd:m/Fr:n/Wgt:n
Crank Angle (top)
(bot)
Time (sec)
Elbow Angle (deg)
Crank Angle (deg:top=0)
Elbow Torque (N-m:ex-)
Radial Force (N:in-)
Force Magnitude (N)
Elbow Power (W:in-)
Tangential Force (N:cw+)
Biceps (solid) & Triceps (dashed)
Crank Power (W:in-)

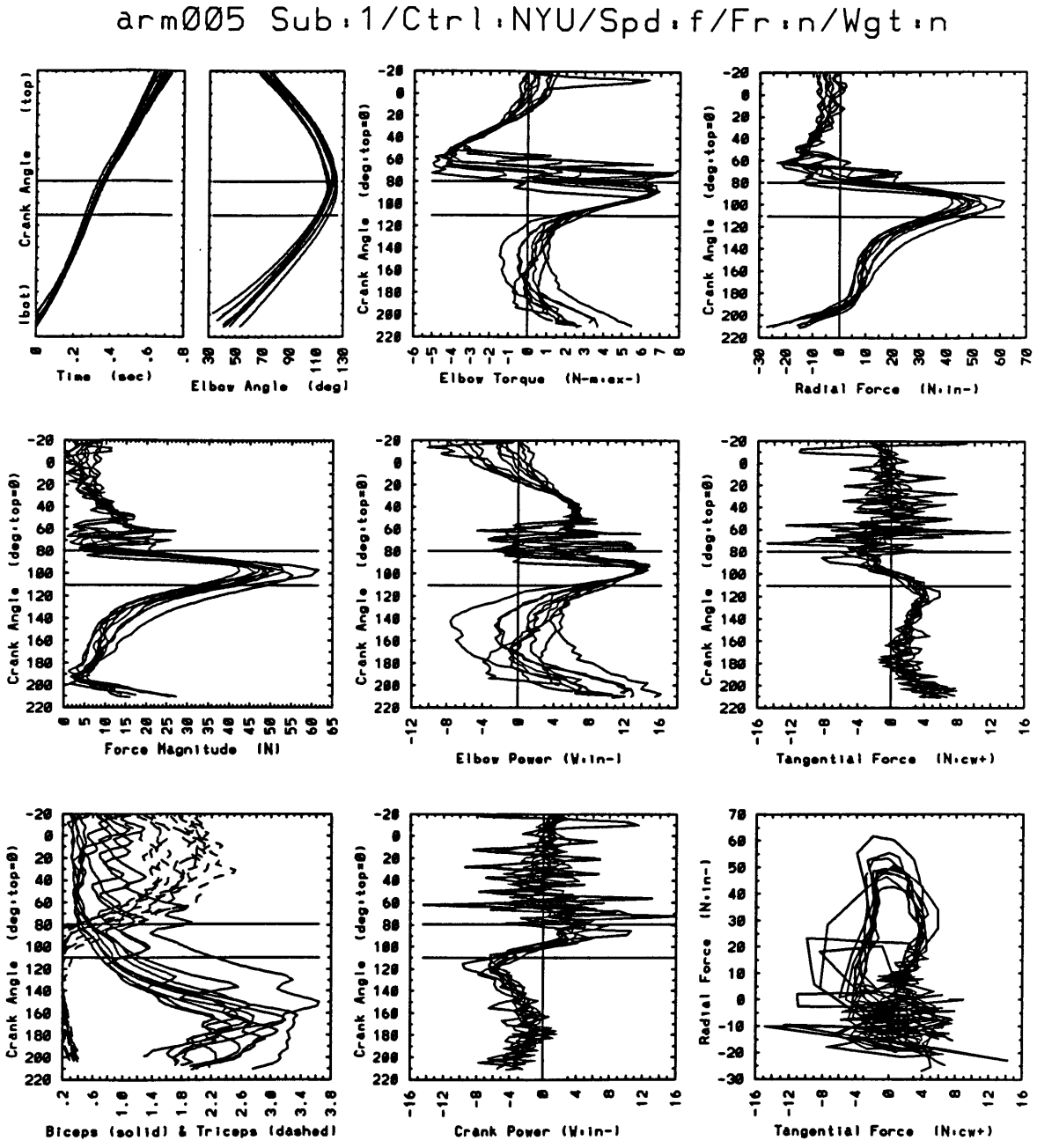
arm005 Sub:1/Ctrl:NYU/Spd:f/Fr:n/Wgt:n
Crank Angle (top) (bot)
Time (sec)
Elbow Angle (deg)
Crank Angle (deg:top=0)
Elbow Torque (N-m:ex-)
Radial Force (N:in-)
Force Magnitude (N)
Elbow Power (W:in-)
Tangential Force (N:cw+)
Biceps (solid) & Triceps (dashed)
Crank Power (W:in-)

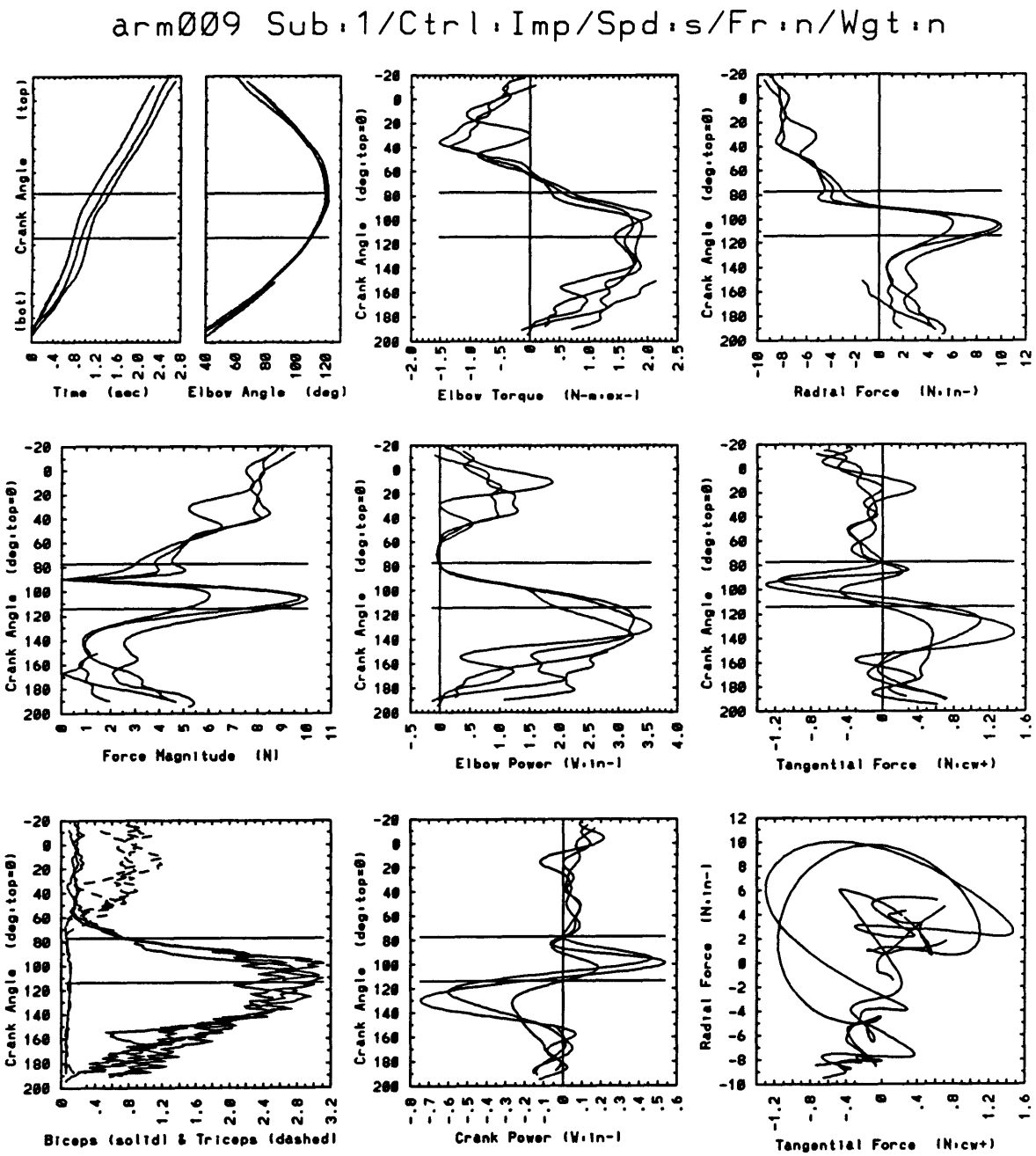
arm009 Sub:1/Ctrl:Imp/Spd:s/Fr:n/Wgt:n
Crank Angle (top)
(bot)
Time (sec)
Elbow Angle (deg)
Crank Angle (deg:top=0)
Elbow Torque (N-m:ex-)
Radial Force (N:in-)
Force Magnitude (N)
Elbow Power (W:in-)
Tangential Force (N:cw+)
Biceps (solid) & Triceps (dashed)
Crank Power (W:in-)
Radial Force (N:in-)
Tangential Force (N:cw+)

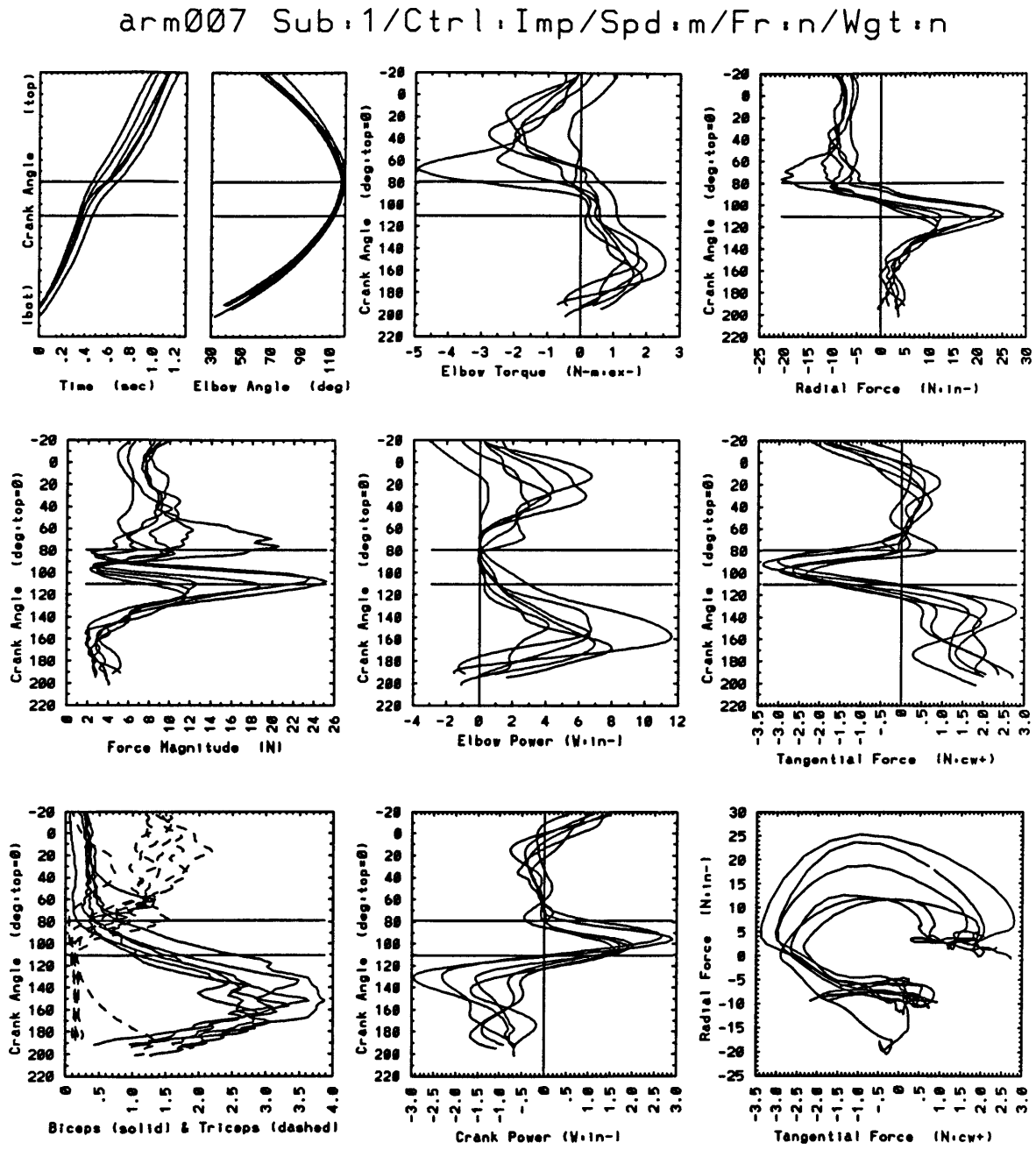
arm00 Sub:1/Ctrl:Imp/Spd:m/Fr:n/Wgt:n
Crank Angle (top)
(bot)
Time (sec)
Elbow Angle (deg)
Crank Angle (deg:top=0)
Elbow Torque (N-m:ex-)
Radial Force (N:in-)
Force Magnitude (N)
Elbow Power (W:in-)
Tangential Force (N:cw+)
Biceps (solid) & Triceps (dashed)
Crank Power (W:in-)
Radial Force (N:in-)
Tangential Force (N:cw+)

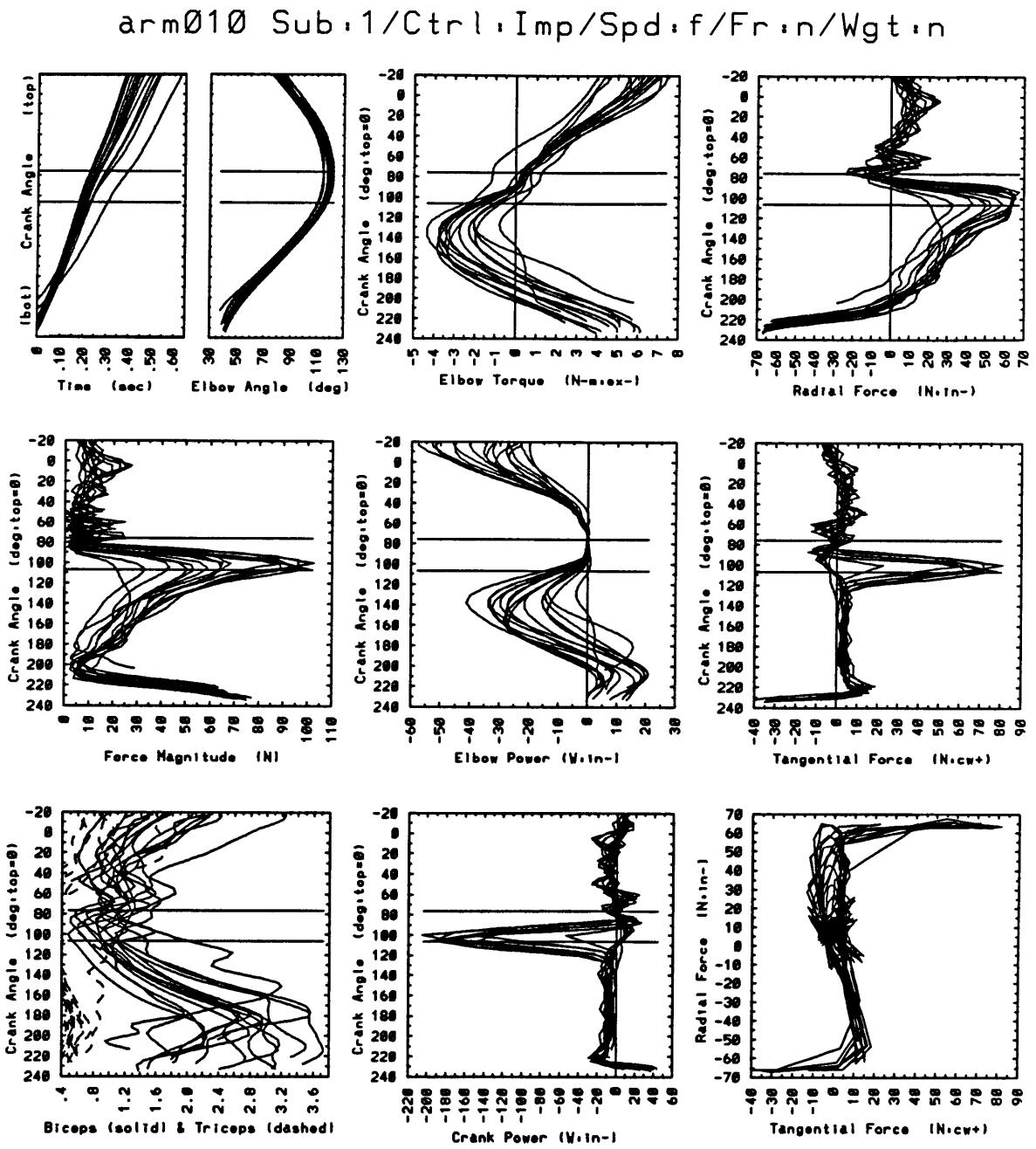
arm010 Sub:1/Ctrl:Imp/Spd:f/Fr:n/Wgt:n
Crank Angle (top)
(bot)
Time (sec)
Elbow Angle (deg)
Crank Angle (deg:top=0)
Elbow Torque (N-m:ex-)
Radial Force (N:in-)
Force Magnitude (N)
Elbow Power (W:in-)
Tangential Force (N:cw+)
Biceps (solid) & Triceps (dashed)
Crank Power (W:in-)
Radial Force (N:in-)
Tangential Force (N:cw+)

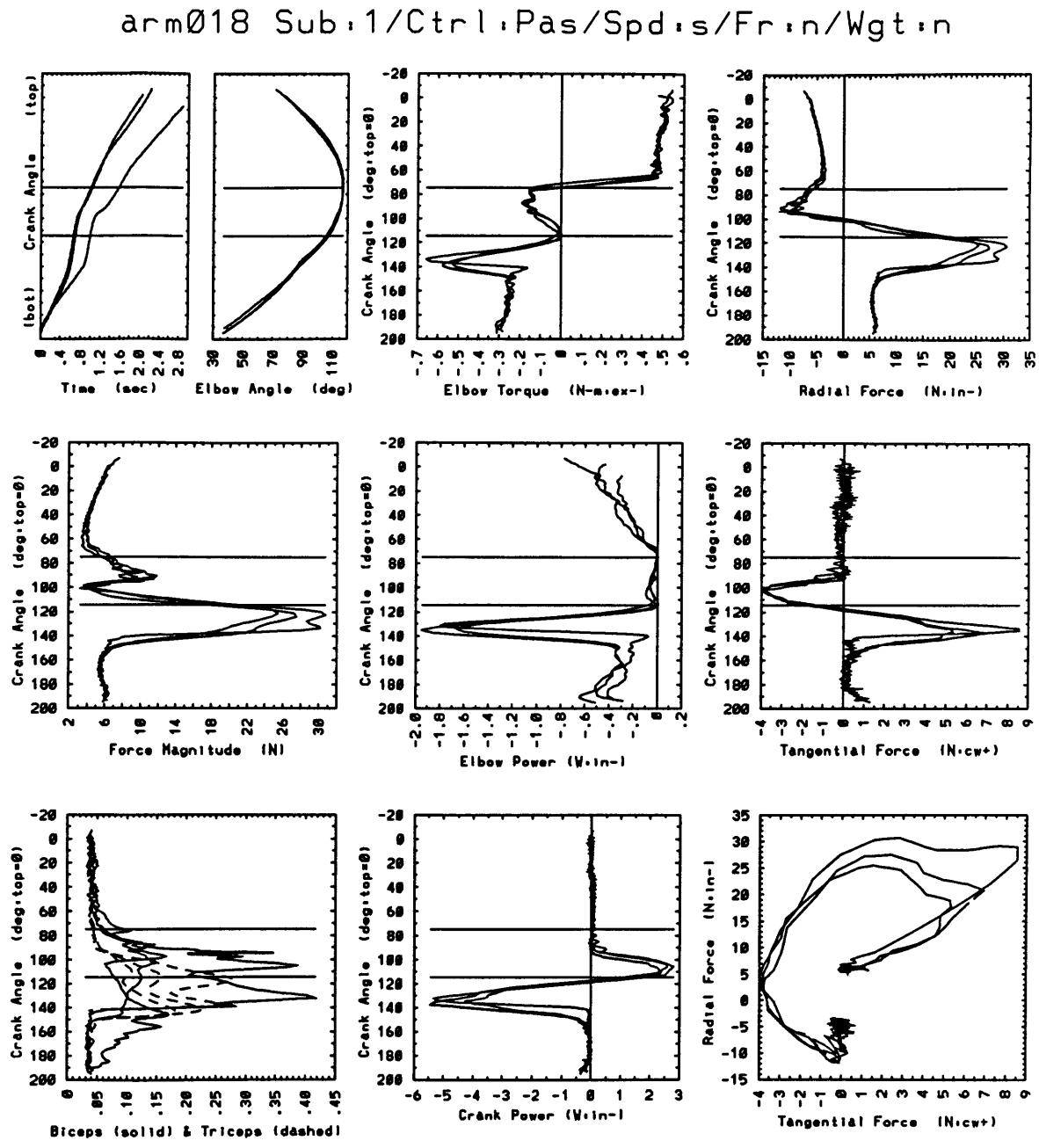
arm018 Sub:1/Ctrl:Pas/Spd:s/Fr:n/Wgt:n
Crank Angle (top) (bot)
Time (sec)
Elbow Angle (deg)
Crank Angle (deg:top=0)
Elbow Torque (N-m:ex-)
Radial Force (N:in-)
Force Magnitude (N)
Elbow Power (W:in-)
Tangential Force (N:cw+)
Biceps (solid) & Triceps (dashed)
Crank Power (W:in-)

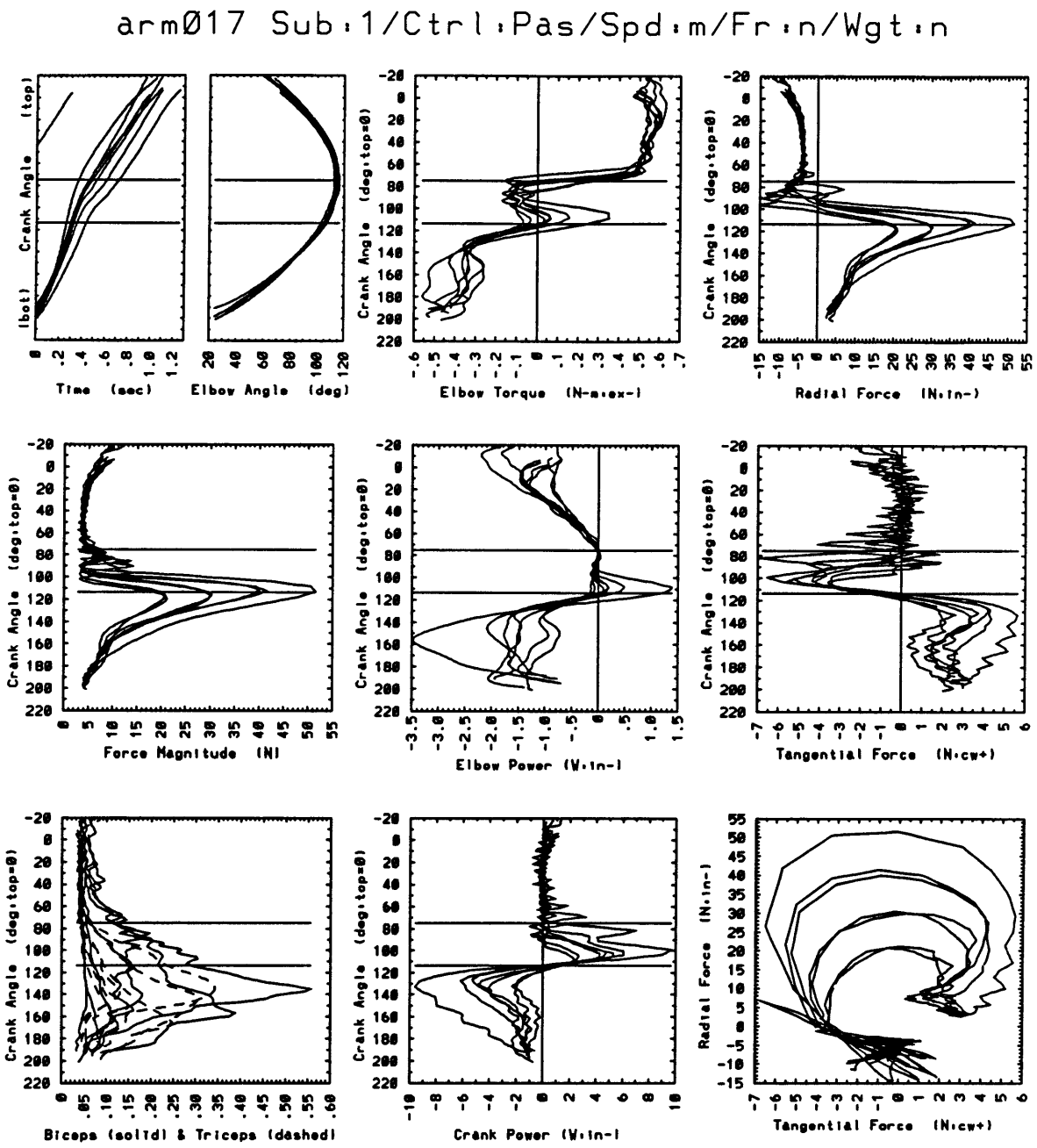
arm017 Sub:1/Ctrl:Pas/Spd:m/Fr:n/Wgt:n
Crank Angle (top) (bot)
Time (sec)
Elbow Angle (deg)
Crank Angle (deg:top=0)
Elbow Torque (N-m:ex-)
Radial Force (N:in-)
Force Magnitude (N)
Elbow Power (W:in-)
Tangential Force (N:cw+)
Biceps (solid) & Triceps (dashed)
Crank Power (W:in-)

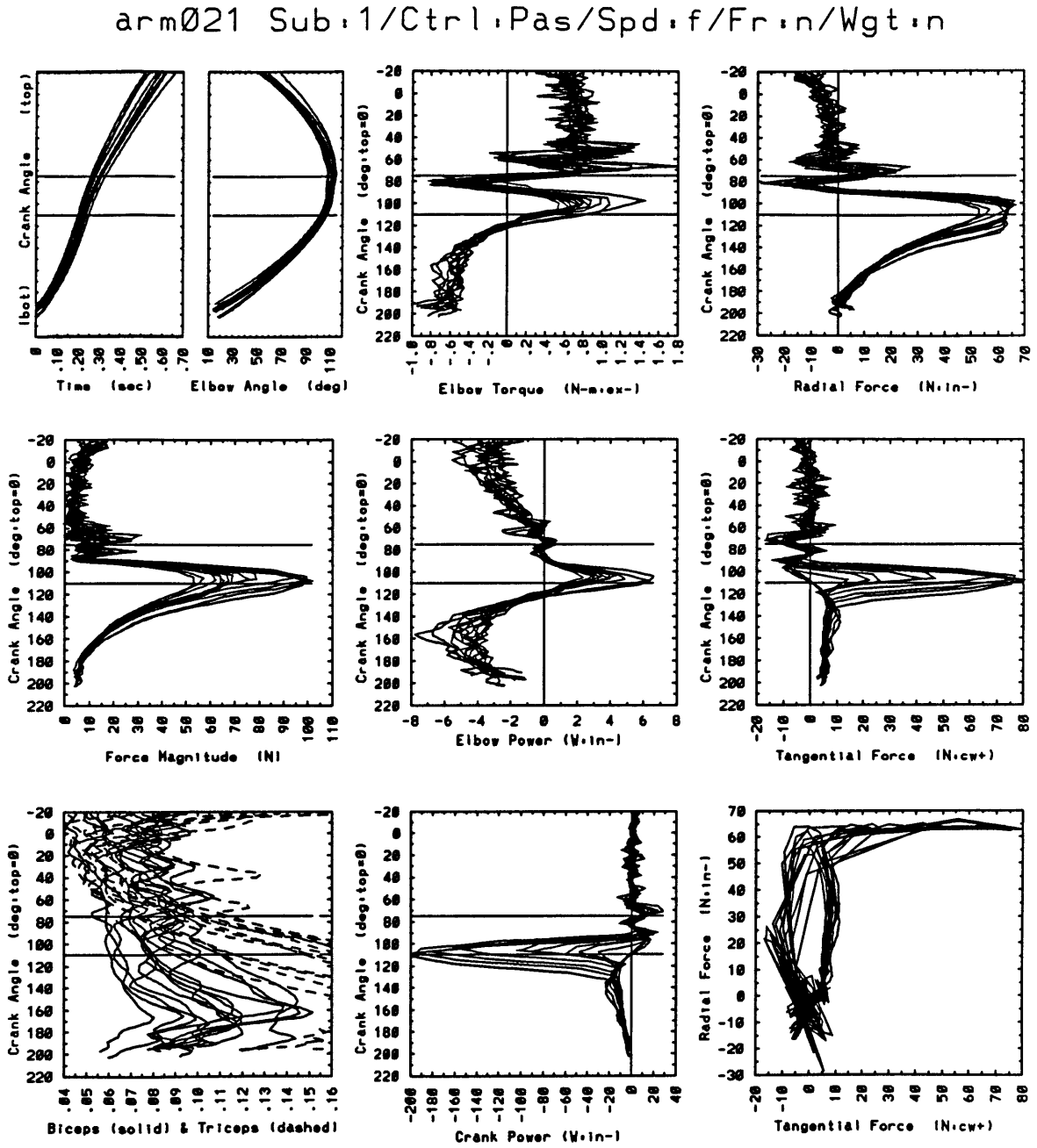
arm021 Sub:1/Ctrl:Pas/Spd:f/Fr:n/Wgt:n
Crank Angle (top)
(bot)
Time (sec)
Elbow Angle (deg)
Crank Angle (deg:top=0)
Elbow Torque (N-m:ex-)
Radial Force (N:in-)
Force Magnitude (N)
Elbow Power (W:in-)
Tangential Force (N:cw+)
Biceps (solid) & Triceps (dashed)
Crank Power (W:in-)

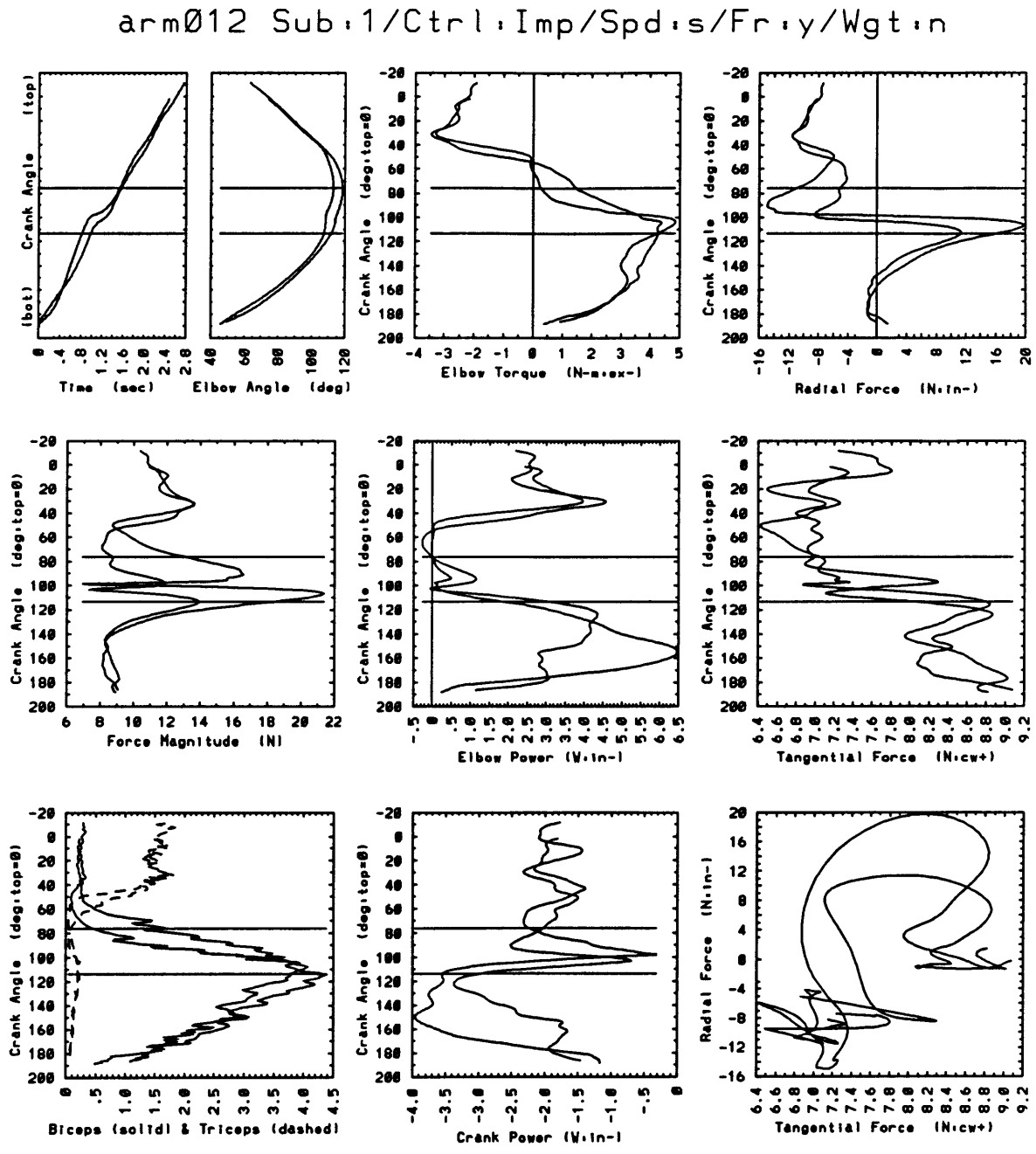
arm012 Sub:1/Ctrl:Imp/Spd:s/Fr:y/Wgt:n
Crank Angle (top)
(bot)
Time (sec)
Elbow Angle (deg)
Crank Angle (deg:top=0)
Elbow Torque (N-m:ex-)
Radial Force (N:in-)
Force Magnitude (N)
Elbow Power (W:in-)
Tangential Force (N:cw+)
Biceps (solid) & Triceps (dashed)
Crank Power (W:in-)

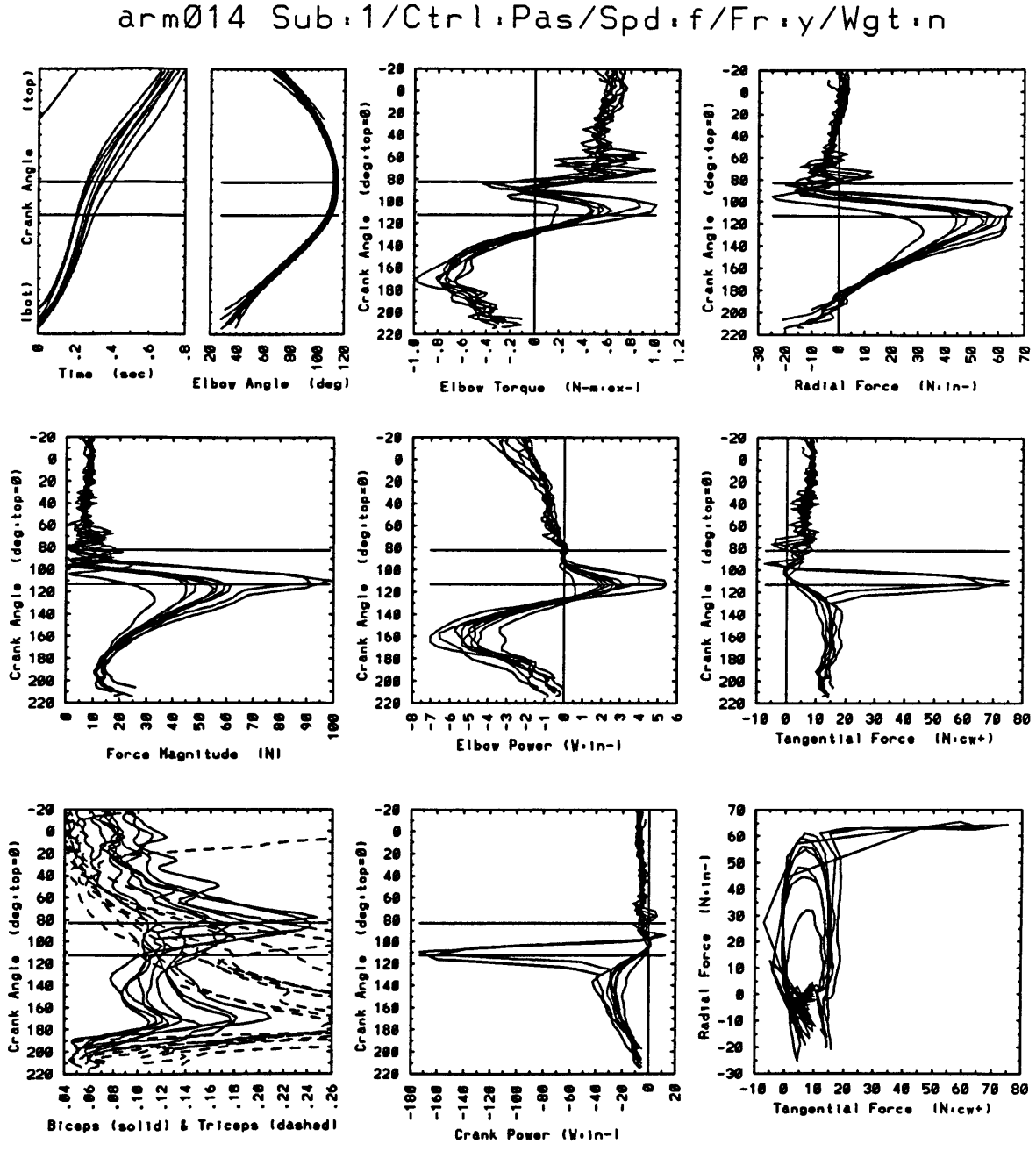
arm014 Sub:1/Ctrl:Pas/Spd:f/Fr:y/Wgt:n
Crank Angle (top) (bot)
Time (sec)
Elbow Angle (deg)
Crank Angle (deg:top=0)
Elbow Torque (N-m:ex-)
Radial Force (N:in-)
Force Magnitude (N)
Elbow Power (W:in-)
Tangential Force (N:cw+)
Biceps (solid) & Triceps (dashed)
Crank Power (W:in-)

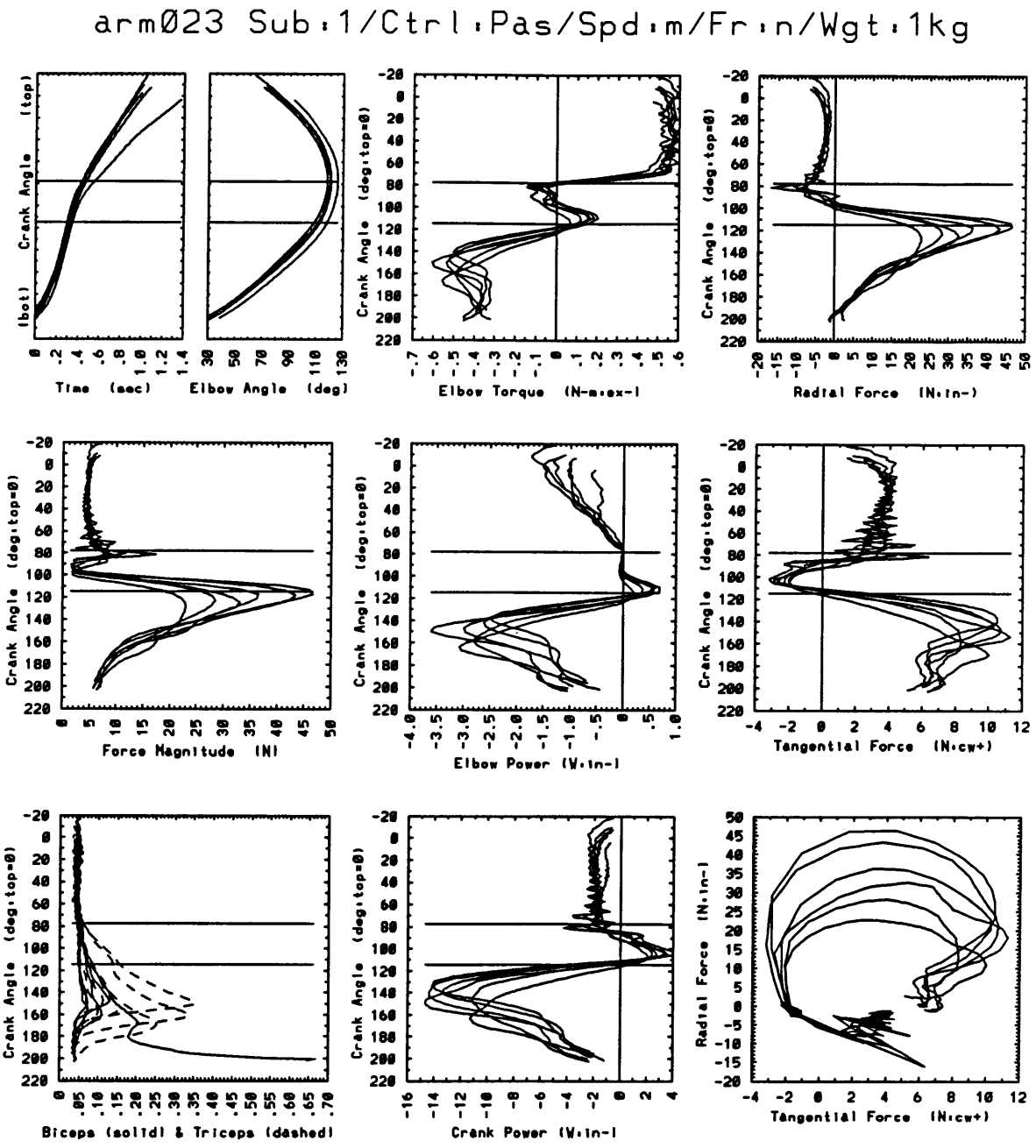
arm023 Sub:1/Ctrl:Pas/Spd:m/Fr:n/Wgt:1kg
Crank Angle (top)
(bot)
Time (sec)
Elbow Angle (deg)
Crank Angle (deg:top=0)
Elbow Torque (N-m:ex-)
Radial Force (N:in-)
Force Magnitude (N)
Elbow Power (W:in-)
Tangential Force (N:cw+)
Biceps (solid) & Triceps (dashed)
Crank Power (W:in-)
Radial Force (N:in-)

SUBJECT 2

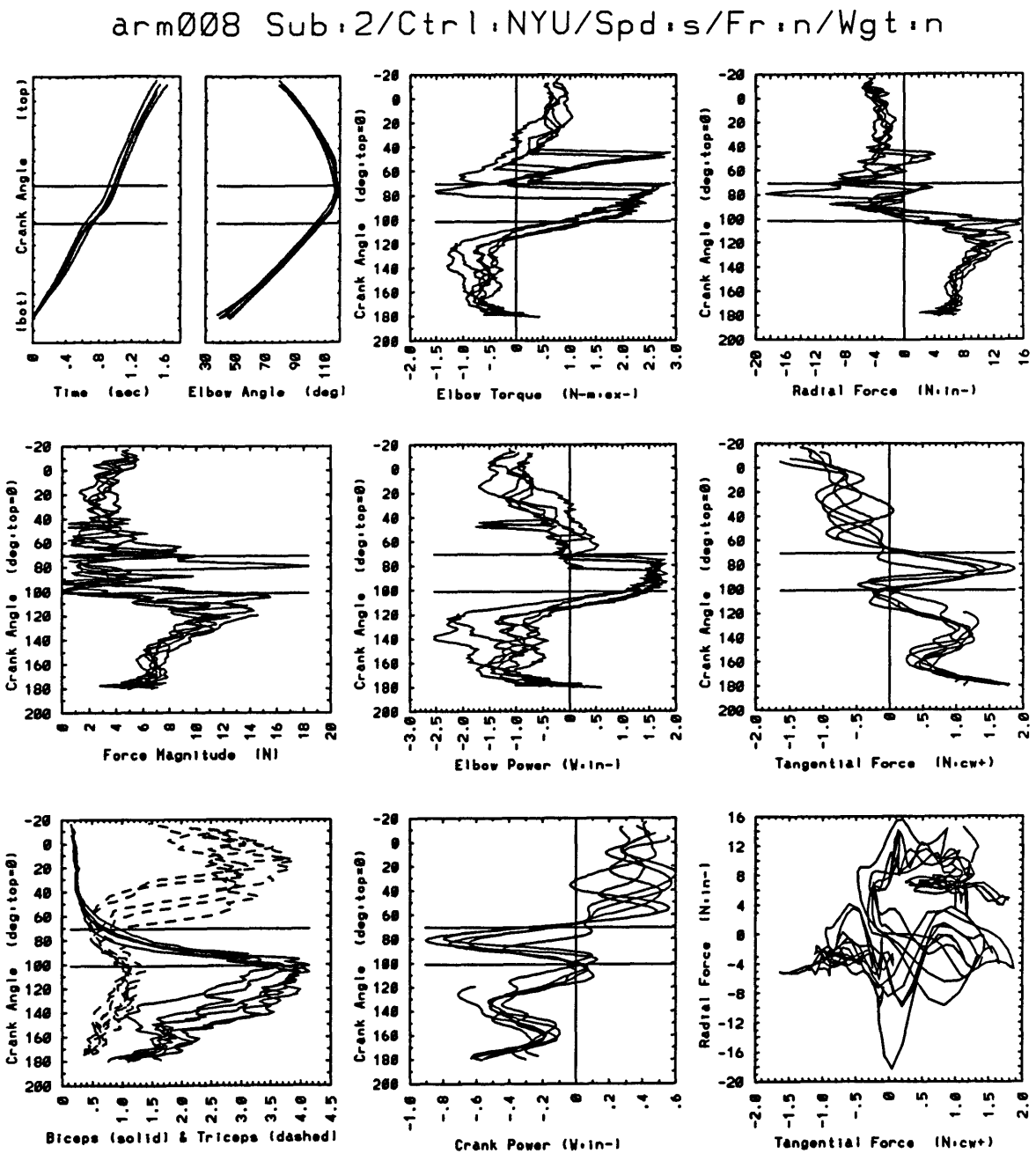
arm008 Sub:2/Ctrl:NYU/Spd:s/Fr:n/Wgt:n
Crank Angle (top)
(bot)
Time (sec)
Elbow Angle (deg)
Crank Angle (deg:top=0)
Elbow Torque (N-m:ex-)
Radial Force (N:in-)
Force Magnitude (N)
Elbow Power (W:in-)
Tangential Force (N:cw+)
Biceps (solid) & Triceps (dashed)
Crank Power (W:in-)
Radial Force (N:in-)
Tangential Force (N:cw+)

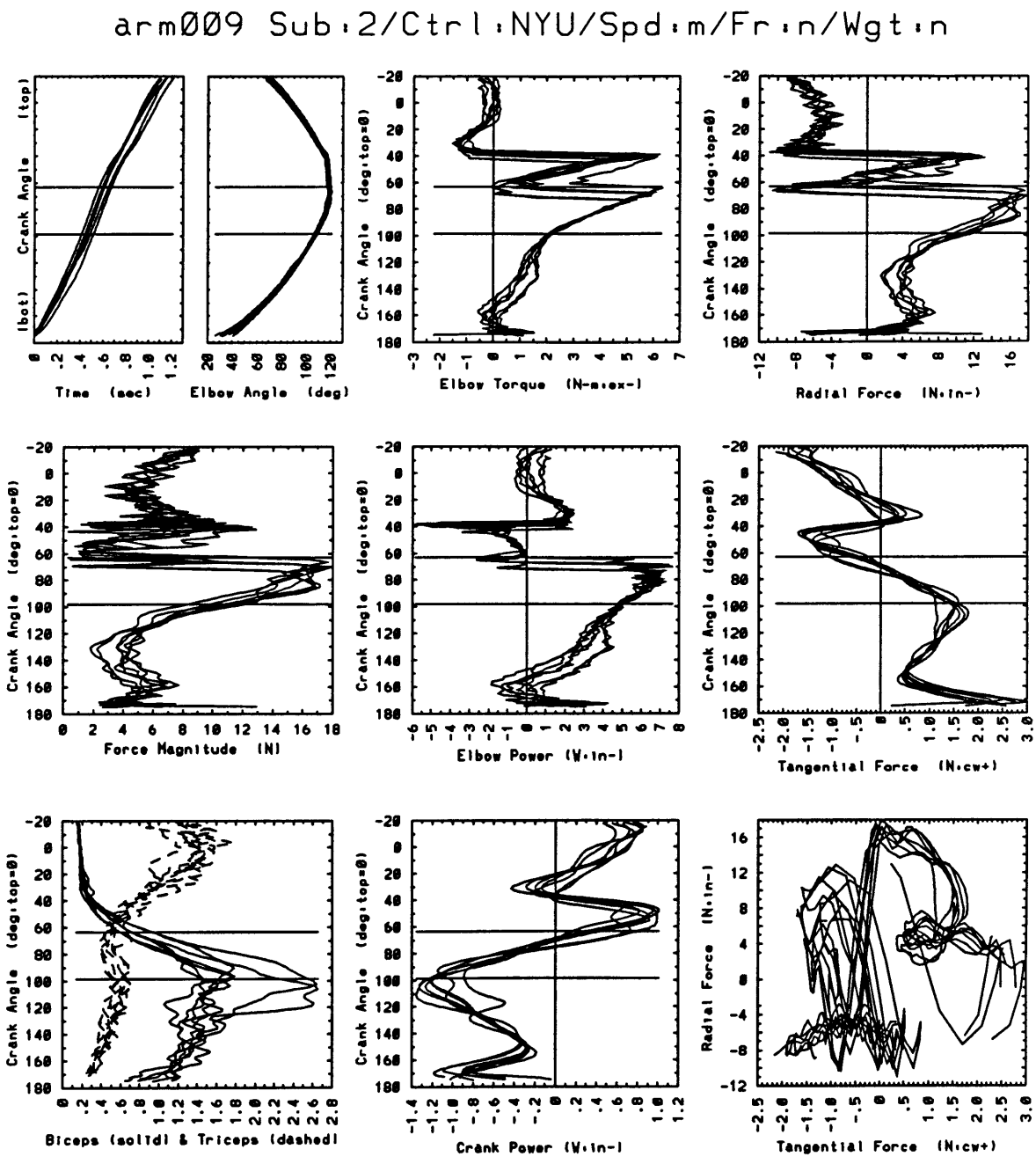
arm009 Sub:2/Ctrl:NYU/Spd:m/Fr:n/Wgt:n
Crank Angle (top)
(bot)
Time (sec)
Elbow Angle (deg)
Crank Angle (deg:top=0)
Elbow Torque (N-m:ex-)
Radial Force (N:in-)
Force Magnitude (N)
Elbow Power (W:in-)
Tangential Force (N:cw+)
Biceps (solid) & Triceps (dashed)
Crank Power (W:in-)
Radial Force (N:in-)
Tangential Force (N:cw+)

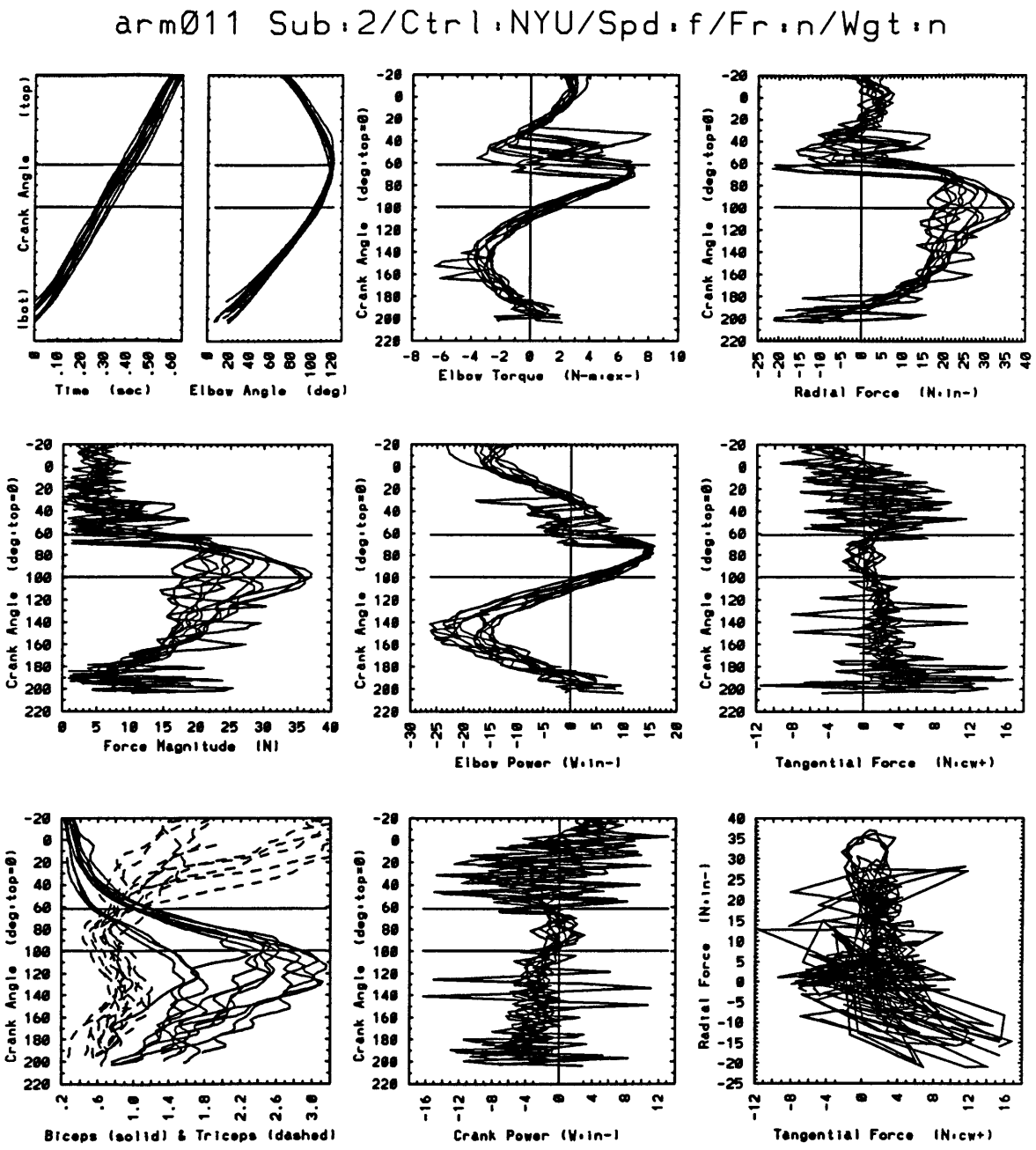
arm011 Sub:2/Ctrl:NYU/Spd:f/Fr:n/Wgt:n
Crank Angle (top) (bot)
Time (sec)
Elbow Angle (deg)
Crank Angle (deg:top=0)
Elbow Torque (N-m:ex-)
Radial Force (N:in-)
Force Magnitude (N)
Elbow Power (W:in-)
Tangential Force (N:cw+)
Biceps (solid) & Triceps (dashed)
Crank Power (W:in-)

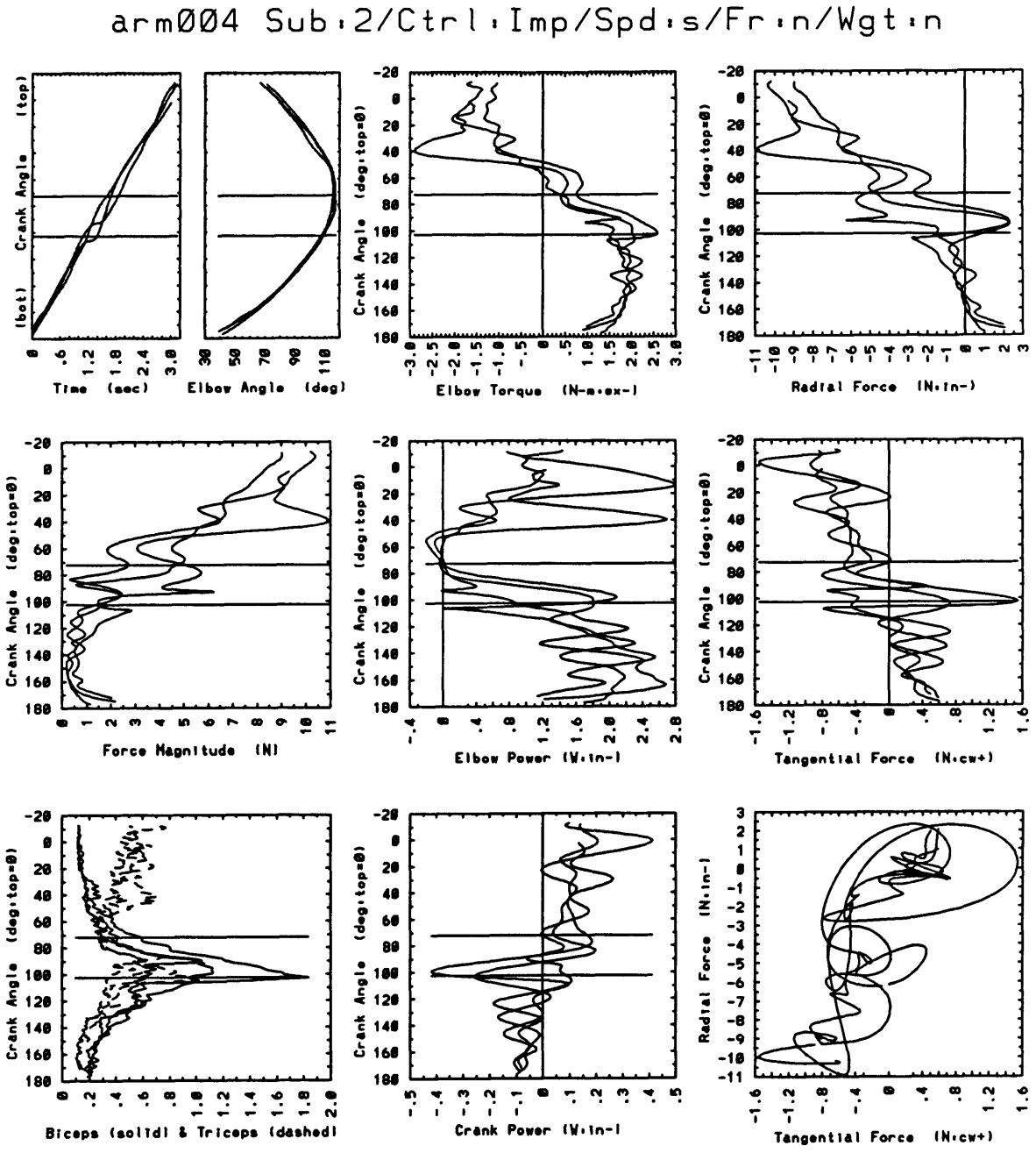
arm00 Sub:2/Ctrl:Imp/Spd:s/Fr:n/Wgt:n
Crank Angle (top)
(bot)
Time (sec)
Elbow Angle (deg)
Crank Angle (deg:top=0)
Elbow Torque (N-m:ex-)
Radial Force (N:in-)
Force Magnitude (N)
Elbow Power (W:in-)
Tangential Force (N:cw+)
Biceps (solid) & Triceps (dashed)
Crank Power (W:in-)

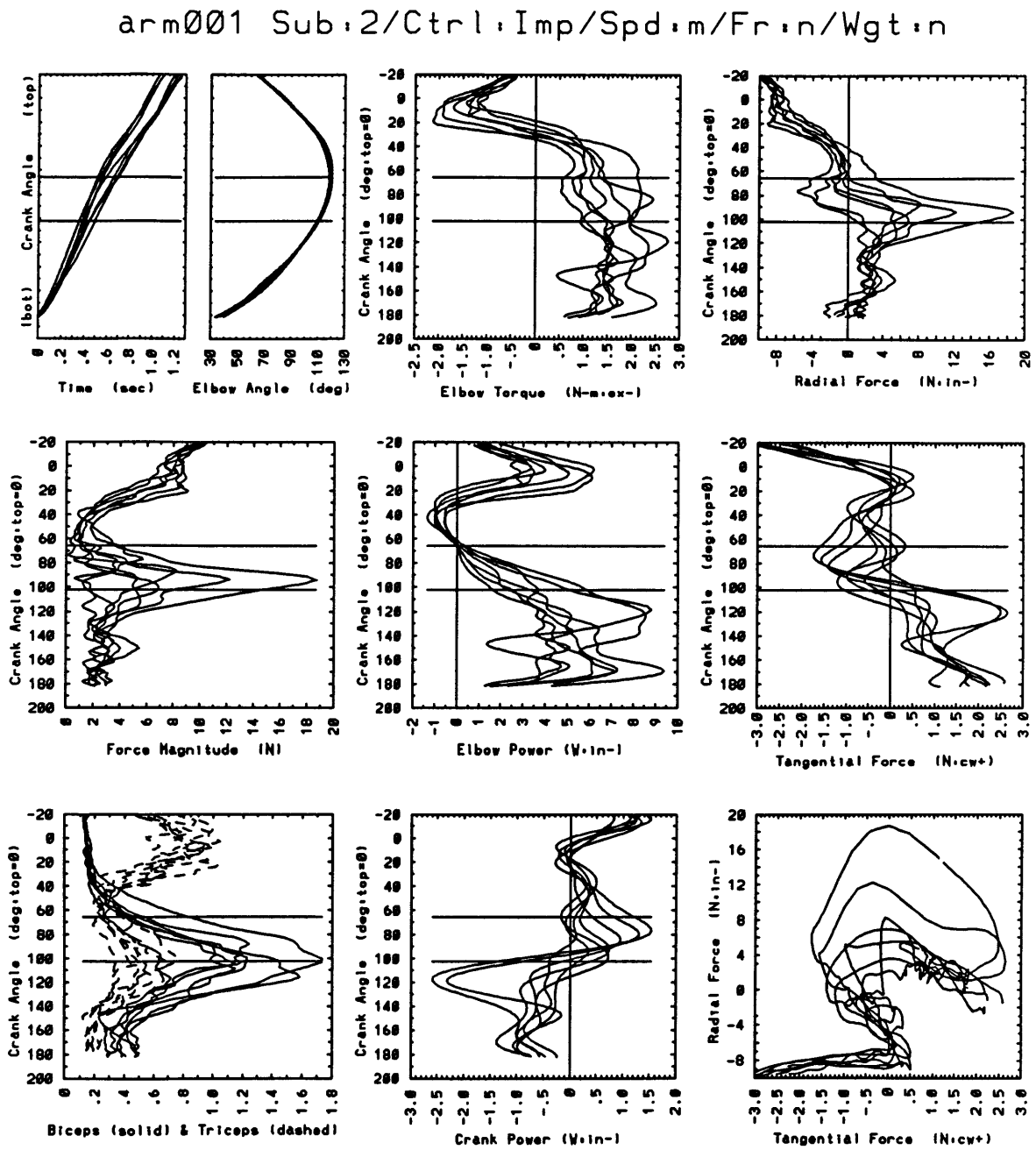
arm00l Sub:2/Ctrl:Imp/Spd:m/Fr:n/Wgt:n
Crank Angle (top)
(bot)
Time (sec)
Elbow Angle (deg)
Crank Angle (deg:top=0)
Elbow Torque (N-m:ex-)
Radial Force (N:in-)
Force Magnitude (N)
Elbow Power (W:in-)
Tangential Force (N:cw+)
Biceps (solid) & Triceps (dashed)
Crank Power (W:in-)
Radial Force (N:in-)
Tangential Force (N:cw+)

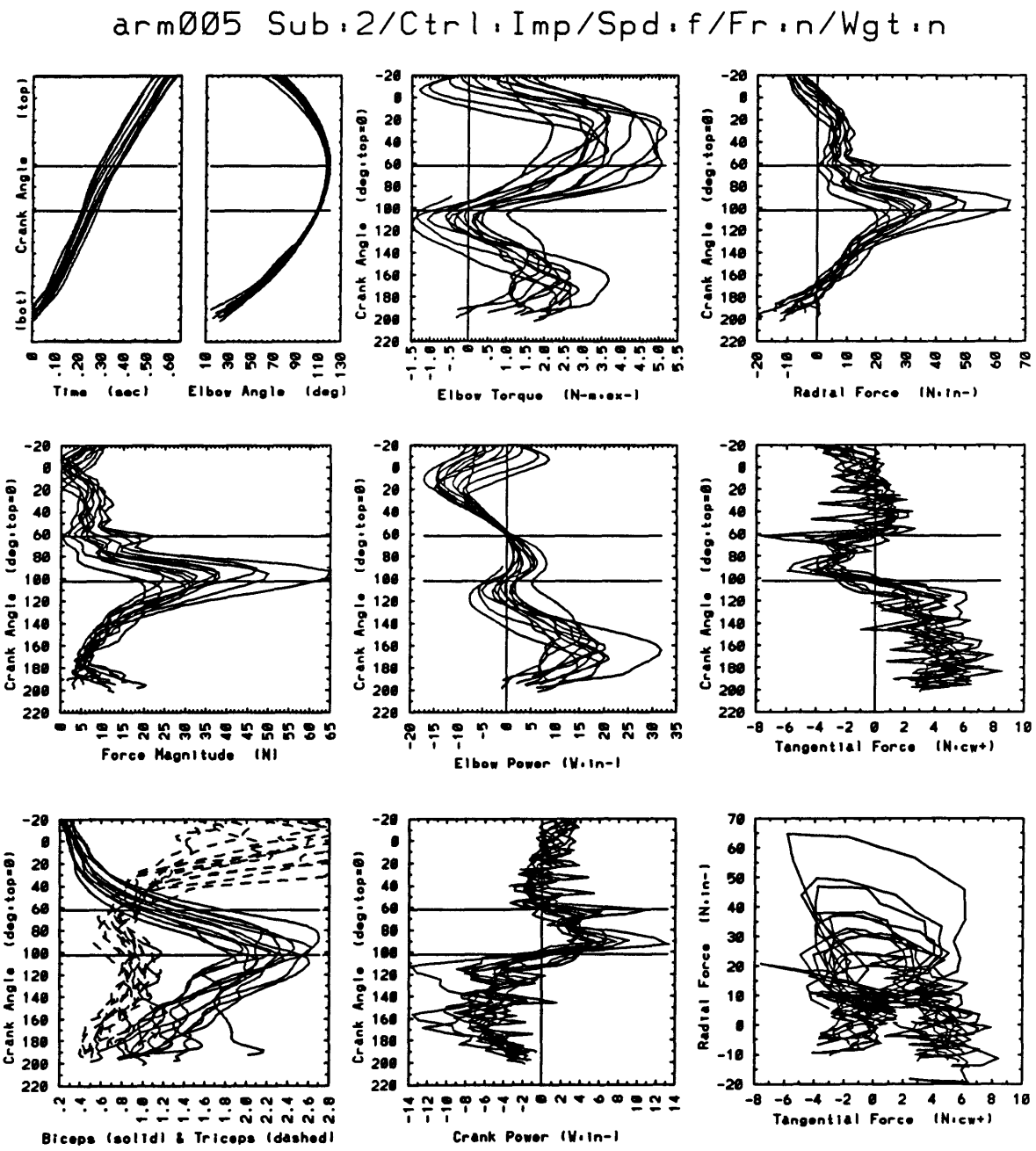
arm005 Sub:2/Ctrl:Imp/Spd:f/Fr:n/Wgt:n
Crank Angle (top) (bot)
Time (sec)
Elbow Angle (deg)
Crank Angle (deg:top=0)
Elbow Torque (N-m:ex-)
Radial Force (N:in-)
Force Magnitude (N)
Elbow Power (W:in-)
Tangential Force (N:cw+)
Biceps (solid) & Triceps (dashed)
Crank Power (W:in-)
Radial Force (N:in-)

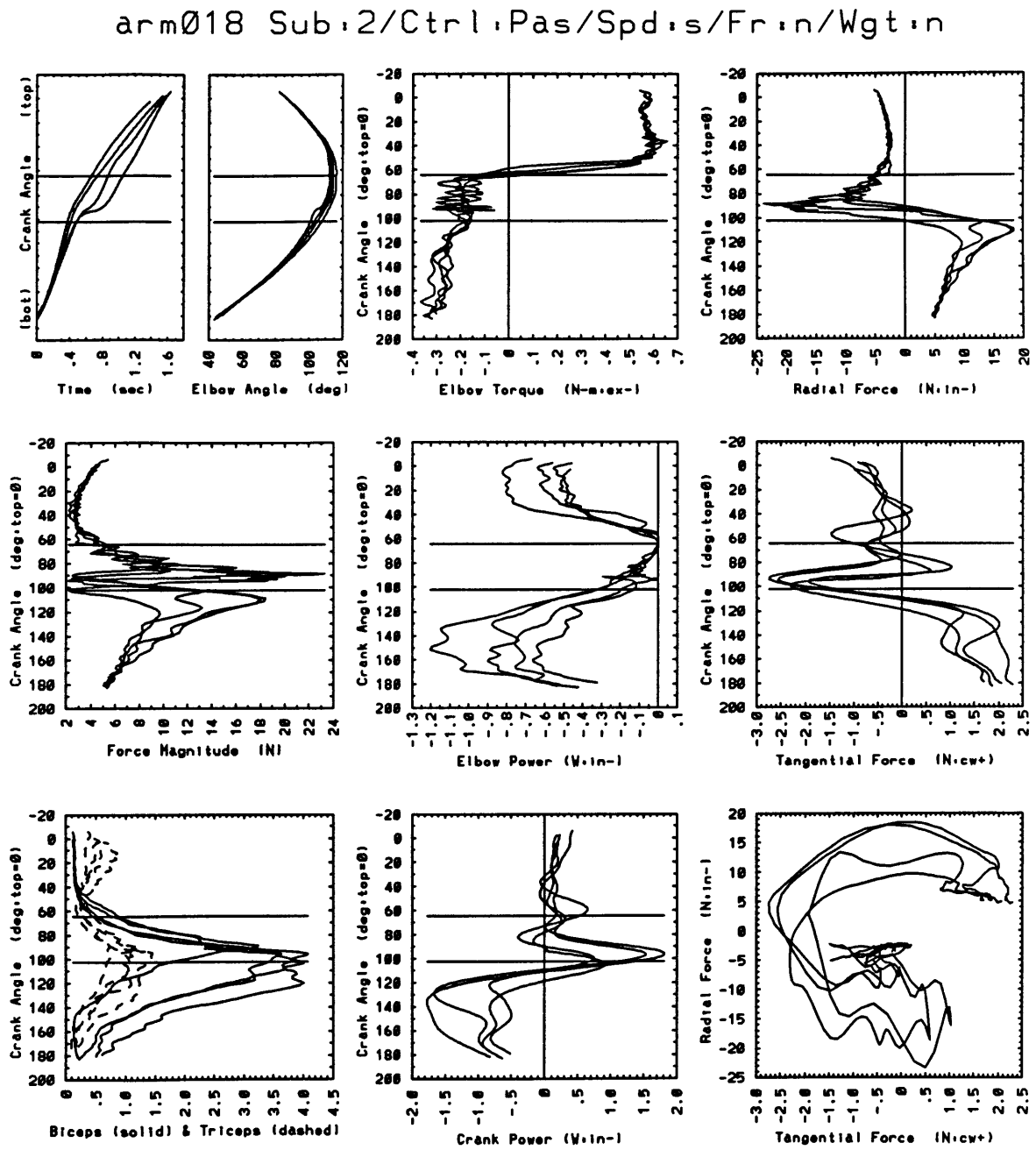
arm018 Sub:2/Ctrl:Pas/Spd:s/Fr:n/Wgt:n
Crank Angle (top) (bot)
Time (sec)
Elbow Angle (deg)
Crank Angle (deg:top=0)
Elbow Torque (N-m:ex-)
Radial Force (N:in-)
Force Magnitude (N)
Elbow Power (W:in-)
Tangential Force (N:cw+)
Biceps (solid) & Triceps (dashed)
Crank Power (W:in-)

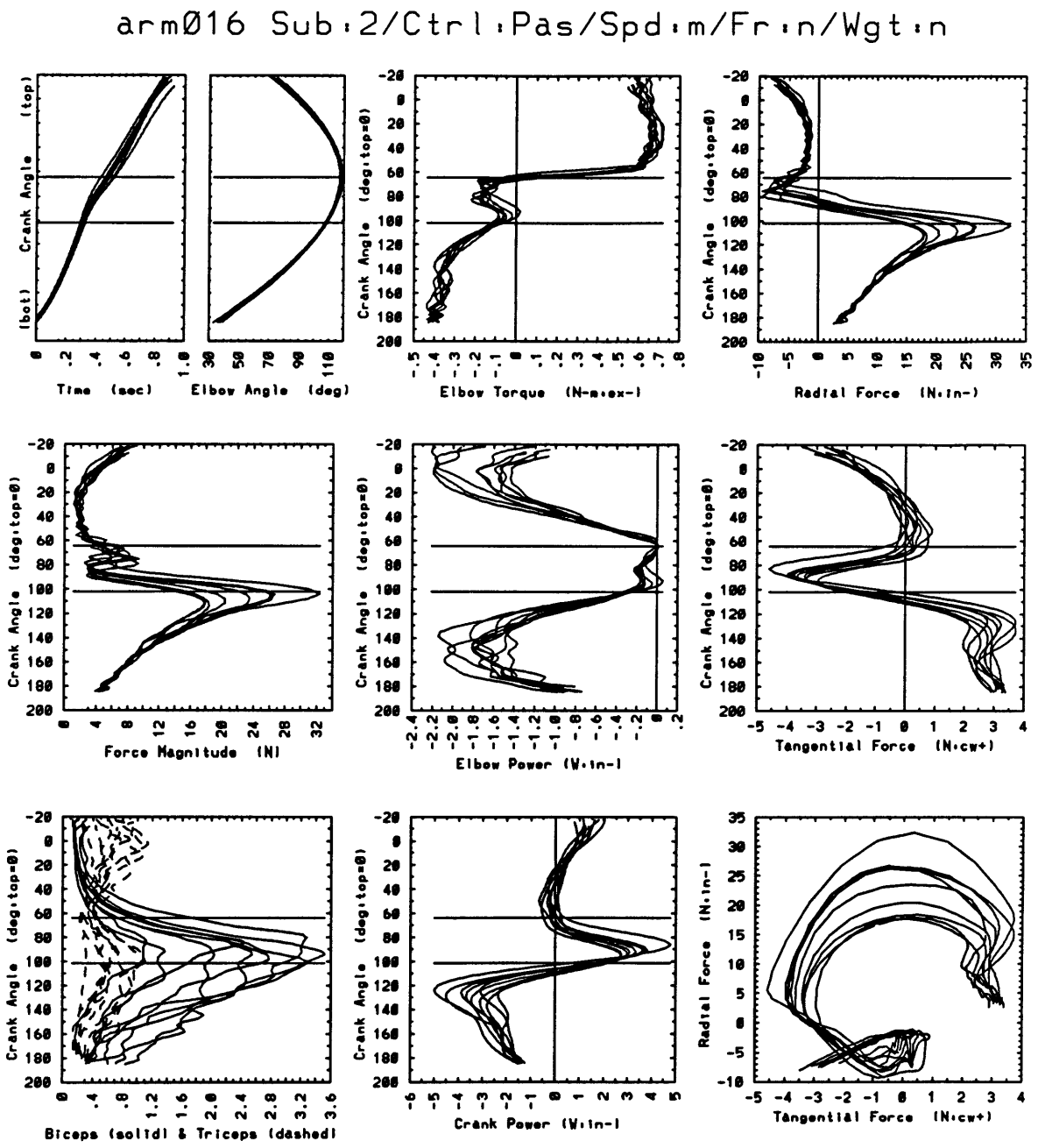
arm016 Sub:2/Ctrl:Pas/Spd:m/Fr:n/Wgt:n
Crank Angle (top)
(bot)
Time (sec)
Elbow Angle (deg)
Crank Angle (deg:top=0)
Elbow Torque (N-m:ex-)
Radial Force (N:in-)
Force Magnitude (N)
Elbow Power (W:in-)
Tangential Force (N:cw+)
Biceps (solid) & Triceps (dashed)
Crank Power (W:in-)

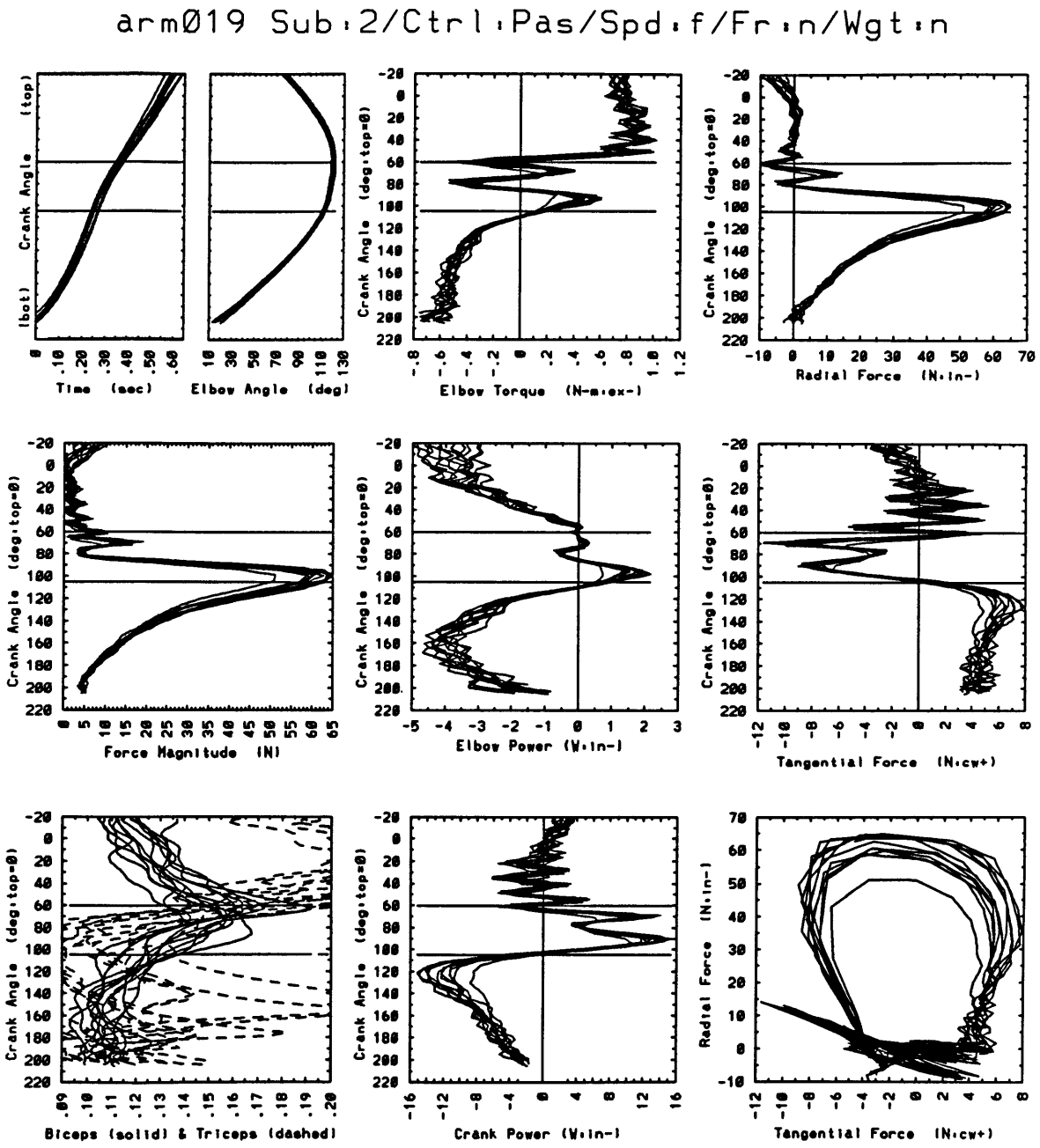
arm019 Sub:2/Ctrl:Pas/Spd:f/Fr:n/Wgt:n
Crank Angle (top) (bot)
Time (sec)
Elbow Angle (deg)
Crank Angle (deg:top=0)
Elbow Torque (N-m:ex-)
Radial Force (N:in-)
Force Magnitude (N)
Elbow Power (W:in-)
Tangential Force (N:cw+)
Biceps (solid) & Triceps (dashed)
Crank Power (W:in-)
Radial Force (N:in-)
Tangential Force (N:cw+)

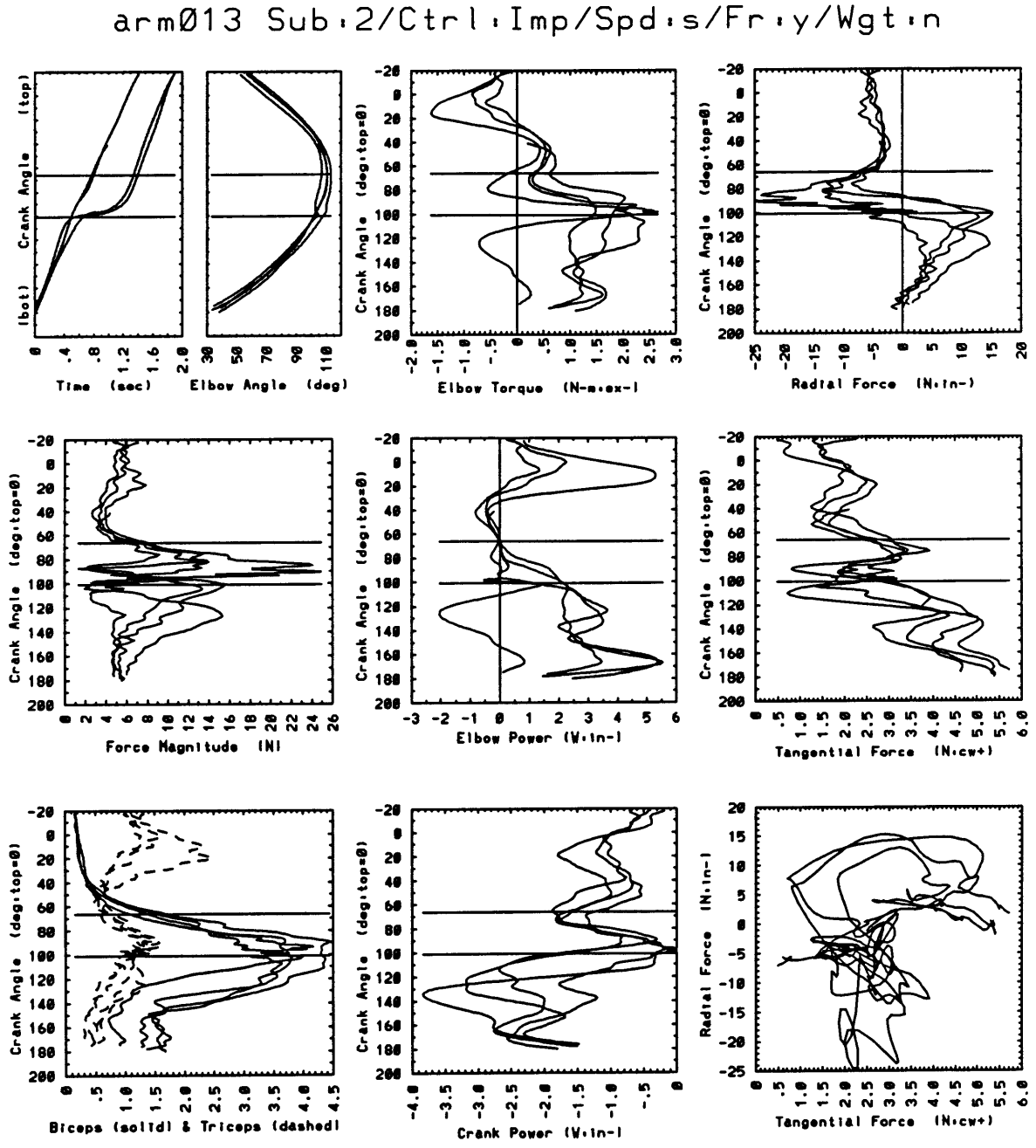
arm013 Sub:2/Ctrl:Imp/Spd:s/Fr:y/Wgt:n
Crank Angle (top)
(bot)
Time (sec)
Elbow Angle (deg)
Crank Angle (deg:top=0)
Elbow Torque (N-m:ex-)
Radial Force (N:in-)
Force Magnitude (N)
Elbow Power (W:in-)
Tangential Force (N:cw+)
Biceps (solid) & Triceps (dashed)
Crank Power (W:in-)
Radial Force (N:in-)
Tangential Force (N:cw+)

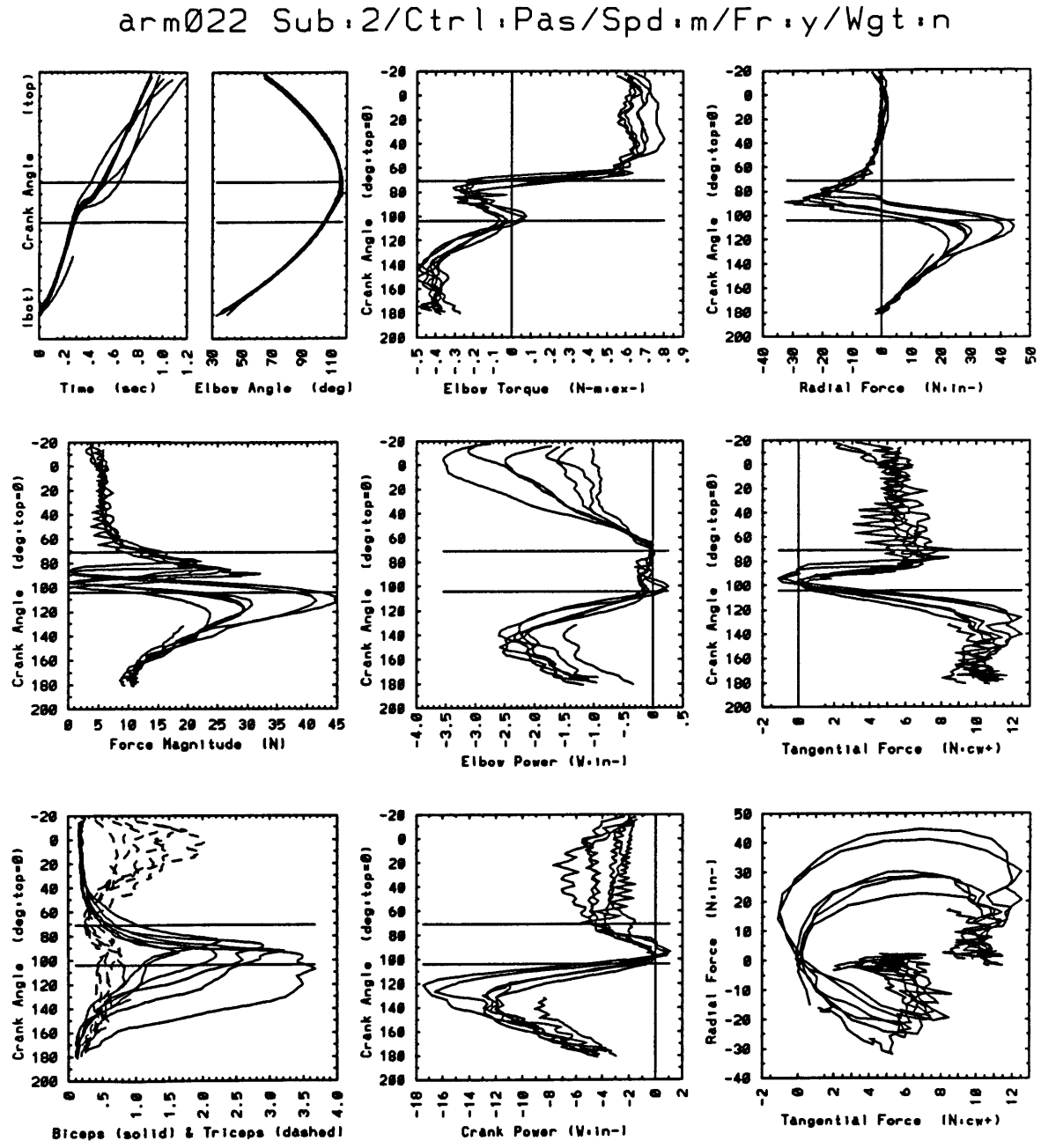
arm022 Sub:2/Ctrl:Pas/Spd:m/Fr:y/Wgt:n
Crank Angle (top)
(bot)
Time (sec)
Elbow Angle (deg)
Crank Angle (deg:top=0)
Elbow Torque (N-m:ex-)
Radial Force (N:in-)
Force Magnitude (N)
Elbow Power (W:in-)
Tangential Force (N:cw+)
Biceps (solid) & Triceps (dashed)
Crank Power (W:in-)
Radial Force (N:in-)
Tangential Force (N:cw+)

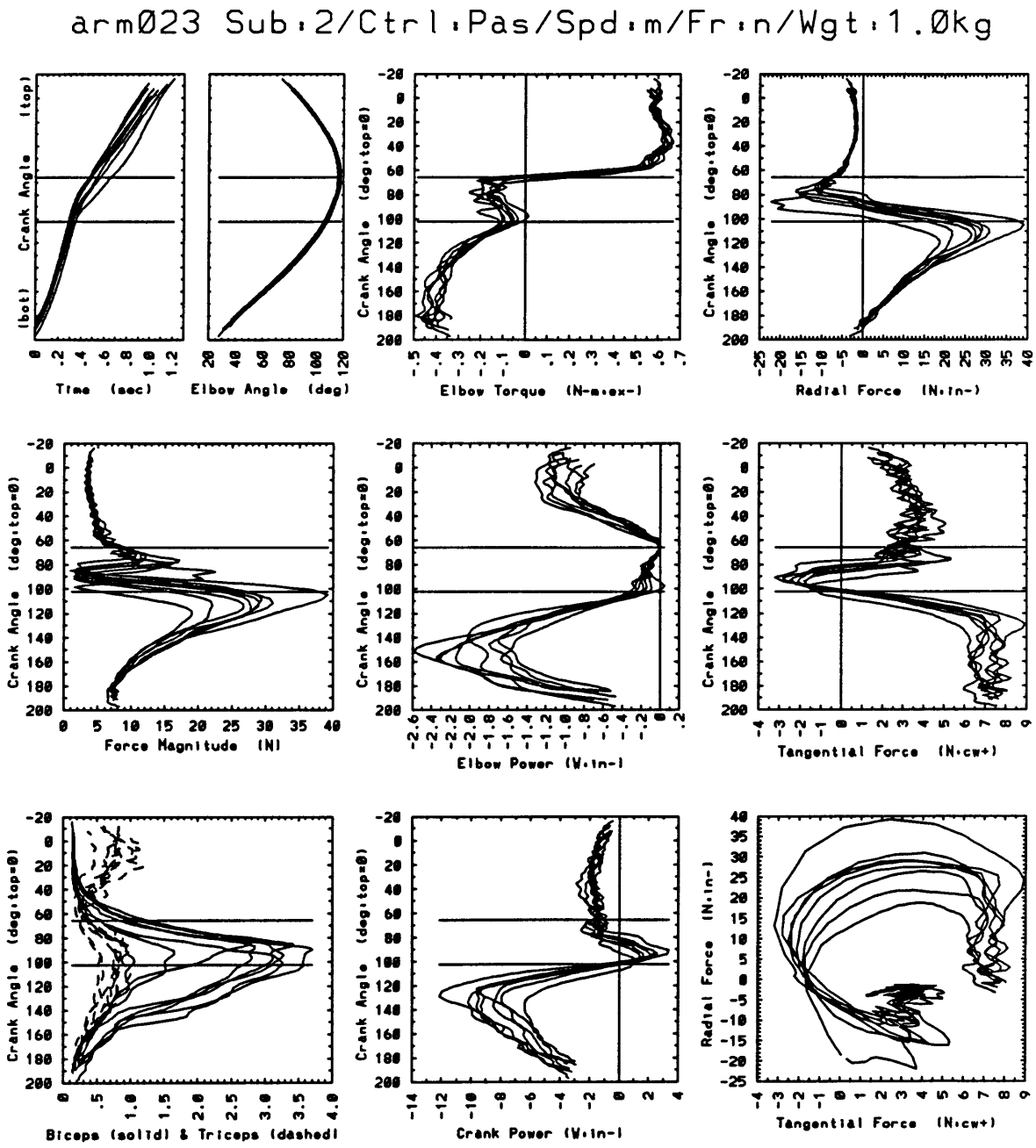
arm023 Sub:2/Ctrl:Pas/Spd:m/Fr:n/Wgt:1.0kg
Crank Angle (top)
(bot)
Time (sec)
Elbow Angle (deg)
Crank Angle (deg:top=0)
Elbow Torque (N-m:ex-)
Radial Force (N:in-)
Force Magnitude (N)
Elbow Power (W:in-)
Tangential Force (N:cw+)
Biceps (solid) & Triceps (dashed)
Crank Power (W:in-)
Radial Force (N:in-)
Tangential Force (N:cw+)

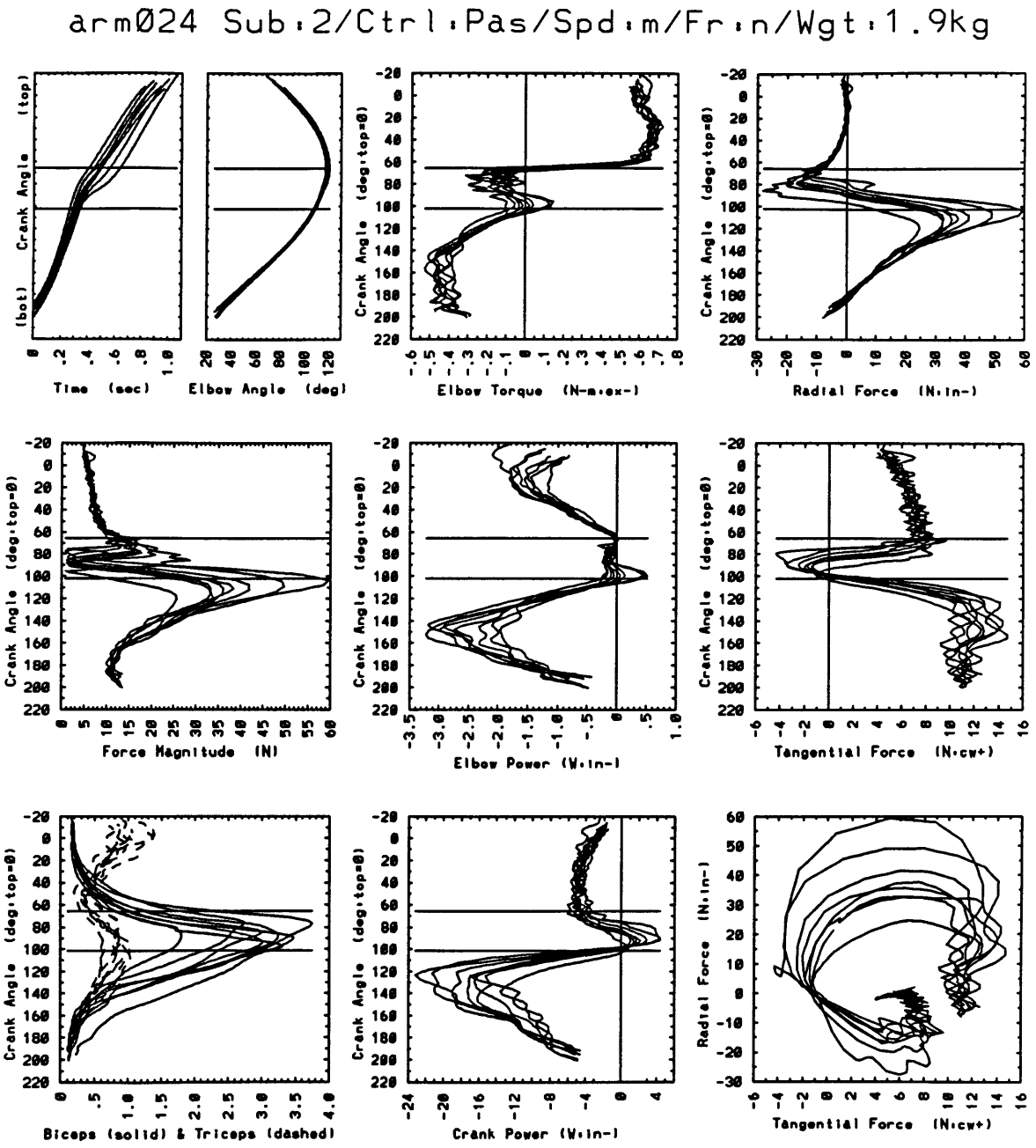
arm024 Sub:2/Ctrl:Pas/Spd:m/Fr:n/Wgt:1.9kg
Crank Angle (top) (bot)
Time (sec)
Elbow Angle (deg)
Crank Angle (deg:top=0)
Elbow Torque (N-m:ex-)
Radial Force (N:in-)
Force Magnitude (N)
Elbow Power (W:in-)
Tangential Force (N:cw+)
Biceps (solid) & Triceps (dashed)
Crank Power (W:in-)
Radial Force (N:in-)
Tangential Force (N:cw+)

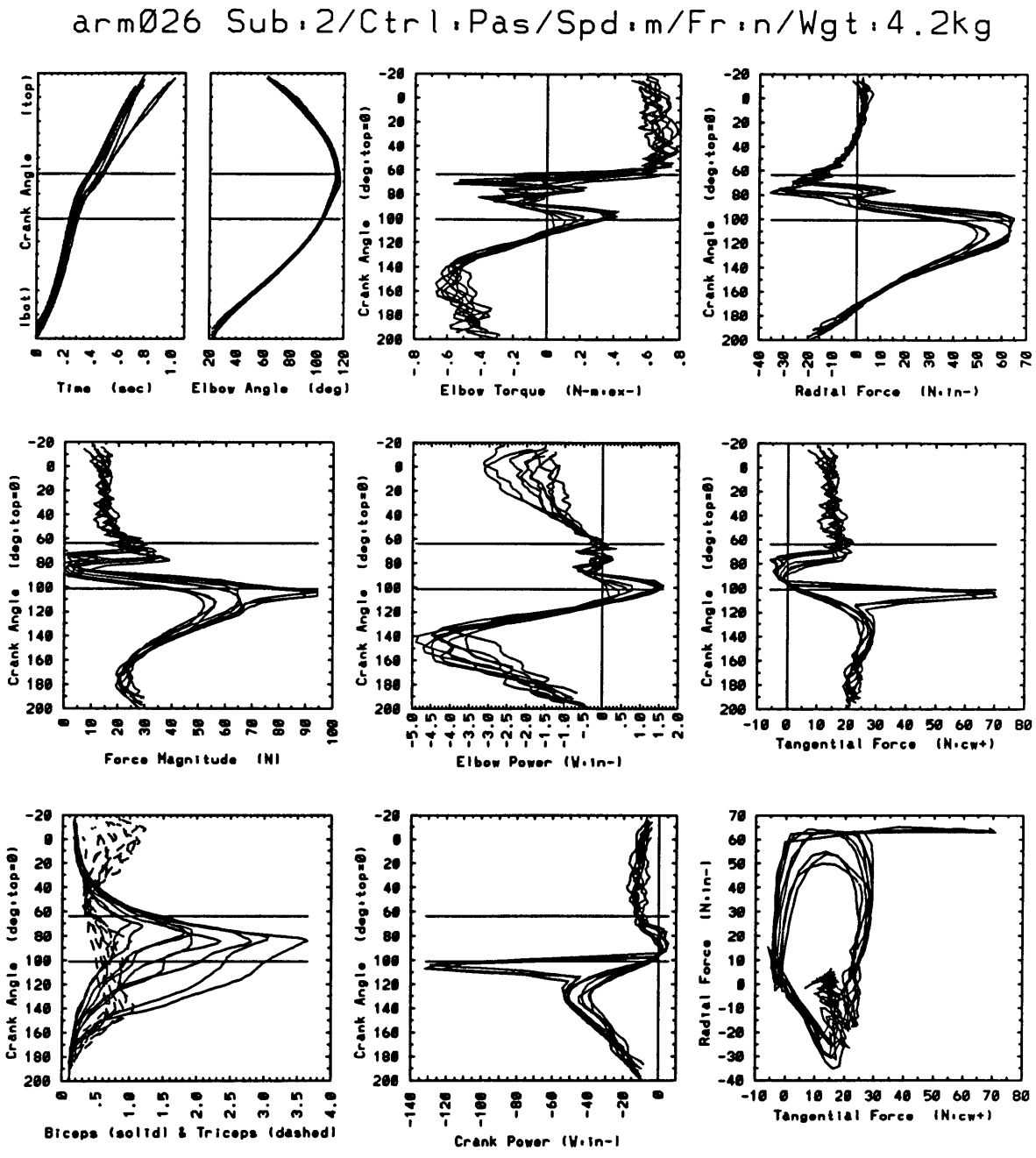
arm026 Sub:2/Ctrl:Pas/Spd:m/Fr:n/Wgt:4.2kg
Crank Angle (top) (bot)
Time (sec)
Elbow Angle (deg)
Crank Angle (deg:top=0)
Elbow Torque (N-m:ex-)
Radial Force (N:in-)
Force Magnitude (N)
Elbow Power (W:in-)
Tangential Force (N:cw+)
Biceps (solid) & Triceps (dashed)
Crank Power (W:in-)
Radial Force (N:in-)

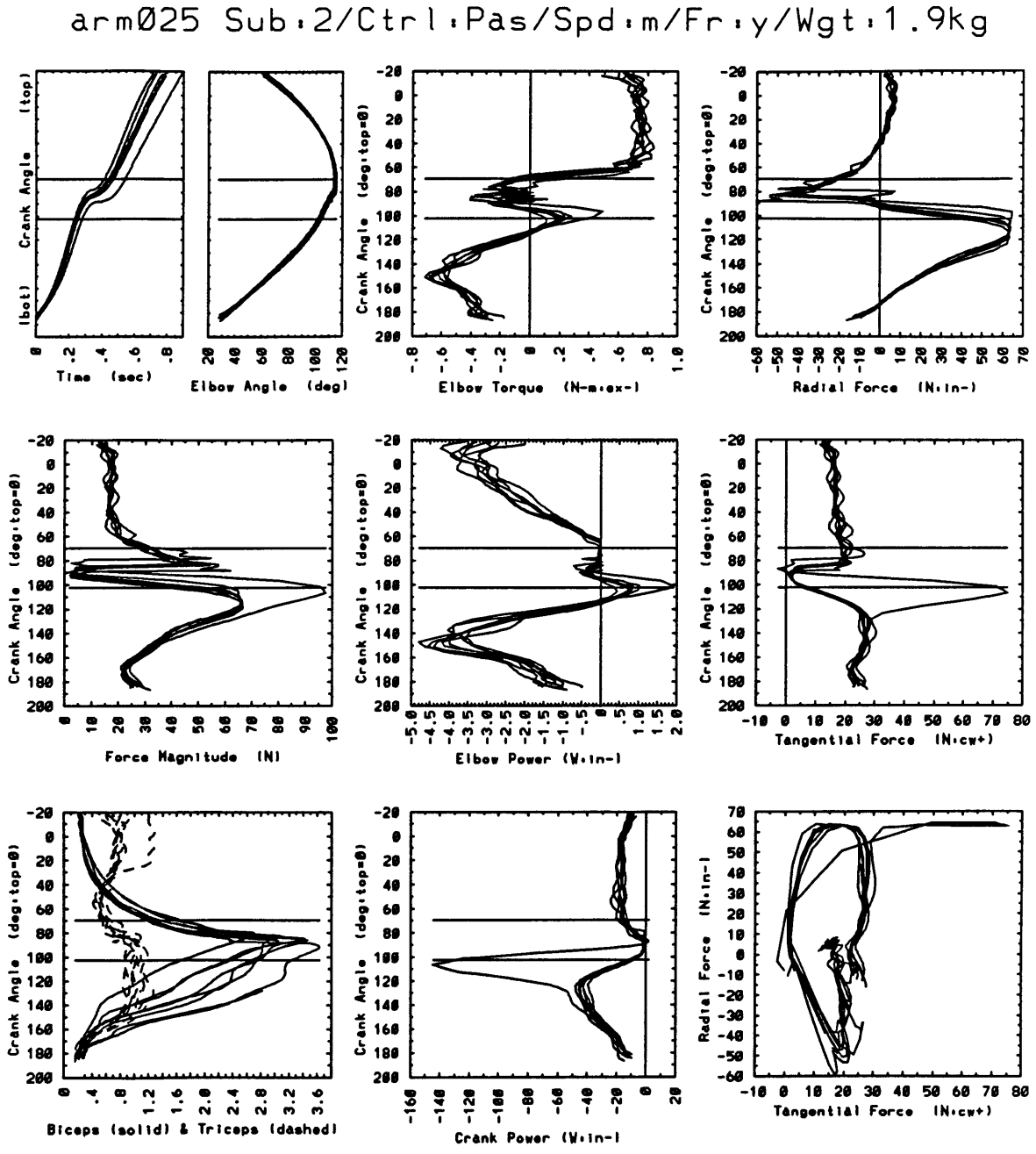
arm025 Sub:2/Ctrl:Pas/Spd:m/Fr:y/Wgt:1.9kg
Crank Angle (top) (bot)
Time (sec)
Elbow Angle (deg)
Crank Angle (deg:top=0)
Elbow Torque (N-m:ex-)
Radial Force (N:in-)
Force Magnitude (N)
Elbow Power (W:in-)
Tangential Force (N:cw+)
Biceps (solid) & Triceps (dashed)
Crank Power (W:in-)

SUBJECT 3

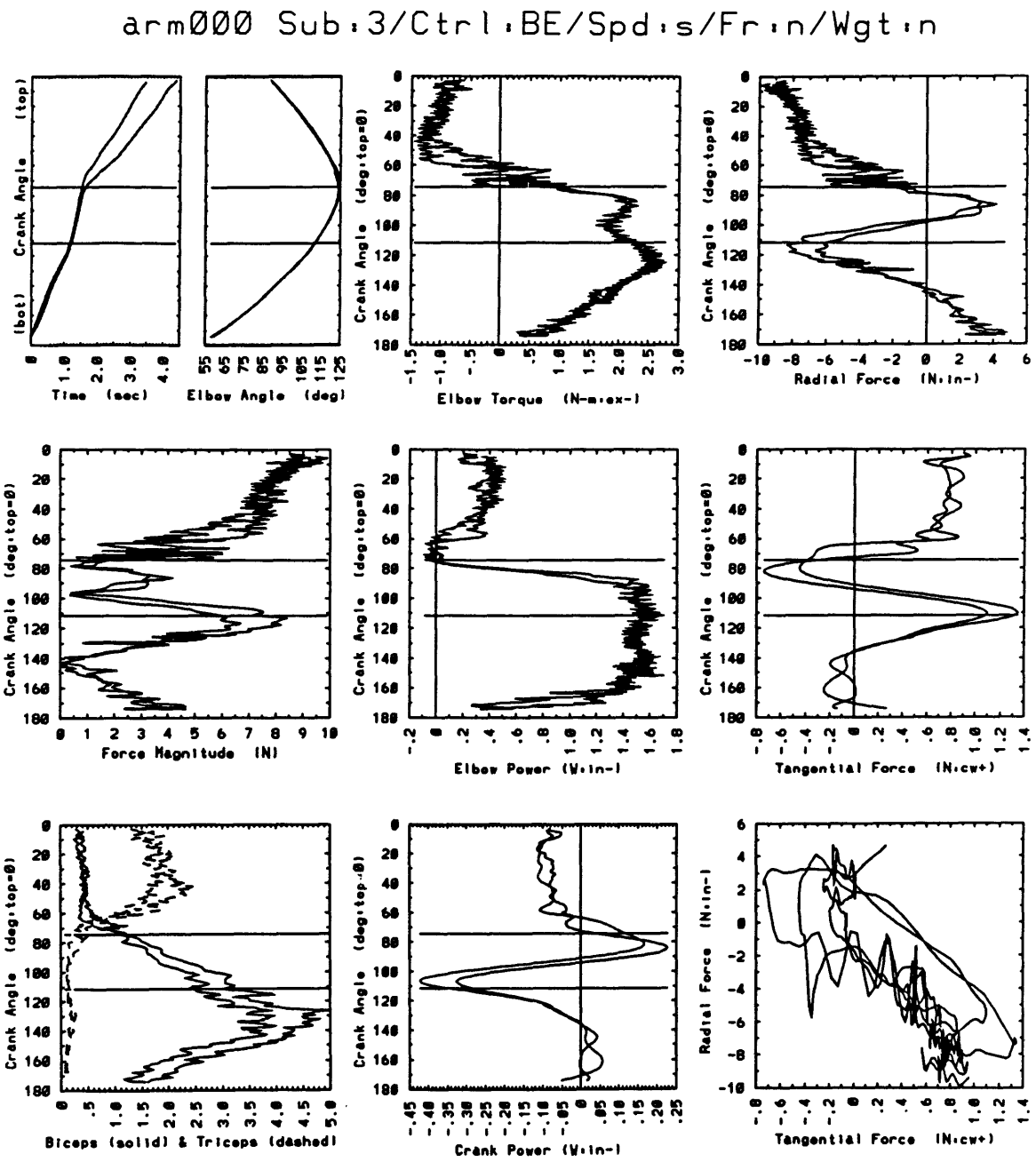
arm000 Sub:3/Ctrl:BE/Spd:s/Fr:n/Wgt:n
Crank Angle (top) (bot)
Time (sec)
Elbow Angle (deg)
Crank Angle (deg:top=0)
Elbow Torque (N-m:ex-)
Radial Force (N:in-)
Force Magnitude (N)
Elbow Power (W:in-)
Tangential Force (N:cw+)
Biceps (solid) & Triceps (dashed)
Crank Power (W:in-)
Radial Force (N:in-)
Tangential Force (N:cw+)

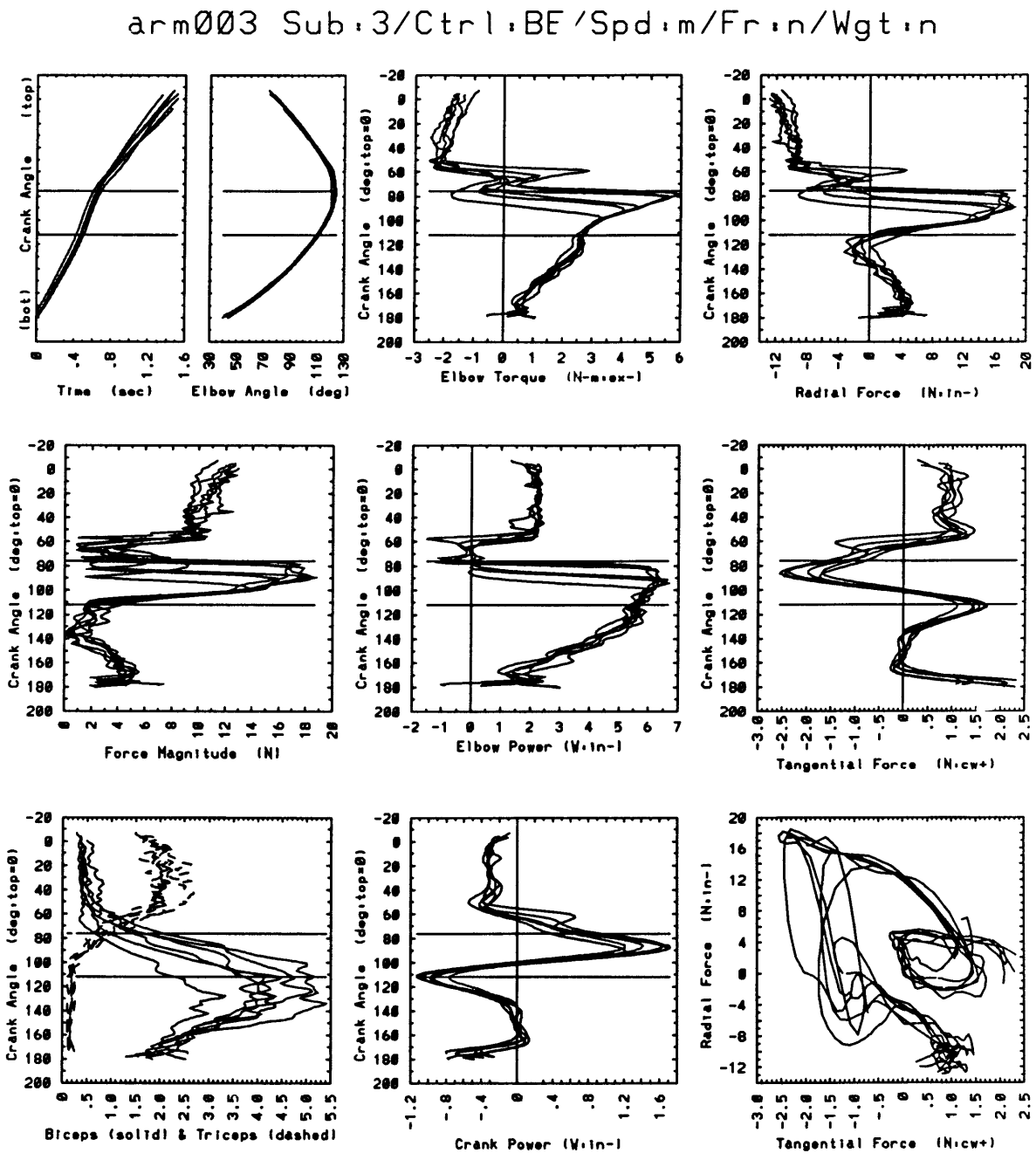
arm003 Sub:3/Ctrl:BF/Spd:m/Fr:n/Wgt:n
Crank Angle (top)
(bot)
Time (sec)
Elbow Angle (deg)
Crank Angle (deg:top=0)
Elbow Torque (N-m:ex-)
Radial Force (N:in-)
Force Magnitude (N)
Elbow Power (W:in-)
Tangential Force (N:cw+)
Biceps (solid) & Triceps (dashed)
Crank Power (W:in-)

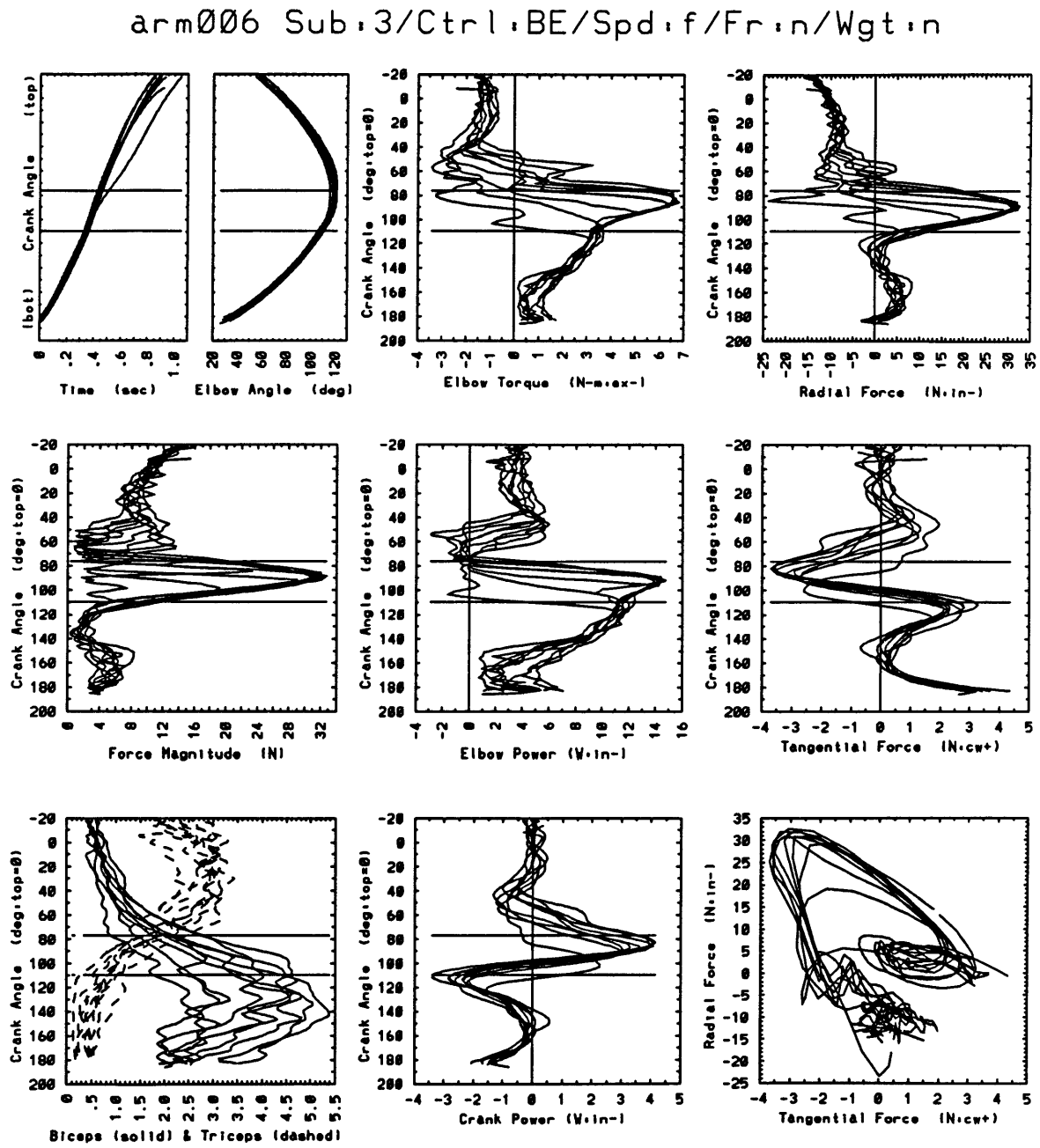
arm00 Sub:3/Ctrl:BE/Spd:f/Fr:n/Wgt:n
Crank Angle (top)
(bot)
Time (sec)
Elbow Angle (deg)
Crank Angle (deg:top=0)
Elbow Torque (N-m:ex-)
Radial Force (N:in-)
Force Magnitude (N)
Elbow Power (W:in-)
Tangential Force (N:cw+)
Biceps (solid) & Triceps (dashed)
Crank Power (W:in-)

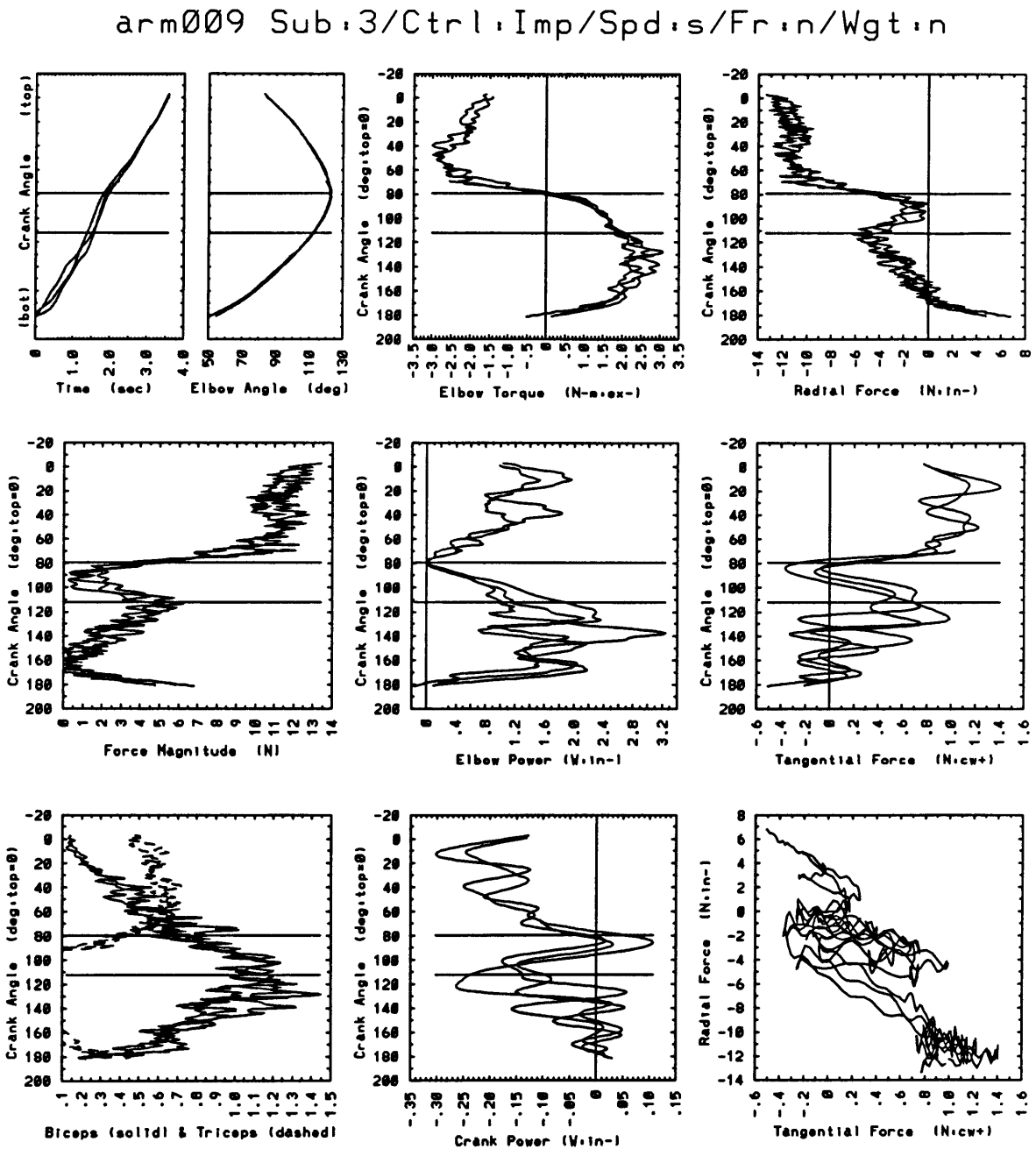
arm009 Sub:3/Ctrl:Imp/Spd:s/Fr:n/Wgt:n
Crank Angle (top)
(bot)
Time (sec)
Elbow Angle (deg)
Crank Angle (deg:top=0)
Elbow Torque (N-m:ex-)
Radial Force (N:in-)
Force Magnitude (N)
Elbow Power (W:in-)
Tangential Force (N:cw+)
Biceps (solid) & Triceps (dashed)
Crank Power (W:in-)

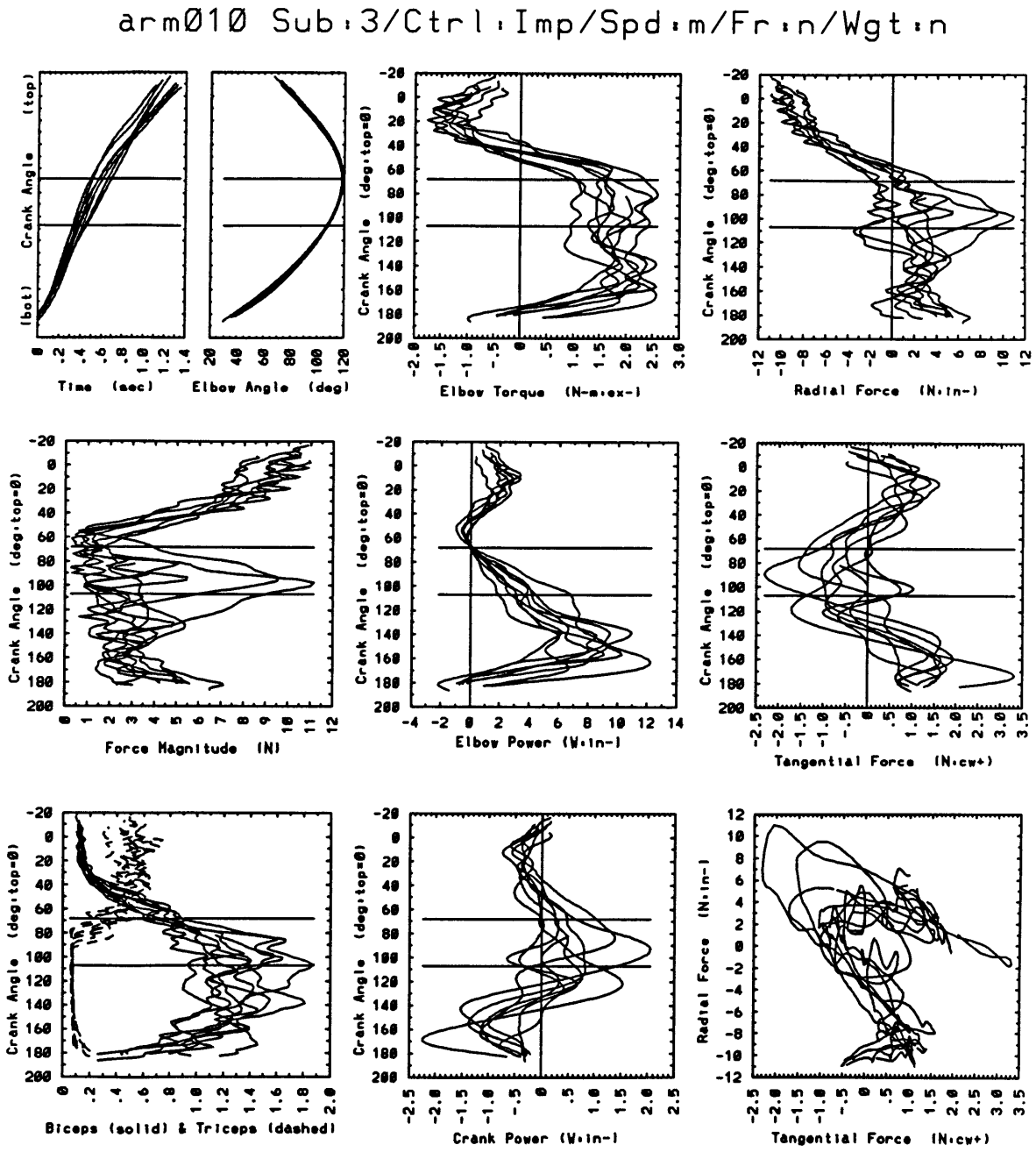
arm010 Sub:3/Ctrl:Imp/Spd:m/Fr:n/Wgt:n
Crank Angle (top) (bot)
Time (sec)
Elbow Angle (deg)
Crank Angle (deg:top=0)
Elbow Torque (N-m:ex-)
Radial Force (N:in-)
Force Magnitude (N)
Elbow Power (W:in-)
Tangential Force (N:cw+)
Biceps (solid) & Triceps (dashed)
Crank Power (W:in-)
Radial Force (N:in-)
Tangential Force (N:cw+)

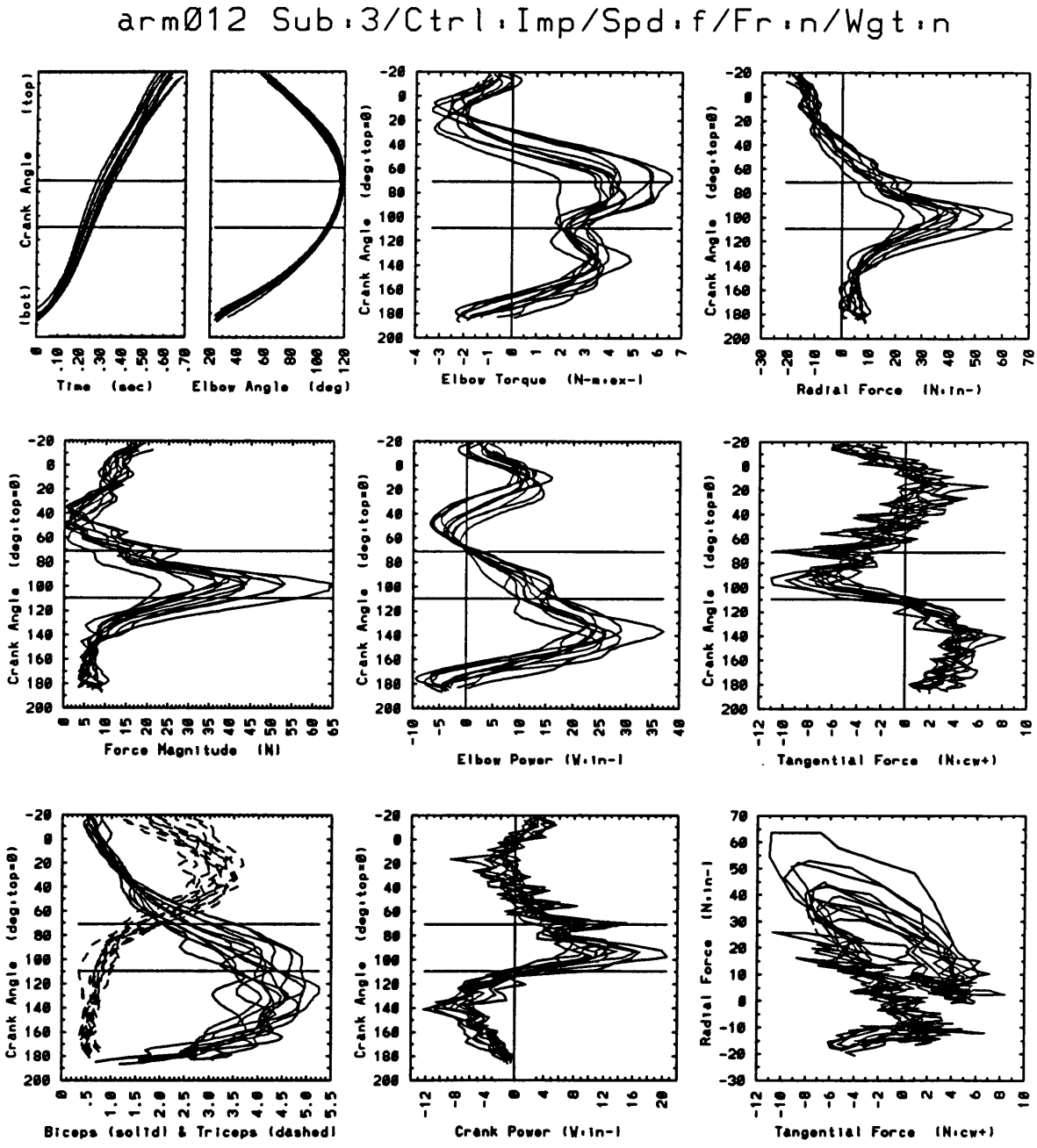
arm012 Sub:3/Ctrl:Imp/Spd:f/Fr:n/Wgt:n
Crank Angle (top)
(bot)
Time (sec)
Elbow Angle (deg)
Crank Angle (deg:top=0)
Elbow Torque (N-m:ex-)
Radial Force (N:in-)
Force Magnitude (N)
Elbow Power (W:in-)
Tangential Force (N:cw+)
Biceps (solid) & Triceps (dashed)
Crank Power (W:in-)

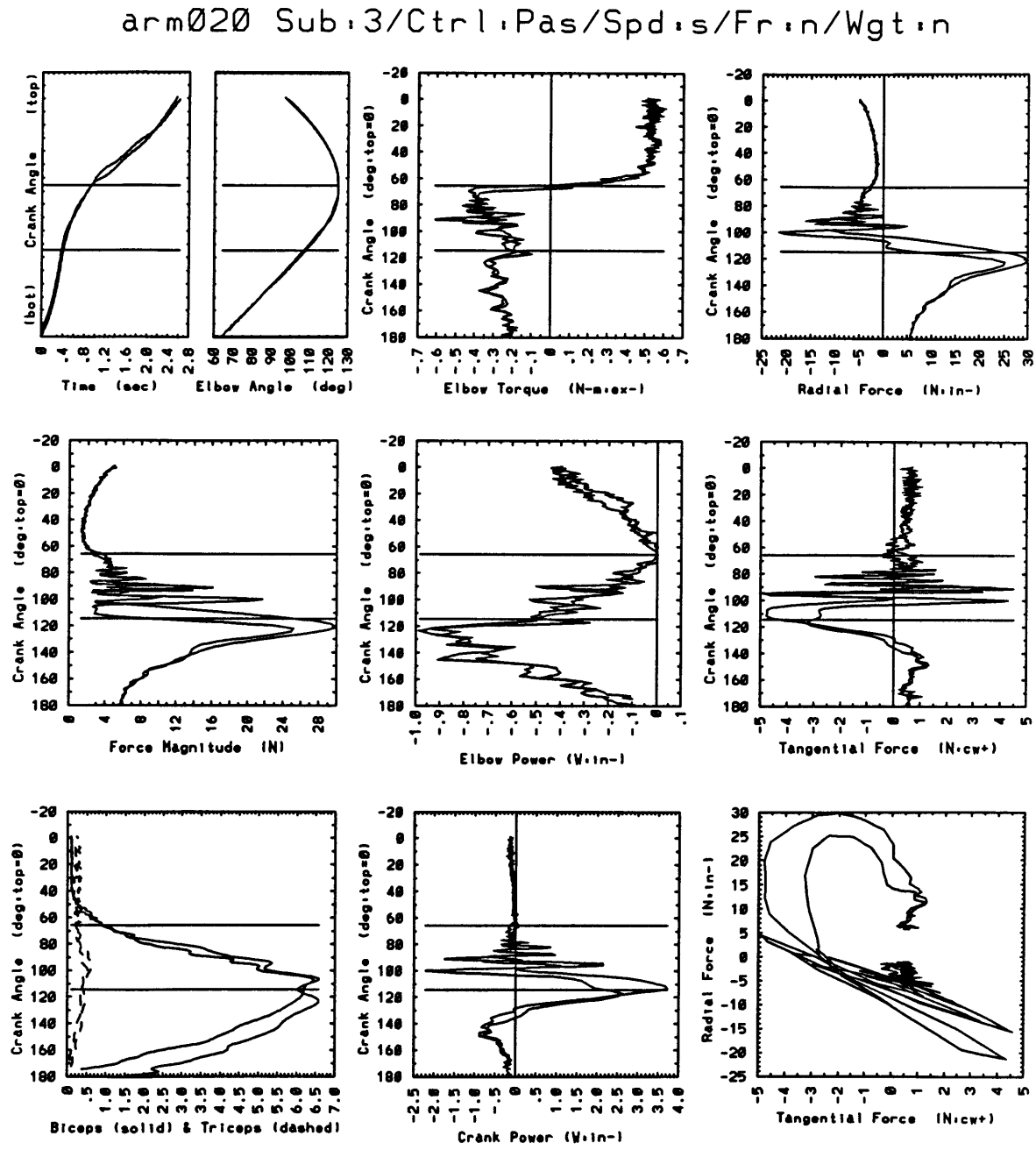
arm020 Sub:3/Ctrl:Pas/Spd:s/Fr:n/Wgt:n
Crank Angle (top) (bot)
Time (sec)
Elbow Angle (deg)
Crank Angle (deg:top=0)
Elbow Torque (N-m:ex-)
Radial Force (N:in-)
Force Magnitude (N)
Elbow Power (W:in-)
Tangential Force (N:cw+)
Biceps (solid) & Triceps (dashed)
Crank Power (W:in-)
Radial Force (N:in-)
Tangential Force (N:cw+)

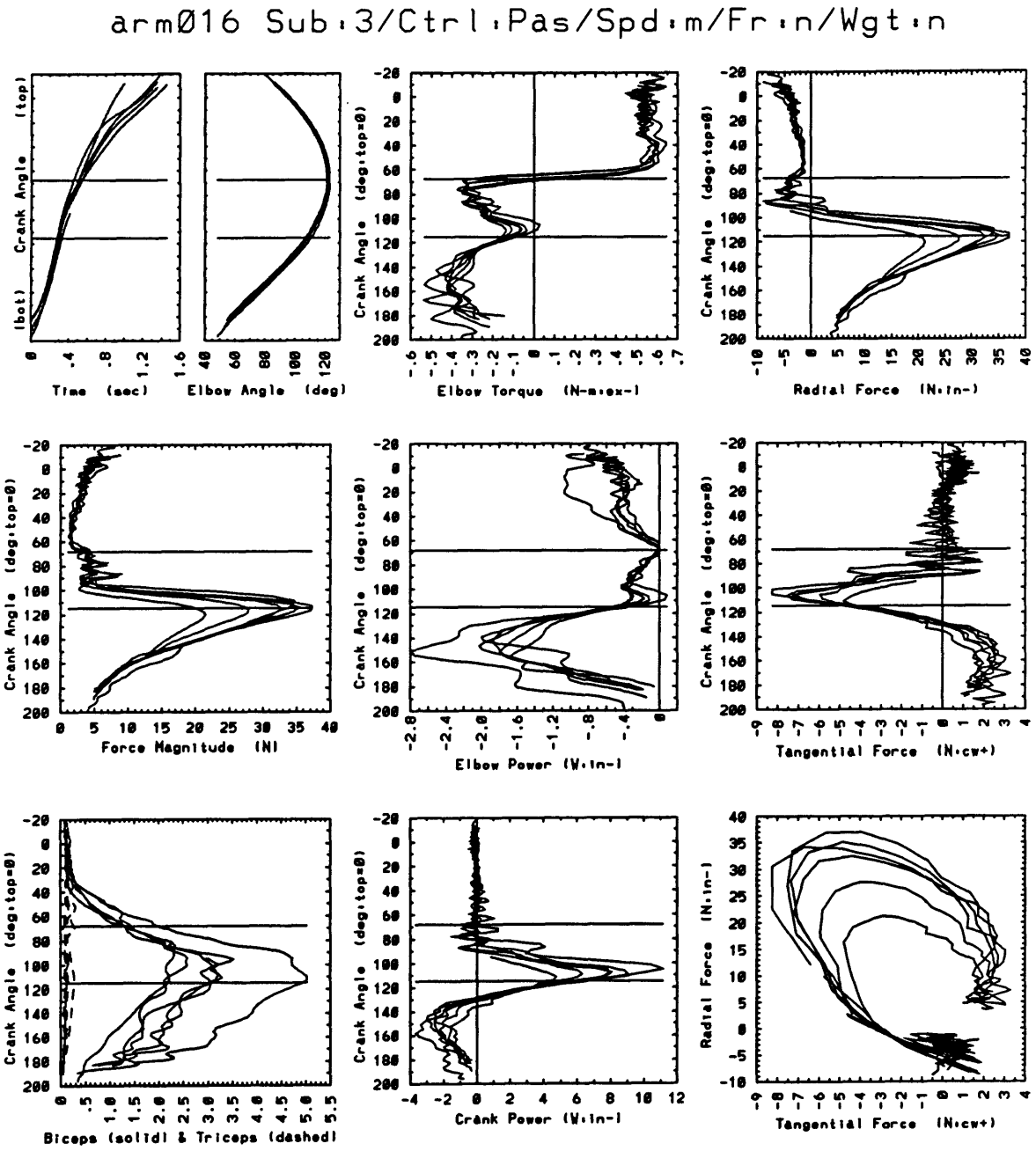
arm016 Sub:3/Ctrl:Pas/Spd:m/Fr:n/Wgt:n
Crank Angle (top) (bot)
Time (sec)
Elbow Angle (deg)
Crank Angle (deg:top=0)
Elbow Torque (N-m:ex-)
Radial Force (N:in-)
Force Magnitude (N)
Elbow Power (W:in-)
Tangential Force (N:cw+)
Biceps (solid) & Triceps (dashed)
Crank Power (W:in-)

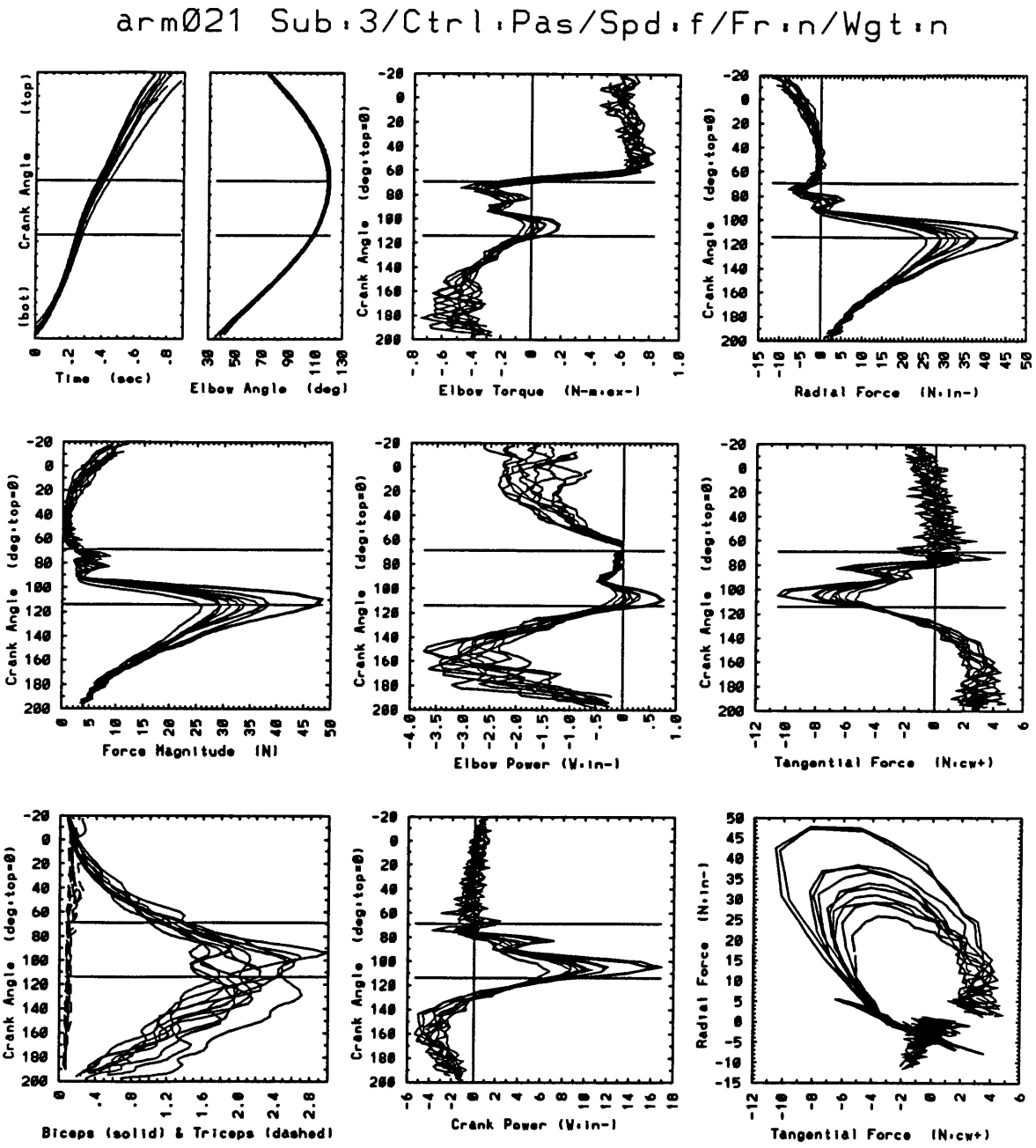
arm021 Sub:3/Ctrl:Pas/Spd:f/Fr:n/Wgt:n
Crank Angle (top) (bot)
Time (sec)
Elbow Angle (deg)
Crank Angle (deg:top=0)
Elbow Torque (N-m:ex-)
Radial Force (N:in-)
Force Magnitude (N)
Elbow Power (W:in-)
Tangential Force (N:cw+)
Biceps (solid) & Triceps (dashed)
Crank Power (W:in-)

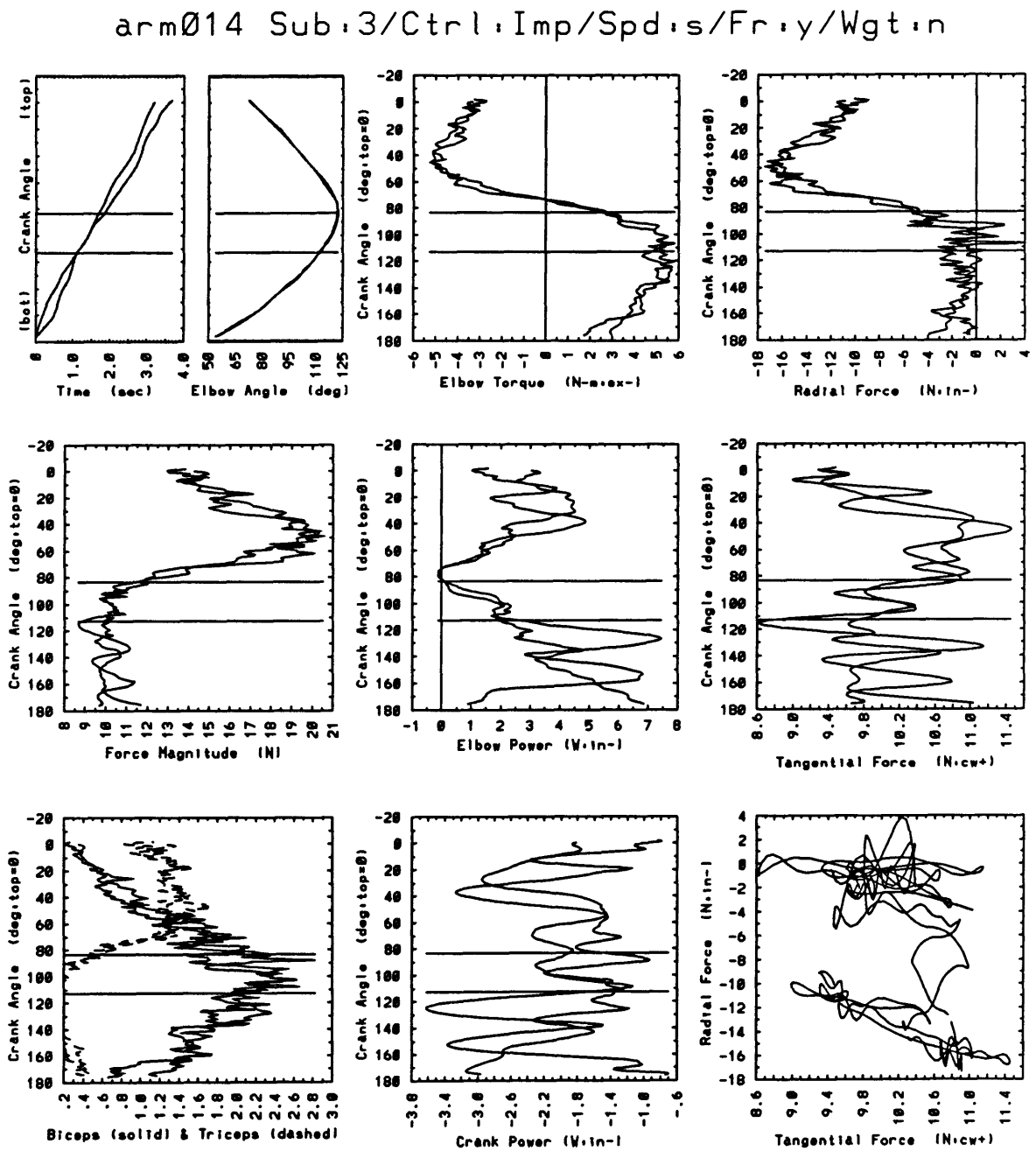
arm014 Sub:3/Ctrl:Imp/Spd:s/Fr:y/Wgt:n
Crank Angle (top)
(bot)
Time (sec)
Elbow Angle (deg)
Crank Angle (deg:top=0)
Elbow Torque (N-m:ex-)
Radial Force (N:in-)
Force Magnitude (N)
Elbow Power (W:in-)
Tangential Force (N:cw+)
Biceps (solid) & Triceps (dashed)
Crank Power (W:in-)

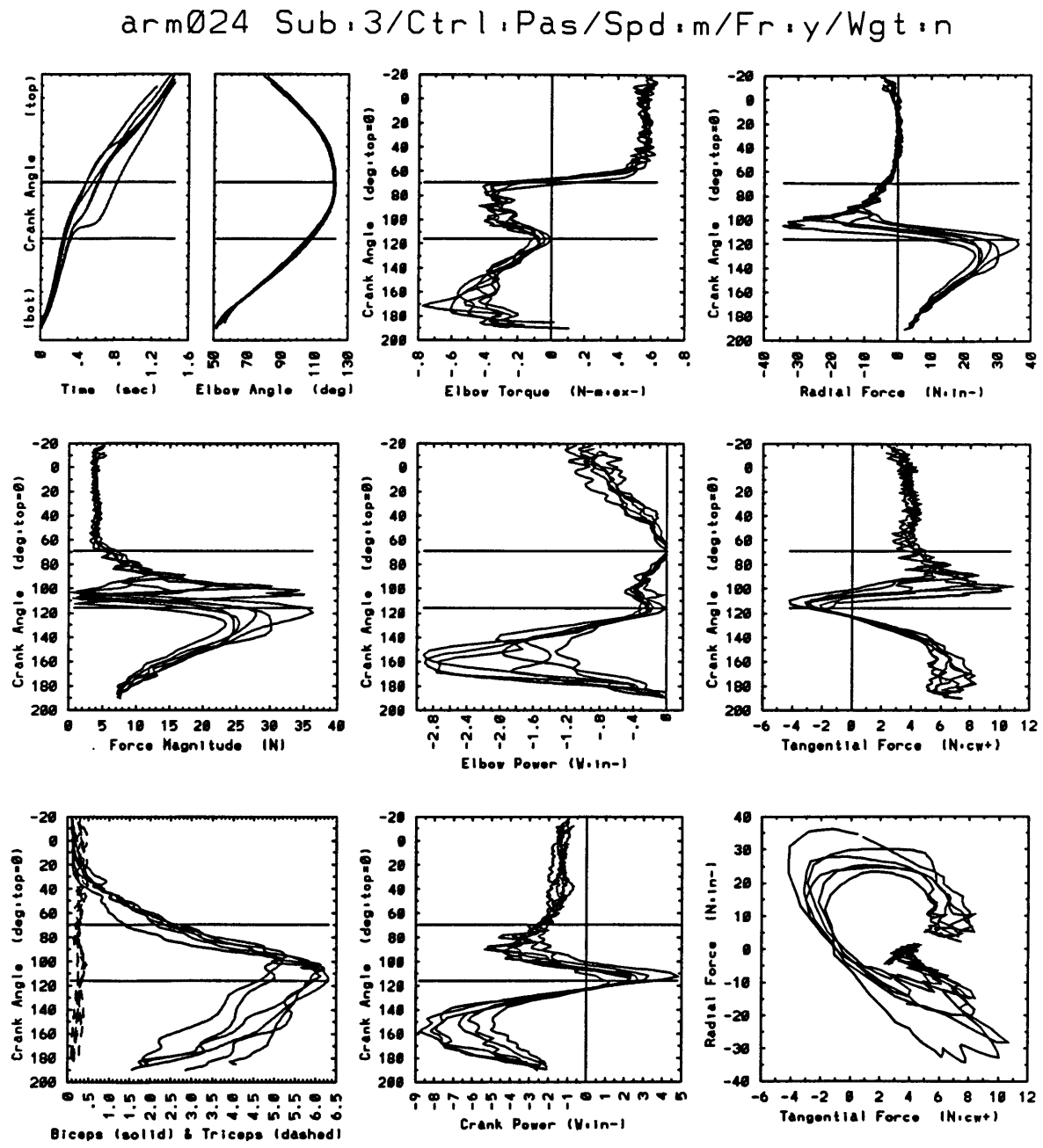
arm024 Sub:3/Ctrl:Pas/Spd:m/Fr:y/Wgt:n
Crank Angle (top)
(bot)
Time (sec)
Elbow Angle (deg)
Crank Angle (deg:top=0)
Elbow Torque (N-m:ex-)
Radial Force (N:in-)
Force Magnitude (N)
Elbow Power (W:in-)
Tangential Force (N:cw+)
Biceps (solid) & Triceps (dashed)
Crank Power (W:in-)

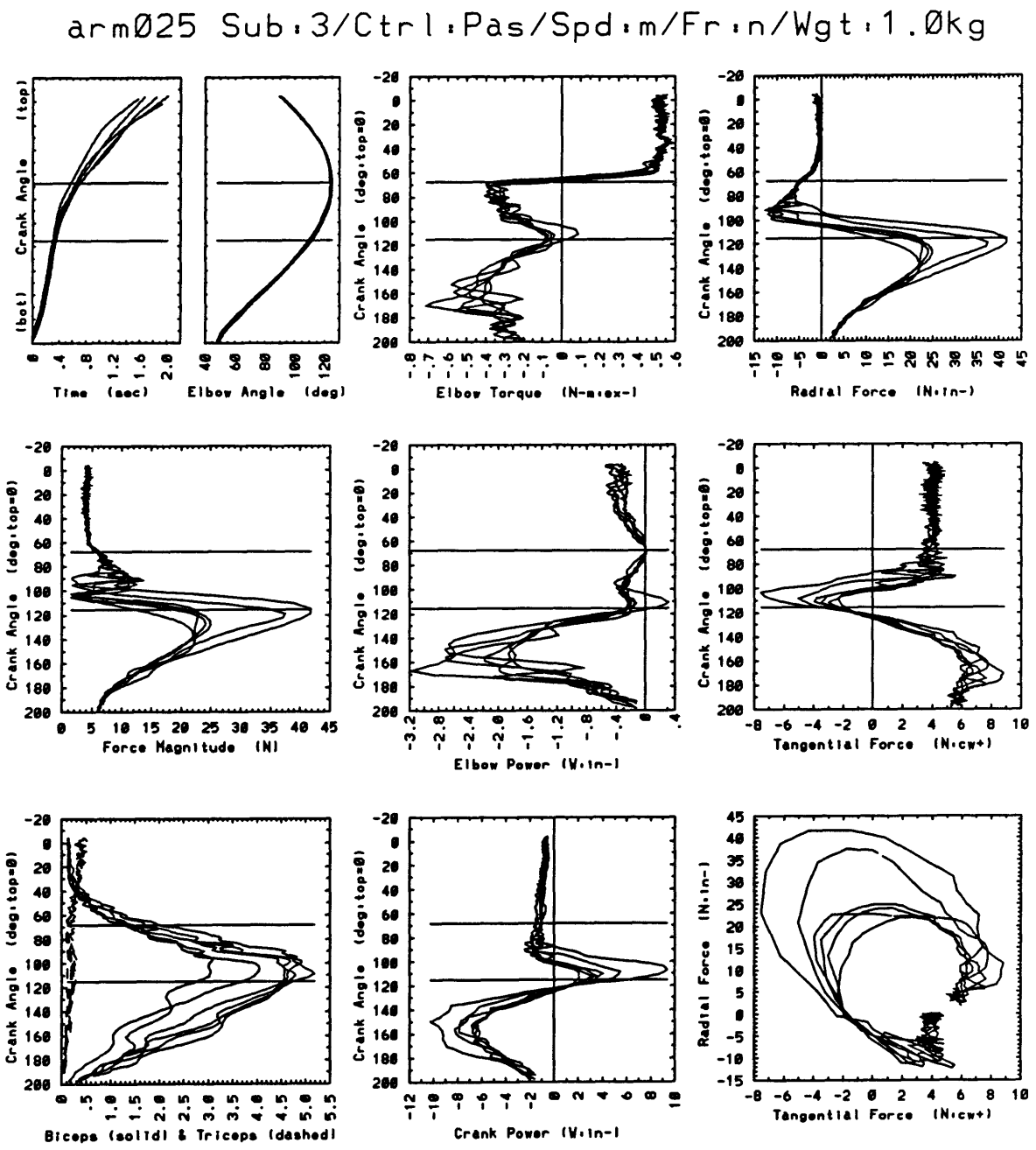
arm025 Sub:3/Ctrl:Pas/Spd:m/Fr:n/Wgt:1.0kg
Crank Angle (top) (bot)
Time (sec)
Elbow Angle (deg)
Crank Angle (deg:top=0)
Elbow Torque (N-m:ex-)
Radial Force (N:in-)
Force Magnitude (N)
Elbow Power (W:in-)
Tangential Force (N:cw+)
Biceps (solid) & Triceps (dashed)
Crank Power (W:in-)
Radial Force (N:in-)
Tangential Force (N:cw+)

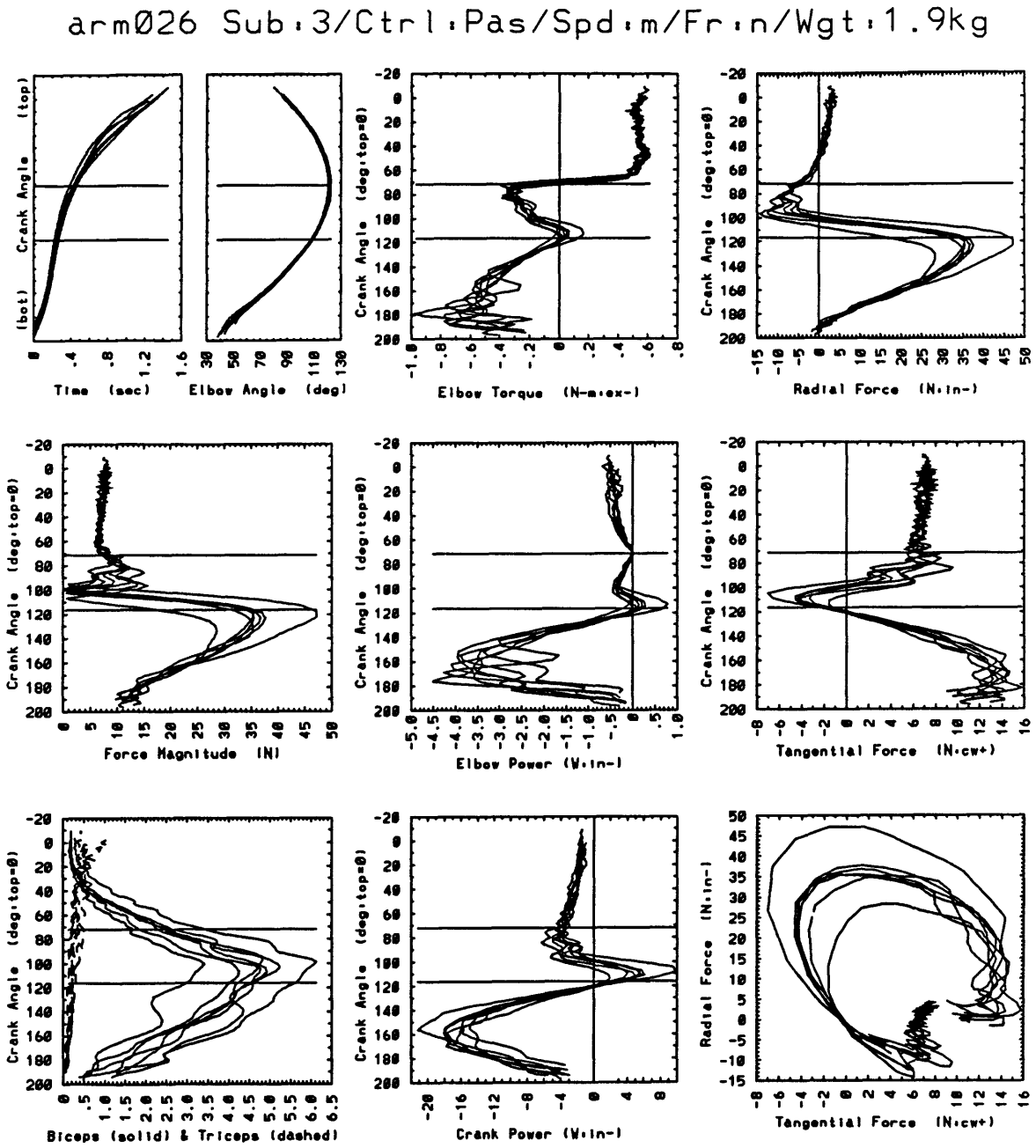
arm026 Sub:3/Ctrl:Pas/Spd:m/Fr:n/Wgt:1.9kg
Crank Angle (top) (bot)
Time (sec)
Elbow Angle (deg)
Crank Angle (deg:top=0)
Elbow Torque (N-m:ex-)
Radial Force (N:in-)
Force Magnitude (N)
Elbow Power (W:in-)
Tangential Force (N:cw+)
Biceps (solid) & Triceps (dashed)
Crank Power (W:in-)
Radial Force (N:in-)
Tangential Force (N:cw+)

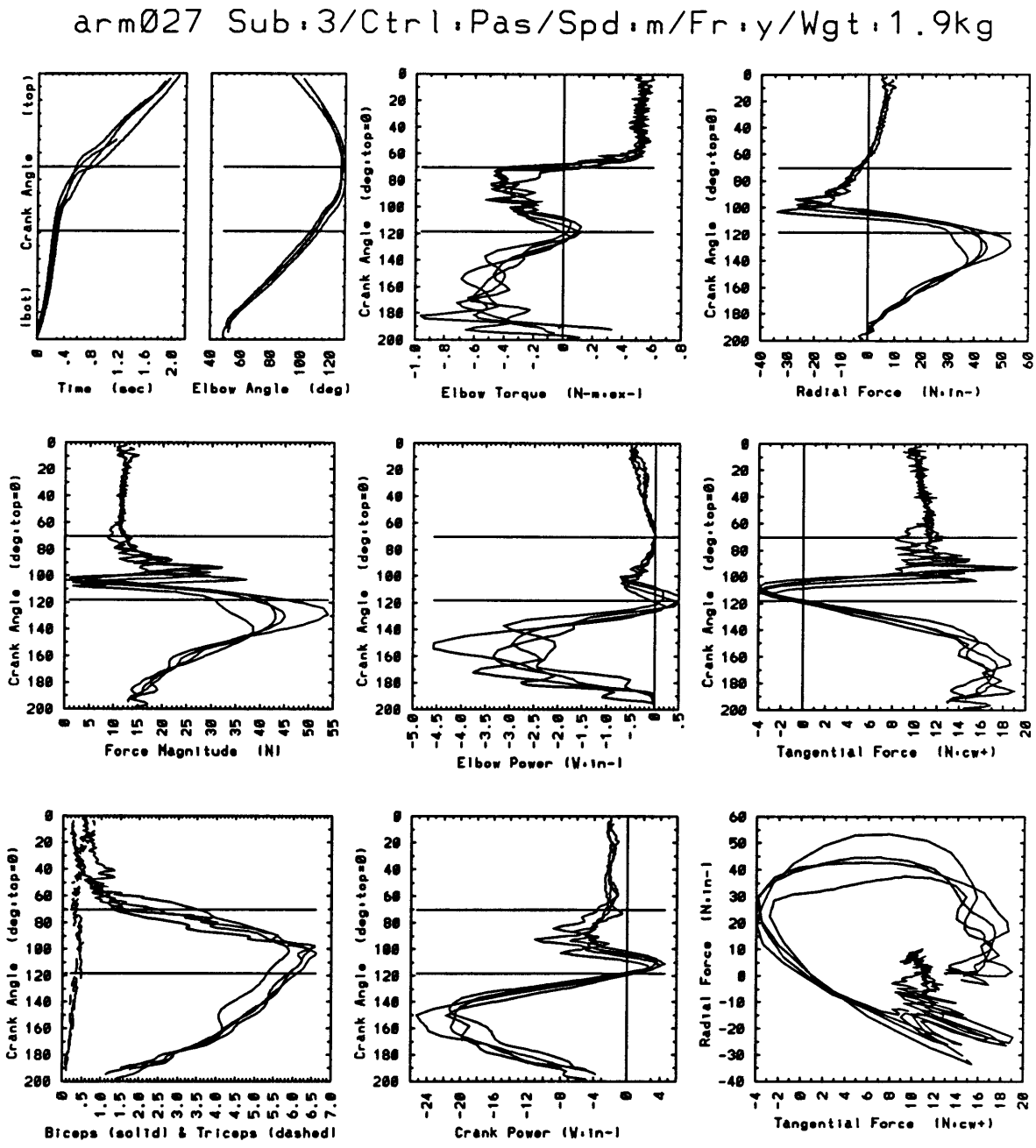
arm027 Sub:3/Ctrl:Pas/Spd:m/Fr:y/Wgt:1.9kg
Crank Angle (top)
(bot)
Time (sec)
Elbow Angle (deg)
Crank Angle (deg:top=0)
Elbow Torque (N-m:ex-)
Radial Force (N:in-)
Force Magnitude (N)
Elbow Power (W:in-)
Tangential Force (N:cw+)
Biceps (solid) & Triceps (dashed)
Crank Power (W:in-)
Radial Force (N:in-)

SUBJECT 4

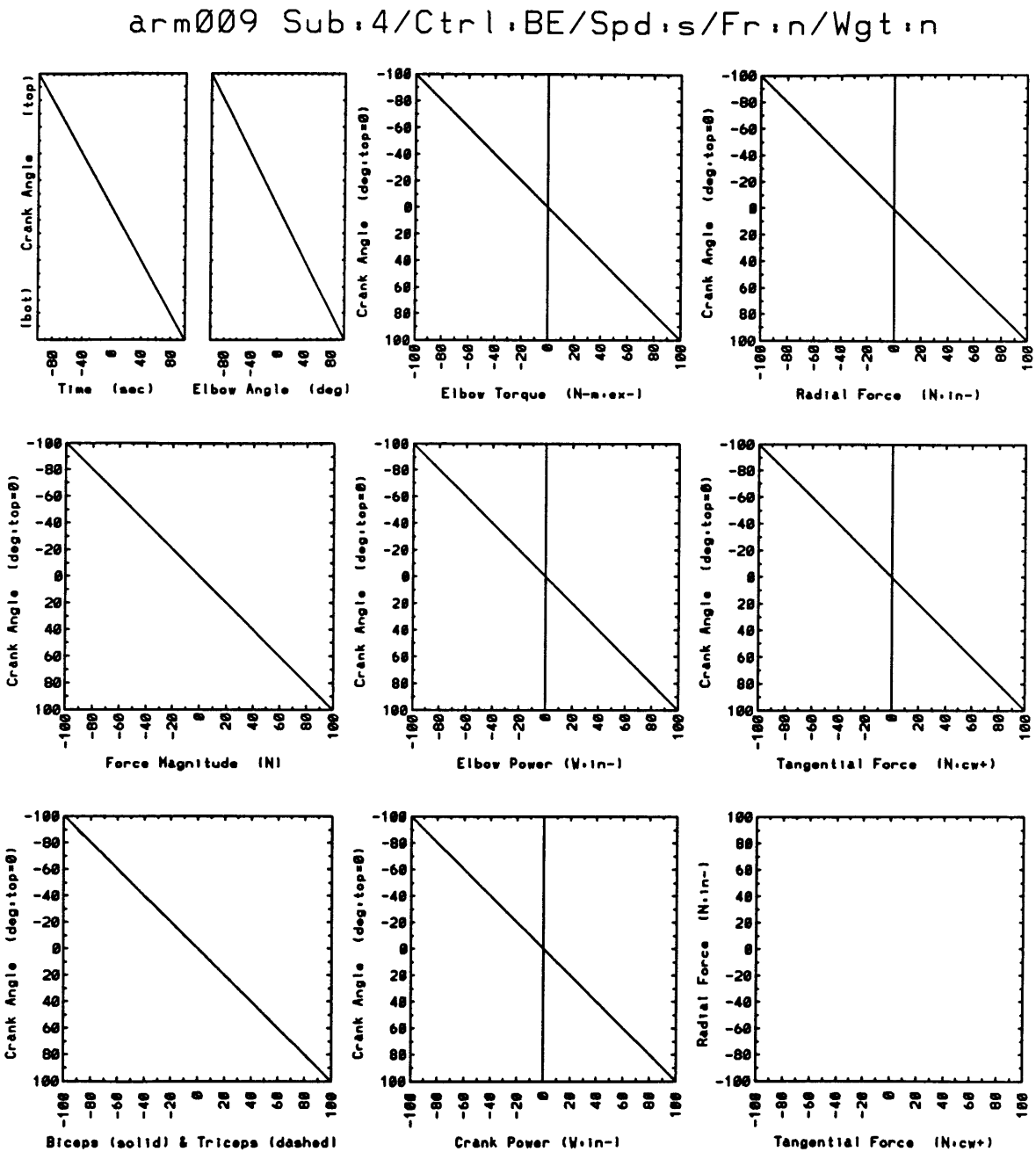
arm009 Sub:4/Ctrl:BE/Spd:s/Fr:n/Wgt:n
Crank Angle (top)
(bot)
Time (sec)
Elbow Angle (deg)
Crank Angle (deg:top=0)
Elbow Torque (N-m:ex-)
Radial Force (N:in-)
Force Magnitude (N)
Elbow Power (W:in-)
Tangential Force (N:cw+)
Biceps (solid) & Triceps (dashed)
Crank Power (W:in-)

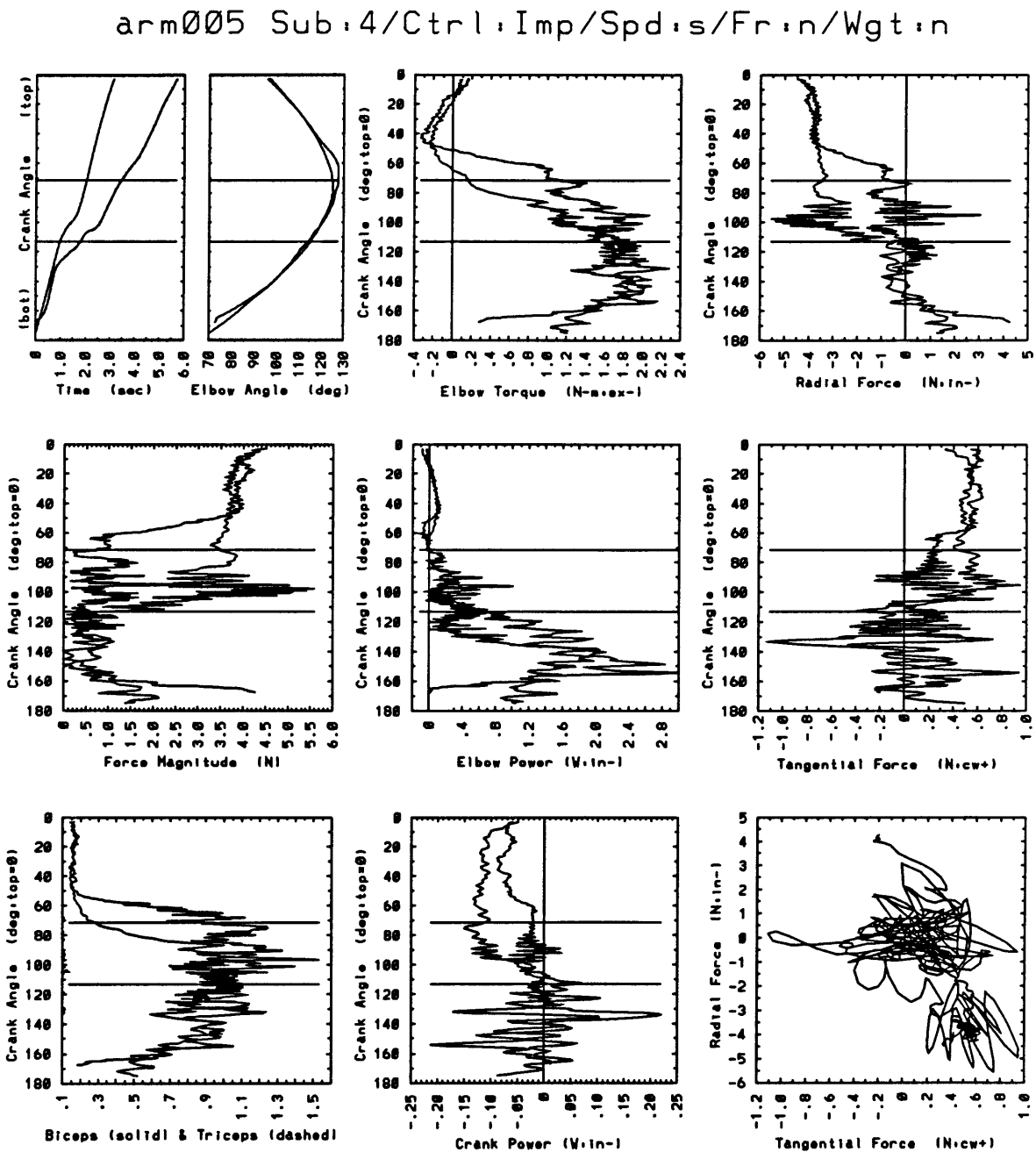
arm005 Sub:4/Ctrl:Imp/Spd:s/Fr:n/Wgt:n
Crank Angle (top)
(bot)
Time (sec)
Elbow Angle (deg)
Crank Angle (deg:top=0)
Elbow Torque (N-m:ex-)
Radial Force (N:in-)
Force Magnitude (N)
Elbow Power (W:in-)
Tangential Force (N:cw+)
Biceps (solid) & Triceps (dashed)
Crank Power (W:in-)

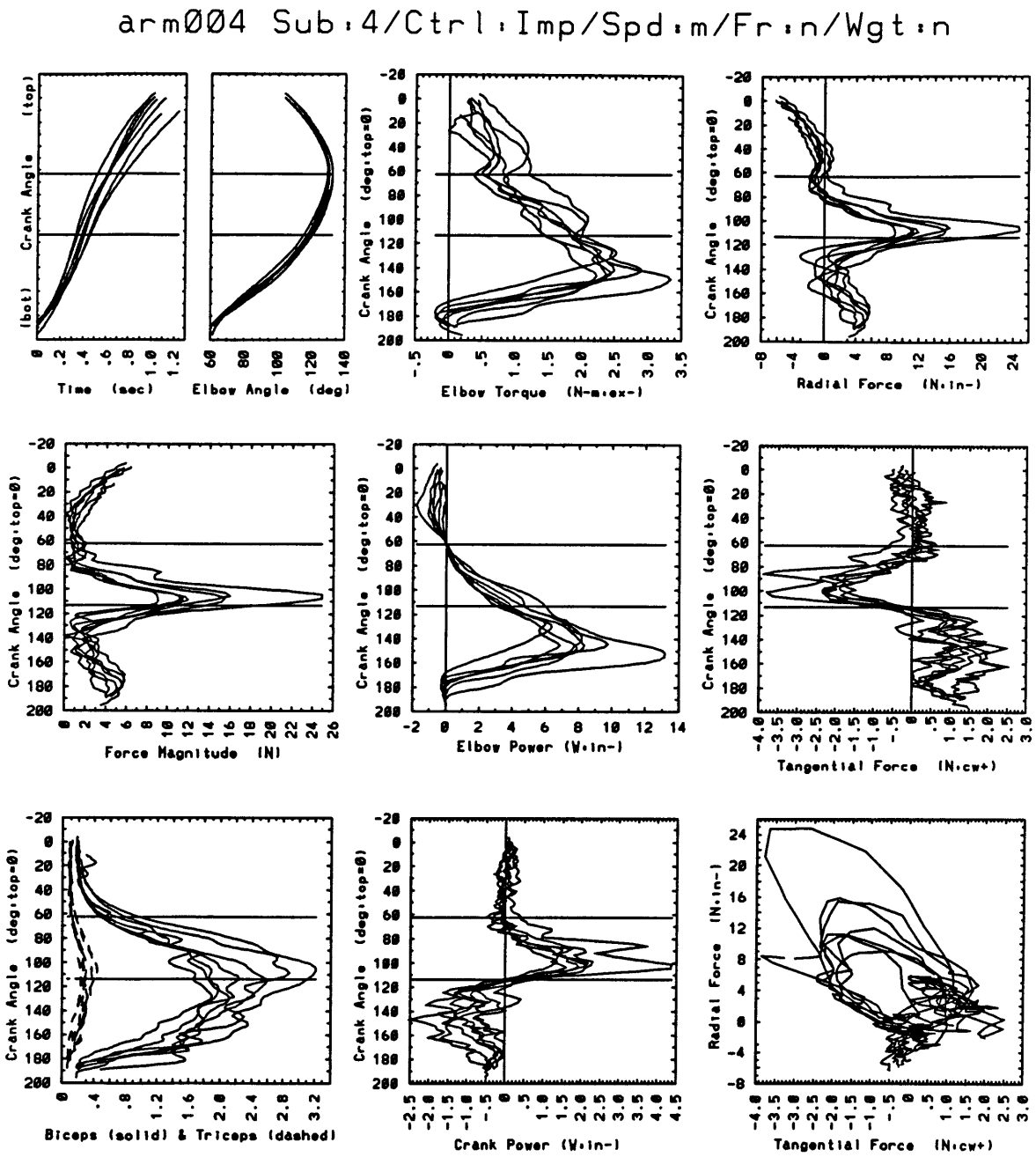
arm004 Sub:4/Ctrl:Imp/Spd:m/Fr:n/Wgt:n
Crank Angle (top) (bot)
Time (sec)
Elbow Angle (deg)
Crank Angle (deg:top=0)
Elbow Torque (N-m:ex-)
Radial Force (N:in-)
Force Magnitude (N)
Elbow Power (W:in-)
Tangential Force (N:cw+)
Biceps (solid) & Triceps (dashed)
Crank Power (W:in-)
Radial Force (N:in-)
Tangential Force (N:cw+)

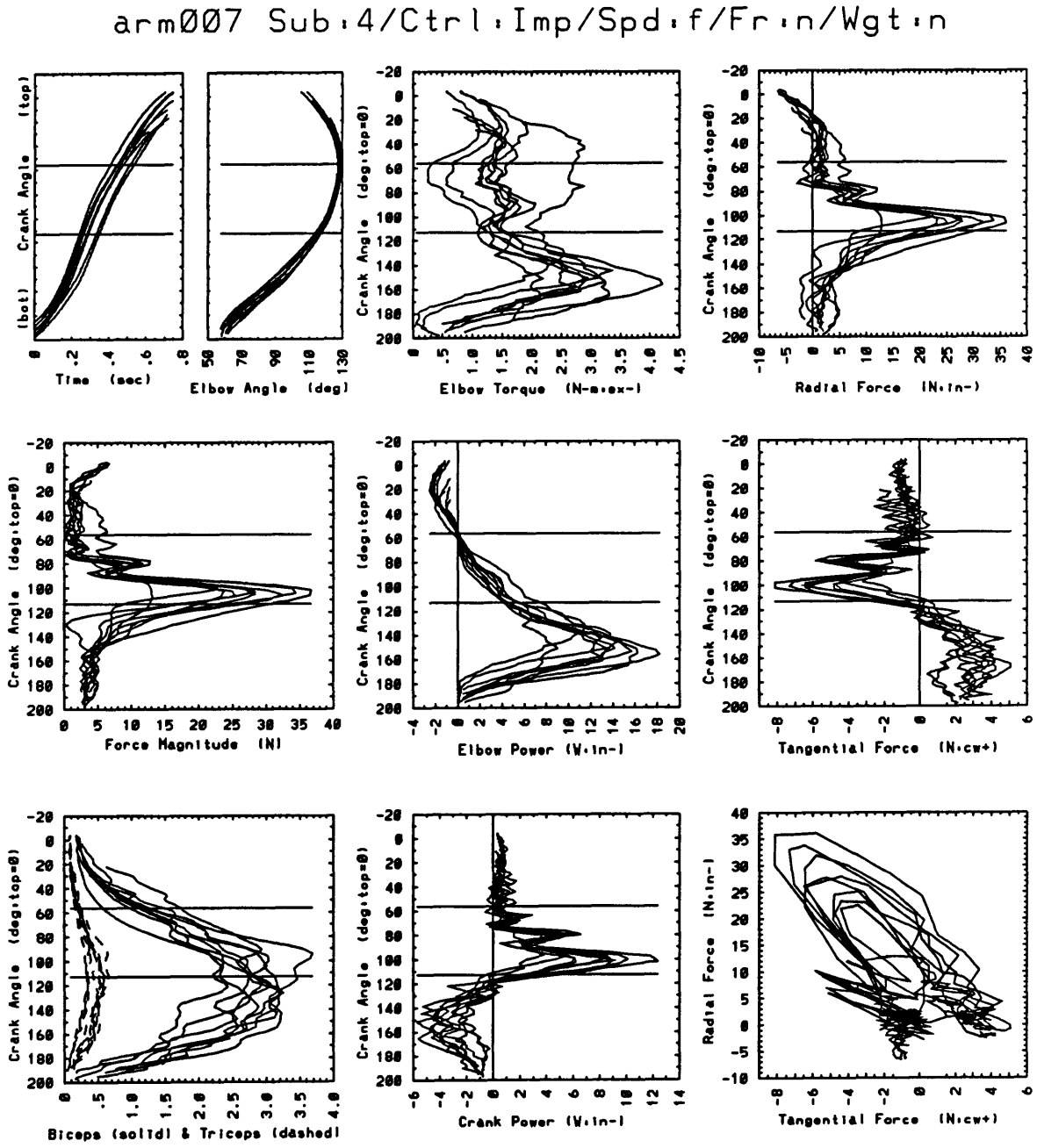
arm007 Sub:4/Ctrl:Imp/Spd:f/Fr:n/Wgt:n
Crank Angle (top)
(bot)
Time (sec)
Elbow Angle (deg)
Crank Angle (deg:top=0)
Elbow Torque (N-m:ex-)
Radial Force (N:in-)
Force Magnitude (N)
Elbow Power (W:in-)
Tangential Force (N:cw+)
Biceps (solid) & Triceps (dashed)
Crank Power (W:in-)
Radial Force (N:in-)
Tangential Force (N:cw+)

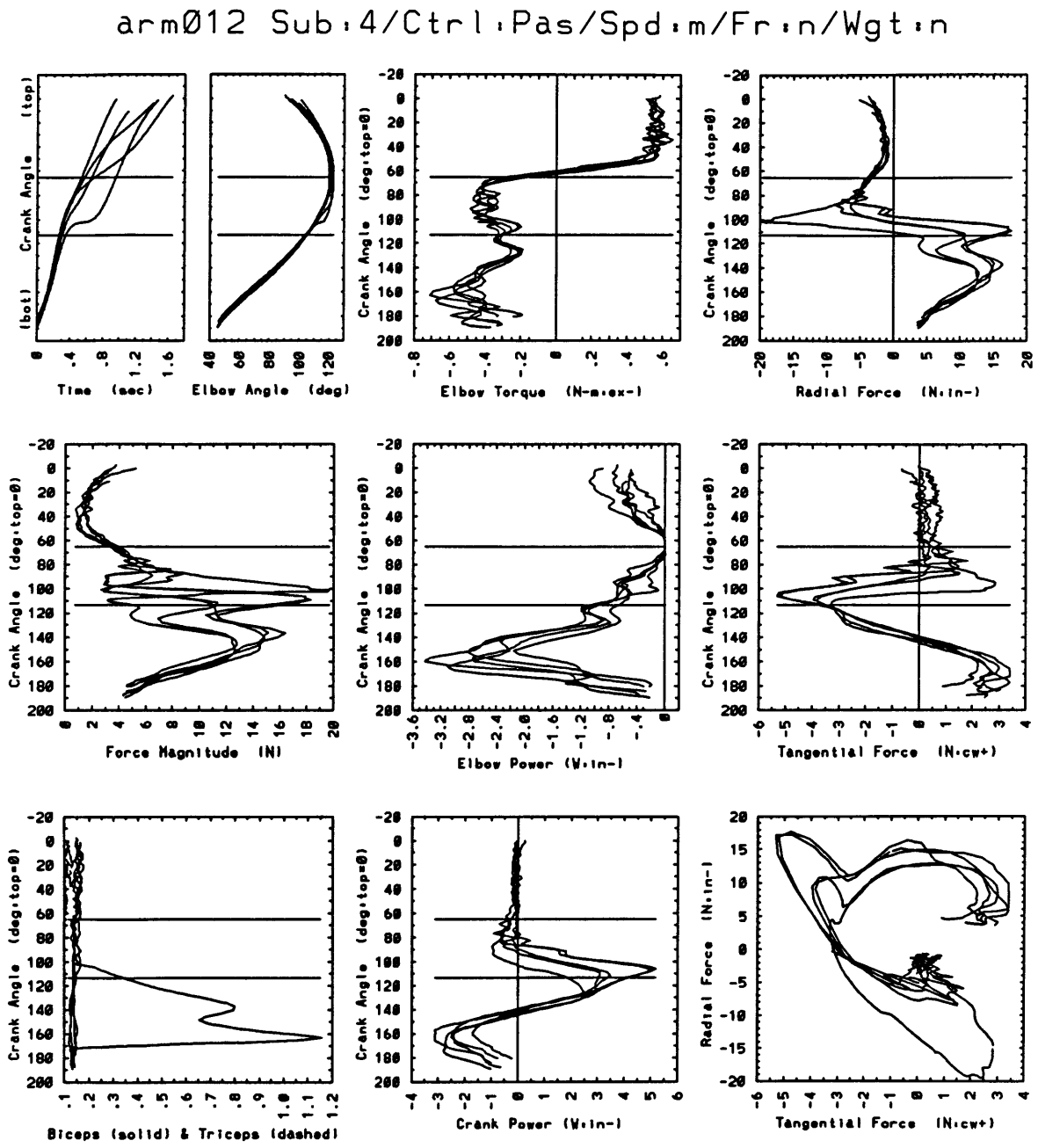
arm012 Sub:4/Ctrl:Pas/Spd:m/Fr:n/Wgt:n
Crank Angle (top) (bot)
Time (sec)
Elbow Angle (deg)
Crank Angle (deg:top=0)
Elbow Torque (N-m:ex-)
Radial Force (N:in-)
Force Magnitude (N)
Elbow Power (W:in-)
Tangential Force (N:cw+)
Biceps (solid) & Triceps (dashed)
Crank Power (W:in-)
Radial Force (N:in-)
Tangential Force (N:cw+)

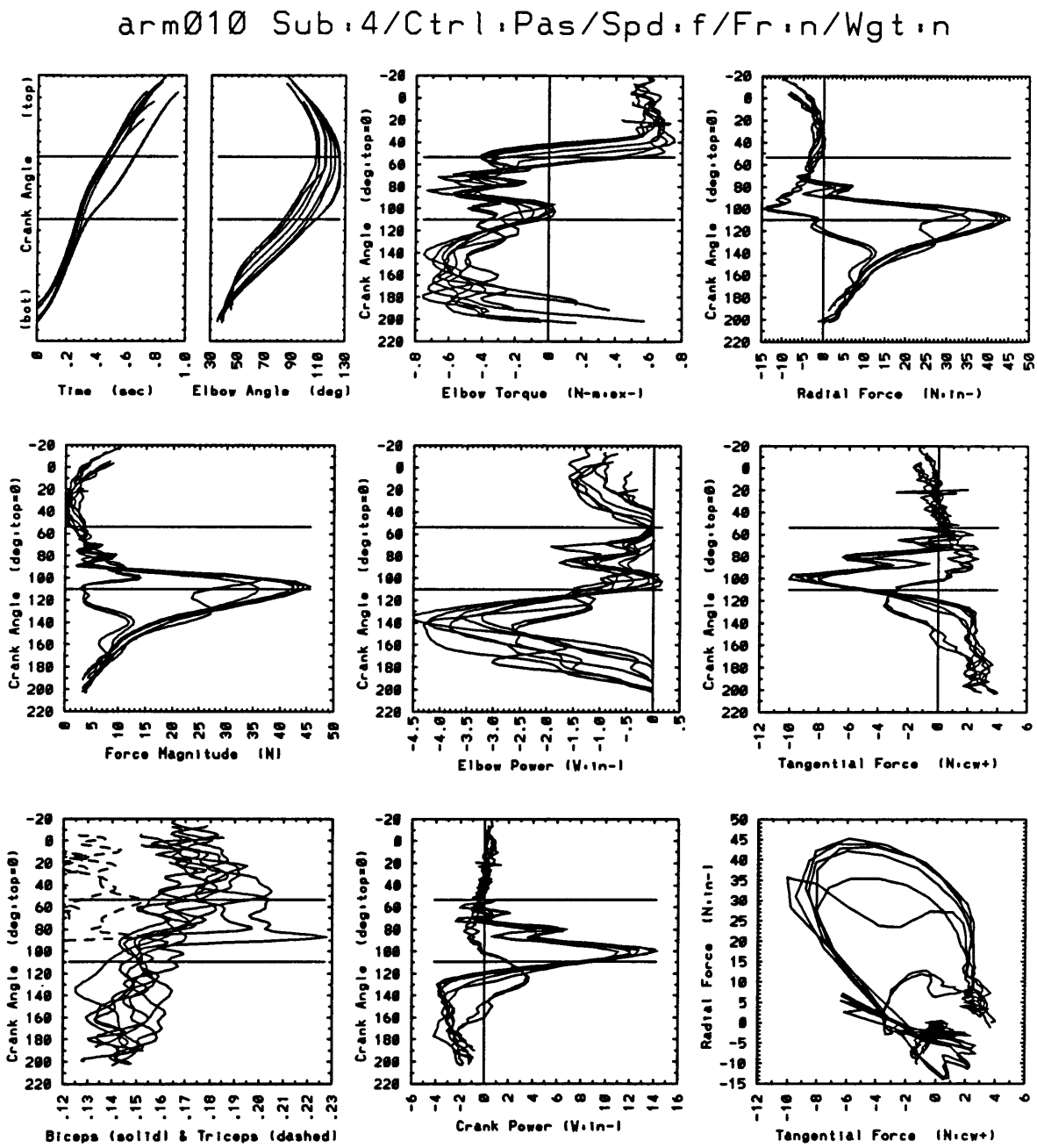
arm010 Sub:4/Ctrl:Pas/Spd:f/Fr:n/Wgt:n
Crank Angle (top)
(bot)
Time (sec)
Elbow Angle (deg)
Crank Angle (deg:top=0)
Elbow Torque (N-m:ex-)
Radial Force (N:in-)
Force Magnitude (N)
Elbow Power (W:in-)
Tangential Force (N:cw+)
Biceps (solid) & Triceps (dashed)
Crank Power (W:in-)
Radial Force (N:in-)

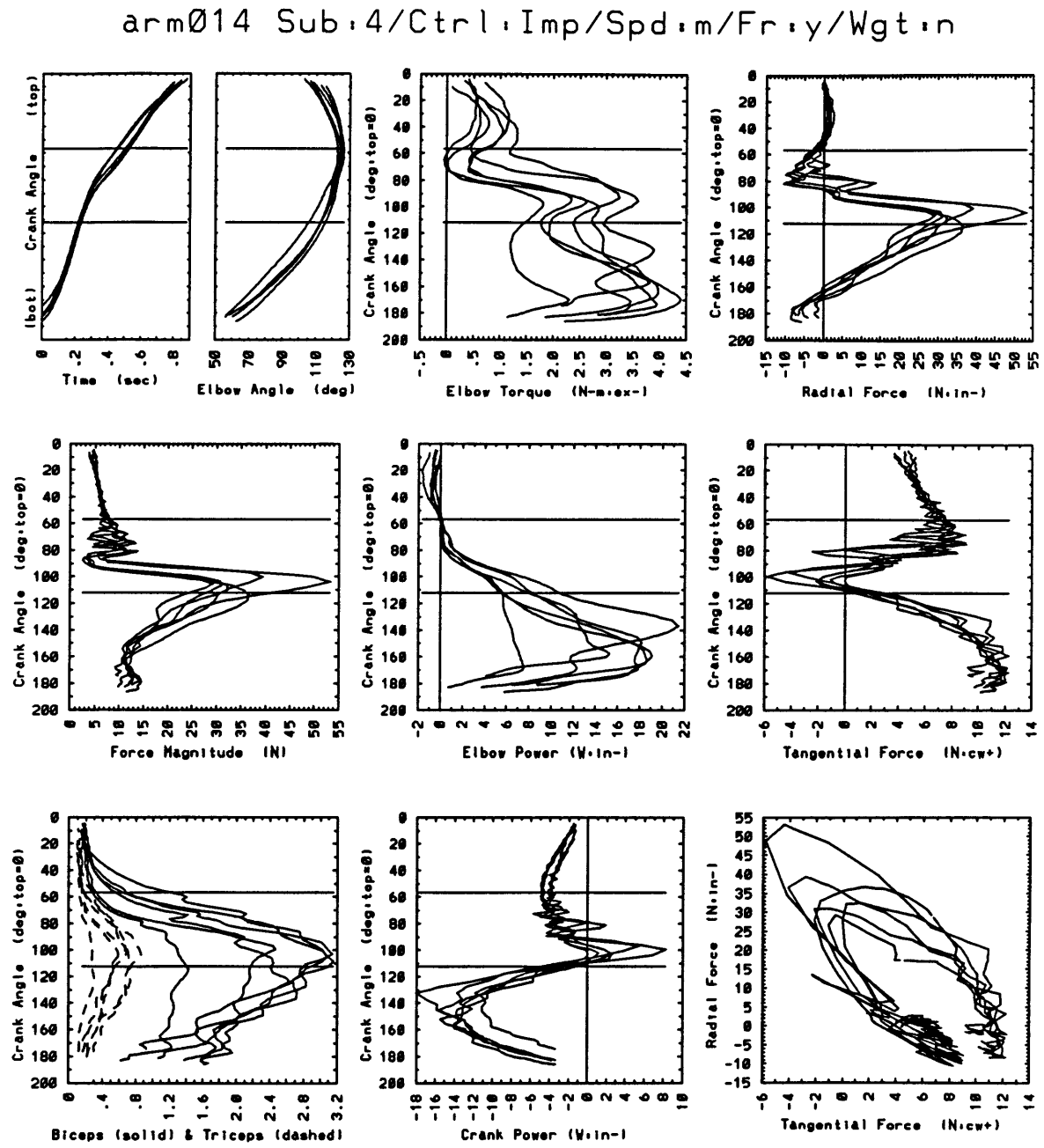
arm014 Sub:4/Ctrl:Imp/Spd:m/Fr:y/Wgt:n
Crank Angle (top) (bot)
Time (sec)
Elbow Angle (deg)
Crank Angle (deg:top=0)
Elbow Torque (N-m:ex-)
Radial Force (N:in-)
Force Magnitude (N)
Elbow Power (W:in-)
Tangential Force (N:cw+)
Biceps (solid) & Triceps (dashed)
Crank Power (W:in-)
Radial Force (N:in-)
Tangential Force (N:cw+)

APPENDIX C

INFORMED CONSENT FORM

INFORMED CONSENT DOCUMENT

Title of Study: A Simulator System for Developing Improved Above-Elbow Prostheses

Principal Investigator: Prof. Neville Hogan
Associated Investigator: John Mansfield

PURPOSE OF STUDY

Externally powered prostheses have proven to be limited in performance and function. In particular, amputees using above-elbow prostheses find many tasks of daily living difficult if not impossible to perform. The purposes of this study are twofold. First, it will compare and quantitatively assess the limitations of past, present, and/or future above-elbow prostheses. The comparison will entail an amputee wearing a specially designed prosthesis simulator while trying to perform various activities of daily living. Second, the study will take advantage of the simulator's capabilities to gain a better understanding of human motion control. The knowledge gained from this second purpose will not only permit enhancement of future powered prostheses but will provide contributions to areas of automatic controls and machine design.

EXPERIMENTAL PROTOCOL

It is desired to test the amputee's ability to perform simple tasks of daily living with various types of prosthesis designs. Such skills as the coordination of the prosthesis with remaining intact joints and the ability to interact with loads or constraints in the environment will be tested. Some examples of such tasks are turning a crank and donning a sock.

PROCEDURE

- ❑ An amputee will be fitted with a socket and the appropriate harnessing so that she can wear the simulator.

- ❑ The amputee will control the simulator using standard, commercially available surface electrodes, switches, and/or cables.

- ❑ If required, surface electrodes will be placed on the amputee in order to measure myoelectric activity of her remaining musculature.

- ❑ The amputee will be asked to perform simple, non-strenuous tasks of daily living in a laboratory environment.

- ❑ Amputee performance will be evaluated:
  - qualitatively by the experimenter and the amputee
  - quantitatively via a computer by measuring the dynamic state of the prosthesis and appropriate intact body segments.

- ❑ Throughout the experiments, comments, suggestions, and inquiries will be welcomed and encouraged.

- ❑ If the amputee grants permission, video-taping of the experiments will be performed.

SAFETY PRECAUTIONS

- ❑ Power to the prosthesis can be turned off in an emergency via any one of six safety switches:
  - the amputee's
  - the experimenter's (4)
  - a switch controlled by the computer

- ❑ Upon emergency shutdown, the prosthesis actuator automatically slows itself down via dynamic braking. This is done to prevent the simulator, which would no longer be under computer supervision, from striking the amputee.

- ❑ The computer will monitor the prosthesis dynamic state to assure that safety speed limits have not been exceeded and that the proposed simulation is stable.

- ❑ When electrodes are used, the computer will also monitor measured myoelectric activity to detect any sporadic signals generated from the MEA processors.

- ❑ During unconstrained tasks, the amputee will be provided with appropriate upper body and face shields if required to prevent him from hitting himself with the prosthesis.

- ❑ All prosthesis electronic components have been grounded to prevent electrical shock.

RISKS AND BENEFITS

The major risk for the amputee is striking herself with the simulator, since unlike the conventional prostheses, the simulator being used is capable of very high speeds. However, by appropriately speed-limiting the device and shielding the amputee during unconstrained tasks, the chance of injury may be virtually eliminated.

The monitoring electrodes are commercial devices which have been used safely for several years now and pose no known risk to the experimental subject.

A possible source of embarrassment may be the video-taping of experimental sessions. The amputee's consent will be obtained in advance of any recording.

There will be no benefits to the experimental subject beyond the personal satisfaction for contributing to the advancement of prosthetics.

SUBJECT AGREEMENT

I volunteer for this project and I am free at any time to seek further information regarding the experiment. In addition, I am also free to withdraw consent and discontinue participation at any time.

If I wish to remain anonymous, I may specify that my name be withheld from any publication resulting from these experiments.

In the unlikely event of physical injury resulting from participation in this research, I understand that medical treatment will be available from the M.I.T. Medical Department, including first aid emergency treatment and follow-up care as needed, and that my insurance carrier may be billed for the cost of such treatment. However, no compensation can be provided for medical care apart from the foregoing. I further understand that making such medical treatment available; or providing it, does not imply that such injury is the Investigator's fault. I also understand that by my participation in this study I am not waiving any of my legal rights. Further information may be obtained by calling the Institute's Insurance and Legal Affairs Office at 253-2822.

I understand that I may also contact the Chairman of the Committee on the Use of Humans as Experimental Subjects, M.I.T. 253-6787, if I feel I have been treated unfairly as a subject.

I have read the above consent document and understand the experiments described in the document. I agree to participate in the experiments as a subject.

The project investigators retain the right to cancel or postpone the experimental procedures at any time they see fit.

Date: _____ Subject's Signature: _____

Subject's Name: _____

APPENDIX D

QUESTIONNAIRE

QUESTIONNAIRE

Candidate Information:

Name _____ Date _____

Address _____

_____

Phone number: Work _____ Home _____

Birth date _____ Sex _____ Height _____ Weight _____

Amputation Side: Right _____ Left _____

Congenital deficiency? _____

Acquired? _____ When _____ Cause _____

Amputation limb length (acromion process to distal bone termination) _____ inches

Sound limb length (acromion process to lateral epicondyle) _____ inches

Special considerations pertaining to amputation limb (scarring, neuroma, adhesion, etc.)

_____

Does the participant currently wear a prosthesis? No _____ Yes _____

If yes, please complete the following questions on this page and page 2 (next page).

When was the first prosthesis received? _____ How long has it been used? _____

Information on the prosthesis:

Harness design _____ Socket design _____

Elbow model _____

Control at elbow: B.P. _____ Switch _____ EMG _____ Type: _____

Wrist unit: B.P. _____ Switch _____ EMG _____ Type: _____

Terminal device type: Hook _____ Hand _____

Control of terminal device: BP _____ Switch _____ EMG _____ Type: _____

Distance from the C7 spinous process to the hook attachment: _____ inches

Researcher's name: _____

Signature: _____

EVALUATION OF PRESENT PROSTHESIS

1. This prosthesis is worn, on average _____ hours per day, _____ days per week.
   On what occasions is the prosthesis particularly useful? _____
   _____

2. The prosthesis is:
   ____ always comfortable.
   ____ comfortable most of the time.
   ____ comfortable about half the time.
   ____ hardly ever comfortable.
   ____ never comfortable.

3. Functionally the prosthesis is:
   ____ very important.
   ____ important.
   ____ sometimes important.
   ____ unimportant.
   ____ very unimportant.

4. The elbow device is:
   ____ very difficult to operate.
   ____ difficult to operate.
   ____ operates satisfactorily.
   ____ easy to operate.
   ____ very easy to operate.

5. Without looking, I can tell about the elbow position and movement:
   ____ never.
   ____ occasionally.
   ____ about half the time.
   ____ almost always.
   ____ always.

Please tell us about your skill with the present prosthesis.

1: Cannot or does not use terminal device for this purpose
2: Performs task poorly or slowly
3: Completes task but with some difficulty
4: Completes task satisfactorily
5: Completes task independently with speed commensurate with nonamputees

____ a. grasp and pull up trouser or skirt
____ b. grasp clothing while zipping zipper
____ c. grasp toothbrush and apply paste
____ d. cut meat with knife and fork
____ e. hold glass and fill from faucet
____ f. dry dish with towel
____ g. donning socks
____ h. carry pail with terminal device
____ i. sharpen a pencil
____ j. hold paper and cut
____ k. hold jar and open
____ l. grasp playing cards
____ m. grasp telephone while dialing
____ n. use a rolling pin

APPENDIX E

EXPERIMENTAL PROTOCOLS

PROTOCOL 1

1. Consent form signed (Y/N) _____
2. Questionnaire form completed (Y/N) _____
3. Training:

   A. With the participant's current prosthesis:

   The participant will practice the following tasks: (refer to Protocol 2 for instructions)

   (i) cutting meat
   (ii) donning socks
   (iii) rolling dough

   The participant will be allowed to practice until he/she is comfortable with the task.

   When the participant confirms familiarity with the task he will be asked to perform a timed trial for all three tasks. Investigator will document the time (Documentation Form, Appendix F).

   Comments on the participant's performance on the above tasks:

   (i) cutting meat: _____

   _____

   (ii) donning socks: _____

   _____

   (iii) rolling dough: _____

   _____

   Height of the chair for: (1) cutting meat_____ cm.

   (2) donning socks _____ cm.

B. Training with the prosthesis emulator:

Participant will don the prosthesis emulator. Training with the two controller emulations (A and B) will be provided on the following activities:

1. Full range of elbow flexion and extension with shoulder at
   - 0°
   - 10° of extension
   - 90° of flexion
2. Grasp a film can with the terminal device, transport it to a distance of at least 30 cm, and release the can.

   Participant is considered having learned the activities when he/she performs them easily, and the investigator judges the participant functionally competent.

3. Pre-test criteria:

   Participant's ability to perform activities in sections A and B comfortably.

PROTOCOL 2: ADL TASKS

TASK 1: CUTTING MEAT

Materials

- 1/2 can of Play- Doh molded into rectangular 1/2" thick patty, surface scored in four strips
- metal knife and fork
- table and stool arranged to allow plate to be placed at or below elbow height

Positions

- participant sits at table
- therapist sits at amputated side to demonstrate;stands behind participant during test with hand near participants mouth

Instructions

- therapist demonstrates
- "Put the fork in your [terminal device], stabilize the meat with the fork. Cut along the mark with the knife held in your hand. Keep the fork in your [terminal device] to remove the piece from the plate and hand it to me as if you were going to eat it. Then cut the next piece. Continue until you have given me all the pieces."
- The therapist collects all the pieces.

Start/Stop

- Start: fork touched
- Stop: fourth piece given to therapist
- Maximum time: 4 minutes

TASK 2: DONNING SOCKS

Materials

- pair of cotton tube socks
- pair of nylon knee-hi hose

Positions

- participant sits with both shoes removed and knee-hi hose applied over each foot
- therapist sits at amputated side to demonstrate
- cotton socks in therapist's pocket

Instructions

- Therapist demonstrates, then hands participant one sock at a time
- "Hold the sock with both [hands] and put it on your foot. Pull it up all the way above your calf muscle, then put on the other sock. Do the [ipsilateral] side first."

Start/Stop

- Start: first sock touched
- Stop: second sock pulled completely on leg above the belly of the gastrocnemius muscle.
- Maximum time: 4 minutes

TASK 3: ROLLING DOUGH

Materials

- rolling pin
- full can of Play-Doh in the form of a cylinder with a 3" diameter
- 4"x 4" surface drawn on a plastic board

Positions

- participant stands at table
- therapist stands at amputated side
- items arranged on table

Instructions

- therapist demonstrates
- "Pick up rolling pin with sound hand then grasp the other end of the pin with your [terminal device]. Flatten the dough with the rolling pin using both hands until all four edges of the dough touch the 4"x 4" square at the same time. Begin now."

Start/Stop

- start: rolling pin touches the Play-Doh
- stop: all four edges of the 4"x 4" are in contact with the Play-Doh
- Maximum time: 4 minutes

APPENDIX F

DATA COLLECTION FORM

Name: _____ Date: _____

Subject's prosthesis: _____

Started with: Controller A_____ Controller B_____

Order of performing tasks: First_____ Second _____ Third_____

Time taken to perform ADL tasks (seconds)						
Controller	**Cutting Meat**		**Donning Socks**		**Rolling Dough**	
	Trial 1	Trial 2	Trial 1	Trial 2	Trial 1	Trial 2
Subject's Prosthesis †						
Controller A						
Controller B						

† subject performed only one trial with his own prosthesis

Comments: _____

_____

_____

_____

_____

_____

Investigator's Name:_____

Signature:_____

APPENDIX G

SUBJECT LINK LENGTHS

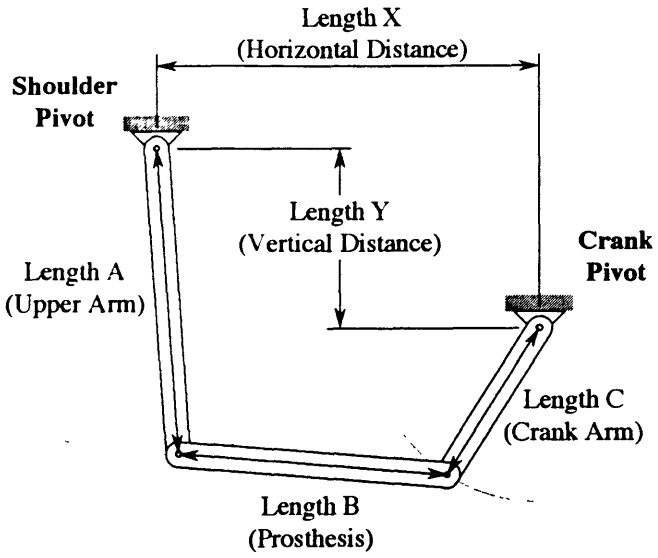

Subject Link Lengths (inches)					
Subject	**A**	**B**	**C**	**X**	**Y**
1	14.0	12.5	8.0	17.5	8.0
2	14.0	13.0	8.0	18.5	6.8
3	14.5	12.8	8.0	18.5	6.0
4	14.0	13.5	8.0	20.0	6.0

APPENDIX H

CALIBRATION

Since the original crank-emulator calibration, some of the system's hardware has been modified or replaced. As a result, conversion factors used for processing the experimental data were obsolete and new conversion factors had to be established. The primary purpose of this appendix is to document the new set of conversion factors for the emulator. In addition, the appendix briefly documents how each sensor was calibrated.

The general procedure for calibrating the emulator was as follows: A reference value was measured by a sensor. The sensor's output was then read by the DEC 11/73's A/D board and displayed in real time on the computer's monitor in digital units. Reference values were chosen such that the A/D board's full range of measurement was exercised (±2048 digital units).

Emulator Position:
For calibrating emulator position, three aluminum gage blocks were used. One block screwed onto the Pope wrist and provided a flat vertical reference surface. The remaining two blocks attached to the turntable and provided 15, 30, 45, 60, 75, 105, 120, and 135 degree reference angles. Before calibrating, the emulator was clamped onto a gage table at 90° with the turntable level. A machinist's protractor was used to determine the 90° of flexion between the emulator wrist and turntable mounting surface. Once a 90° reference was established, gage blocks were attached onto the turntable and leveled to produce additional angles. The best fit line for the data was:

$$\text{Degrees} = (0.0693)(\text{digital units}) + 4.2162$$

Emulator Velocity
Emulator velocity comes from an operational amplifier differentiating elbow position. A function generator created reference velocities by supplying triangular wave, position signals to the differentiator. The output signals, which were square waves, were measured. A universal counter was used to measure the period of the triangle waves and a scope was used to

measure the amplitudes of the triangle and square waves. Elbow flexion produced positive angular velocity. The best fit line for the data was:

$$\text{Deg/sec} = (0.3793)(\text{digital units}) - 1.4565$$

Emulator Torque

The best way to calibrate the elbow torque transducer would have been to apply a known force directly to the strain gage element as was performed from the past calibration. Unfortunately, this was not possible since many of the emulator's wires and strain gage components have been permanently glued together. Gaining direct access to the strain gage would have risked damaging part or all the current strain gage assembly.

The following method was used to check the past calibration: The emulator was clamped and leveled on its side to eliminated any torques resulting from gravity. The program **em1for.sav** (compiled from **em1for.for** and **em1mac.mac**) was run with the KEPCO power supply in manual voltage control mode. Both positive and negative voltages were applied to the emulator motor to produce motor currents as high as ±2 amps when the emulator reached its mechanical stops. The applied motor current was converted to its theoretical elbow torque and plotted against the measured elbow torque using the past calibration. Theoretically, the resulting cross-plot should be a line with a 45° slope.

The cross-plot results showed that the slope from the past calibration was accurate but the intercept required a minor adjustment. Elbow flexion produces a positive elbow torque and elbow extension produces a negative elbow torque. The resulting line was:

$$\text{N-m} = -(0.00448)(\text{digital units}) + 0.1696$$

The primary reason for keeping the slope from the past calibration was the inability to apply known torques directly to the torque sensor in the present calibration set-up. In addition, except for the zero intercept, there is little reason to believe that the past calibration results for the torque transducer have changed.

Crank Axis Position

The crank axis position was calibrated using a level and the same gage blocks used for calibrating the emulator. The crank is either at 0° or 360° when pointing straight up, 90° when pointing to the left, 180° pointing down, and 270° when pointing to the right. The best fit line for the data was:

$$\text{Degrees} = -(0.1898)(\text{digital units}) + 363.297$$

Crank Handle Position

The crank handle angular position is defined as the relative angle between the crank arm centerline and the attached emulator centerline. When the emulator is collinear with the crank, the handle position is defined to be 0°. Counter-clockwise rotation relative to this zero position gives positive angles and clockwise rotation results in negative angles.

A true zero reference for the handle was determined by leveling the crank at 90° and then leveling the handle. The handle was leveled by resting a level on the threaded steel coupler (one of three parts of the universal joint) with the threads pointing *away* from the crank axis.

One might expect that the zero reference position could be determined by setting the crank at 180° (pointing downward), screwing a weight onto the handle, and letting the entire double

pendulum system come to rest at its steady-state equilibrium position. Unfortunately, there are enough misalignments in the crank/universal joint system that this is not possible. There was a 0.7° deviation between the actual zero reference and the "free hanging" zero reference. Knowing the existence of the 0.7° deviation, handle calibration was performed by hanging a weight from the handle and taking measurements at various crank axis positions and then accounting for the deviation. The best fit line for the data was:

$$\text{Degrees} = -(0.1036)(\text{digital units}) + 1.0030$$

Crank Radial Force
The radial force was calibrated by hanging weights from the crank at 0° and 180° positions. The zero reference was found by averaging the measurements found at the 0° and 180° positions with no weights hanging and the universal joint's steel coupler removed.

The apparent mass of the force sensor and attached universal joint (without the steel coupler) was found to be 95 grams. The steel coupler by itself was 162 grams. Inward radial forces produce a negative output. The best fit line for the data was:

$$\text{Newtons} = (0.0312)(\text{digital units}) - 0.1080$$

Crank Tangential Force
The tangential force was calibrated by hanging weights from the crank at 90° and 270° positions. The zero reference was found by averaging the measurements found at the 90° and 270° positions with no weights hanging and the universal joint's steel coupler removed. A clockwise tangential force produces a positive output. The best fit line for the data was:

$$\text{Newtons} = (0.0331)(\text{digital units}) + 0.2404$$

MEA Zero References
Since MEA voltage measurements are directly converted to A/D units, only a zero reference voltage needs to be found for calibration. (The A/D conversion factor is 10/2048 = 0.00488 volts/unit.) In both cases (biceps and triceps), the intercept at zero digital units was 0.0150 volts. Thus, the conversion line for MEA measurements was:

$$\text{Volts} = (0.00488)(\text{digital units}) + 0.0150$$

Motor Zero References
Similar to the MEA calibration, only a zero reference is required for motor voltage and current calibration. The zero voltage reference was 0.0400 volts and the current reference was 0.0020 amps. The A/D conversion factor is 10/2048 = 0.00488 volts/unit. The KEPCO amp-to-voltage and voltage-to-voltage conversion factors are 4/10 = 0.4 amp/volt and 10 volt/volt respectively. The conversion line for motor voltage was:

$$\text{Volts} = (0.0488)(\text{digital units}) + 0.0400$$

The conversion line for motor amperage was:

$$\text{Amps} = (0.00195)(\text{digital units}) + 0.0020$$

5628-24